Design and Synthesis of New Photolabile Protecting Groups

Dissertation

zur Erlangung des Doktorgrades

der Naturwissenschaften

vorgelegt beim Fachbereich Biochemie, Chemie und Pharmazie

der Johann Wolfgang Goethe -Universität

in Frankfurt am Main

von

Matīss Reinfelds

aus Rīga (Lettland)

Frankfurt am Main, 2018

(D30)

Vom Fachbereich Biochemie, Chemie und Pharmazie

der Johann Wolfgang Goethe -Universität als Dissertation angenommen.

Dekan: Prof. Dr. Clemens Glaubitz

Erster Gutachter: Prof. Dr. Alexander Heckel

Zweiter Gutachter: Prof. Dr. Jens Bredenbeck

Datum der Disputation:

If the universe hands you a hard problem, try to solve an easier one instead, and hope the simple version is close enough to the original problem that the universe doesn't object.

Jordan Ellenberg

Manai ģimenei

To my family

Abstract

Photolabile protecting groups (PPGs, cages, photocages) are molecules which can block the activity of a functional group and be removed by irradiation of light of an appropriate wavelength. One of the goals of this work was to design new photolabile protecting groups, based on a literature known one. The far-UV absorbing diethylamino benzyl (DEAMb) photocage, developed by Wang *et al*., was selected as structural basis for this work. In order to trigger the uncaging reaction with longer wavelengths (≥365 nm), thus allowing also biological applications, its structure was optimized. This was done by elongating the π-orbital conjugation using biphenyl derivatives instead of a single aromatic moiety. The photocage was loaded with glutamic acid as the leaving group.

The highest bathochromic shift was shown by compounds, which had the smallest sterical hindrance imposed on the second aromatic ring. The absorption spectrum was more redshifted if the second aromatic ring contained an electron withdrawing group. However, the stronger the substituents electron withdrawing strength was, the lower the uncaging quantum yield was. It was rationalized, that this is due to a decreased excited state electron density at the benzylic carbon of the DEAMb core which is necessary to trigger bond dissociation. This has been confirmed using TDDFT (time-dependent density functional theory) computations done by Jan von Cosel, Konstantin Falahati and Carsten Hamerla (from the group of Irene Burghardt). The best uncaging quantum yield was 42% for *m*-phenyl substituted DEAMb, while if a strong electron withdrawing group was present (nitro group), there was no photoactivity at all.

In order to achieve a better π-orbital conjugation of the non-coplanar biphenyl derivatives, a C-C bond was introduced between the benzylic carbon and the second aromatic ring. The resulting planar compounds belong to the fluorene class. The computational data predicted the photochemical meta effect to some extent to be preserved in these molecules. A set of fluorene derivatives was synthesized and photochemically characterized. The molar absorption coefficients of all prepared fluorene derivatives were higher than for any of the biphenyl derivatives. Quantum yields of the acetate release ranged between 3-42%, thus being as good as the best glutamic acid releasing biphenyl compounds. The highest uncaging cross section ($\varepsilon\Phi_{365}$) of the acetate release from the prepared fluorene derivatives was above 5000 M^{-1} cm^{-1}. This value proves the high

potential of the new fluorene based photocages developed in this work. Furthermore, release of hydroxide ion from fluorenol could be shown along with generation of, presumably, fluorenyl cation. These intriguing results paves a way for further exploration of fluorene based photocages for the release of bad leaving groups.

The second part of this work describes the custom synthesis of ^{13}C labeled compounds for the VIPER (VIbrationally Promoted Electronic Resonance) project. In the VIPER pulse sequence, a molecule is vibrationally excited by a narrow band IR-pump pulse. The following Vis-pump pulse will promote the vibrationally pre-excited molecules to an electronically excited state. This Vis-pump pulse is offresonant for the not vibrationally pre-selected species and only resonant with the molecules, which are already pre-excited by the IR-pump pulse. Since the IR absorption bands usually are well resolved, a selective excitation of one molecule in an ensemble of similar ones is possible in the IR frequency range. Isotopologues and isotopomers are an extreme case of molecules which are near identical and differ only by isotopic composition or position. As a result in solution and at room temperature they have an identical UV-Vis absorption spectrum but different IR spectrum. This allows vibrational excitation of only one isotopologue (or isotopomer).

Isotopic labels were introduced in known photocages: 7-diethylamino coumarin (DEACM) and *para*-hydroxy phenacyl (*p*HP). The position for isotopic label incorporation in these molecules was guided by computations done by Jan von Cosel and Carsten Neumann. To allow control of the photoreactions in an ultrafast timescale, an IR active leaving group was used. The uncaging behavior of the prepared molecules in steady state was tested using chromatography (HPLC) and spectroscopy (^{1}H NMR, FTIR and UV-Vis). The VIPER experiments were performed by Daniela Kern-Michler, Carsten Neumann, Nicole Mielke and Luuk van Wilderen (from the group of Jens Bredenbeck). A selective uncaging of only the vibrationally pre-excited molecules could be achieved.

Zusammenfassung

Photolabile Schutzgruppen (*eng*. photolabile protecting groups, photocages) sind Moleküle, die die Aktivität einer funktionellen Gruppe blockieren und durch Bestrahlung mit Licht einer geeigneten Wellenlänge entfernt werden können. Eines der Ziele dieser Arbeit war, neue photolabile Schutzgruppen zu entwickeln, die auf einer bereits literaturbekannten Verbindung basieren. Als Ausgangspunkt für diese Arbeit wurde das kürzlich veröffentlichte Diethylaminobenzyl (**DEAMb**) als photolabile Schutzgruppe gewählt. Es ist bekannt, dass dieser einfache Chromophor selbst schlechte Abgangsgruppen (AG) wie Alkohole, Amine oder Diole freisetzen kann (P. Wang, *J. Photochem. Photobiol., A*, **2017**, 335, 300–310.). Gleichzeitig können damit auch gute Abgangsgruppen wie Ester freigesetzt werden.

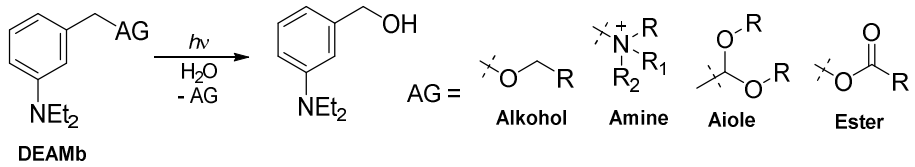

Der einzige Nachteil ist die Notwendigkeit, UV-Licht (<330 nm) für die Photoaktivierung des DEAMb zu verwenden. Ein Ziel dieser Arbeit war es daher, die DEAMb-Struktur so zu modifizieren, dass längere Wellenlängen (≥365 nm) zum Starten der Photoreaktion genutzt werden können. Dies wurde durch Verlängerung der π-Orbitalkonjugation unter Verwendung von Biphenylderivaten anstatt einzelner aromatischer Einheiten erreicht.

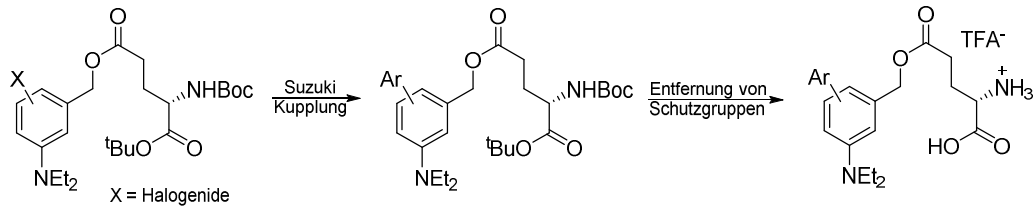

Die von DEAMb abgeleiteten Halogenide wurden hergestellt und mit Glutaminsäure als Abgangsgruppe synthetisiert. Danach wurde ein Arylsubstituent durch Suzuki-Kopplung an verschiedene Positionen des DEAMb eingebaut und die Schutzgruppen der Glutaminsäure mit Trifluoressigsäure entfernt.

Zuerst wurde der Einfluss der Substituentenposition getestet. Die UV-vis-Absorptionsmessungen wurden in 0,1M TEAA-Puffer (mit 20% MeCN) durchgeführt. Dabei wurde die Aufmerksamkeit auf die Absorptionsbande bei der längsten Wellenlängen gerichtet, die einem S_0-S_1-Übergang zugeordnet werden kann. Die *para*-Substitution (relativ zur NEt_2-Gruppe) hat den höchsten Extinktionskoeffizienten, der aus einem sogenannten *push-pull-effekt* resultiert. Solch ein intramolekularer Ladungstransfer erhöht üblicherweise den Extinktionskoeffizienten und verschiebt das Absorptionsmaximum zu längeren Wellenlängen, kann jedoch die Reaktivität in einer nicht vorhersagbaren Weise beeinflussen. Das *meta*-Isomer hat einen kleineren Extinktionskoeffizienten, aber das Absorptionsmaximum ist im Vergleich zum *para*-Isomer (Absorptionsmaximum = 335 nm) bathochrom um 20 nm auf 355 nm verschoben. Verbindungen mit Substituenten in *ortho*-Position hatten aufgrund sterischer Hinderung die geringsten Extinktionskoeffizienten. Die sterische Hinderung zwingt die aromatischen Ringe aus der Planarität heraus und reduziert die Überlappung der π-Obritale. Die Quantenausbeuten der Photoreaktion bei 365 nm sind für alle gering (<0,1%).

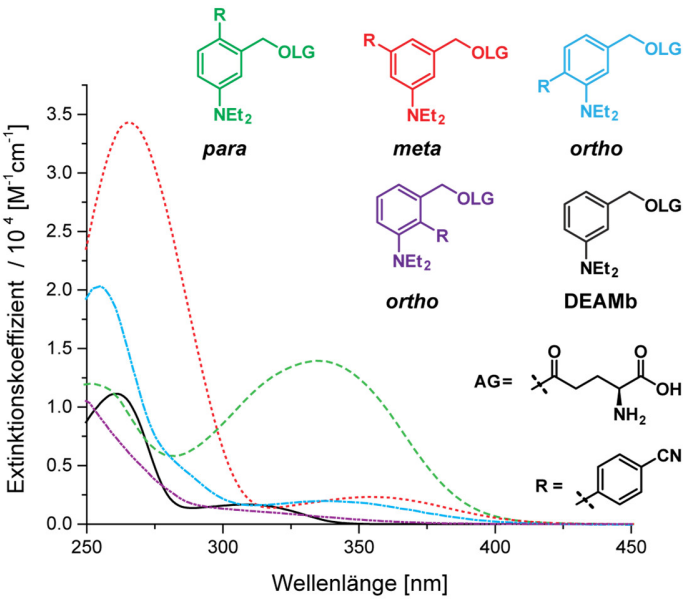

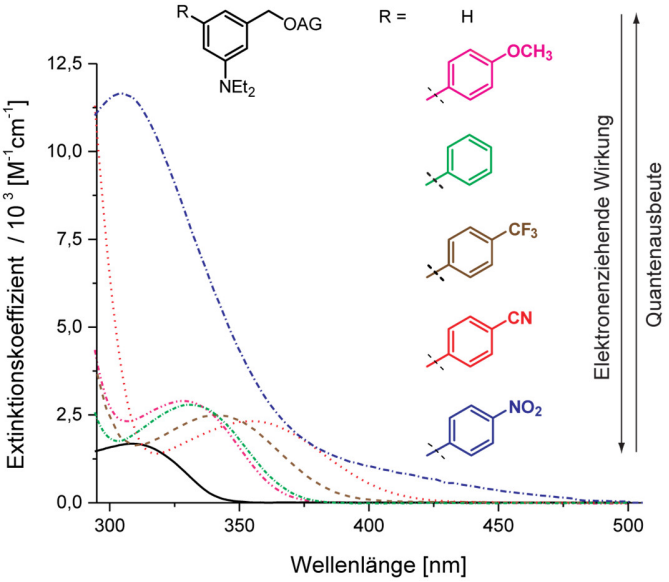

Die elektronischen Effekte des Substituenten in der *meta*-Position des DEAMb wurden dann getestet. Ein klarer Trend konnte festgestellt werden, der die elektronenziehende Wirkung eines Substituenten mit dem Absorptionsmaximum und der Quantenausbeute der Reaktion verbindet. Die Absorptionsspektren sind für Moleküle mit einem Elektronenakzeptor-Substituenten am stärksten rotverschoben. Gleichzeitig sind

die Quantenausbeuten verringert. Die beste Quantenausbeute betrug 42% für *m*-Phenyl-substituiertes DEAMb (ein Photon-Wirkungsquerschnitt $\varepsilon\Phi_{365}$ = 225 $M^{-1}cm^{-1}$), während, wenn eine starke Elektronen abstoßende Gruppe vorhanden war (Nitrogruppe), überhaupt keine Photoaktivität vorlag. Die Freisetzung von Glutaminsäure konnte direkt (mittels ^{1}H-NMR und HPLC) oder durch Derivatisierungsreaktionen (mittels Dünnschichtchromatographie oder HPLC) nachgewiesen werden.

Die Beobachtung, dass Derivate mit einer stark elektronenziehenden Gruppe photoinaktiv sind, kann durch die verringerten Orbitalkoeffizienten in der *meta*-Position des DEAMb-Gerüsts erklärt werden. Diese sind notwendig, um eine Bindungsdissoziation im angeregten Zustand auszulösen, wie es von Zimmerman beschrieben wurde (H. E. Zimmerman, V. R. Sandel, *J. Am. Chem. Soc.* **1963**, 85, 915–922).

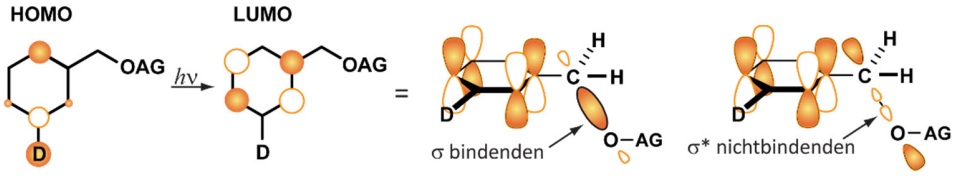

Im HOMO von Benzol mit einer Elektronendonor-Gruppe ist die Elektronendichte in *para*- und *ortho*-Position lokalisiert. Somit findet eine elektrophile Substitution in diesen Positionen statt. Bei Anregung im LUMO wird die Elektronendichte in die *ortho*- und *meta*-Positionen überführt. Durch Elektronendichte-Änderungen in einem Molekül, das eine -CH_2-AG Substitution in der *meta*-Position zur Elektronendonorgruppe hat, kann die erhöhte Elektronendichte der *meta*-Position in den LUMO die anionische Abstoßung der AG (zB Acetat) auslösen. Dies ist möglich aufgrund einer partiellen Population des σ^*-nichtbindenden Orbitals des benzylischen Kohlenstoffs und der Abgangsgruppe durch die Elektronen des aromatischen Rings. Dies ist bekannt als Meta-Effekt nach Zimmermann.

Durch TDDFT-Rechnungen von Jan von Cosel, Konstantin Falahati und Carsten Hamerla (Arbeitskreis Irene Burghardt) konnte qualitativ gezeigt werden, dass die LUMO-Formen und -koeffizienten für Derivate mit variierender Elektronendonor- oder – ziehenden Gruppe mit unserer beobachteten Reaktivität überein stimmten und unsere Schlussfolgerungen bestätigten. Die berechneten Anregungsenergien stimmten gut mit den experimentell beobachteten überein.

Um eine bessere π-Orbital-Konjugation der nicht-koplanaren Biphenyl-Derivate zu erreichen, wurde eine C-C-Bindung zwischen dem Benzyl-Kohlenstoff und dem zweiten aromatischen Ring eingeführt.

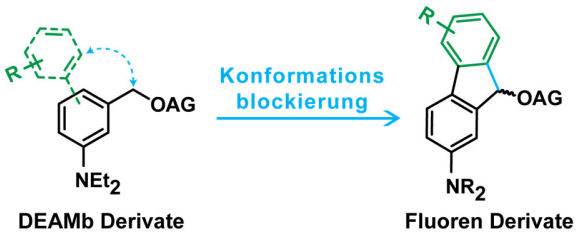

Die daraus resultierenden planaren Verbindungen gehören zur Klasse der Fluorene. Die Computerdaten sagten voraus, dass der photochemische Meta-Effekt in diesen Molekülen erhalten bleibt. Eine Reihe von Fluoren-Derivaten wurde synthetisiert und photochemisch charakterisiert. Um den Synthesebedarf zu reduzieren, wurde die Abgangsgruppe in Acetat umgewandelt. Somit wurden die Verbindungen weniger polar und daher musste organisches Lösungsmittel als Additiv zugegeben werden (MeCN mit 10% 0,1M TEAA-Puffer), um die photochemischen Eigenschaften zu messen.

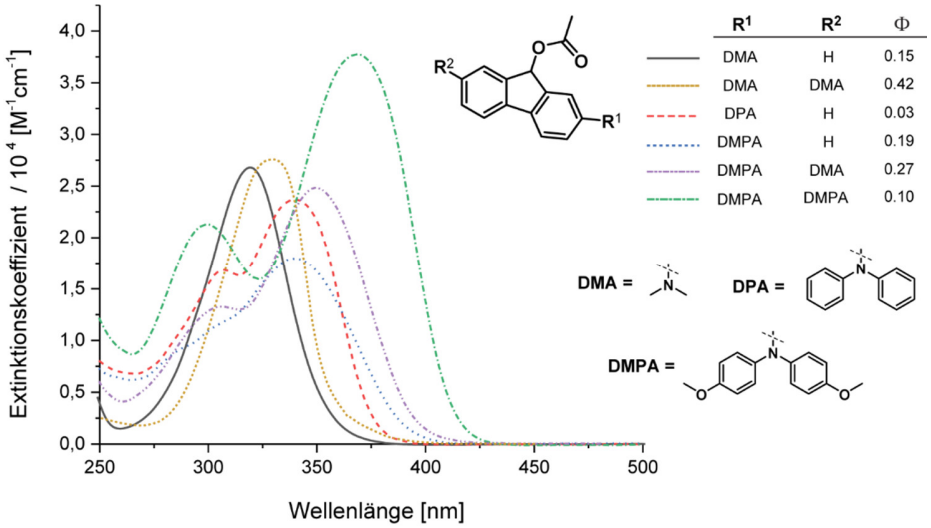

Die molaren Absorptionskoeffizienten aller hergestellten Fluoren-Derivate waren höher als die der Biphenyl-Derivate. Die Quantenausbeuten der Acetat-Freisetzung lagen zwischen 3-42% und sind vergleichbar mit den besten zuvor entwickelten Glutaminsäure-freisetzenden Biphenylverbindungen. Der höchste Photonen-Wirkungsquerschnitt ($\varepsilon\Phi_{365}$) der Acetatfreisetzung aus den hergestellten Fluoren-Derivaten lag über 5000 $M^{-1}cm^{-1}$. Dieser Wert belegt das hohe Potential der neuen fluoren-basierten PPGs, die in dieser Arbeit entwickelt wurden. Die Ergebnisse bestätigen auch, dass die berechneten Vorhersagen erfolgreich verwendet werden können, um die photochemischen Eigenschaften einer photolabilen Schutzgruppe zu verbessern.

Darüber hinaus konnte die Freisetzung von Hydroxid-Ionen aus Fluorenol zusammen mit der Bildung von einem langlebigen Zwischenprodukt, das vermutlich ein Fluorenyl-Kation ist, gezeigt werden. Diese faszinierenden Ergebnisse ebnen den Weg für die weitere Erforschung von Fluoren-basierten Molekülen zur Freisetzung von schlechten Abgangsgruppen sowie zur Verwendung des Fluorenylcarbokation als photochemisch erzeugbares Elektrophil.

Der zweite Teil dieser Arbeit beschreibt die Synthese von ^{13}C-markierten Verbindungen für das VIPER-Projekt (VIbrationally Promoted Electronic Resonance). Mit der VIPER-Pulssequenz wird ein Molekül von einem schmalbandigen IR-Pump-Puls vibrationsangeregt. Der folgende Vis-Pump-Puls versetzt die vibrationell vorangeregten Moleküle in einen elektronisch angeregten Zustand. Dieser Vis-Pump-Puls kann nur von den Molekülen absorbiert werden, die bereits durch den IR-Pump-Puls vorangeregt sind. Für die nicht schwingungsmäßig vorausgewählten Spezies ist der sichtbare Anregepuls nicht resonant. Da die IR-Absorptionsbanden in der Regel gut aufgelöst sind, ist eine selektive Anregung eines Moleküls in einem Ensemble von ähnlichen Molekülen im IR-Frequenzbereich möglich. Isotopologe und Isotopomere sind ein Extremfall von Molekülen, die nahezu identisch sind und sich nur durch Isotopenzusammensetzung oder -position unterscheiden. Somit haben sie in Lösung bei Raumtemperatur identische UV-Vis-Absorptionsspektren, aber unterschiedliche IR-Spektren. Die verschiedenen IR-Spektren erlauben die Vibrationsanregung von nur einem Isotopolog (oder Isotopomer).

Isotopenmarkierungen wurden in bekannte Photolabile Schutzgruppen eingeführt: 7-Diethylaminocoumarin und *para*-Hydroxyphenacyl (*p*HP).

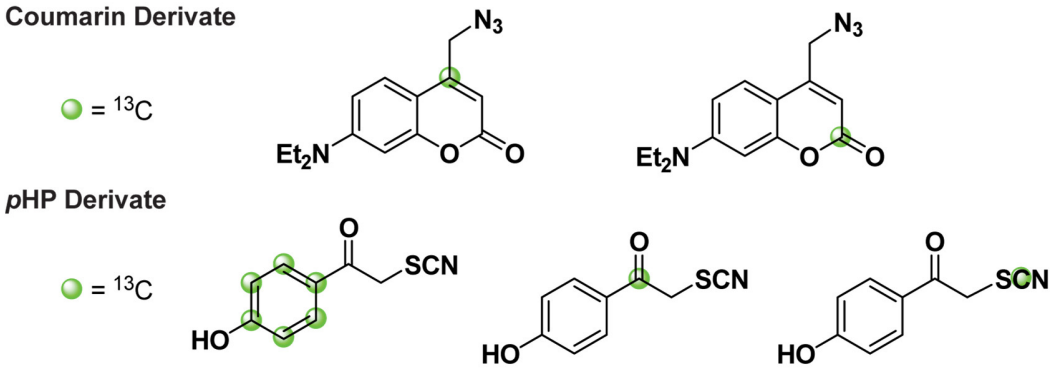

Die Position für den Isotopenmarkierungseinbau in diese Moleküle wurde durch Berechnungen von Jan von Cosel und Carsten Neumann bestimmt. Um die Photoreaktionen auf einer ultraschnellen Zeitskala kontrollieren zu können, wurde eine IR-aktive Abgangsgruppe

verwendet. Das Uncaging-Verhalten der hergestellten Moleküle im stationären Zustand wurde mittels Chromatographie (HPLC) und Spektroskopie (^{1}H-NMR, FTIR und UV-Vis) getestet. Die VIPER-Experimente wurden von Daniela Kern-Michler, Carsten Neumann, Nicole Mielke und Luuk van Wilderen (Arbeitskreis Jens Bredenbeck) durchgeführt. Eine selektive Photoreaktion von nur den vibrationsvorangeregten Molekülen konnte beobachtet werden.

Table of Content

1. Introduction

1.1. Photocages and photochemical orthogonality

Photolabile protecting groups (PPGs), also known as cages or photocages, are used just like other protecting groups to mask the activity of some functionality of a molecule. The key feature is that photocages can be removed by irradiation of light with an appropriate wavelength. The possibility to trigger the reaction by light allows spatiotemporal control over the release of the photocaged molecule. Thus, photocaged molecules are often used to study biological processes.[1,2] However, photolabile protecting groups have found application also in other fields, such as organic synthesis,[3,4] and super resolution microscopy.[5,6]

The specific properties a photocage should possess will always depend on the application. Usually it would be profitable to have the absorption maximum at longer wavelengths to avoid damage from irradiation with far-UV light to the studied system. The molar absorption coefficient and uncaging quantum yield of a photocage should be as high as possible to achieve maximal effect with minimal amount of light. Finally, the compound should be stable in the dark, easy to prepare and install on the substrate.

It is unlikely that one photocage would fulfill all of these criteria, but the task of an organic chemist is to design new photolabile protecting groups which would maximally approach them. It is a challenging goal, since photochemical reactivity often is opposite to the ground state reactivity. At the same time, the reaction pathways which are followed by a molecule in its excited state will often resemble the rationales of the ground state reactivity. Photochemistry as a separate subject is rarely included in the curriculum of university chemistry programs, thus is often misjudged by chemists as random and irrational.[7] Luckily, there exist textbooks which prove the opposite.[8,9]

There are many factors which influence the photochemical properties and the reactivity of a molecule. For example, the solvent[10] or photocage's concentration,[11] the local environment[12] and the solution's pH[13] or temperature.[14] Thereby, by adjusting some external factor it is possible to control the photoreactivity[15] and even achieve selective uncaging of two functionalities from the same chromophore.[16] A selective uncaging from the same photocage can be achieved also by the release rate selectivity, for example, by photocaging different functional groups[17] or by kinetic isotope effect.[18]

The complexity of the systems where photocages are used are ever increasing. For example, orthogonal addressing of more than one photocage in a mixture is still a challenge. The simplest way to achieve orthogonality in photo release reactions would be the selection of photocages whose chromophores absorb in a different spectral region. Such a wavelength selective cleavage has been extensively studied by the group of Bochet since the year 2000,[19,20] and up to four layers of a selective, sequential uncaging have been achieved from Si surfaces[21] or from oligonucleotides (the latter by the group of Heckel).[22] For a more comprehensive review the reader is referred to the literature.[23] However, the visible spectral range lacks reliable photolabile protecting groups which could be addressed orthogonally from each other. Thus, further development of PPGs is still important.

A large number of already known photocages have been discovered as results of experimental observations rather than a rational design. Thus, the current challenge of the field is to use computational predictions to guide the synthesis of new photocages.[24] Computational chemistry can give many answers, but the right questions have to be asked. As a result, in order to design a new photolabile protecting group, a detailed knowledge of the already known ones is essential.[25] Particularly, the underlying mechanisms of their photoactivity is important. For that reason, in the following chapters an overview of the photoreaction mechanism for the most relevant photolabile protecting groups will be given. Also the known examples for the redshifting of the absorption spectra for these photocages will be shown.

Generally, photocages can be divided into two categories by the means of how the leaving group is released after excitation. The first group would consists of molecules, where the leaving group is not being released directly after excitation. Instead, some intermediate (dark) processes has to happen before bond cleavage. In the second group of photocages, the uncaging event takes place directly after excitation as a result of electron density changes in the molecule. Currently, the computational predictions are more suitable to guide the design of the latter group. Thus, in the following text the focus will be on the photocages within this group, while for the former group only the most relevant or recent examples will be given.

Photochemistry is not limited to linear optics. A selective photoactivation is possible also by two photon activation which is especially widely used in biological applications due to high spatiotemporal resolution.[1,26,27] Among other nonlinear optical methods which have the potential to expand the toolbox of a selective photoactivation can be mentioned quantum dots[28–30] and upconverting nanoparticles.[31,32] Furthermore, multidimensional spectroscopy enables control of

the excited state processes in an ultrafast timescale.[33,34] One multidimensional spectroscopy method, which has the potential to be used for selective photochemistry, is called VIPER and is described separately in Chapter 1.4.

1.2. The first photocage category – leaving group release is dark reaction

Photocages can be divided into two categories by the means of how the leaving group (LG) is released. In one case light triggers only the first of an entire cascade of processes which leads to the bond cleavage. Since the actual bond breaking event is a thermal (dark) reaction, the release of bad leaving groups (bad nucleofuges) can be achieved. To this category belongs such long-known photocages as *ortho*-nitrobenzene (*o*NB) and *ortho*-hydroxycinnamyl (*o*HC). In the following, a short overview of these photolabile protecting groups along with most recent examples will be given.

1.2.1. *ortho*-Nitrobenzyl (*o*NB) based photocages

Engels[35] and Kaplan[36] were the pioneers of the photocaging of biologically active molecules to temporarily block their activity. In their studies they used the *ortho*-nitrobenzyl (*o*NB) photocage to release organic phosphates. Since then the *o*NB and its derivatives are among the most often used photocages.

The primary step after photoexcitation of *o*NB based compounds (**1**, Figure 1) is excited-state hydrogen atom transfer. The aci-nitro compound **2** then undergoes intramolecular cyclization to give compound **3** from which subsequently the release of the leaving group happens.[37,38] The product of the uncaging reaction is the nitroso compound **4**.

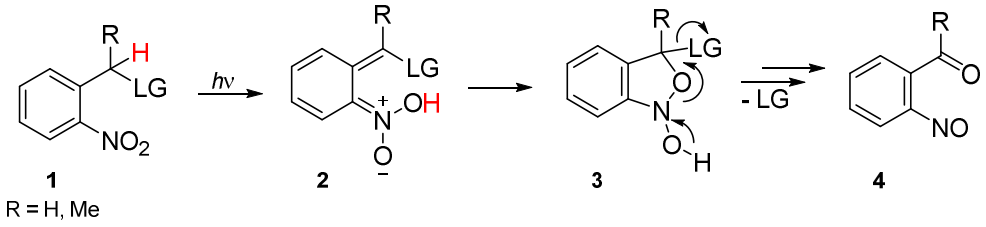

Figure 1: Simplified release mechanism from the oNB photocage.

One of the tactics to redshift the absorption spectra of the *o*NB is extension of the π-system by installing electron donating substituents.[39] Fusing of further aromatic rings seems to be a better method to improve the spectral properties, as has been shown for nitrodibenzofuran.[40] The main

drawbacks of the *o*NB derived photocages are the generation of plausibly toxic nitroso photoproduct, which also absorbs light at the irradiation wavelengths.

1.2.2. *ortho*-Hydroxycinnamic acid (*o*HC) based photocages

The *ortho*-hydroxycinnamyl group (**5**, Figure 2), which was first reported by Porter,[41] undergoes isomerization of the double bond upon irradiation (**6**). This makes intramolecular *trans*-esterification possible, leading to the release of a leaving group in the timescale of microseconds.[42]

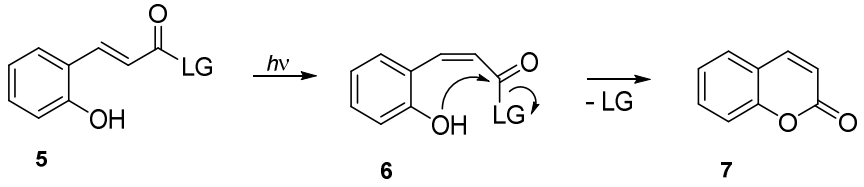

Figure 2: Simplified release mechanism of the *o*HC photocage.

Similar to the *o*NB photocage, also for the *o*HC photocage the absorption spectra have been bathochromically shifted by introducing electron donating substituents and fusing a further aromatic ring.[43] The most recent literature example is carbazole based *o*HC derivatives which can release two leaving groups from one chromophore.[44]

1.2.3. Miscellaneous visible light absorbing, recently reported photocages

Photoinduced energy transfer usually is associated with intermolecular sensitization. But Falvey achieved release of carboxylic acids from *N*-alkyl-4-pyridinium esters by demonstrating a creative use of charge transfer complex built between pyridinium cation and iodide ion (**8**, Figure 3).[45]

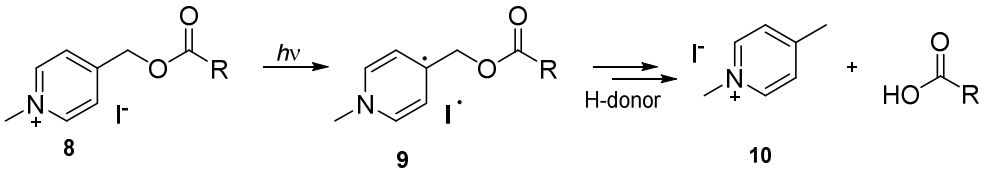

Figure 3: Charge transfer excitation of *N*-methylpyridinium iodide esters.

Photoexcitation with visible light triggers electron transfer from iodide to the pyridinium ion, resulting in a pyridyl radical (**9**), which then fragmentizes, releasing the leaving group and pyridinium iodide **10**. However, so far only the release of esters have been shown.

Dougherty combined the ease of the photochemical reduction of quinones with the reactivity of the trimethyl lock to obtain the visible light absorbing photocage **11** (Figure 4).[46] Trimethyl lock is known for rapid intramolecular cyclization once the phenolic oxygen is revealed.

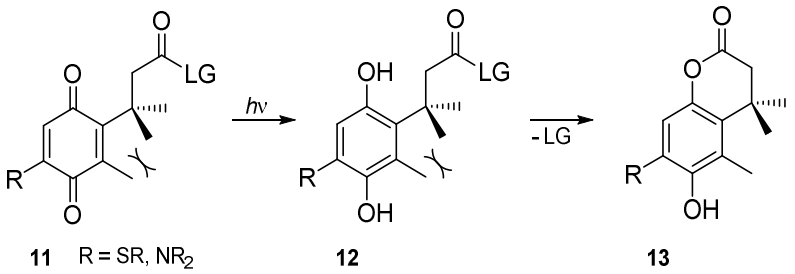

Figure 4: Uncaging strategy based on a trimethyl lock.

The absorbance spectra of the synthesized molecules reach up to 600 nm. Upon excitation an intramolecular electron transfer from the sulfur or nitrogen substituent to the quinone ring happens, followed by hydrogen abstraction (**12**). The reaction seems to happen both from singlet and triplet states, the latter having lifetimes in the range of nanoseconds. The subsequent lactonization happens thermally, with a high efficiency to release the leaving group and give the product **13**.[47] Further advantage of this photocage is that the charge-transfer absorption band of starting material depletes during the reaction because the carbonyl group of the quinone is reduced. Thus, the reaction's product is not competing for the irradiation light. A similar photocage was recently reported by Wang and Kalow.[48]

Another fabulous system, absorbing in the near-IR range, was proposed by Schnermann and coworkers.[49] The heptamethine cyanine based molecule **14** (Figure 5) after excitation sensitizes singlet oxygen. This leads to photooxidative C-C bond cleavage within cyanine itself (**15**), followed by hydrolysis of the oxidation product **16** to give the compound **17**. The leaving group is released after intramolecular cyclization of the amine **17** to give the carbamide **18**. Photooxidation can happen at each of the acyclic double bonds (only one is shown in Figure 5).

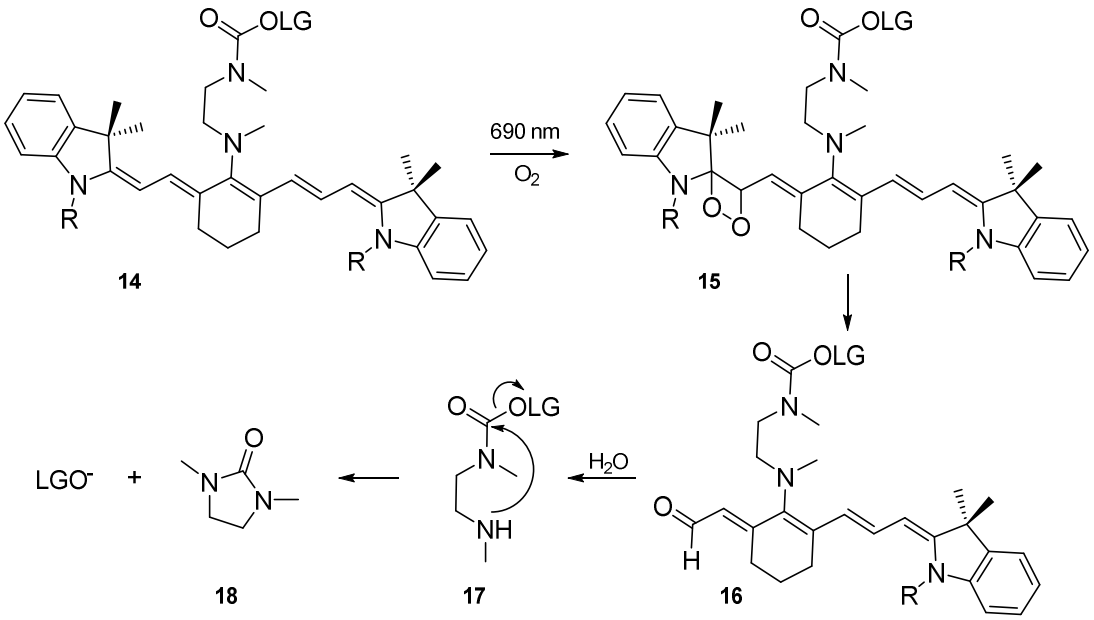

Figure 5: Uncaging reaction of the cyanine dye based photocage.

The photooxidation of the cyanine dyes happens at the positions which have increased electron density in the excited state. Electron density changes can be easily predicted by DFT computations, but the hydrolysis and the following cyclization to release the leaving group have to be tailored by the chemist's intuition. Thus, one cannot expect such photocages to be discovered on a regular basis. The use of a simple computations in search for a new photocage within this category is limited. From the application point of view photocages within this category are less suitable if ultrafast release of the leaving group is necessary.

1.3. The second photocage category – leaving group release is light reaction

The second photocage category consists of photocages, which release their leaving groups directly as a result of an electron distribution change in the excited state. Thereby, even the simple Hückel MO theory can be used to find molecules, which might be photoactive and belong to this photocage category.

A high speed of uncaging is characteristic of these photocages. They are more suitable for a release of good leaving groups, such as esters. Highly nucleophilic anions are prone to recombination. In the following, an overview of the most relevant PPGs belonging to this group will be given with a focus on the origin of the photoactivity. The coumarin photocage will be used as a case study about the tuning of the absorption properties.

1.3.1. The *p*-hydroxyphenacyl (*p*HP) photocage

The *para*-hdroxyphenacyl (*p*HP) photocage was first reported in 1996 by Givens and Park.[50,51] They demonstrated that the irradiation of *p*HP caged adenosine triphosphate (ATP) **19** yielded the phenylacetic acid derivative **20** and the released ATP with good quantum yields (Figure 6).

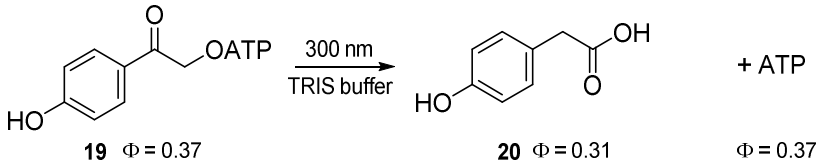

Figure 6: The photorelease of ATP from *p*HP photocage.

The quantum yield of the **20** formation is slightly smaller than that of the starting material **19** disappearance, indicating formation of also other photoproducts. The mechanism of the release has been well studied and is shown in Figure 7.

The lifetime of the excited singlet state produced upon excitation of the compound **21** is estimated to be only 4 ps, as it undergoes very rapid intersystem crossing ($k_{ISC} = 4 \cdot 10^8\ s^{-1}$) to triplet state. The fast intersystem crossing (ISC) is possible because the orbital type is changed from $^1n,\pi^*$ to $^3\pi\pi^*$ (El-Sayed rule). Also this triplet is short lived (aprox. 60 ps) and the leaving group is released with the phenolic proton (water assisted) to generate triplet biradical ^{3}**22**, which again undergoes ISC, generating ^{1}**22**. This can be trapped by water, to give the alcohol **23**, but this is a minor product.

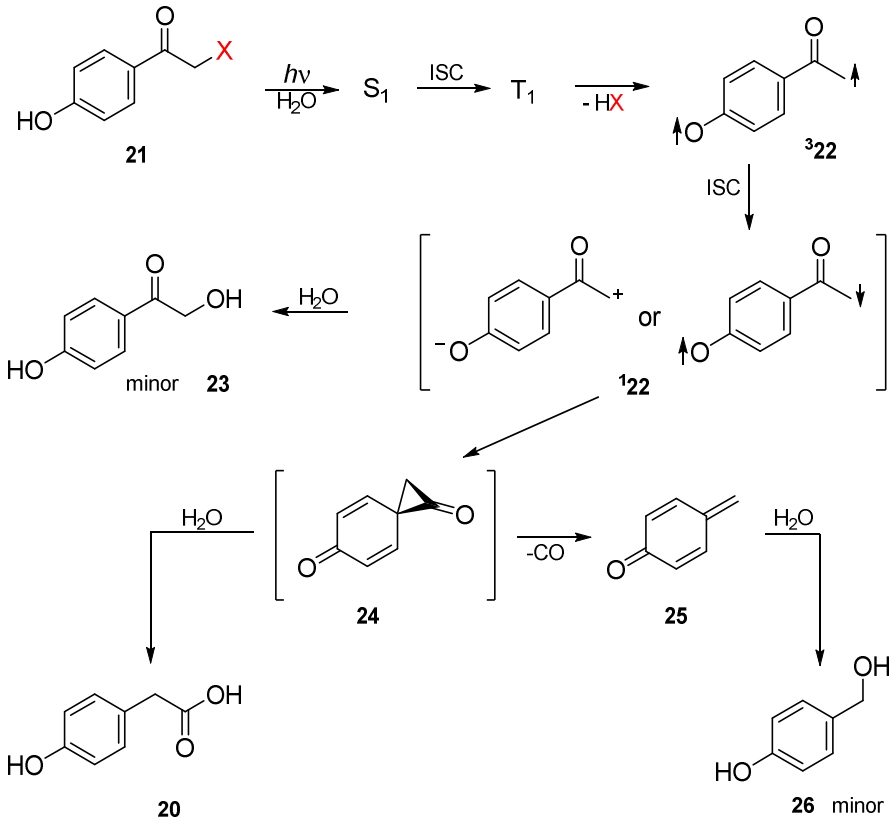

Figure 7: The uncaging mechanism of the *p*HP photocage.

The main product results from Favorskii-like rearrangement in which the spiroketon **24** is produced. It can hydrolyze, to yield the major photoproduct **20** or decarbonylate to give benzyl alcohol **26** (after hydrolysis of the quinone methide **25**). The major photoproduct **20** appears with a rate constant of $2 \cdot 10^9\ s^{-1}$, while the decay of the ^{3}**21** has a rate constant of $3 \cdot 10^9\ s^{-1}$.[52] Thus, the release of the leaving group is very fast. For a more detailed discussion of this mechanism please see the review by Klán *et al.* and references therein.[53]

The absorption maximum can be shifted to longer wavelengths (however, still staying below 330 nm) by installing aromatic substituents without much influencing the photoreaction quantum yields. Nevertheless, the substituents can influence the pK_a of the phenolic proton. Formation of a phenolate redshifts the absorption maximum, but decreases the uncaging quantum yield. The rate of the triplet formation in early stages of the photoreaction was not altered by *p*H. Thereby, the lower uncaging quantum yields of the deprotonated phenols probably are due to other deactivation channels available for its triplet state.[13] The quantum yields are higher for leaving groups who´s pK_a is below 11, thus the *p*HP photocage is not suitable for releasing leaving groups like alcohols and amines.[54] In spite of its absorption in the far UV region, *p*HP is still recognized

as a good photolabile protecting group due to its robust photochemistry and aqueous solubility. This is confirmed by multiple reports about the *p*HP and its derivatives published in the last 5 years. Leaving groups like nicotinamide,[55] fluoride ion,[56] amines[57] (in acidic and neutral pH) and triazole[58] have been successfully released. Furthermore, its absorption spectra tail has been shifted to visible[59] and also two photon activation[60] has been reported.

1.3.2. The benzoin group

The photocyclization of benzoin acetate to give 2-phenylbenzofuran and expelling of a leaving group was reported by Sheehan and Wilson in 1964.[61] It was recognized, that cyclization yield is the highest for 3,3-dimethoxy substituted molecules. In a follow-up article it was discovered that particularly efficient cyclization happens if the phenyl ring, which is not conjugated to the carbonyl group (**27**), has *meta*-methoxy substituents (Figure 8).[62]

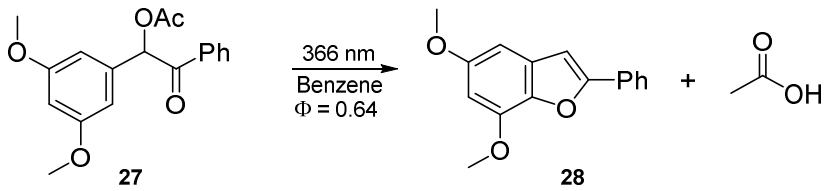

Figure 8: The photoinduced benzoin cyclization.

In the years to follow, the benzoin photocage has found a broad scope of application for the release of various leaving groups. For details, the reader is suggested the review by Klán *et al.* and references therein.[53] The uncaging mechanism of the benzoin photocage is shown in Figure 9.

Upon irradiation of the benzoin **29**, a singlet excited state exciplex (charge transfer complex) **29a** is generated within 2 ps. This is followed by rapid conversion (again, in few picoseconds) to biradical **32**. This can directly decay into the product **28** (and release the leaving group in ns time scale) or first generate the cation **33**, which then deprotonates to give the product **28**.[63] An alternative pathway is direct heterolysis from **29a** to release the leaving group and give carbocation **30**, which is trapped by water to give compound **31**.[64] The latter mechanistic pathway would be in line with Zimmerman's meta effect, which is described in the next chapter.

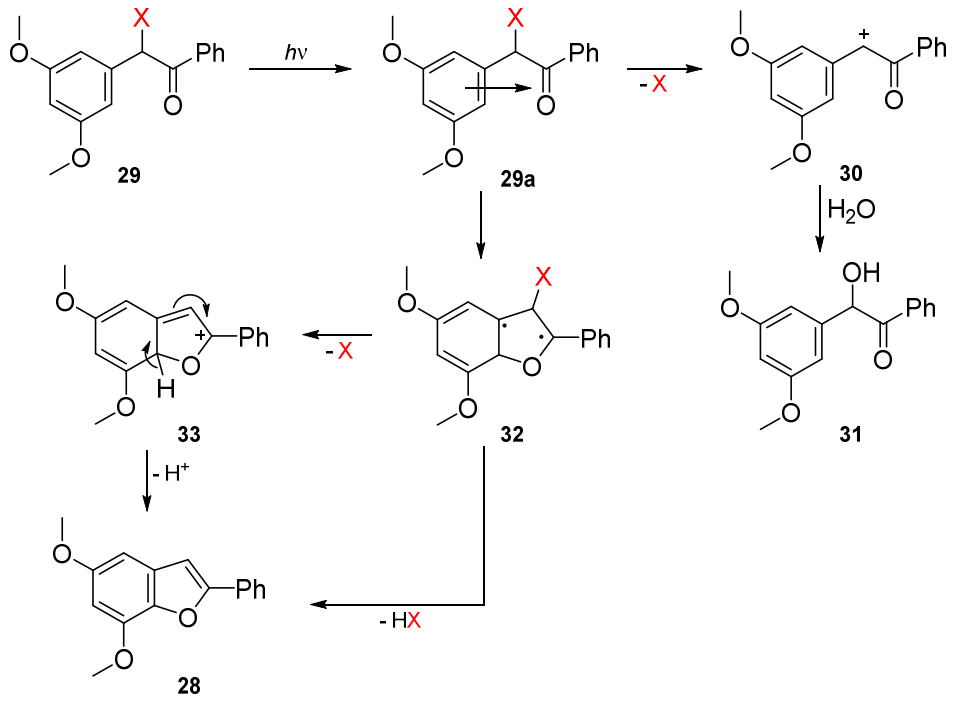

Figure 9: The uncaging mechanism of the benzoin photocage.

The fast photoreaction, which gives only one main photoproduct (the benzofurane **28**)[63] and the small influence of the leaving group on the uncaging quantum yield[64] are the advantages of benzoin based photocages. However, the absorption in UV region and the formation of a product, which has more redshifted absorption spectrum might be the reason why in last 5 years no new reports using the benzoin **29** photocage have been published (to the best knowledge of the author of this work). This benzoin based photocage is interesting because it combines two molecules, which also each separately could release the leaving group – acetophenone with a leaving group at the α-carbon and *meta*-electron donor containing an aromatic ring with a leaving group at the benzylic carbon. The latter will be reviewed more detailed in the next chapter.

1.3.3. The benzyl ethers and meta effect

In the year 1963, Zimmerman and Sandel published the fundamental report on *meta*-substituted benzyl acetate photoactivity. The 3,5-dimethoxy benzyl acetate **34** underwent a photosolvolysis to give benzyl alcohol **35** with a high chemical yield (79%) and 10% quantum yield (Figure 10).[65]

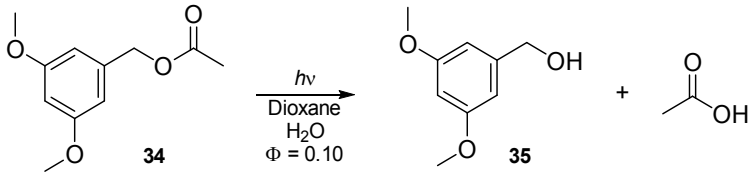

Figure 10: Photosolvolysis of 3,5-dimethoxy benzyl acetate.

More importantly, the authors gave a mechanistic justification based on molecular orbital computations. Their explanation has stood the test of time till nowadays, in spite of being made in the very early stages of mechanistic organic photochemistry.

Figure 11 shows the π-electron distribution characteristics for two model cases, the benzyl carbocation (W = CH_2^+) and benzyl carbanion (D = CH_2^-). The carbocation represents benzol, substituted with an electron withdrawing group (*e.g.* NO_2) while the carbanion represents an electron donating substituent (*e.g.* OMe).

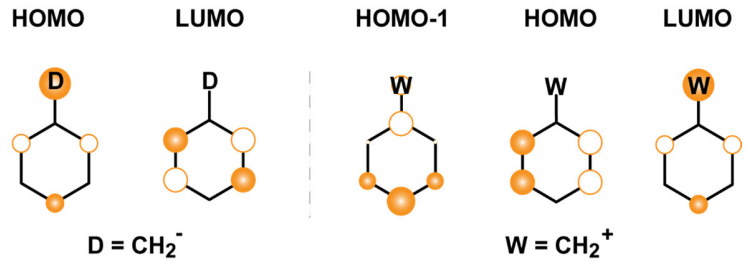

Figure 11: The frontier molecular orbitals of benzol bearing an electron withdrawing (W) and donating (D) group. Computations were done by program HuLiS.[66]

In the HOMO of an electron donating substituent-bearing benzene electrons are localized in *para* and *ortho* positions. Thus, electrophilic substitution reactions happen in these positions. But upon excitation to LUMO, the electron density is transferred to *ortho* and *meta* positions. The increased electron density can change the reactivity in the excited state (vide infra).

The HOMO and HOMO-1 orbitals of the benzyl carbanion are almost degenerated, in one case directing electrophilic attack to the *para* position (HOMO-1) while in other case to *ortho* and *meta* (HOMO). Thus, to explain the ground state reactivity normally observed for benzol with a strong electron withdrawing group as NO_2, the atomic charges have to be taken into account. Such analysis reveals decreased electron density in all positions of the aromatic ring (comparing to unsubstituted benzene), but the *meta* position has slightly smaller reduction of atomic charge than the *para* and *ortho*, thus the ground state reactivity.[67] For electronic excitation, the highest oscillator strength is associated with a transition to LUMO in which the electron density in *meta* position is depleted.

The consequences of the electron density changes upon electronic excitation in each case (W = donor or acceptor) are different. For a molecule which has –CH_2-LG substitution in the *meta* position to the electron donating group, the increased electron density of the *meta* position in LUMO orbitals can trigger the anionic repulsion of the LG (*e.g.* acetate).[65] This is possible due to partial population of the σ^* antibonding orbital of the benzylic carbon and the leaving group by the electrons of the aromatic ring (Figure 12).

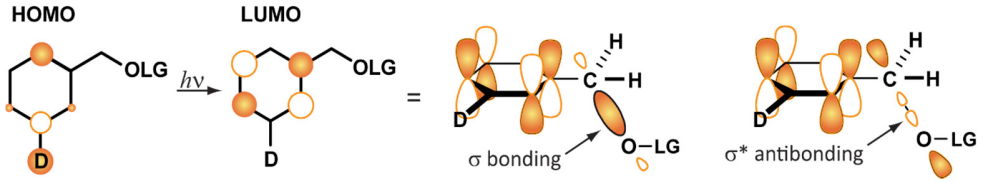

Figure 12: Zimmerman's meta effect.

The ability of the electron donors to promote photolysis at the *meta* benzylic carbon now is known as Zimmerman's meta effect. Despite the fact that the electron density is increased also in the *ortho* position upon excitation, the difference between the electron density in HOMO and LUMO for the *meta* position is larger. As a consequence, historically the main interest has been oriented to the *meta* position thus also the term "meta effect".

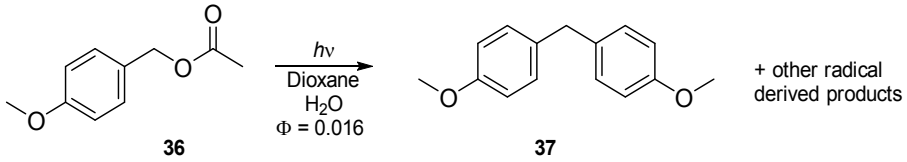

Figure 13: Photolysis of *para*-methoxy benzylacetate.

The photolysis of the *para*-methoxy benzyl acetate **36** has a much lower quantum yield and gives only free radical derived products (**37**, Figure 13). Meanwhile, the photolysis of 3-methoxybenzyl acetate yielded products from heterolysis and homolysis reaction with a quantum yield similar to that of dimethoxy substituted compound **34** (Figure 10). These results further support the role of electron density change upon excitation.

Qualitative computations of the methoxy substituted benzyl cation energies in the excited state revealed that the *meta* substituted compounds have lower energy excited state cations (Figure 14). Furthermore, the energy difference between the ground and excited state cations decreases going from *p*-MeO to *m*-MeO to 3,5-diMeO substituents. The excited state electron density located on the sp^2 hybridized carbon to which the methylene group is attached increases in the same order.

The low quantum yield of the *p*-MeO benzyl acetate (**36**) photolysis is explained by the smaller electron density at the benzylic carbon in the excited state.

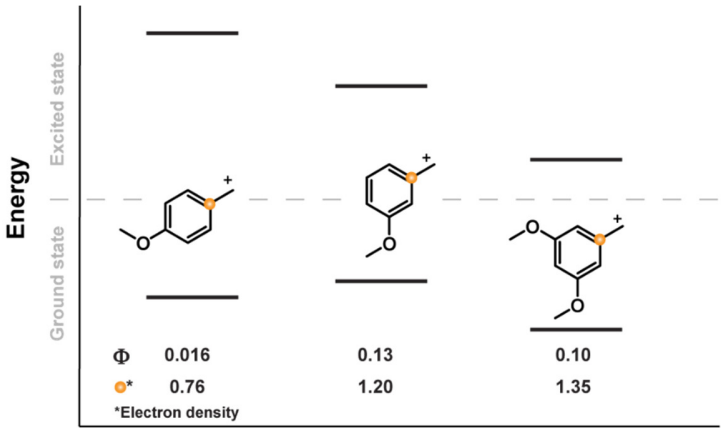

Figure 14: The relative energies of various substituted benzyl cations and the electron density at the benzylic carbon in the excited state. The graph was prepared using values from literature.[65]

Although the meta effect has been overall accepted, the nature of the bond cleavage process has been at dispute. The excited singlet state **39**, produced by irradiation of the compound **38**, could undergo homolytic bond cleavage to give radical ion pair **40** (Figure 15). By hydrogen abstraction from solvent, the photoproduct **41** (along with other radical derived side products) would be formed. Such products were observed in the irradiation the 3-methoxy benzyl acetate already in the first Zimmerman's publication,[65] thus there has been no discussion about the formation of the radical pair **40**. The origin of the ion pair **42** has been the topic of the debate instead.

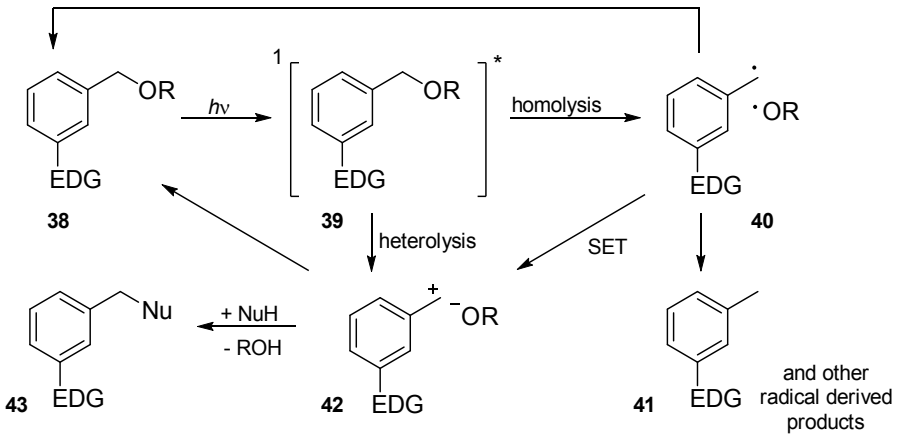

Figure 15: The reaction mechanism of the *meta* substituted benzylether photolysis.

Pincock promoted for generation of the ion pair by rapid single electron transfer of the radical pair **40**,[68] while Zimmerman defended direct formation of the ion pair **39**.[69,70] When the

ion pair is generated it can recombine to give the starting material **38** or react with the solvent, to give the compound **43** and free the leaving group.

No clear answer regarding the mechanism of the ion pair **42** formation can be given. However, in favor of a direct heterolysis from the S_1 excited state speaks experimental data on the uncaging of the 3,5-dimethoxy benzylphospate.[63]

The homolysis/heterolysis product ratio can be influenced by multiple factors, such as the nature of the *meta*-substituents,[71] or the solvent.[72] Generally, strong electron donating substituents (3,5-dimethoxy, m-diethylamino, 3,5-dialkylamino) and polar solvents favor heterolysis derived photoproducts.[65,73–75]

For the 3,5-dimethoxy benzyl cation a conical intersection has been located above the equilibrated excited state singlet geometry by only 7.19 kcal mol^{-1} with the energy gap between S_1 and S_0 at the nearest approach being only 0.31 kcal mol^{-1}. The ground and excited state radical surfaces are separated by a much larger energy (16.8 kcal mol^{-1}) gap which is located 164 kcal mol^{-1} from the equilibrated excited state radical geometry.[70] Conical intersections nearby to the excited state of *meta*-electron donating substituted benzyl cations have been recently confirmed also by Winter *et.al*.[76] These data are explaining why the 3,5-dimethoxy benzyl acetate upon irradiation yielded only heterolysis products.

Computations of Winter *et al*. showed that benzyl cation **45a** (Figure 16) with two strong electron donating substituents has nearly degenerate ground singlet and triplet states, thus it might exist as triplet diradical cation **45b**.[77]

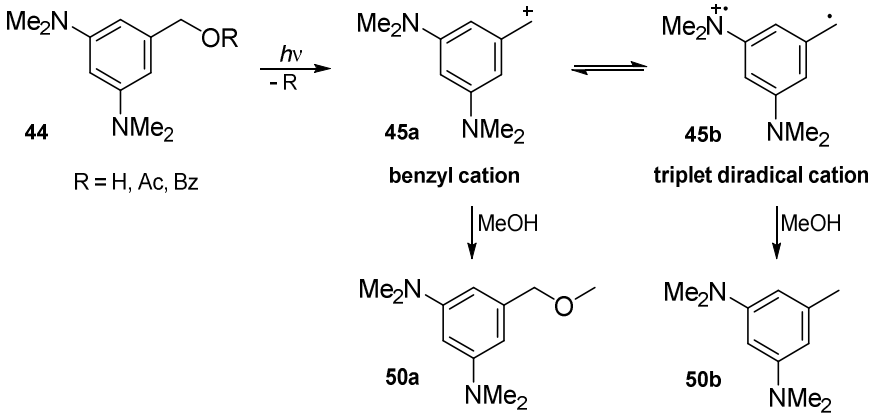

Figure 16: The singlet and triplet derived products from irradiation of the 3,5-di(dimethylamino) benzyl ethers.

Experimentally it was shown that irradiation of benzyl alcohol and its derivatives (**44**) produces the photosolvolysis product **50a** (major product) and the radical derived hydrogen

abstraction product **50b** (minor product). Due to lack of radical derived products from the leaving group and no dependence of the product ratio on the solvent, authors proposed that initial bond photolysis to be heterolytic.[73]

Later computations suggested also other compounds which might have ground state open shell singlet (or triplet) diradical cation configuration, for example 7-dimethylamino coumarin (coumarin photolabile protecting groups are described in the chapter 1.3.4). Speculatively it was suggested, that molecules with such a ground state carbocations potentially could be photocages and have a nearby conical intersection between the closed shell singlet and open shell singlet configurations.[78] A Coumarin diradical cation derived uncaging product was also confirmed experimentally by another group.[12]

Some examples for the applications of the 3,5-dimethoxybenzyl protecting group include the release of glycine (caged *via* amino group using a carbamate linker),[79,80] nitric oxide (from photocaged diazeniumdiolate)[81] and to unmask carboxylic acid in a polymer film.[82] The enhanced susceptibility of the *meta*-methoxybenzyl photocage to undergo bond cleavage homolytically has been used for photocrosslinking of DNA.[83] 3,5-Dimethoxybenzyl protecting group with a phenolic modification in the *ortho* position to the benzylic carbon was shown to release carbonyl compounds efficiently.[84] Introduction of two methyl groups at the benzylic position resulted in depleted photoactivity while two phenyl groups enhanced the photoactivity. Replacement of the two methoxy substituents with one dimethylamino bathochromically shifted the longest wavelength absorption band by approximately 30 nm without significantly influencing the uncaging quantum yield.[85] Later it was demonstrated by Wang *et al*. that the simple diethylamino benzyl photocage (**51**, Figure 17) can release not only carboxylic acids but also alcohols,[86] amines[87] and diols.[88]

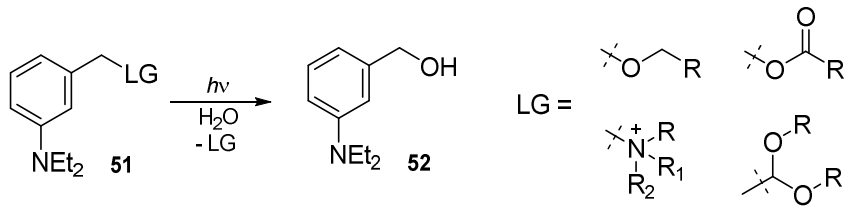

Figure 17: The release of alcohols, amines and diols.

The release of amines is accompanied also by products arising from radical reactions. Authors proposed that they result from single electron transfer between the released amine and the benzyl carbocation. The formation of radical derived products could be suppressed by changing the solvent.

Alcohols, amines and diols were released with large chemical yields. Irradiation was done with a medium pressure mercury lamp and Pyrex filter ($\lambda > 300$ nm). The quantum yields of release were good (alcohol 0.26, tertiary amine 0.18, diol 0.08). Thus, this structurally simple photolabile protecting group has a remarkable power to release even bad leaving groups. The main drawback is the need to use far UV light for photoactivation. The research about trityl and benzyl photocages done by Wang and coworkers has been summarized in detailed account.[89]

Photosolvolysis has been reported also from *ortho*-benzyl ethers.[74] However, the sterical hindrance between the electron donating group and the *ortho* substituent has a negative influence on absorption spectrum.[90] *Ortho* substituted compounds also are photoactive, because the electron density increase upon excitation of the donor substituted benzene is observed not only in the *meta* but also in the *ortho* positions (Figure 11-Figure 12).

In contrast to electron donating substituent promoted benzyl ether photosolvolysis reactions, electron withdrawing groups decrease electron density in these positions, yielding different reactivity.

Havinga *et al*. in 1956 reported light promoted phosphate ester hydrolysis (Figure 18). The *meta* isomer showed the highest reactivity.[91] This reactivity was later explained by Zimmerman to be a result of decreased electron density in the *meta* position relative to nitro group upon excitation (see also Figure 11 and discussion there).[92]

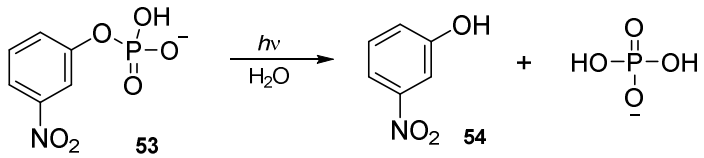

Figure 18: Light promoted hydrolysis of phosphate ester.

Benzene with electron donating or withdrawing groups are also reactive towards nucleophiles in their excited state. The reactions often happen at the positions, which have reduced electron density. These reactions are certainly of a theoretical interest, but lay outside of the scope of photolabile protecting groups. Thus, for more details, the reader is referred to literature.[93] There are not many examples of photolabile protecting groups, which would be based at the "negative" meta effect. Some are given in the following.

The nitro acetates **55-58** undergo photohydrolysis to give the corresponding phenols upon irradiation at 313 nm (Figure 19).

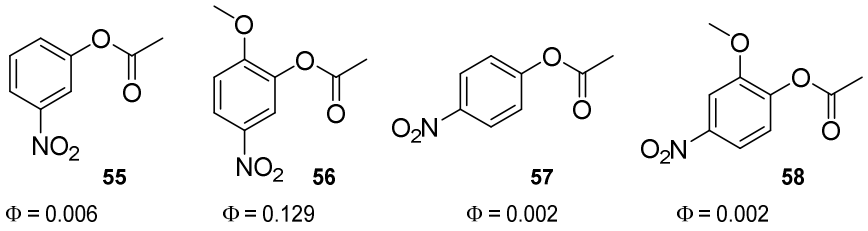

Figure 19: The quantum yields of nitro acetate photohydrolysis.

The uncaging quantum yield is higher if the nitro group is in the *meta* position relative to the acetate. The highest quantum yield is demonstrated by the compound **56** which contains a *para*-methoxy group. The quantum yield decreases in presence of a triplet quencher.[94]

The structurally similar nitro compound **59** also releases esters (**61**) upon irradiation and has redshifted absorption spectra, but the uncaging quantum yield is smaller (Figure 20). Interestingly, the quantum yield decreases if the irradiation is done with light of a longer wavelength.[95]

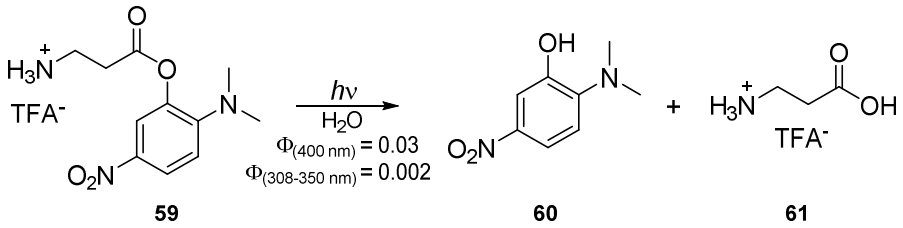

Figure 20: The release of β-alanine from nitrophenol ester.

Most likely the reason is the charge transfer character of the longest wavelength absorption band (from the amino group to the nitro group). As a result, the decrease of the electron density (which is a potential prerequisite for bond cleavage) at phenolic oxygen in this excited state might be not significant. A similar effects has been observed in *o*NP photocages.[96]

At the same time, the uncaging quantum yield of the compound **56** (Figure 19) was higher than its analogue without a methoxy group (**55**). Although the methoxy group is a weaker electron donor than the dimethyl amino, the charge transfer should be observed also in this case. Thus, it would be of high interest to understand the underlying mechanistic reasons for the observed reactivity of compounds **55**, **56** and **59**, especially in the light of the recently reported *two-photon only* effect from Heckel lab.[97]

Another example of the intriguing nitrophenyl chemistry is the photoinduced decarboxylation of the acetates **62.** The nitro group in all of the isomers is withdrawing the electron density from the benzylic carbon, thus depopulating its bonding orbital to the carboxylate which results in release of CO_2. However, the reaction does not happen *via* the same mechanistic

pathways for all regioisomers.[98] The *para* isomer decarboxylates from relaxed triplet state (in a 200 ps time scale), while the *ortho* isomer reacts exclusively from hot singlet state releasing CO_2 in less than 1 ps. The *meta* isomer reacts *via* both of these channels. Since the electron density change at the benzylic carbon on the potential energy surface from which decarboxylation happens is more pronounced for the *meta* and *ortho* isomers, one can speculate that the ultrafast release arises from meta(-ortho) effect. However, when the *meta* isomer undergoes ISC, as further decarboxylation happens in the same manner and speed as for the *para* isomer.

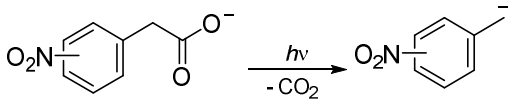

-NO_2	Φ
para	0.6
meta	0.6
ortho	0.1

Figure 21: Decarboxylation of nitrophenyl acetates.

The decarboxylation quantum yield for the *ortho* isomer is low due to the competing hydrogen transfer reaction from benzylic carbon which is well known in the *o*NB photocages.

Meta substituted benzyl phenyl sulfide **64** undergoes homolytic bond cleavage to give radical derived products such as **65** (where R = –CH_2-PhX) and diphenyldisulfide **66** (Figure 22). It was observed that quantum yield is higher if the aromatic ring contains an electron withdrawing substituent, such as NO_2 or CN, possibly due to their radical stabilizing abilities.[71]

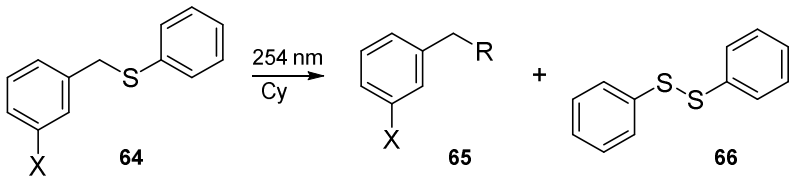

X	Φ
-OCH_3	0.020
-CH_3	0.047
-CF_3	0.053
-NO_2	0.071
-CN	0.39

Figure 22: Photoreaction of benzyl phenyl sulfide.

The photocages described in this chapter are interesting from the theoretical point of view, due to their simple structure and efficient photoreactions. Furthermore, even small changes in the substituent pattern can greatly influence the mechanism of the uncaging reactions. Despite the first theoretical study of substituted benzyl alcohol photoreactions being published more than five decades ago, many theoretical aspects of the photoreaction mechanism of these compounds are not yet clear, especially for the compounds containing electron withdrawing groups. For the compounds bearing electron donating substituents, there is a lack of studies regarding shifting of the absorption maximum to longer wavelengths while preserving the good reactivity. To that end, the next chapter will be focused on the coumarin photocage and the design principles to redshift its

absorption maximum. Since the frontier molecular orbitals of the coumarin photocage are isolobal with the photocage which are based on meta effect (e.g. DEAMb), the origins of photoactivity are the same. Thus, the design principles which are successful to redshift the absorption spectra for coumarin, could be used also for DEAMb derived photocages.

1.3.4. The coumarin photocage

The photoactivity of 4-substituted coumarin derivatives was first demonstrated by Givens and Matuszewski, by irradiation of coumarin phosphate ester by 360 nm light in presence of nucleophiles (Figure 23A).[99] In the years following their report, countless new studies have emerged, which have been reviewed neatly.[54,100]

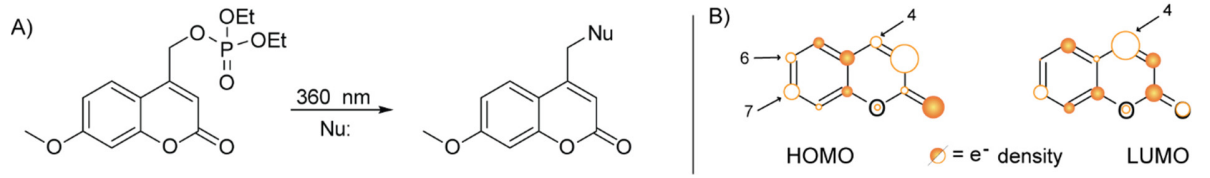

Figure 23: *A* – The cleavage of coumarin phosphate ester in presence of nucleophiles after irradiation with 360 nm light. *B* – electron density distribution of the coumarin in HOMO and LUMO state as predicted by program HuLiS.[66]

The photoactivity of the position 4 in the coumarin molecule can be rationalized by means of the molecular orbital theory. As calculated using software HuLiS,[66,101] in the ground state (HOMO) the electron density in the position 4 is small, while in the excited state (LUMO) the electron density in this position is much larger (Figure 23B). The size of the circles in the figure are proportional to atomic orbital contributions, however should be viewed only qualitatively. For quantitative characterization the reader is referred to literature.[102,103] This increased electron density in the excited state can lead to a bond cleavage between benzylic carbon and a leaving group, if those are attached to position 4 of the coumarin, similarly as described for photolabile protecting groups, based on Zimmerman's meta effect (Chapter 1.3.3).

Before the use of coumarin derivatives as photocages, they were widely exploited as laser dyes. Thereby, the influence of various aromatic ring substituents on the spectral properties was well understood.

For unsubstituted coumarin the S_0-S_1 transition (λ_{max} = 313 nm) is of $\pi \rightarrow \pi^*$ type,[102,104] however some literature sources suggest it to be of $n \rightarrow \pi^*$ type.[105,106] The molar absorption coefficient of this band is ca. 5000 (M^{-1} cm^{-1}),[105] what would suggest $\pi \rightarrow \pi^*$ type transition, since $n \rightarrow \pi^*$ are symmetry forbidden and typically have lower molar absorption coefficients.

Most likely, misinterpretation in some literature sources is a result of the closely located energies of the two states.[102,107]

The S_0-S_1 absorbance band is long axis polarized (Figure 24A, the dashed arrow),[104] thereby introducing further substituents in positions 3, 6 and 7 has the highest influence on the absorbance spectra.[108] However, electron donating substituents (*e.g.* amino group) will have a different effect on the absorbance spectra depending whether it's in the position 6 or 7.[106] When the amino substituent is located at position 6, the transition energy is lower than that for the 7-substituted analogue.

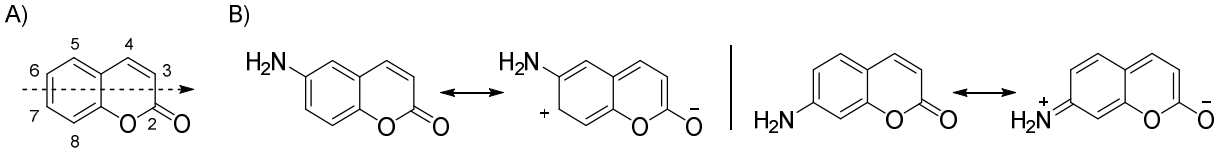

Figure 24: *A* – The atom numbering and the long axis (dashed line) of the coumarin molecule. *B* – The resonance structures of coumarin bearing amino substituent in the position 6 and 7.

This can be rationalized by comparing the electron densities of those positions in HOMO and LUMO state (Figure 23B). In the HOMO state both the positions 6 and 7 have some electron density, thereby attaching an electron donating group will have a destabilizing effect. Meanwhile in the LUMO state there is a very small electron density in position 6, while it is significant in position 7. Thereby, an electron donating substituent in position 7 would equally destabilize HOMO and LUMO state, while in position 6 it would have such an effect only in HOMO, resulting in a smaller energy gap between both states. But the 7 substituted isomer has much larger oscillator strength of the S_0-S_1 transition due to efficient delocalization (Figure 24B) over the entire coumarin π-system, what is not possible for the isomer with the amino substituent in position 6.[103]

Further bathochromic shift of the absorbance spectra is achieved if an electron acceptor group is installed in position 3 or 4 of the coumarin molecule.[106] The effect is more prominent (lower excitation energy, higher molar absorption coefficients) if the substituent is installed in position 3. That can be explained by the closer alignment of the substituents in this position with the coumarin long axis absorbance band (Figure 24A). Substituents in this position also have smaller sterical hindrance when compared to position 4, allowing them to adopt a more planar configuration. This results in a better π-orbital conjugation both in HOMO and LUMO state, yielding higher transition oscillator strengths.[109] For example, substitution of the julolidine-derived coumarin dye **67** with an electron donating phenyl group (**68**) shifts the absorbance to

longer wavelengths by 22 nm, while the electron withdrawing benzothiazol substituent (**69**) redshifts the absorbance by 87 nm (Figure 25).[110]

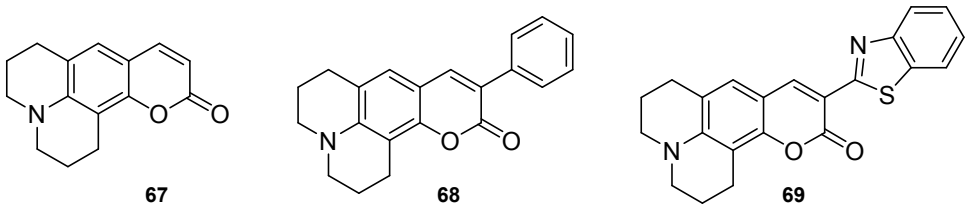

Figure 25: Structure formulas and absorbance maximum (in EtOH) of selected coumarin dyes.

Comprehensive understanding of the structure-properties relationships in the coumarin dyes allowed rather rapid development of coumarin derived photocages. Bendig *et al.*[107] showed the release of adenosine 3′,5′-cyclic monophosphate from coumarin and its derivatives with electron donating substituents in position 6 and/or 7 (Figure 26).

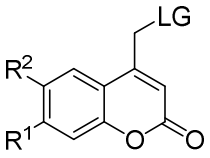

Nr.	R^1	R^2	λ_{max} (nm)	ε (M^{-1} cm^{-1})	Φ (nm)
70	H	H	314	5900	0.085 (313)
71	H	OCH_3	346	4500	0.03 (333)
72	OCH_3	H	328	13200	0.13 (333)
73	OCH_3	OCH_3	349	11000	0.04 (333)
74	NMe_2	H	397	17200	0.28 (365)
75	NEt_2	H	402	18600	0.21 (365)

LG =

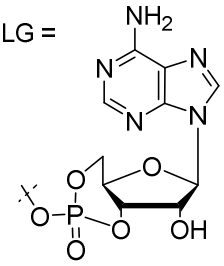

Figure 26: Photochemical properties of coumarin derived photocage with substituents in position 6 and 7. The measurements are done in MeOH:HEPES (1:4), the leaving group (LG) was adenosine 3′,5′-cyclic monophosphate.[107]

A trend connecting the wavelength of the absorbance maximum and its molar absorption coefficient can be recognized as described for coumarin dyes. Coumarin with an electron donating methoxy group in position 6 (**71**) has a lower molar absorption coefficient then position 7 substituted analogue (**72**), but the absorbance maximum is shifted to longer wavelengths. Introducing the methoxy substituent in both positions (6 and 7) has an additive effect (redshifted absorbance spectra and higher molar absorption coefficient). The best results by the means of absorbance band maximum and its intensity are shown by the 7-amino substituted compounds (**74-75**).

The uncaging mechanism of coumarin has been studied extensively.[107,111,112] An excited singlet state of the compound **76** (Figure 27) is generated upon irradiation. A homolytic bond cleavage to give a radical pair **76a** is possible, however, the absence of radical-derived

photoproducts (such as 4-methyl-7-metoxy-coumarin), suggests direct heterolytic bond cleavage to give ion pair **76b**. A tight ion pair, which then escapes solvent cage (**76c**) has been proposed, however, no direct experimental evidence has been obtained. In diluted water containing solvents the major coumarin-derived photoproduct is the alcohol **76-OH**. The oxygen atom (Figure 27, red) in the alcohol **76-OH** rises from solvent (as shown by isotopic labeling experiment). Absence of phosphorescence (in EtOH at 77 K) also excludes significant intersystem crossing to triplet state of the excited compound **76** (ISC quantum yield was estimated to be below 0.05).

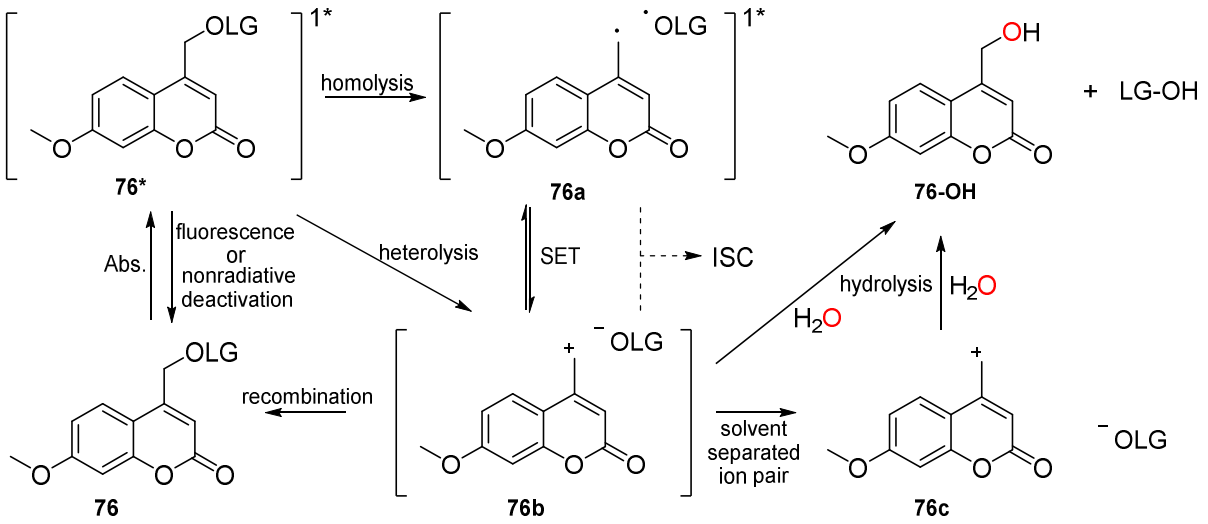

Figure 27: Uncaging mechanism of the 7-metoxy coumarin derivatives.[111]

Although the described mechanism holds true for the studied coumarin derivatives (plus the leaving groups and the solvent used), for other, although very similar systems, some minor changes are possible. For example, the rate of the leaving group release has been determined to be in a nanosecond[113] or in a picosecond time scale.[114] Direct generation of a solvent separated ion pair without the intermediate tight-ion pair,[114] or release of Br and SPh radicals from excited singlet state *via* homolytical bond cleavage has been shown.[115] Thus, the mechanism shown in Figure 27 is a good approximation, but should not be viewed as a universal truth. When two coumarin derivatives with different leaving groups are compared, the reported quantum yields should be viewed more qualitatively than quantitatively (this applies to photocages in general). Thereby, in the following review of the coumarin photocages the reader should try to recognize only the general trends connecting the uncaging quantum yields with the substitution pattern of the various coumarin derivatives. Generally, the uncaging quantum yield is higher if the coumarin molecule contains electron donating groups (which stabilize the coumarin cation). A higher uncaging quantum yield has leaving groups which form resonance-stabilized anions (such as

mesylate, phosphate, and benzoic acid derivatives with electron accepting substituents in the aromatic ring). Thereby, also pH can have an influence on the quantum yield for the release of multiprotolytic anions.[116]

Fusing another aromatic ring on the coumarin scaffold has a small positive impact on the absorption properties as shown by Costa, Gonçalves *et al*.[117] For example, the absorbance spectra of compounds **77** and **78** have a very similar maximum to that of the compound **71** but the molar absorption coefficients are two times higher (Figure 28). However, release of simple amino acids happens with a one order of magnitude smaller quantum yield (at 254 nm). Replacing the oxygen atom in the pyrone side of the coumarin molecule by nitrogen (**79**) only slightly redshifts the absorbance maximum when compared to the oxygen containing analogue (**71**) without improving the molar absorption coefficient.[118] Expanding the aromatic ring by an oxazole derivative (**80**) is not improving absorption properties when compared to 7-metoxy substituted analogue (**72**).[119] No photoreaction quantum yields for compounds **79** and **80** were reported.

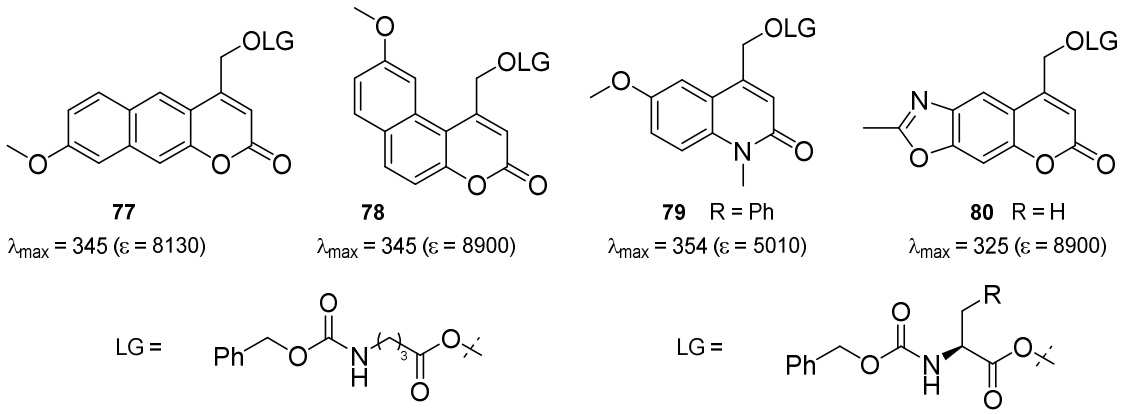

Figure 28: Photochemical properties of coumarin derived photocage with extended aromatic ring. The measurements were done in EtOH, λ_{max} is given in nm, ε is given in M^{-1} cm^{-1}.

Furuta *et al.* in 1999 already reported the brominated 7-hydroxy coumarin (**81**, Bhc), which has been one of the most often used coumarin PPGs since then (Figure 29).[120] The bromine atom in position 6 lowers the *p*Ka of hydroxy group in position 7, thereby in physiological pH the phenol is in its anionic form, exhibiting a higher molar absorption coefficient and redshifted absorption spectra. Additionally, the presence of a heavy atom would promote ISC to triplet state thus elongating the lifetime of the excited state.

In a later study the effect of substitution of a carbon with a nitrogen atom in the aromatic ring was tested (**82**). This resulted in a decreased *p*Ka value of the hydroxy group along with a higher molar absorption coefficient at 365 nm.

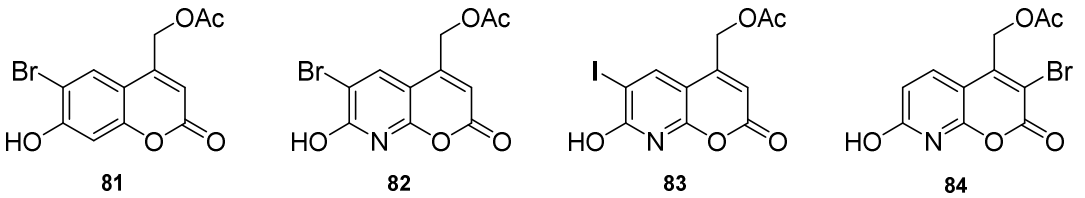

Figure 29: Photochemical properties of coumarin halogen derivatives. The measurements were done in KMOPS buffer which contains 10 mM 4-morpholinepropane-1-sulfonic acid (MOPS), and 100 mM KCl, with 0.1% DMSO (pH 7.14). λ_{max} is given in nm, ε is given in M^{-1} cm^{-1}.

Further replacement of the bromine with iodine is increasing the uncaging quantum yield (**83**). Placing of the bromine atom in position 3 of the coumarin aromatic ring (**84**) redshifts the absorbance spectrum maximum to 378 nm as a result of the push-pull character.[121]

Expanding the π-conjugation in position 7 by installing a second aromatic ring (Figure 30, **85**) only slightly shifts the absorbance maximum in comparison to a simple methoxy substitution (**72**).[122] The similar *p*-EtO-aryl substituent, connected to coumarin rings position 7 *via* an ethylene linker (**86**), has an absorbance maximum redshifted by 30 nm and a higher molar absorption coefficient.[123]

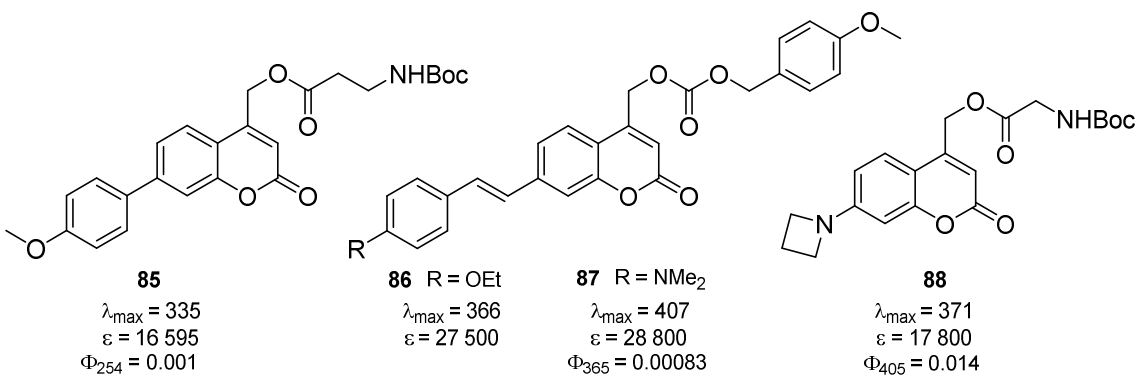

Figure 30: Photochemical properties of 7-substituted coumarin derivatives. The measurements were done in MeCN (compound **85**), in MeCN : H_2O (9:1)(compound **86-87**), in PBS (pH = 7.4) buffer with MeCN (3:7) (compound **88**). λ_{max} is given in nm, ε is given in M^{-1} cm^{-1}.

In biphenyls the two aromatic rings have an approximately 20° dihedral angle[124] while *ortho*-unsubstituted stilbenes are planar,[125] which is likely the reason why compound **86** has a more redshifted absorbance maximum and a higher molar absorption coefficient than the structurally similar compound **85**. Just as in the case of methoxy and dimethylamino substituted compounds (**72** and **74**), also the stilbene derivative **87** has more redshifted absorbance spectrum

than compound **86** due to stronger electron donating properties of the amino group. However, the uncaging quantum yield for the compound **87** is 2-3 orders of magnitude smaller when compared to other coumarin derivatives with similar leaving groups (**81-84**, **88**).[123] This is probably due to an additional nonradiative relaxation pathway available due to the double bond.

Introduction of an azetidinyl substituent (**88**) significantly blueshifts (aprox. 30 nm) the absorbance maximum if compared to the NEt_2 substituted analogue (**75**) due to reduced electron donating strength of the azetidinyl substituent. But the uncaging quantum yield of the same leaving group in the same conditions is slightly higher than for the NEt_2 substituted analogue.[126] The lability of the azetidinyl ring to even mild nucleophiles (chloride) makes the use of this coumarin derivative impractical.[127]

Of the so far described coumarin derivatives, the 7-diethylamino coumarin (**75**, DEACM) has the best photochemical properties. Consequently it has been extensively used as a basis for further optimization of the pyrone part of the molecule. A significant absorption redshift to the visible spectral range can be achieved by replacing the oxygen atom by sulfur (Figure 31, **89**) or by malononitrile (**90**).[11]

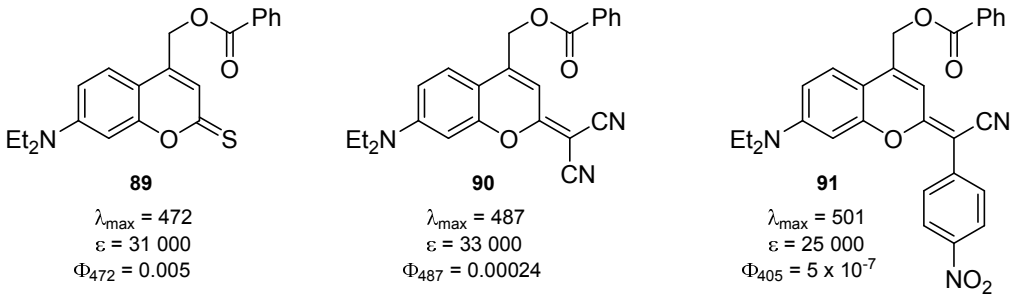

Figure 31: Photochemical properties of coumarin derivatives with modified carbonyl group. The measurements were done in TRIS (pH = 7.5) buffer with MeCN (1:1) (compound **89-90**); in CH_2Cl_2 (compound **91**). λ_{max} is given in nm, ε is given in M^{-1} cm^{-1}.

The latter has a bad uncaging quantum yield (the parent DEACM releases benzoic acid with a nearly 10 times better quantum yield), while the thiocoumarin **89** has two times better uncaging quantum yield than parent DEACM. Interestingly, the uncaging quantum yield of the compound **89** significantly increases if the solution concentration is increased (this effect was not observed for parent DEACM or derivative **90**). The thiocoumarin **89** is prone to a side reaction (hydrolysis of the C=S bond to give C=O) but this reaction has more than 10 times smaller quantum yield than the uncaging reaction, thereby does not disturb the application of thiocoumarin caged biologically active molecules in living Zebrafish embryos.[128] The coumarin-malononitrile derivative **91** has an

even more redshifted absorbance spectrum maximum, but due to the strong electron accepting nature of this substituent the uncaging quantum yield is very low.[129]

As described for coumarin based laser dyes, the absorbance maximum of DEACM photocages has been bathochromically shifted by installing substituents in position 3. The electron donating *p*-NMe_2-phenyl substituent (Figure 32, **92**) changes the absorbance maximum of the parent DEACM only slightly (less than 10 nm).[130] Electron withdrawing substituents has larger impact, for example, propargylic derivative **93** has its absorption maximum at 430 nm.[131] A similar molecule with a cyano substituent in this position has λ_{max} at 443 nm (ε = 26 000 M^{-1} cm^{-1}) but it releases benzoic acid with a small quantum yield (0.0005).[11] Coumarin derivative with a *p*-CN-phenyl substituent in position 3 has a similar absorbance maximum and releases glutamic acid with a better quantum yield (0.05, exact data about absorbance maximum and molar absorption coefficient was not given).[132] The compound **94**, whose absorbance maximum is located at 450 nm, demonstrates superior photochemical properties and has a high molar absorption coefficient and good quantum yield of glutamic acid release.[133]

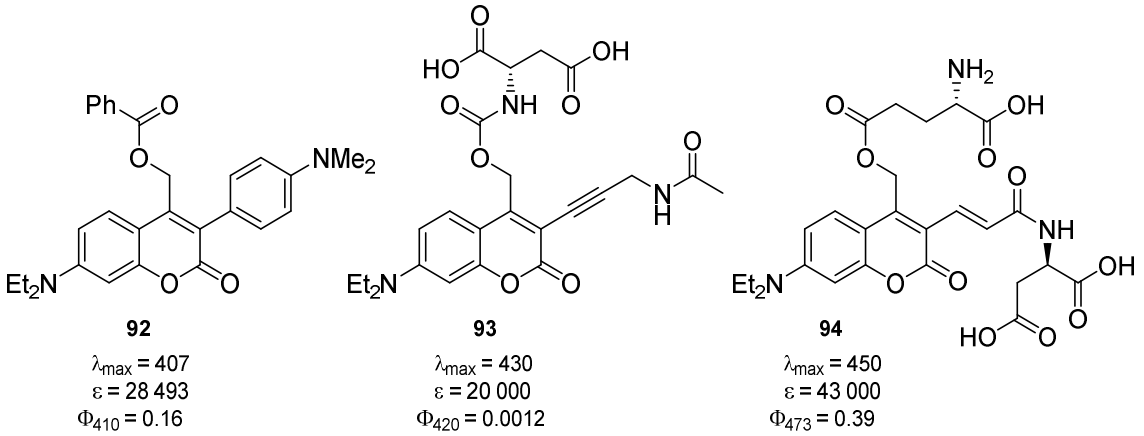

Figure 32: Photochemical properties of 3-substituted coumarin derivatives. The measurements were done in DMSO (compound **92-93**); in phosphate buffer (pH = 7.4)(compound **94**). λ_{max} is given in nm, ε is given in M^{-1} cm^{-1}.

The aspartic acid (attached *via* an amide bond to the acryl substituent in the position 3 of the coumarin molecule) has been introduced to increase the aqueous solubility of the compound for use in biological applications. Other methods for the increasing of the aqueous solubility of coumarin photocages are known, for example, introduction of substituents with a polar side chain,[134] replacing the diethyl substituents in DEACM with a carboxymethyl[135] or by attaching 2,2-bis(methylol)propionic acid dendrimer which at the same time acts to sterically hinder the binding of caged gamma-aminobutyric acid (GABA) to its receptors in neurons.[136] The molecules,

to which the photocage is attached, often are also highly soluble in aqueous media (for example, DNA[137] or RNA[138]). Thereby, if the photolabile protecting group has favorable photochemical properties for a biological application, but on its own it is not water soluble, a way to prepare a more soluble analogue can be found.

The stilbene coumarin derivatives **95a-d** (Figure 33) demonstrates interesting properties. Depending on the substituent pattern its absorbance spectrum maximum can be shifted even to 515 nm (**95d**) without losing good uncaging quantum yields. Upon irradiation a cyclic photoproduct **97a-d** is formed as a result of intramolecular cyclization of the carbocation **96a-d**. The cyclic photoproduct does not have the π-conjugation with the substituent in position 3, thereby its absorbance maximum is shifted to blue and does not compete with **95a-d** for the irradiation light.

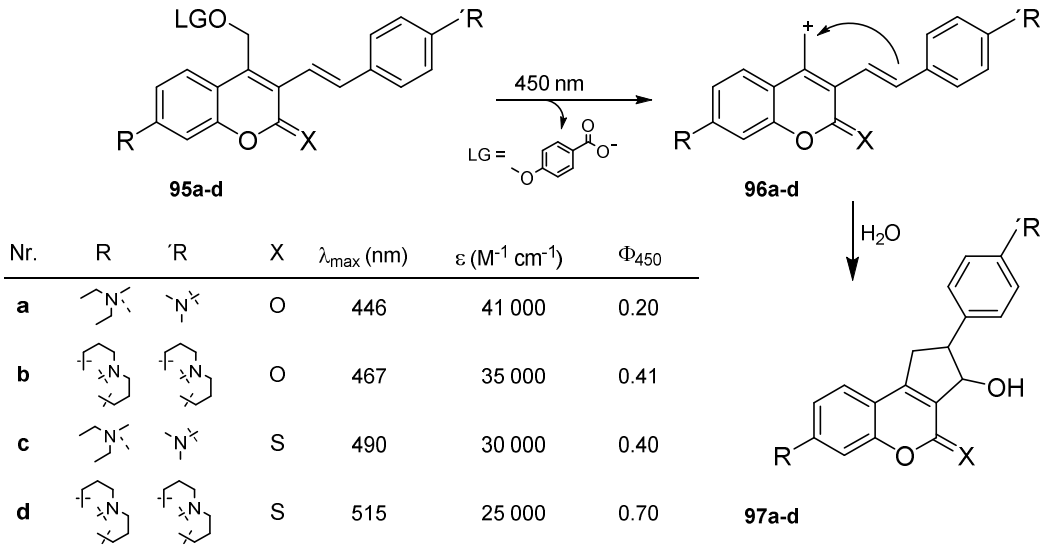

Nr.	R	´R	X	λ_{max} (nm)	ε (M^{-1} cm^{-1})	Φ_{450}
a			O	446	41 000	0.20
b			O	467	35 000	0.41
c			S	490	30 000	0.40
d			S	515	25 000	0.70

Figure 33: Photochemical properties of 3-styril substituted coumarin derivatives. The measurements were done in MeOH : H_2O (1:9).

Various coumarin derivatives, reported during more than three decades following the first report about the use of coumarin as a photocage, now cover a broad spectral range from far UV to green light. A graphical summary of the previously reviewed molecules is given in Figure 34. Some general trends can be recognized. For example, the size of a substituent's π-electron system is not the major factor which influences the molar absorption coefficient. More important is the substituent's position and how efficient the π-orbital overlap is. Charge transfer systems (and in general, more polarized systems) have the highest molar absorption coefficients

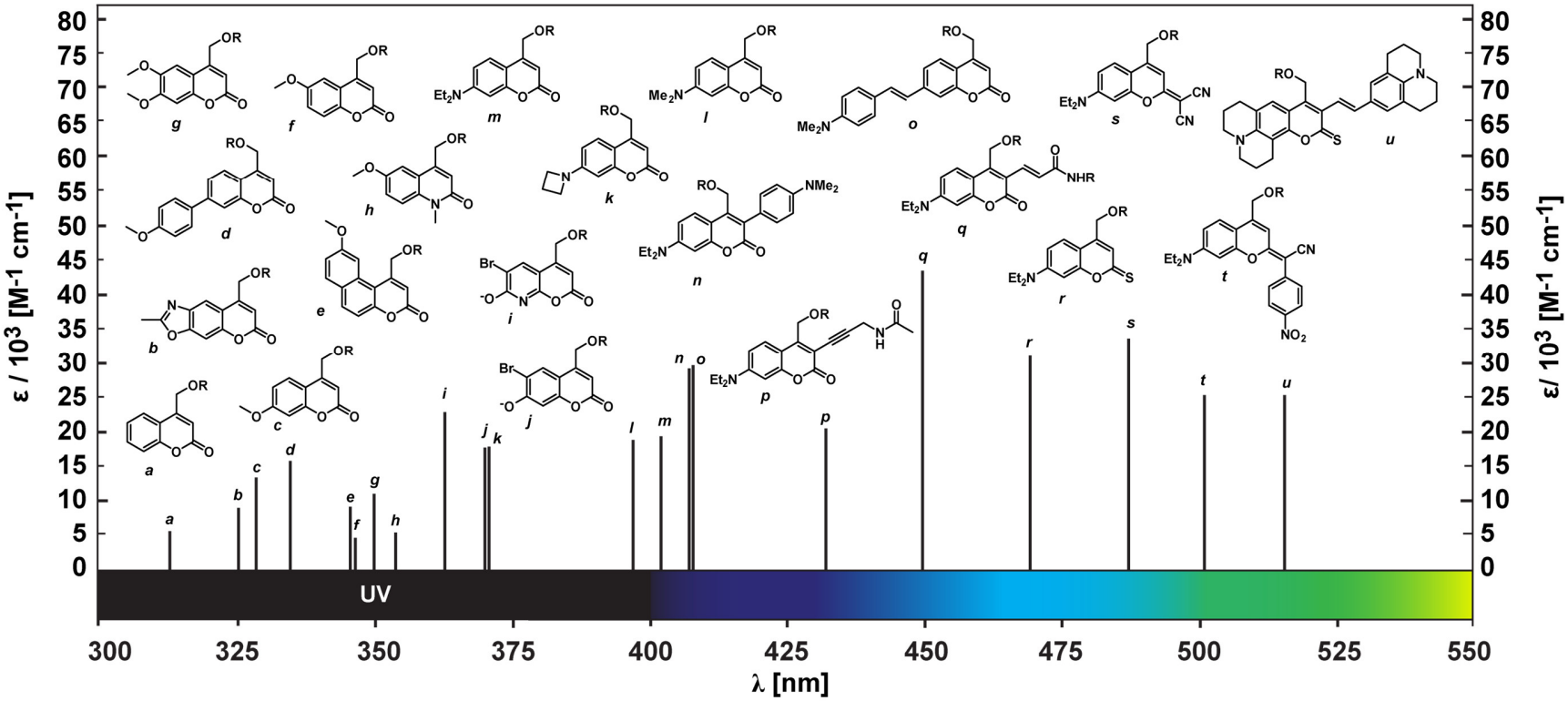

Figure 34: The absorption maximum of various coumarin derivatives used as photocages. For more details and literature sources please see text and figures of the Chapter 1.3.4.

1.3.5. Miscellaneous visible light absorbing, recently reported photocages

The toolbox of visible light absorbing photocages has been expanded over the last years, starting from a milestone publication by Šebej *et al*. who reported a photocage based on visible light absorbing dye fluorescein (**98**, Figure 35).

The compound **98** (X = *O*,*O*-diethyl phosphate, Br, OAc) could be synthesized only as an equimolar complex with oxidizing reagent DDQ (2,3-Dichloro-5,6-dicyano-1,4-benzoquinone), however, it is expected that in water it decomposes rapidly, thus the complex is dissolved. The molar absorption coefficient of these xanthene based molecules is around $4 \cdot 10^4$ (M^{-1} cm^{-1}) in the absorption maximum (520 nm) and the uncaging quantum yields reach up to 2.4%.[139]

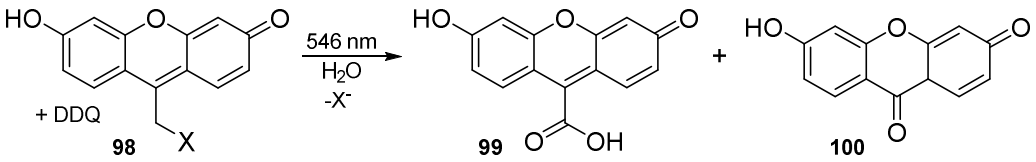

Figure 35: The photoreaction of fluorescein based photocage.

Two photoproducts were isolated, the acid **99** and the keton **100**. It was suggested, that DDQ hydrolysis products serve as oxidants to produce the keton **100**. However, later it was revealed that the acid **99** releases CO upon irradiation.[140]

The photoactivity of the compound **98** was predicted by simple Hückel MO computation. As already described (vide supra, Zimmerman's meta effect and coumarin photocages), increased electron density in the position, to which benzylic carbon is attached can trigger the uncaging reaction. Figure 36 shows the frontier molecular orbitals of coumarin along with xanthene, BODIPY (boron-dipyrromethene) and trimethine cyanine. For already described molecular fragments (coumarin and xanthene) a trend connecting the excited state (LUMO) electron density at the meso position and an uncaging of compounds bearing a benzylic carbon with a leaving group at this position can be recognized. Thus, also from BODIPY (Figure 36, panel c) and cyanine dyes (panel d) photoactivity could be expected. And indeed, the photooxidation of the cyanine dyes was described in Chapter 1.2.3. Also BODIPY derivatives has been shown to be photoactive.

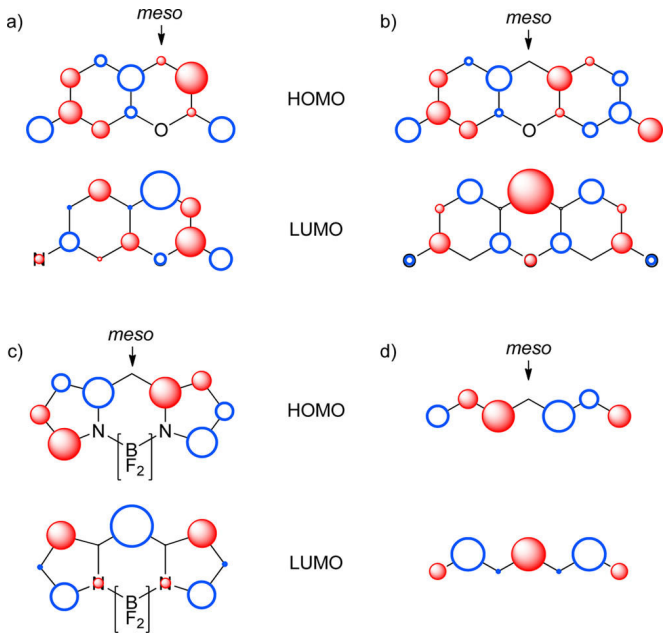

Figure 36: Frontier molecular orbitals of: *a)* coumarin *b)* xanthene *c)* BODIPY *d)* trimethine cyanine. Reprinted with permission from L. A. P. Antony, T. Slanina, P. Šebej, T. Šolomek, P. Klán, *Org. Lett.* **2013**, 15, 4552–4555. Copyright 2013 American Chemical Society.

Winter *et al.*[141] and Weinstain *et al.*[142] published structurally very similar BODIPY photocages with a leaving group attached to the *ipso* position (

Figure **37**). BODIPY photocages reported by Winter and coworkers use acetate as a leaving group. The most redshifted absorption maximum (553 nm, $\varepsilon = 4.9 \cdot 10^4$ M^{-1} cm^{-1}) and highest quantum yield is demonstrated by a compound substituted with two iodine atoms (**101**). The BODIPY derived photoproduct is its methyl ether **103**, thus suggesting formation of a carbocation which is then trapped by the solvent - methanol.

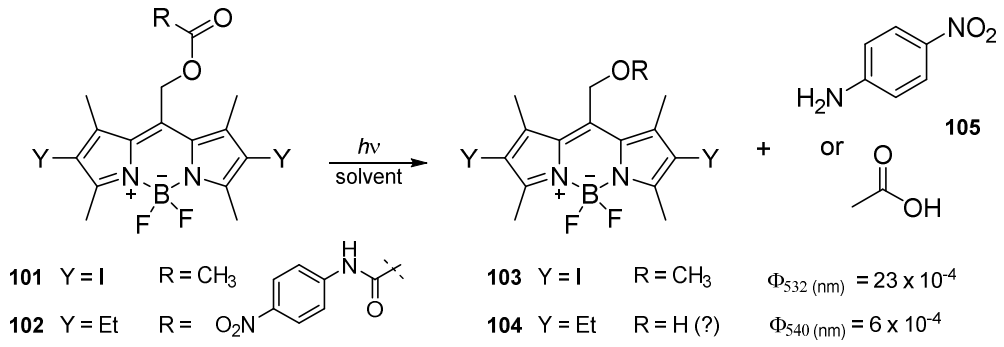

Figure 37: First generation of BODIPY derived photolabile protecting groups.

The quantum yields reported by Weinstain and coworkers are similar. For example, the ethyl substituted BODIPY (**102**) releases the *para*-nitro aniline (**105**) leaving group (caged *via*

carbamate linker) in PBS buffer (and 5% MeCN) with $6 \cdot 10^{-4}$ quantum yield. It was not specified what BODIPY derived photoproduct are produced, but in the aqueous solution it probably was alcohol **6**. The spectral properties of BODIPY derivatives reported in the two articles also are similar. Both groups demonstrated application in vivo.

A year earlier Urano with coworkers also published a BODIPY based uncaging strategy. It is based on photoinduced electron transfer from BODIPY core to a self immolative linker from which the leaving group is then released.[143] Due to a different other uncaging mechanism, it will not be discussed here further. Instead, the reader is referred to literature.[144,145]

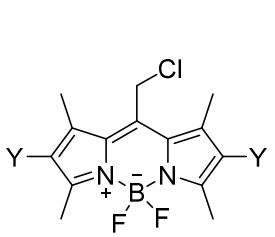

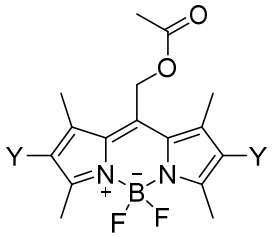

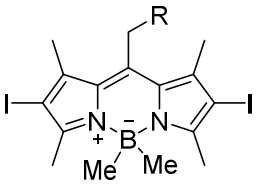

Nr.	Y	λ_{max}	$\varepsilon_{(\lambda max)}$	Φ(%)
106	H	523	44 400	2
107	Cl	549	34 600	20
108	Br	549	55 700	50
109	I	556	59 300	80

Nr.	Y	λ_{max}	$\varepsilon_{(\lambda max)}$	Φ(%)
110	H	517	71 000	0.34
111	Cl	544	48 000	0.74
112	Br	545	56 300	1.47
113	I	553	49 000	2.35

Nr.	R	λ_{max}	$\varepsilon_{(\lambda max)}$	Φ(%)
114	Cl	542	62 400	95
115	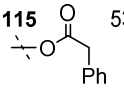	538	60 700	28

Figure 38: The photochemical properties of selected BODIPY derivatives.

A detailed investigation of the photochemical properties of the BODIPY photocage was published later by the group of Winter and Weinstain together with the group of Klán.[146] Systematic screening of the substituent effects reveals that the uncaging quantum yield increases if the chromophore contains a halogen atom, and the higher the period number of the halogen substituent is, the higher the quantum yield is (Figure 38, **106-109**). The quantum yield of ISC (compounds **110-113**) increases in the same order: H < Cl < Br < I (0.05; 22; 54; 84%). If the sample is not degassed, the uncaging quantum yield is usually decreased by half. However, the decomposition of the chromophore is not accelerated, thus sensitization of oxygen seems to be just an additional pathway for relaxation. Photobleaching of the BODIPY chromophore has been also observed, but the quantum yield is small (0.04%). The quantum yields are higher for the leaving groups which have lower pK_a values (compare **106-109** with **110-113** and **114** with **115**). Increasing the electron density of the BODIPY core increases the quantum yield. This effect can be seen by replacing the fluorine atoms with methyl groups (**114-115**), which results in a higher quantum yield of uncaging (compare the compounds **109** and **114**). The reported molecules have

outstanding uncaging cross sections for a visible light absorbing photocage, reaching even 40 000 (M^{-1} cm^{-1}).

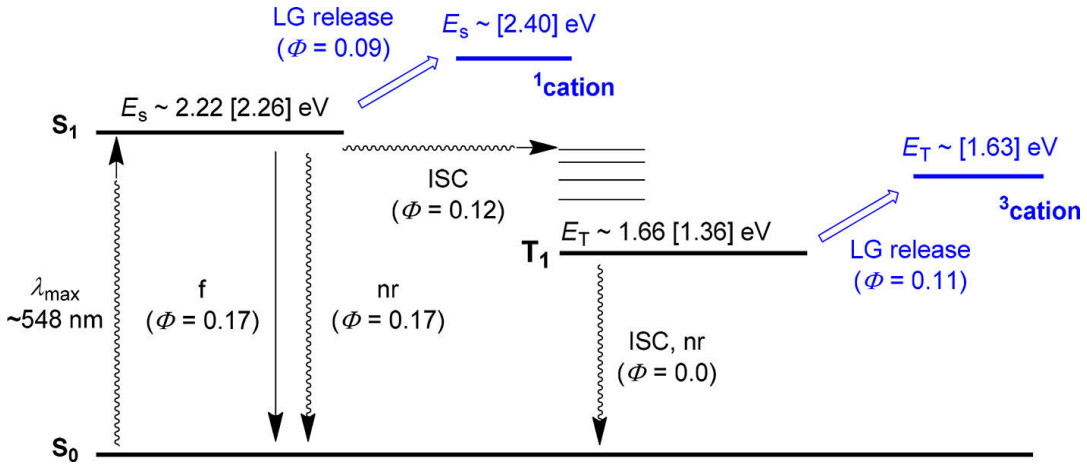

Figure 39: Jablonski diagram for the uncaging of BODIPY chloride **107**. The values in square brackets were determined by computations. Reprinted with permission from T. Slanina, P. Shrestha, E. Palao, D. Kand, J. A. Peterson, A. S. Dutton, N. Rubinstein, R. Weinstain, A. H. Winter, P. Klán, *J. Am. Chem. Soc.* **2017**, 139, 15168–15175. Copyright 2017 American Chemical Society.

Figure 39 shows the Jablonski diagram of the photochemistry from compound **107**. This molecule in its first excited state can undergo uncaging (LG release). The generated ion pair can still recombine (which might be a major nonradiative deactivation process). Nonradiative deactivation and fluorescence have the same quantum yields (17%). The ISC happens with a 12% quantum yield, generating a triplet state which is approximately 0.5-0.9 eV lower in energy than the excited singlet. Practically all molecules from triplet state undergo an uncaging reaction. However, it was proposed that in case of mediocre leaving groups (as acetate), also the triplet state can be depopulated by nonradiative decay.

In summary, this publication can be considered as an excellent example for a state of the art report on the rational design of a photolabile protecting group. It can be expected that in the years to come, BODIPY will establish its place among photocages as coumarin and *o*NB. For example, release of CO,[147] uncaging of amines (photocaged *via* carbamate linker),[148] alkynoic acids[149] and near-IR absorbing BODIPY photocages have recently already been reported.[150]

1.4. The VIPER pulse sequence

The VIPER (VIbrationally Promoted Electronic Resonance) pulse sequence has been developed in the lab of Jens Bredenbeck as an analytical tool in 2D IR spectroscopy.[151] It is a mixed pulse sequence (Figure 40), where a molecule is vibrationally excited by a narrow band IR-pump pulse (Figure 40A, bold arrow). The following Vis-pump pulse will promote the vibrationally pre-excited molecules to an electronically excited state. This Vis-pump pulse is off-resonant for the not vibrationally pre-selected species and only resonant with the molecules, which are already pre-excited by the IR-pump pulse. Thus, selective excitation is possible (Figure 40A, dashed arrows).

In contrast to UV-Vis absorption, the IR absorption bands usually are well separated from each other, thereby with a narrow band IR-pump selective pre-excitation of one molecule in an ensemble of similar molecules should be possible. The pump-induced spectral changes of the electronically excited molecules are then monitored by a broadband IR-probe pulse.

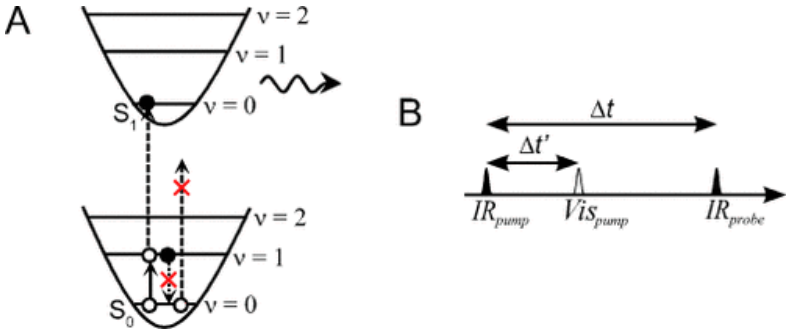

Figure 40: Principle of VIPER 2D IR. *A* – Schematic Jablonski diagram of the VIPER process; *B* – The pulse sequence used in VIPER. Figure reproduced from reference [151] with a permission; Copyright 2014 Wiley-VCH Verlag GmbH & Co. KGaA, Weinheim.

Van Wilderen *et al*. proposed that this method could be used more than just for analytical purposes if the electronically excited molecules would undergo photochemical transfiguration, naming, uncaging. To test this hypothesis and demonstrate the high potential of this method, the proof of principle study should show selective excitation of a single molecule in presence of near-identical ones.

A potential test system would be two isotopologues or isotopomers of the same photocage. These two species have the same UV-Vis absorption spectra, rendering it impossible to select only one of them for uncaging by direct UV-Vis irradiation. Incorporation of the isotopic label does not change the UV-Vis absorbance spectrum of a molecule, but does change its IR spectrum, thereby

allowing selective pre-excitation of only one of the isomers by a narrow band IR pulse. In order to enable a sufficient shift of the UV-Vis absorption spectrum, the IR pulse has to be centered on a vibrational mode which is coupled to an electronic transition. Computational predictions can and shall be used to guide the synthetic incorporation of an isotopic label in a position which would have the largest effect of an vibrational pre-excitation and thereby yield the largest VIPER signals, while other factors influencing the VIPER efficiency, such as the delay between the IR-pump and the Vis-pump pulse (the visible pulse must arrive within the lifetime of vibrationally excited state), should be determined experimentally. Thereby a collaborative effort of theoretical predictions with organic synthesis and spectroscopy is necessary to test the VIPER pulse sequence for applications in photo release.

2. Objective

The objective of this work is the design and synthesis of new photolabile protecting groups. This will be done following the rational design principles from most recent literature as described in the introduction. The results should yield not only a new photocage, but also a further understanding of their rational design principles to give the opportunity to design *de novo* photocages.

The 3-diethylaminobenzyl (DEAMb, see Chapter 1.3.3) photocage was selected as the structural base of this work. Wang *et al*. have demonstrated the remarkable power of its simple chromophore to release even bad leaving groups with good quantum yields. The main drawback of this photocage is the need to use a far UV light to trigger the photoreaction.

In order to improve its spectral properties, the π-system of the DEAMb photocage will be expanded by installing further aromatic substituents, for example, a second aromatic ring. Glutamic acid will be used as a leaving group. It is often used for photocage development due to its biological relevance. Furthermore, its polar nature increases the loaded photocage's water solubility, thus a predominantly aqueous solvent system for characterization can be used. The molar absorption coefficient and the uncaging quantum yield of the newly synthesized compounds will be measured. The experimental data will be further analyzed by computational predictions. The results of the computational predictions will then be used to further optimize the structure of the new photocage.

For a proof of principle VIPER study, coumarin (see Chapter 1.3.4) and *p*HP (see Chapter 1.3.1) derived photocages loaded with a simple, IR active leaving group (*e.g.* azide, thiocyanate) will be prepared and their photochemical properties tested. Synthetic methods for the preparation of the same compounds, but with a ^{13}C isotopic label in certain positions, will be developed and used to synthesize the isotopically labeled compounds. The exact positions of the ^{13}C label incorporation will be guided by computational predictions done by Jan von Cosel (group of Irene Burghardt) and Carsten Neumann (group of Jens Bredenbeck). The photochemical characterization of the photocages will be done in collaboration with Daniela Kern-Michler, Carsten Neumann, Nicole Mielke and Luuk van Wilderen (group of Jens Bredenbeck) while the VIPER experiments will be done exclusively by the mentioned members of the group of Jens Bredenbeck.

3. Results and Discussion

3.1. A new photolabile protecting group

In the following chapter, the design and synthesis of a new photolabile protecting group is described. The work was started by testing the possibility of improving the photochemical properties of a literature known photocage (DEAMb, see Chapter 1.3.3) by elongating its π-orbital conjugation. In order to prepare relatively fast a small library of compounds with varying substituent effects a palladium catalyzed cross coupling reactions was chosen as a key step. Some of the results reported in Chapter 3.1 have been published in the bachelor theses of Lennart Alsheimer,[152] Jennifer Breitenbach[153] and Vivien McKenney.[154] These results have been obtained under the supervision of the current author and will not be referenced separately.

3.1.1. Synthesis and photochemical characterization of biphenyl derivatives

The commercially available 3-amino benzoic acid **116** was used as a starting material (Figure 41). In a reaction with thionyl chloride the corresponding acyl chloride is formed, which reacts with the solvent (ethanol) *in situ*, to give the ethyl ester **117**. The reaction takes place with a high yield and no purification is necessary. In the next step the amino group is alkylated by ethyl bromide in presence of KI. The role of potassium iodide is to form the more reactive EtI from the EtBr directly in the reaction mixture. Also the 3-diethylamino benzoic acid ethyl ester **118** was used in the next step without chromatographic purification.

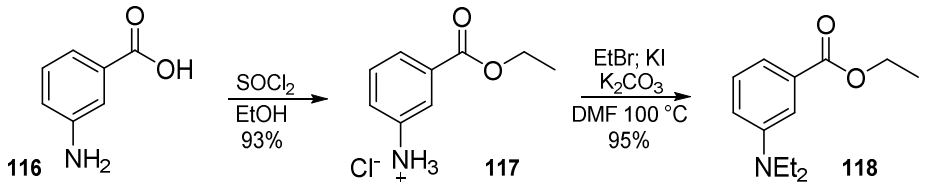

Figure 41: Synthesis of 3-diethylamino benzoic acid ethyl ester **118**.

The ethyl ester **118** was reduced to alcohol by $LiAlH_4$ (Figure 42). The alcohol **119** was halogenated in a reaction with molecular iodine. The amino group directs the S_EAr reaction to happen in the *para* positon.

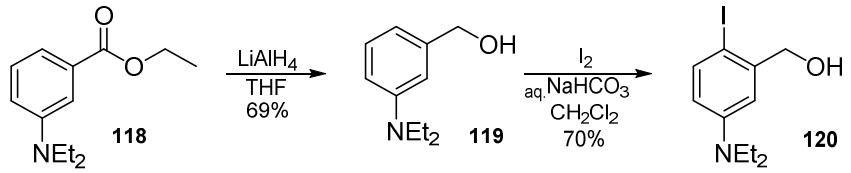

Figure 42: Preparation of the alcohol **120** from ester **118**.

The alcohols (**122-123**) were condensed with the protected glutamic acid **121** in a Steglich-type reaction (Figure 43). Esters are often chosen as model leaving groups due to their non-nucleophilic nature. Glutamic acid was used because of its biological importance and polar nature, which enables performing photochemical characterization of loaded photocages in predominantly aqueous conditions.

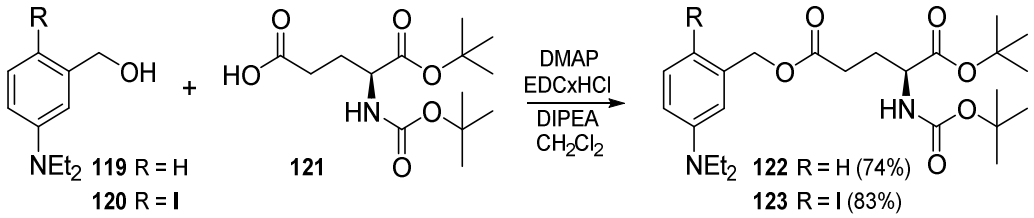

Figure 43: Steglich-type esterification of alcohols with glutamic acid.

The compound **123** was used in palladium catalyzed cross couplings. Suzuki reaction was successful and the biphenyl compound **124** was isolated in a good yield (Figure 44A). Also the Sonogashira coupling was successful (Figure 44C), but no product could be obtained in the Heck reaction (Figure 44B). The reactions were conducted according to procedure described in literature and no optimization of the reaction conditions was done.[39]

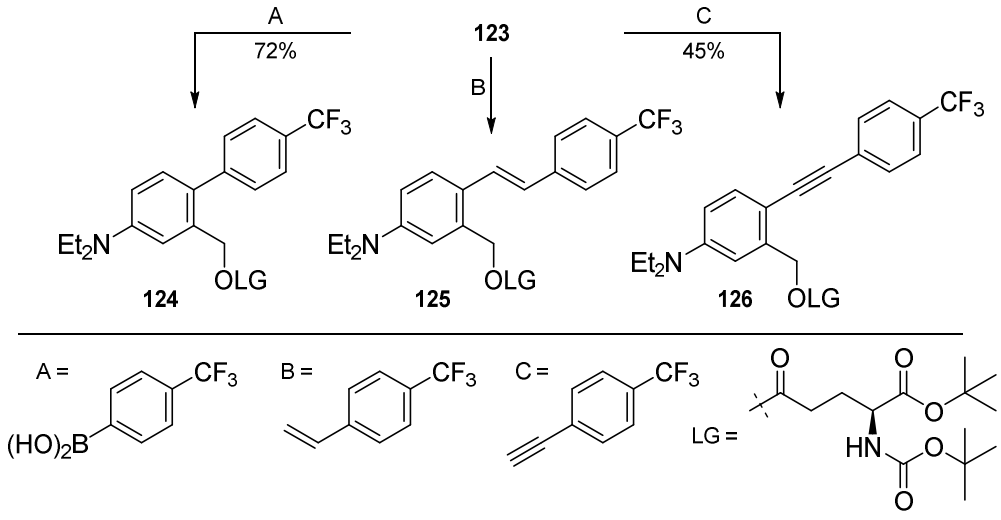

Figure 44: Palladium catalyzed cross coupling reactions. For reaction conditions A and C please see the experimental part.

The glutamic acid protecting groups of the compound **9** were removed using trifluoroacetic acid in CH_2Cl_2 (Figure 45). Cleavage of the Boc groups happens within the first hour of the reaction, while the *tert*-butyl ester takes longer time, hence the reaction mixture was stirred in room temperature for ca. 16 hours.

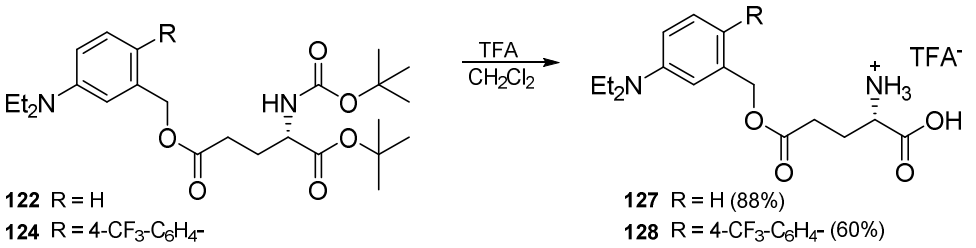

Figure 45: Cleavage of glutamic acid protecting groups from the biphenyls **122** and **124**.

In the same reaction conditions the protecting group cleavage from alkyne **127** did not yield the expected product. Instead, hydrolysis of triple bond was observed to give the compound **129** (Figure 46). The structure of this product was proposed based on the results of NMR and mass spectral analysis. However, the exact position of the carbonyl group in the product was not assigned.

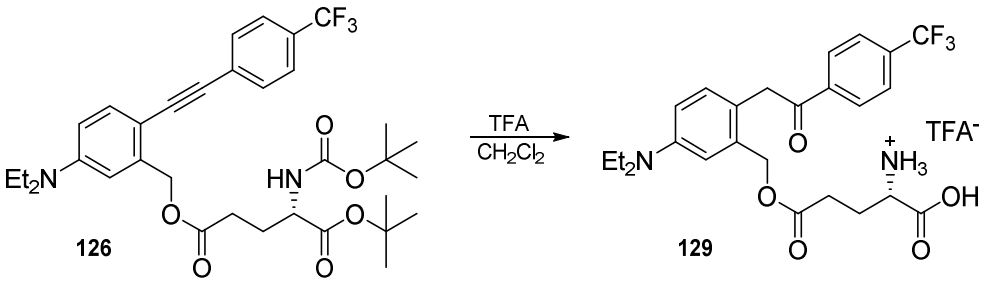

Figure 46: The protecting group cleavage from alkyne **126** resulting in a hydrolysis of the triple bond. The exact position of carbonyl group was not assigned.

Thus, the photochemical properties were tested only for the compounds **127**-**128**. The UV-Vis absorption spectra of these compounds are shown in Figure 47. It can be seen, that the attachment of a second aromatic substituent does not change the maximum of the longest wavelength absorbance band, but the molar absorption coefficient is increased 9-fold. For the sake of simplicity, the longest wavelength absorption band will be called the "absorption maximum" also in further text despite it not always being the absorption band with the highest molar absorption coefficient.

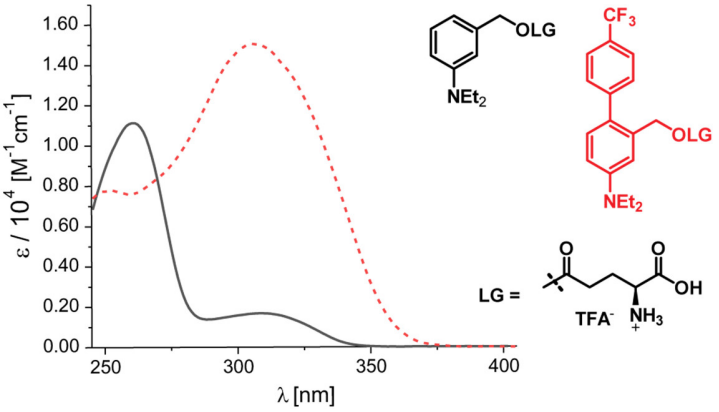

Figure 47: The molar absorption coefficients of the compounds **127-128**. Measurements were done in 0.1M TEAA buffer (+ 20% MeCN).

Compounds **127** and **128** were irradiated to test their photoactivity. The parent DEAMb (**127**) uncaged with a 12% quantum yield upon irradiation at 310 nm (Figure 48). This result is comparable to a similar photocage (3-dimethylamino benzyl) from literature, which released acetate with a 8% quantum yield (at 254 nm).[74] The biphenyl compound **128** had better uncaging quantum yield (19%) at a longer wavelength (365 nm). Here and further, the quantum yield of the starting material disappearance is reported.

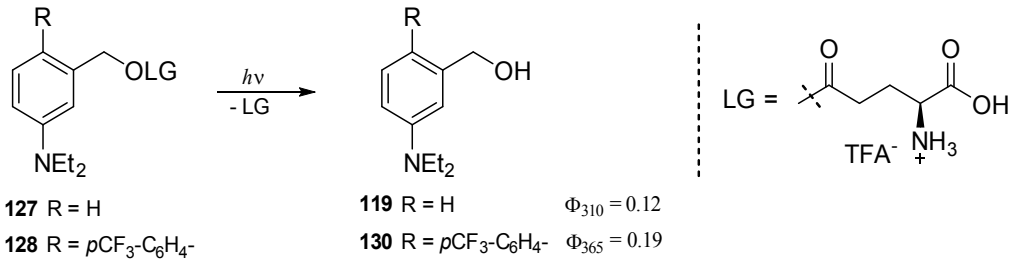

Figure 48: Irradiation experiments of the compounds **127-128**. Measurements were done in 0.1M TEAA buffer (+ 20% MeCN).

In Figure 49 HPLC analysis of the irradiation is shown. Irradiation of the compound **127** yields only one photoproduct, while for the compound **128** also other minor photoproducts can be seen.

The improved spectral properties and uncaging quantum yield of the biphenyl compound **128** in comparison to the parent DEAMb photocage **127** were encouraging to continue the DEAMb photocage optimization.

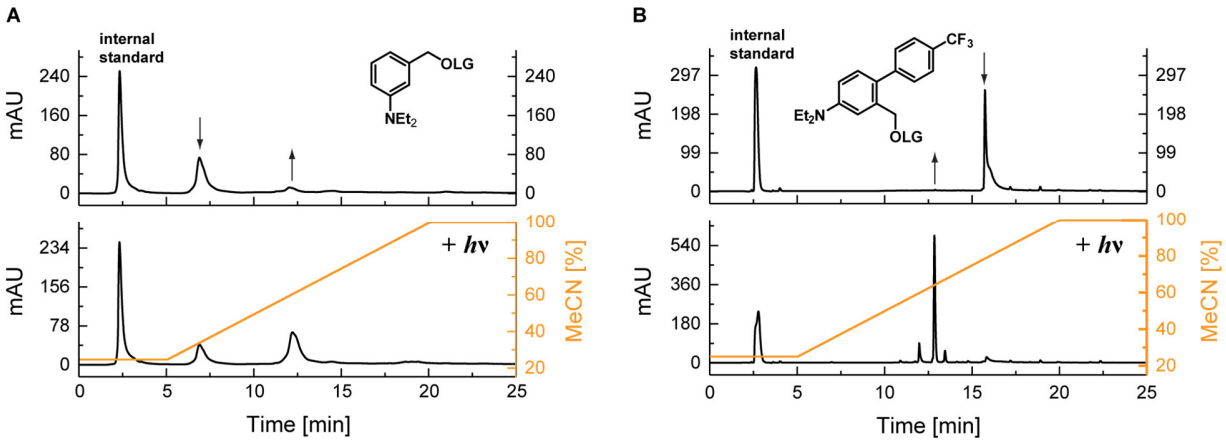

Figure 49: The HPLC analysis of compounds **127** (A) and **128** (B) irradiation. The upper panel shows the sample before irradiation, lower panel – after irradiation. Phenylalanine was used as internal standard.

Since the synthesis of stilbene derivative **125** was not successful and the alkyne derivative **126** was unstable in the reaction conditions used for removal of glutamic acid protecting groups, only the biphenyl systems were further investigated.

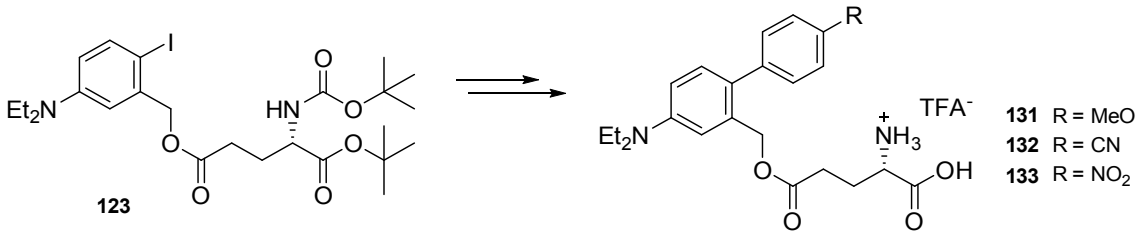

Figure 50: Synthesis of *para*-substituted biphenyl derivatives.

The iodide **123** was used to prepare biphenyl derivatives with other substituents in the second aromatic ring (Figure 50). The synthesis was done analogous to compound **130** (Suzuki coupling followed by the protecting group cleavage). For synthesis details please see the experimental part.

The photochemical properties of these compounds are shown in Figure 51. For comparison, also the parent DEAMb (**127**) and compound **128** are shown. The electron donating substituent *p*-MeO **131** (green, Figure 51) does not shift the absorbance maximum to longer wavelengths, but does increase the molar absorption coefficient. Since it does not absorb light at 365 nm, no quantum yield of uncaging was determined (but the compound was photoactive upon irradiation at 280 nm). The molecule **132**, which contains the strong electron withdrawing –CN substituent (blue, Figure 51) has redshifted absorbance maximum and a high molar absorption coefficient at 365 nm. However, the good spectral properties cannot compensate the small uncaging quantum yield (Φ_{365}= 0.25%), thereby the uncaging cross section is also small ($\varepsilon\Phi_{365}$= 21 $M^{-1}cm^{-1}$). The

uncaging cross section at 365 nm is comparable to the compound **128** ($\varepsilon\Phi_{365}$= 75 $M^{-1}cm^{-1}$), so no clear preference to one of these compounds can be drawn.

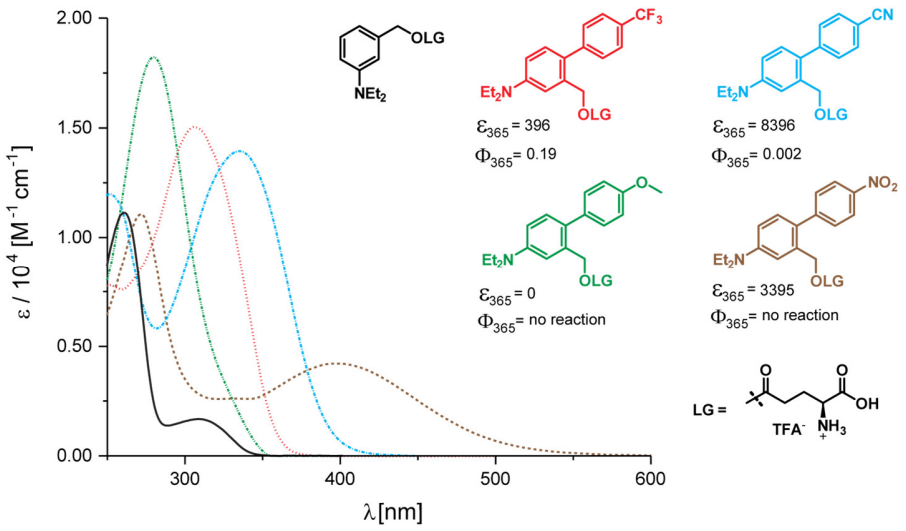

Figure 51: Photochemical properties of *para* substituted biphenyl derivatives. Measurements were done in 0.1M TEAA buffer (+ 20% MeCN). **ε** is given in $M^{-1}cm^{-1}$.

The nitro substituted compound **133** has the most redshifted absorbance spectrum which expands even into the visible spectral range, but the molar absorption coefficient is smaller than that of other biphenyls and the molecule was not photoactive.

It is known, that push-pull systems bathochromically shift the absorbance spectrum and increase molar absorption coefficients[155] and this can indeed be seen in the spectral properties of the so far prepared biphenyls **128**, **131-133**. It has been shown, that the push-pull effect can also lead to a depletion of photoactivity,[15] which can be observed also in the case of these biphenyl compounds. For this reason it was decided to test the photochemical properties of biphenyl compounds, derived from substitution of DEAMb chromophore in other positions.

To that end, aryl halides **134-136** were prepared (Figure 52), following the route described for the compound **119**. Since the 3-amino benzoic acid precursors of the compounds **134-136** already contained a bromine atom, no halogenation was necessary. For synthesis details please see the experimental part.

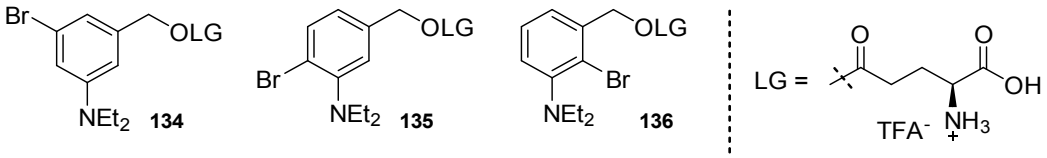

Figure 52: Aryl halides used to prepare *ortho* and *meta* (relative to the amino group) biphenyls.

These halides were used in a Suzuki coupling reaction to prepare biphenyl derivatives (Figure 53). The synthesis was done analogous to compound **128** (Suzuki coupling followed by the protecting group cleavage).

Some general conclusions could be made about the Suzuki reaction. The reaction happened fastest and gave highest yields for the substrates, which have a halogen atom in the *para* (**123**) and *meta* (**134**) position (relative to the amino group). This is probably due to sterical hindrance in the *ortho* positions. Particularly bad reactivity was observed for the compound **136**. Increased reaction time did not result in higher yields but gave more side products, for example, hydrodehalogenation of the starting material.[156] Also hydrolysis of coupling products could be observed (to give corresponding biphenyl benzyl alcohol). Homocoupling of boronic acid always happened to some extent.[157] The symmetric biaryls produced proved to be difficult to separate from the desired biphenyls due to their similar structures. Separation was easy by reverse phase chromatography, especially if done after cleavage of glutamic acid protecting groups.

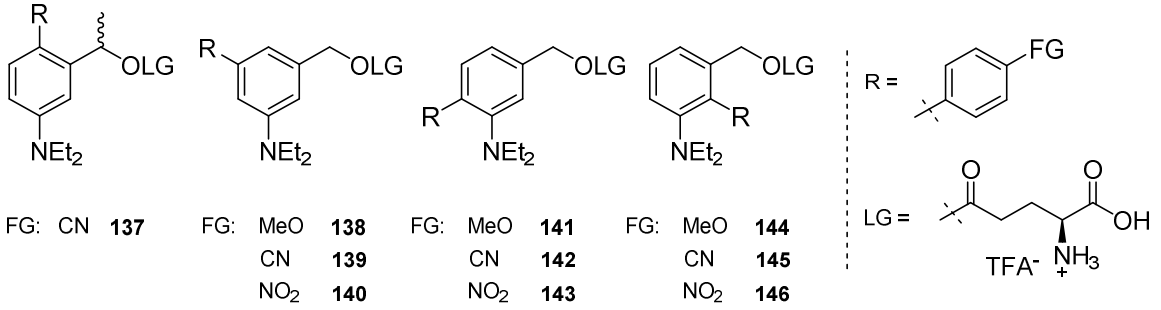

Figure 53: The structures of DEAMb derived biphenyls.

All four possible regioisomers of the electron donating methoxy substituent containing molecules were compared (Figure 54), however for the compound **141** incomplete analytical data was gathered (please see experimental part for further information). The *meta* isomer **138** has the best spectral properties even though the molar absorption coefficient at 365 nm is small (484 $M^{-1}cm^{-1}$). Both *ortho* isomers have particularly low molar absorption coefficients (**141** and **144**) probably as a result of sterical hindrance from the diethylamino substituent and the benzylic carbon (in case of the compound **144**). Quantum yield of uncaging was determined only for the isomer **138** (Φ_{365}=19%) since it is the only one to absorb at 365 nm. However, all other isomers demonstrated photoactivity if irradiated at 280 nm (data not shown).

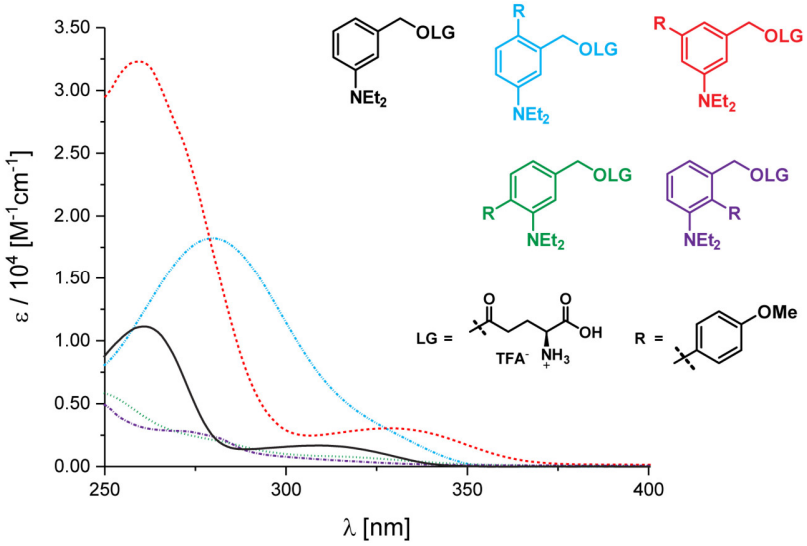

Figure 54: The molar absorption coefficients of methoxy substituted biphenyl derivatives **131**, **138**, **141** and **144**. Measurements were done in 0.1M TEAA buffer (+ 20% MeCN).

The effect of the substituent position was further tested by CN functionalized molecules. Analogous to the methoxy substituted ones, all four possible regioisomers were prepared and their spectral properties measured (Figure 55). Shifting the substituent from *para* (**132**, **137**) to the *meta* position (**139**) results in depletion of the molar absorption coefficients of the longest wavelength absorbance band. This is due to the lost conjugation of the amino group with the electron withdrawing substituent in *para* position (push-pull system).

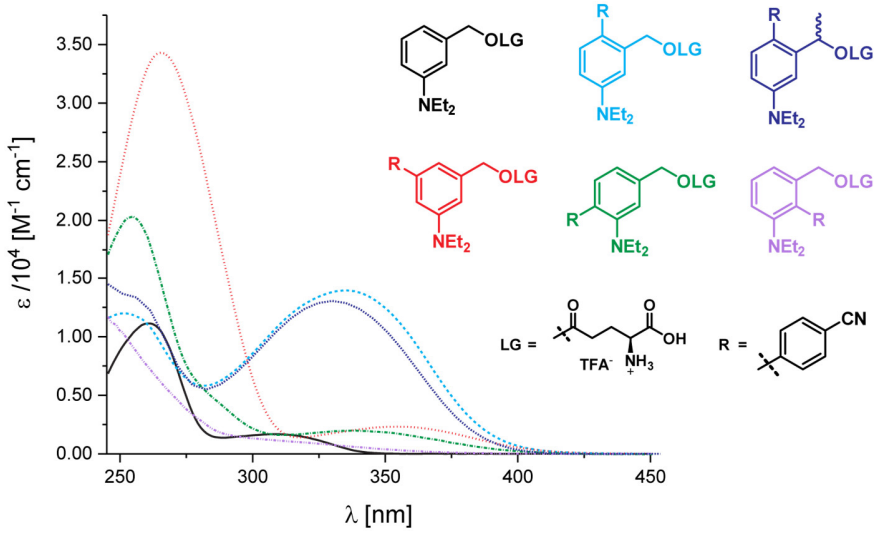

Figure 55: The molar absorption coefficients of cyano substituted biphenyl derivatives **132**, **137**, **139**, **142** and **145**. Measurements were done in 0.1M TEAA buffer (+ 20% MeCN).

Nevertheless the absorbance maximum of the *meta* substituted compound is more redshifted (see also Table 1). Also for these substrates the lowest molar absorption coefficients are

demonstrated by the compounds, which are substituted in the *ortho* positions (**142** and **145**). The effect of steric hindrance can also be observed when compounds **132** and **137** are compared. The only structural difference is the methyl group on the α-carbon, but it is enough to decrease the molar absorption coefficient and blueshift the absorbance maximum.

The uncaging quantum yield of the cyano substituted regioisomers are shown in Table 1. Installation of the methyl group on the benzylic carbon (**137**) slightly increases the uncaging quantum yield if compared to the analogue compound without the methyl group (**132**). This might be a result of the stabilizing effect of the methyl group on the carbocation, generated upon uncaging (see the uncaging mechanism, Figure 15). In either case quantum yields are small.

Table 1: Photochemical properties of the cyano substituted biphenyls. Table reproduced with modifications from Reinfelds, M. *et al*. *Chem. Eur. J.* **2018**, 24 (doi: 10.1002/chem.201802390) with permission; Copyright 2018 Wiley-VCH Verlag GmbH & Co. KGaA, Weinheim.

Compound Nr.[a]	Isomer	λ_{max} (nm)[b]	$\varepsilon_{\lambda_{max}}(\mathrm{M^{-1}cm^{-1}})$	$\varepsilon_{365}(\mathrm{M^{-1}cm^{-1}})$	$\Phi_{365}(\%)$	$\Phi\varepsilon_{365}(\mathrm{M^{-1}cm^{-1}})$[c]
127	DEAMb	309	1681	0	12[d]	200[d]
132	*para*	335	13 950	8396	0.25	21
137	*para*	330	13 050	5845	0.37	22
139	*meta*	355	2320	2156	0.04	<1
142	*ortho*	338	1980	1330	4	53
145	*ortho*	254	10420	205	0.6	1

[a] Measurements were done in 0.1M TEAA buffer (+ 20% MeCN). [b] The value of the absorbance band at the longest wavelength where it is possible to distinguish. [c] Uncaging cross section. [d] Determined at 310 nm.

The *para* and *ortho* isomers gave one photoproduct upon irradiation, while *meta* isomer **139** produced a complex mixture of photoproducts (see appendix, Figure 143). By TLC-MS analysis it was shown, that upon irradiation of compound **132** benzyl alcohol is produced (see appendix, Figure 144). The uncaging quantum yields exceed 1% only for the *ortho* substituted compound **142** but its uncaging cross section is small ($\varepsilon\Phi_{365}$= 53 $\mathrm{M^{-1}cm^{-1}}$) thereby neither of these compounds can be considered to be a useful photocage. These results suggest that installing electron withdrawing substituents in any position of the aromatic ring influences the photoactivity negatively.

This claim is further supported by biphenyls, which contained a nitro substituent. Even though all of these derivatives have absorbance in visible range (Figure 56), neither of these compounds was photoactive.

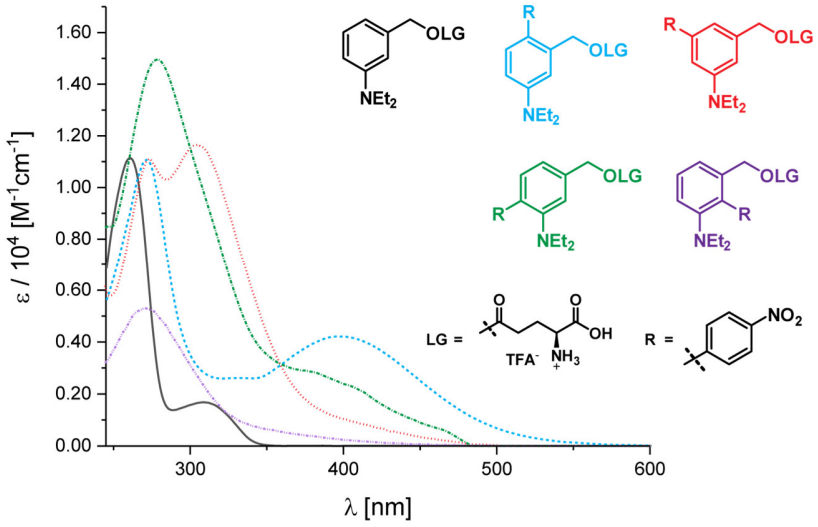

Figure 56: UV-Vis of the nitro compounds **133**, **140**, **143** and **146**. Measurements were done in 0.1M TEAA buffer (+ 20% MeCN).

The molar absorption coefficients of the nitro substituted biphenyls also further support the destructive influence of the sterical hindrance in the *ortho* positons to the absorption spectra. This can be explained by the increased torsion angle between the two aromatic rings (Figure 57).

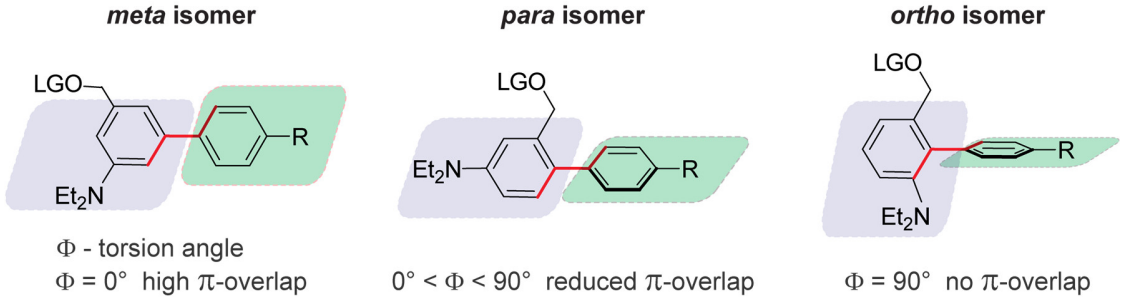

Figure 57: Torsion angle in biphenyl derivatives. Figure reproduced from Reinfelds, M. *et al. Chem. Eur. J.* **2018**, 24 (doi: 10.1002/chem.201802390) with permission; Copyright 2018 Wiley-VCH Verlag GmbH & Co. KGaA, Weinheim.

The best π–orbital overlap in biphenyl derivatives is possible, if the two aromatic rings are in the same plane (torsion angle = 0°). In reality the angle is larger due to steric repulsion between the adjacent hydrogens in *ortho*-position (in case of simple biphenyl). In the gas phase the angle is 44-45° with a small rotational barrier (6-8 kJ mol^{-1} at 0 K) while in solution the torsion angle is 20°.[124,158,159] Introduction of *ortho* substituents limits the free rotation of the two aromatic rings

and forces them out of the coplanarity (torsion angle is about 70°), resulting in a reduced π–orbital overlap. As a result the absorption spectrum is hypsochromically shifted and the molar absorption coefficient decreased.[160] The same can be observed in DEAMb derived biphenyls (Figure 54-Figure 56).

In order to better understand the substituent electronic effects, additional compounds were prepared. The understanding of the sterical effects made us choose the *meta* position for further derivatization. To that end, four compounds were prepared (Figure 58).

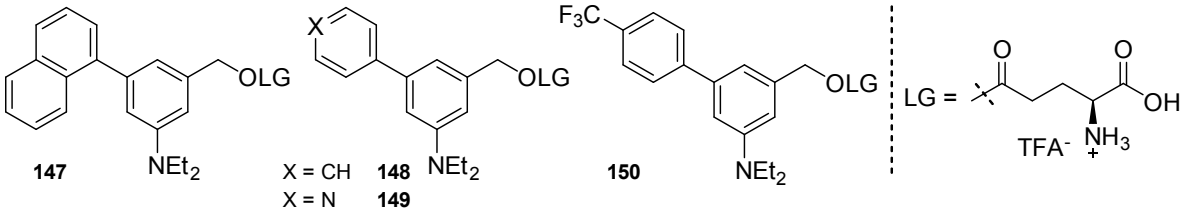

Figure 58: Structure of the *meta* substituted biphenyl derivatives.

The absorption spectra of compounds **147-150** are shown together with previously described biphenyls **138-140** in Figure 59.

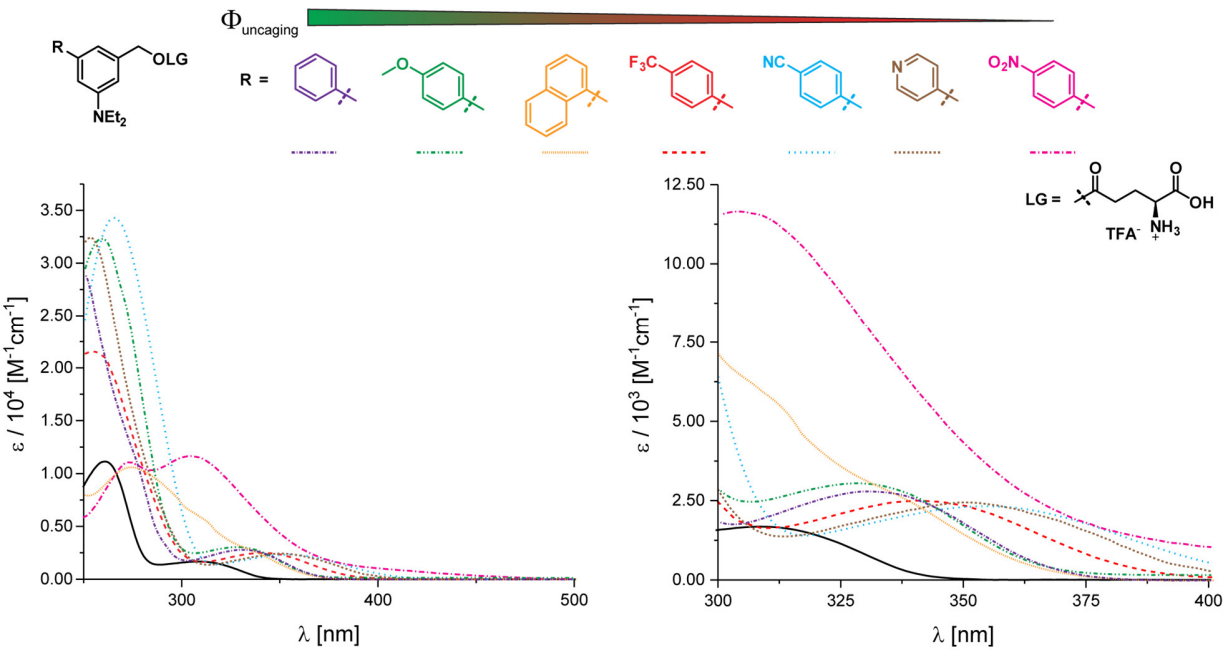

Figure 59: The absorbance spectra of all prepared *meta* substituted biphenyls and the trend of uncaging quantum yield change (shown by the arrow). Full spectra is shown in the left side, only the longest wavelength absorbance band is shown on the right side. Measurements were done in 0.1M TEAA buffer (+ 20% MeCN). The spectra shown in the right part of figure is reproduced from Reinfelds, M. *et al. Chem. Eur. J.* **2018**, 24 (doi: 10.1002/chem.201802390) with permission; Copyright 2018 Wiley-VCH Verlag GmbH & Co. KGaA, Weinheim.

Simple substituents like phenyl, *p*-methoxyphenyl and napthyl shift the absorption maximum of the DEAMb longest wavelength absorbance band and nearly double the molar absorption coefficient if compared to the unsubstituted DEAMb (**119**).

Introduction of a weak electron accepting group (CF_3, **150**) further shifts the absorption maximum. If a stronger electron withdrawing substituent is used, like CN (**139**), pyridine (**149**) or nitro (**140**) the effect is more pronounced.

The opposite effect is shown by the uncaging quantum yield. The stronger is the electron withdrawing group the smaller is the quantum yield. The results of quantum yield measurements and the absorption properties are shown in Table 2.

Table 2: The photochemical properties of *meta* substituted biphenyls. Table reproduced with modifications from Reinfelds M. *et al*. *Chem. Eur. J*. **2018**, 24 (doi: 10.1002/chem.201802390) with permission; Copyright 2018 Wiley-VCH Verlag GmbH & Co. KGaA, Weinheim.

Compound Nr.[a]	R	λ_{max} S_0-S_1 (nm)[b]	Excitation energy S_0-S_1 (nm)[c]	Oscillator strength[c]	$\varepsilon_{\lambda_{max}}$ S_0-S_1 ($M^{-1}cm^{-1}$)	ε_{365} ($M^{-1}cm^{-1}$)	Φ_{365}(%)	$\Phi\varepsilon_{365}$($M^{-1}cm^{-1}$)[d]
127	H	309	n.d. [e]	n.d.	1681	0	12[f]	200[f]
148	Ph	331	307	0.0598	2825	535	42	225
147	Napthyl	334	n.d.	n.d.	2860	400	1.9	8
138	OMe	327	299	0.0824	3048	484	19	92
150	CF_3	340	328	0.0513	2504	1472	4.6	68
139	CN	355	354	0.0456	2320	2156	0.04	<1
149	Py	349	n.d.	n.d.	2245	2038	0.01	<1
140	NO_2	304	308[g]	0.2494[g]	11651	2463	No reaction	No Reaction

[a] Measurements were done in 0.1M TEAA buffer (+ 20% MeCN). [b] The value of the absorbance band at the longest wavelength where it is possible to distinguish (S_0-S_1 transition). [c] Corresponding computed excitation energies obtained at the TD-PBE0/Def2-TZVP level of theory. At the amino group ethyl was replaced with methyl, the leaving group replaced with –OH. [d] Uncaging cross section. [e] Not determined. [f] Determined at 310 nm. [g] The S_3 state was assigned to the experimental value in this case.

3.1.2. TDDFT computations of the biphenyl derivatives

The observed trends of reactivity for the described biphenyl derivatives show the negative influence of electron withdrawing groups. It can be expected that they decrease the electron density at the *meta* position to which the benzylic carbon and a leaving group is attached, which is a

prerequisite for a bond dissociation according to Zimmerman's meta effect (see Chapter 1.3.3). This was qualitatively confirmed by TDDFT computations (done by Jan von Cosel, Konstantin Falahati, Carsten Hamerla, group of Irene Burghardt).

Using Gaussian16 program package and PBE0/Def2-TZVP level of theory an excited state analysis was performed.[161–163] Ground state structures were optimized and all minima verified by frequency calculations. The computed excitation energy (S_0-S_1 transition) and oscillator strength are shown in the Table 2. The results are in a good agreement with the experimental data.

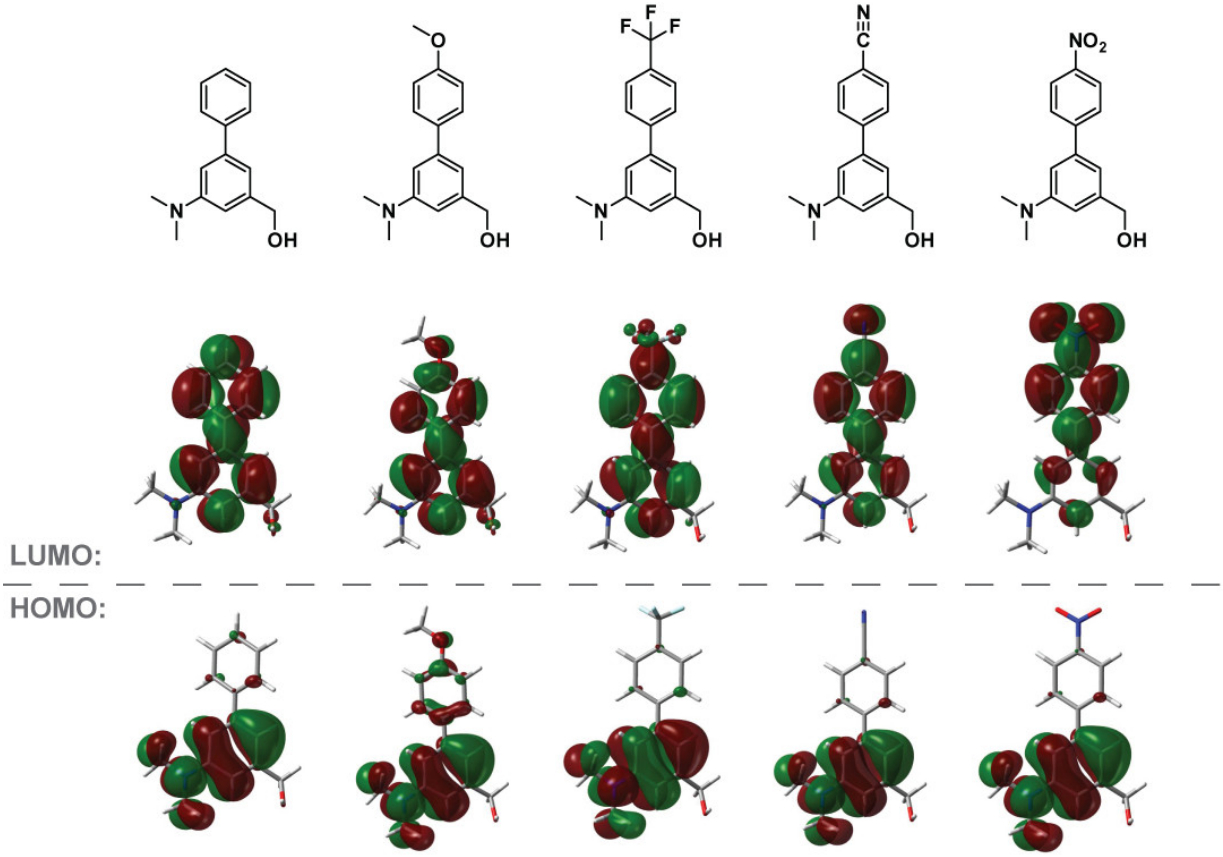

Figure 60: The frontier orbitals of selected biphenyl compounds (**148**, **138**, **150**, **139** and **140**), obtained at the TD-PBE0/Def2-TZVP level of theory. To reduce the calculation times, the ethyl group was replaced by methyl, an OH group was used as leaving group. The figure was prepared in a collaboration with Jan von Cosel, Konstantin Falahati, Carsten Hamerla, from the group of Irene Burghardt. Figure reproduced from Reinfelds, M. *et al*. *Chem. Eur. J*. **2018**, 24 (doi: 10.1002/chem.201802390) with permission; Copyright 2018 Wiley-VCH Verlag GmbH & Co. KGaA, Weinheim.

The frontier molecular orbitals for selected biphenyls are shown in Figure 60. For the compounds which contain electron donating substituents such as phenyl (**148**) and methoxyphenyl (**138**), an increased local orbital contribution at the *meta* position, to which the benzylic carbon is

attached, can be seen. This is in contrast with molecules containing a strong electron withdrawing groups such as cyano (**139**) and nitro (**140**) which in the excited state have a very small electron density in this position. As a result, these molecules have little or no photoactivity. This is in agreement with the experimental results.

3.1.3. Detection of the glutamic acid leaving group

The direct detection of glutamic acid leaving group is a complicated task due to its polar nature and absorption in the far UV range. Therefore indirect methods are often used, such as detection of CO_2 in the IR frequency range, which is released upon uncaging if the glutamic acid is caged trough an amino group *via* a carbamate linker.[131] Another example is the detection of electric impulses in neuronal cells upon light induced release of glutamic acid, however, this method is complicated and expensive due to the need for neuronal cells.[133] In both cases, equipment which is not available in a standard organic chemistry laboratory is necessary.

A classical method for the detection of amino acids is ninhydrin staining. An example is demonstrated for the compound **150**. Upon irradiation of this compound (Figure 61), the glutamic acid **152** is released (panel A). The amino group (**152a**) of the glutamic acid reacts with the dione **153** (ninhydrin) the give the colored compound **153** (panel B).

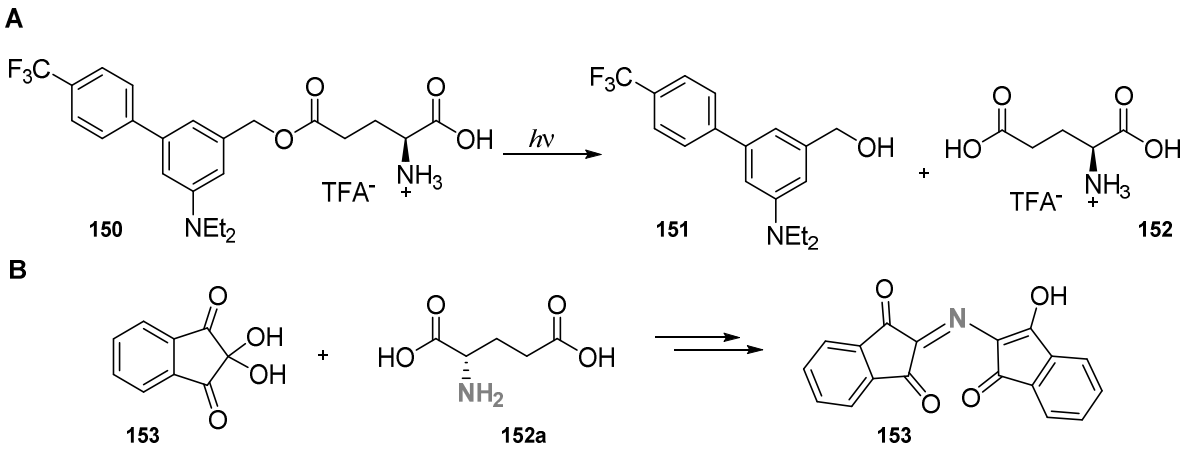

Figure 61: Uncaging of the compound **150** and subsequent reaction of the released glutamic acid with ninhydrin.

Since the amino group is available for a reaction with ninhydrin also in the caged form (compound **150**) a positive signal is expected before the irradiation as well. This can be seen in Figure 62 which shows the TLC analysis before and after irradiation.

In panel A the fluorescent TLC plate is shown. The left line is compound **150** before uncaging (labeled with a circle and number 1), the middle line is the compound **150** after irradiation and the right line is glutamic acid standard. A complete conversion of the starting material can be seen.

When the TLC plate is sprayed with ninhydrin solution and gently heated, red colored spots appear (panel B and C). As expected, coloring can be observed also for the not irradiated sample (labeled with a circle and number 1), but the irradiated sample (middle line) shows coloring in the same height as the glutamic acid standard (labeled with a circle and number 2 for the irradiated sample and 3 for the glutamic acid standard). Thus, glutamic acid has been released.

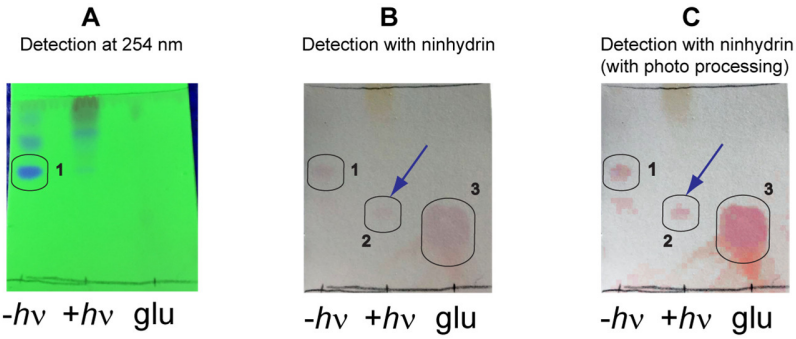

Figure 62: Glutamic acid detection in the irradiated mixture of a photocaged glutamic acid using TLC and ninhydrin. This figure is reused in a modified form from the bachelor thesis of Jenifer Breitenbach.[153]

The ninhydrin staining can be used as a fast on-bench control for the glutamic acid release, however, it's not suitable for quantification and is not un-doubtful. In contrast, the ^{1}H NMR spectroscopy gives certain proof of the structure of the released molecule and could be used for quantification. Thus, the compound **150** was irradiated in a NMR solvent (MeOH-d_4 + D_2O) and compared to the glutamic acid standard (Figure 63). Clear release of glutamic acid could be seen, proving the NMR to be a good method for determination of the glutamic acid release.

The experiment was repeated for the best photochemically performing biphenyl compound **148** using MeCN-d_3 + D_2O as a solvent. The results are shown in appendix (Figure 146). However, the drawback of the NMR analysis is the high concentration of the starting material necessary to achieve a good signal to noise ratio. Thus, even using high power LED long irradiation times might be necessary if the uncaging quantum yields are low.

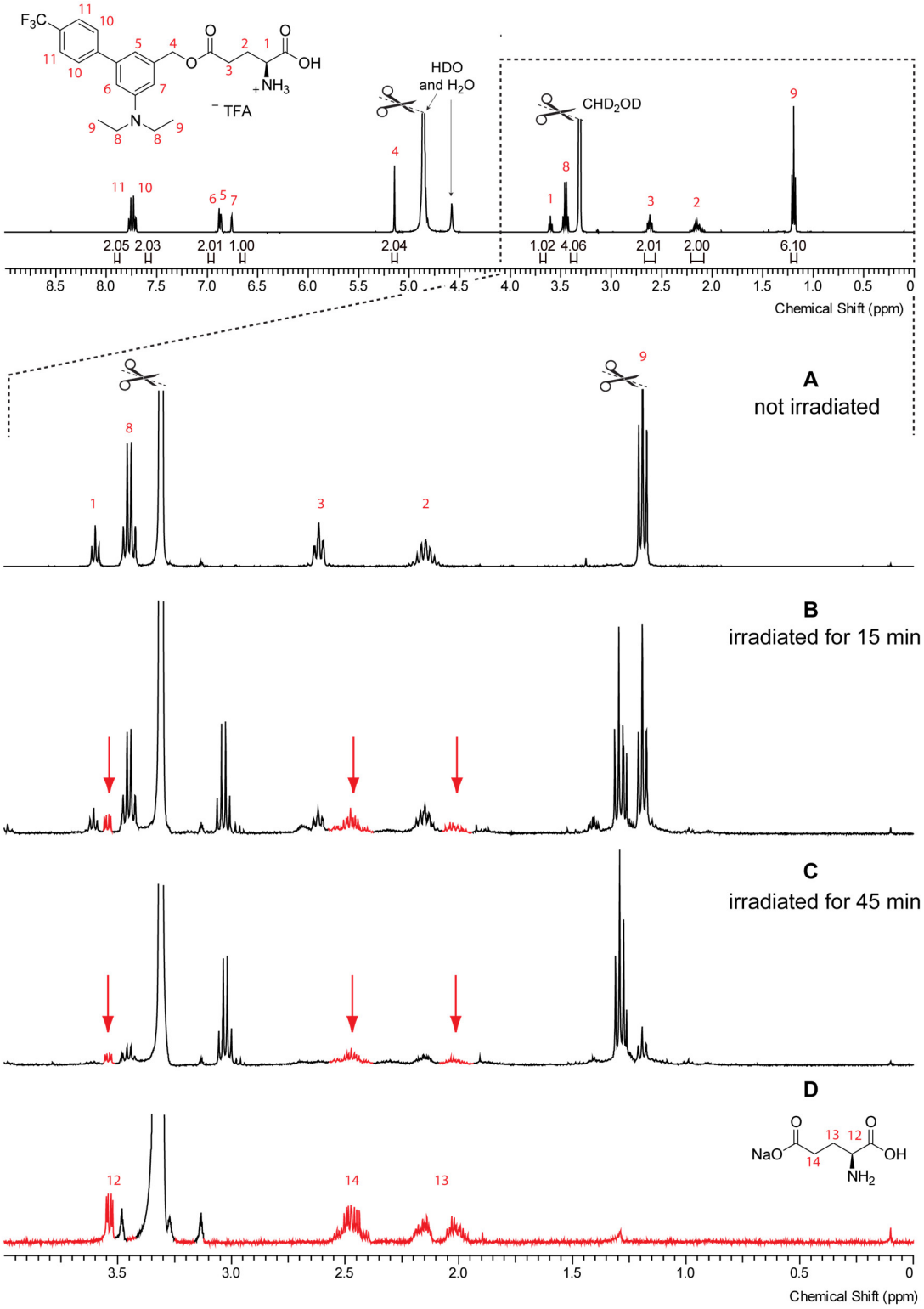

Figure 63: ^{1}H NMR (400 MHz) control of the glutamic acid release from the biphenyl **150**. Measurements were done in in MeOD-d_4 + D_2O, irradiation at 365 nm. This figure is reused in a modified form from the bachelor thesis of Jenifer Breitenbach.[153]

Indirect proof of a glutamic acid release can be shown also by HPLC analysis, if the irradiated mixture is compared to the expected photoproduct – benzyl alcohol. To that end, the glutamic acid loaded biphenyl **148** (Figure 64, panel A) and the expected photoproduct (panel B) were analyzed with HPLC. The compound **148** was then irradiated at 365 nm using solutions with a µM (panel C) and mM (panel D) concentration (the latter being the sample from NMR determination of glutamic acid, Figure 146). In both cases the same photoproduct is produced, whose retention time corresponds to the expected benzyl alcohol.

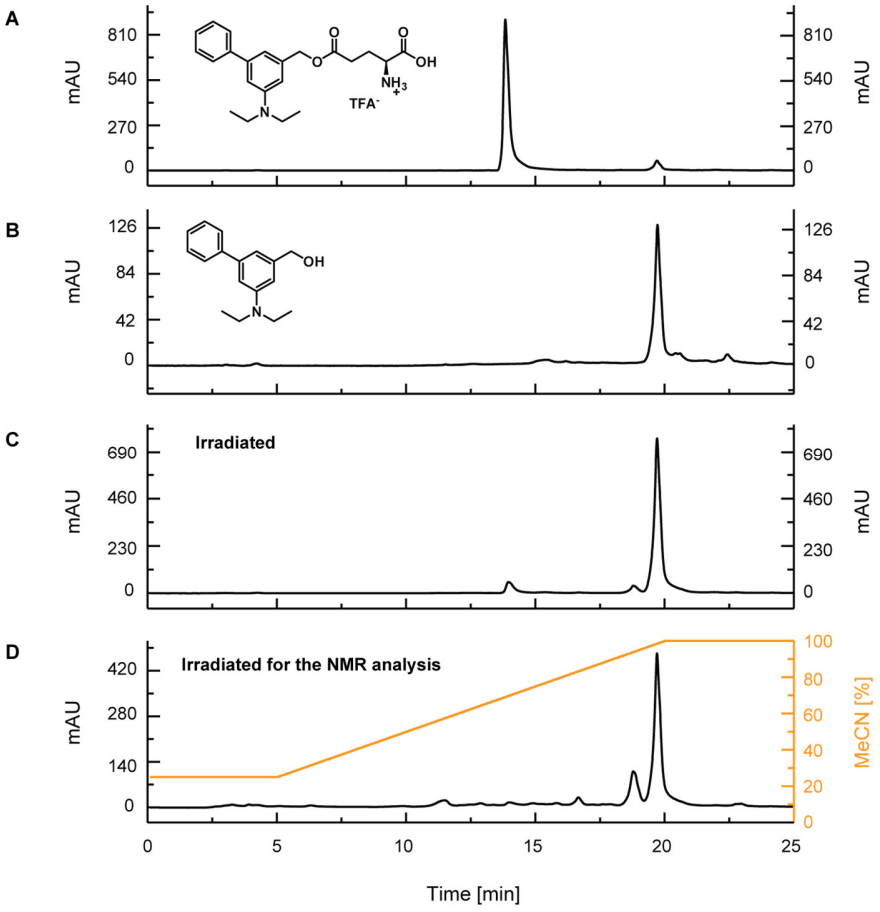

Figure 64: HPLC before and after irradiation of the **29** (0.03 mM). The irradiation power (LED 365 nm) was close to 165 mW, volume - 200 µL. The concentration of NMR sample (last chromatogram) was ca. 10 mM and volume ca. 600 µL. Figure reproduced from Reinfelds, M. *et al*. *Chem. Eur. J.* **2018**, 24 (doi: 10.1002/chem.201802390) with permission; Copyright 2018 Wiley-VCH Verlag GmbH & Co. KGaA, Weinheim.

Direct determination of the glutamic acid release by HPLC would be favorable since it would also allow quantification. However, due to a low molar absorption coefficient which lies in the far-UV region, it is difficult to determine glutamic acid using UV-Vis detectors. As a result of the highly polar nature of glutamic acid, its retention time on standard reverse phase (C18) columns

is very short, eluting close to dead volume of the column, often together with buffer used for sample preparation.

The results obtained using a C18 modified column which is suitable for elution with 100% water are shown in Figure 65 (panels A-E). For elution, a phosphate buffer (NaH_2PO_4/H_3PO_4 1:1, pH = 2.6) was used because it has low absorption in the detection wavelength (210 nm). If no injection is done, only a slight shift of the baseline can be observed. This probably is a result of an insufficiently washed HPLC system still containing buffer salts left by previous users (panel A). The 0.1M TEAA buffer can be detected as two broad signals, one for AcOH and one for triethylammonium phosphate (panel B). Glutamic acid is eluted at a similar time (panel C, red). If the sample contains a large amount of glutamic acid (mM range), the signal can suppress the TEAA buffer (panel D). However, the glutamic acid could not be detected in the irradiation experiment of biphenyl **145**, probably due to the low concentration (irradiation was done in µM concentration, data not shown).

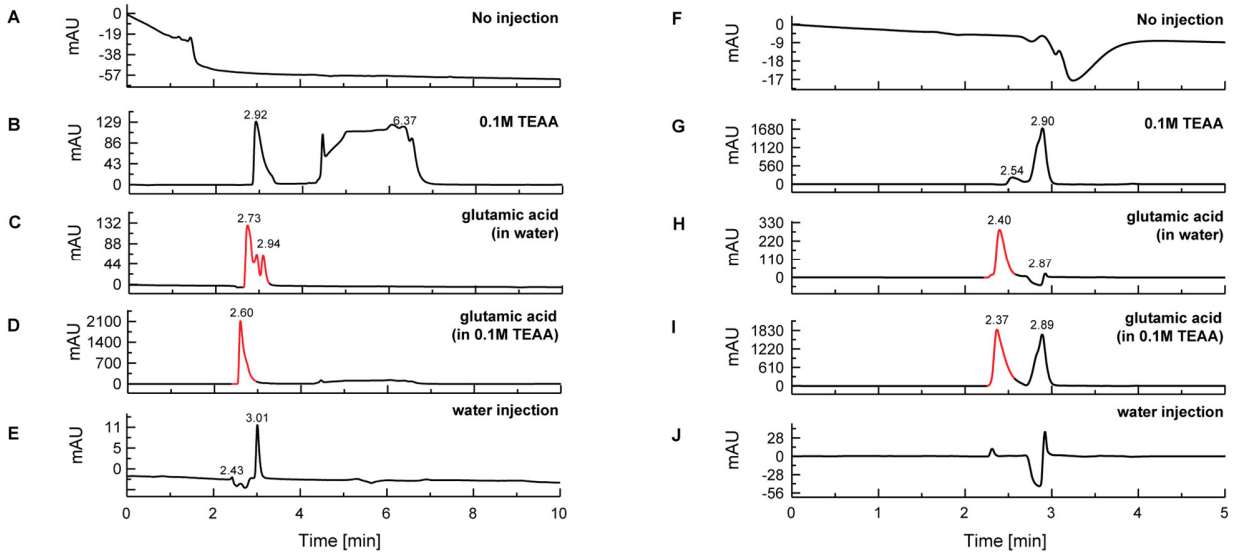

Figure 65: Determination of glutamic acid using a HPLC. Panels A-E shows analysis performed on a Multokrom 100-5 C18 AQ (4.6 x 250 mm) column, using only phosphate buffer (10 mM, pH = 2.6) for elution (isocratic, flow 1.0 mL/min), detection at 210 nm. Panels F-J shows the analysis performed on a reverse phase Nucleosil 300-5 C8 (4.6 x 250 mm) column, elution was done by MeCN and 10mM phosphate buffer (pH = 2.6) in an isocratic ratio 5:95 (flow 1.0 mL/min), detection at 210 nm.

Also a column with a shorter alkyl chain (C8) solid phase was tested. A shorter alkyl chain should increase retention of polar analytes. Furthermore, the used column was not endcapped. Endcapping is a process in which the silanol groups, which could not be modified by alkyl chains during the manufacturing process due to sterical hindrance, are alkylated by short alkyl chains (for

example, -Si(CH_3)$_3$). If the silanol groups are not endcapped, they can interact with analytes. It was expected, that in the case of highly polar glutamic acid this interaction would increase the retention time. Yet, the results are similar to those obtained with the C18 AQ column.

Just as for the C18 AQ column, also C8 was eluted using phosphate buffer (NaH_2PO_4/H_3PO_4 1:1, pH = 2.6) but also 5% of MeCN was part of a mixture. If no sample is injected (Panel F, Figure 65) only one negative signal around minute 3 can be seen, indicating the dead volume of the HPLC system. The signal of 0.1M TEAA buffer (panel G) is sharper than that of the same buffer injected to the other column (panel B). This might be due to MeCN in the elution mixture or the different column material and pore size. After injection of glutamic acid (dissolved in water), a signal at 2.40 min can be seen which is thus assigned to glutamic acid. The same signal, together with the signal of a buffer can be seen if glutamic acid is dissolved in 0.1M TEAA (panels C-D). Yet, also using this column glutamic acid can be detected only if a large concentration (mM) sample is injected. The irradiation experiments were done in the µM range, thus the release of glutamic acid could not be detected (data not shown).

A HPLC system equipped with ELSD (evaporative light scattering detector) was also tested, however the results obtained were not unambiguous due to early elution times of glutamic acid.

To circumvent the early elution time a HILIC stationary phase was tested. Hydrophilic interaction chromatography (HILIC) is particularly good to analyze highly polar or charged species which have a bad retention in reverse phase chromatography. This is achieved by the functionalization of solid phase by a polar substituent. Typical gradient elution for HILIC analysis is opposite to C18 modified silica - analysis is started with high content of organic solvent (such as MeCN) and then the amount of an aqueous eluent is gradually increased. Polar species have larger retention times than unpolar ones accordingly.[164] In this work an HILIC column functionalized with zwitterionic sulfobetaine was used (NUCLEODUR® from Machenrey-Nagel). This stationary phase is incompatible with phosphate salts, thus ammonium acetate buffer was used. This buffer absorbs also in the wavelength which is used for the detection of glutamic acid (210 nm), thus isocratic elution was done to ensure stable baseline.

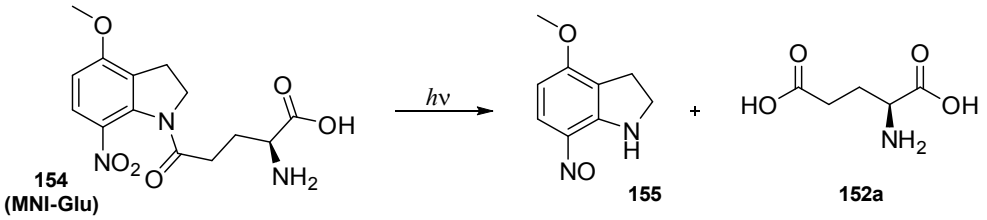

Figure 66: Irradiation reaction of the MNI glutamate **154**.

First, a commercially available standard of photocaged glutamic acid – the MNI-glutamate (**154**) was employed for testing of the HILIC column (Figure 66). Upon irradiation in aqueous solvent it releases glutamic acid and produces nitroso side product **155**.[165] A solution of **154** was prepared in the elution solvent which consists of MeCN (60%) and 40% of an ammonium acetate buffer (10mM, pH = 5). A solvent mixture instead of a pure buffer was used in order to avoid baseline shifts at the detection wavelength due to a change of the solvent composition.

The results are shown in Figure 67. The MNI-glu (**154**) is eluted in 4.23 min (panel A) but the photoproduct **155** is eluted one minute earlier (panel B). A new peak rises also in minute 7.61 (for better visibility compare the panels A1 and B1). If an aliquot of glutamic acid is added to the irradiated sample of MNI-glu, the peak intensity at 7.65 rises (panel C and C1), thus confirming that it originates from released glutamic acid. A signal with the same elution time can be seen if a solution containing only glutamic acid is injected (panel D and D1).

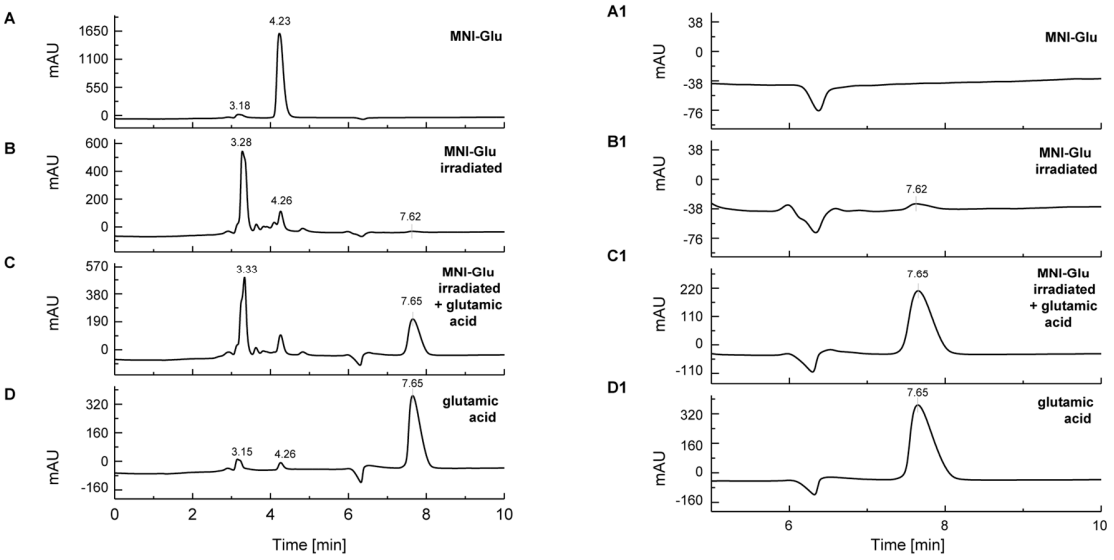

Figure 67: Determination of glutamic acid release from MNI-glu (**154**) using a HPLC. Analysis was performed on a NUCLEODUR® 300-5 HILIC (4.6 x 250 mm) column, using MeCN and 10mM acetate buffer (pH = 5.0) in an isocratic ratio 60:40 for elution (flow 0.8 mL/min), detection at 210 nm. Panels A-B shows elution time from 0 to 10 min, the panels A1-D1 only the time between 5-10 min.

By changing the ratio of MeCN and ammonium acetate buffer in the isocratic solvent mixture, the retention time of glutamic acid and MNI-glu **154** changes (Table 3). The retention time shift is much larger for the glutamic acid **153a** due to its more polar nature in comparison to the MNI-glu **154**.

Table 3: The change of the retention time of glutamic acid and MNI-glu (**154**) on a HILIC column depending on MeCN content in the eluent.

MeCN (%)[a]	Retention time (min)[b]	
	MNI-glu (**154**)	Glutamic acid (**152a**)
50	3.99	5.52
60	4.23	7.65
70	4.97	13.61

[a]Second component of the elution mixture was 10mM ammonium acetate buffer (pH = 5.0) [b] Analysis was performed on a NUCLEODUR® 300-5 HILIC (4.6 x 250 mm) column using isocratic elution mixture (flow 0.8 mL/min).

The developed chromatographic method for glutamic acid detection was used also to control the release of glutamic acid from the biphenyl **132**. The results are shown in Figure 68.

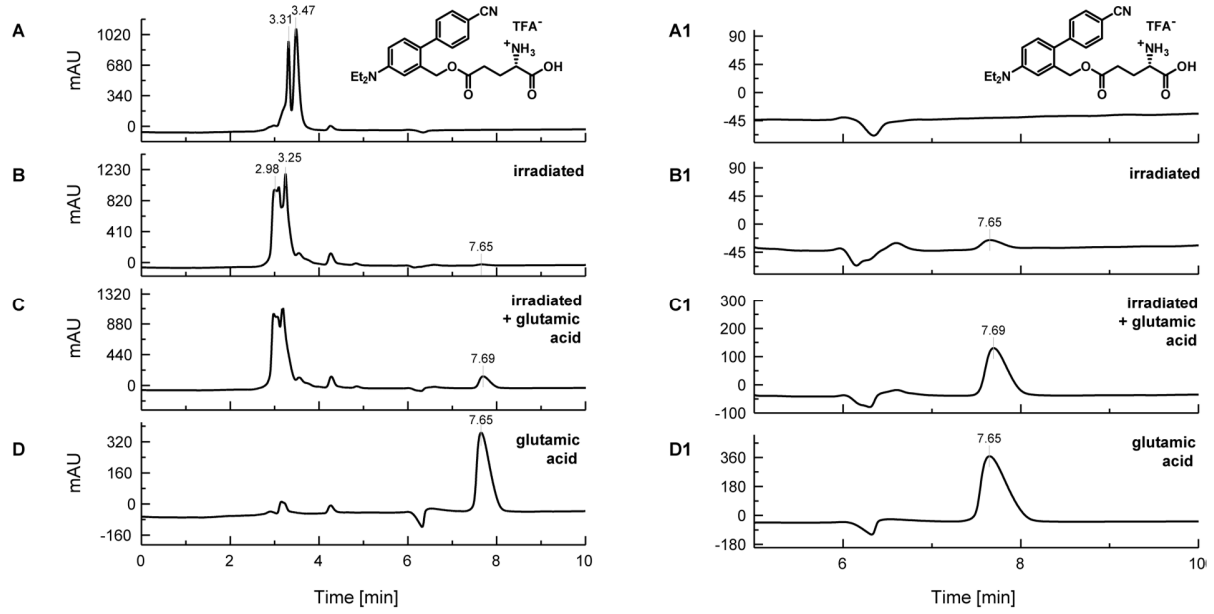

Figure 68: Determination of glutamic acid release from biphenyl **132** using a HPLC. Analysis was performed on a NUCLEODUR® 300-5 HILIC (4.6 x 250 mm) column, using MeCN and 10mM acetate buffer (pH = 5.0) in an isocratic ratio 60:40 for elution (flow 0.8 mL/min), detection at 210 nm. Panels A-B shows elution time from 0 to 10 min, the panels A1-D1 only the time between 5-10 min.

The retention time of the biphenyl compound **132** is very short (panel A). After irradiation the signals are slightly shifted to early elution times, but still are not suitable for a reaction control. However, a new signal rising at 7.65 min can be seen (compare the panels A1 and B1), indicating the release of glutamic acid. Just as for the MNI-glutamate **154** (Figure 67), also this time the identity of this peak was further confirmed by adding glutamic acid to the irradiated sample (panel C and C1) and comparing it to the glutamic acid injected alone (panel D and D1).

The *ortho*-phthaldialdehyde **156** is a popular reagent for spectroscopic determination of amino acids (Figure 69). In presence of thiols (such as mercaptoethanol) the compound **156** reacts with primary amines to give a fluorescent product.[166]

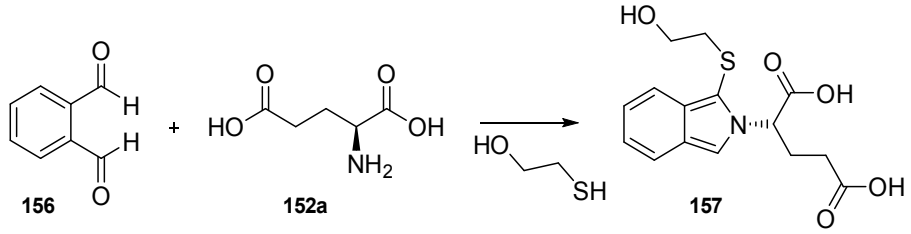

Figure 69: Derivatization of a glutamic acid with *ortho*-phthaldialdehyde (OPA).

In order to test this reaction for determination of a photoreleased glutamic acid, a commercially available solution of **156** together with mercaptoethanol, NaOH and boric acid in methanol was used (in further text called simply OPA reagent). An aliquot of this solution was mixed with equal volume of glutamic acid (5 mM) and the fluorescence of the resulting mixture measured using a plate reader. The compound **157** shows fluorescence with an emission maximum at 450 nm (Figure 70A). The OPA reagent (Figure 70B, gray) and the biphenyl **132** have practically no fluorescence at 450 nm (Figure 70B, orange).

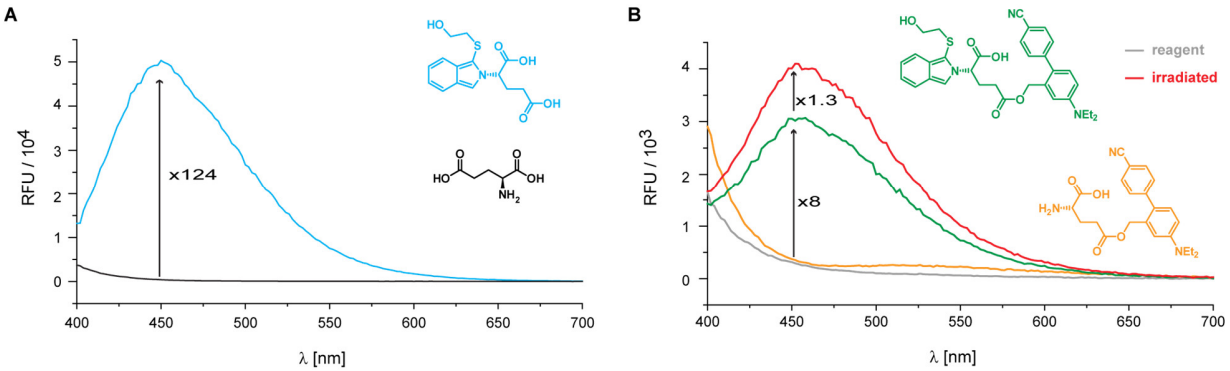

Figure 70: Fluorescence measurements of the OPA derivatization reaction. *A* – glutamic acid (black), glutamic acid after the reaction (blue); *B* – OPA **156** with mercaptoethanol (gray), biphenyl **132**(orange), biphenyl **132** with OPA reagent (green), irradiated biphenyl **132** with OPA reagent (red). Excitation at 300 nm, instrument gain adjusted to the positive control (blue, panel A).

When the OPA reagent is mixed with biphenyl **132**, a fluorescence increase can be observed (Figure 70B, green) which becomes only slightly larger if the biphenyl has been irradiated before. This result is not surprising, because the amino group is available for a reaction also in caged form, since the photolabile protecting group is attached *via* an ester bond.

Furthermore HPLC analysis of the derivatization's reaction was done (Figure 71). The panel A shows the OPA reagent mixture alone. It is followed by panel B which shows the positive control – wildtype glutamic acid after the derivatization. Due to the polar nature of the isoindole **157**, the elution time is very fast. Inlay in panel B shows its absorption spectrum.

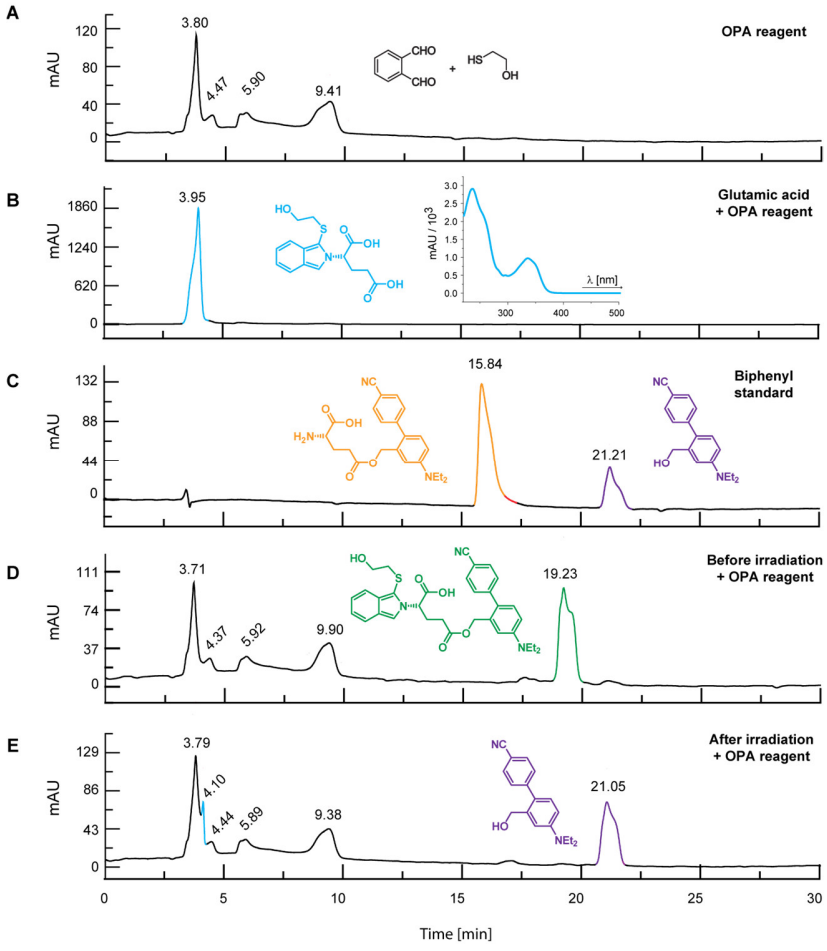

Figure 71: Determination of glutamic acid using a HPLC. The analysis was performed on a Multokrom 100-5 C18 (4.6 x 250 mm) column, using MeCN and sodium acetate buffer (50 mM, pH = 5.0) for elution (gradient content of MeCN: 0-2 min 25%, then over 31 min to 100%), detection at 240 nm.

The panel C shows the biphenyl **132**, loaded with glutamic acid (orange, 15.84 min) together with the expected photoproduct, biphenyl benzylalcohol (violet, 21.21 min). When the

biphenyl **132** is mixed with OPA reagent, a new peak, eluting at 19.32 min is produced (panel D, green). This is a result of the derivatization reaction happening even before the uncaging, as could be seen also in the fluorescence measurements (Figure 70). If the OPA reagent is mixed with the biphenyl **132** after irradiation, the peak at 19.23 min is not formed. Instead, a new peak can be seen at 4.10 min (panel E, blue), which corresponds to the positive control for the product **157** (panel B, blue). Thus, the release of glutamic acid could be detected.

However, these results are far from optimal. Better results could be obtained by using a fluorescence detector, because then the detection of the analyte **157** would not be disturbed by OPA reagent leftovers (in contrast to UV-vis detection). Furthermore, the unselective reaction of the OPA reagent with both, released and still caged glutamic acid could be circumvented if a post-column derivatization would be done.

The chromatographic analysis using the HILIC column (vide supra) could solve one of the problems, naming, the early elution time of the isoindole **157** which is causing signal overlay with the OPA reagent. Thus, the derivatization experiments were repeated, this time using biphenyl **150**, from which a successful release of the glutamic acid was shown by ^{1}H NMR spectroscopy (Figure 63). The results are shown in Figure 72.

In Figure 72 only the elution time between 5 and 10 min is shown, thus the signals from OPA reagent and the biphenyl **150** before and after irradiation cannot be seen (they are eluted in the first 5 minutes, see also Figure 68 and the discussion there). Panel A shows the baseline (no injection), panel B and C show the chromatograms of the glutamic acid and OPA reagent. The detection is done at 365 nm, thus no glutamic acid signal is expected. If the glutamic acid is reacted with the OPA reagent, a large signal from produced isoindole **157** can be seen at 6.97 min (panel D). The analysis of glutamic acid loaded biphenyl **150** looks the same (panel F) as the analysis of the OPA reagent (panel B), thus suggesting that this signal is just a ghost peak (see the signal intensity on *y*-axis). When the OPA reagent is mixed with the not irradiated biphenyl **150**, a small intensity signal of the isoindole **157** can be seen at 6.97 (panel G) resulting from the glutamic acid traces present in the sample because of the dark hydrolysis reaction. This peak increasey its intensity nearly 18-fold if the biphenyl **150** has been irradiated before, indicating successful detection of the glutamic acid release.

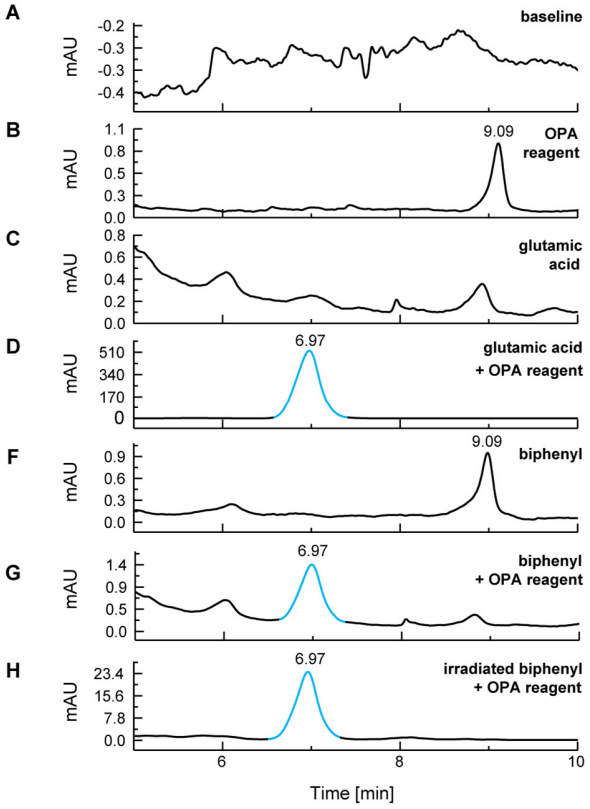

Figure 72: Determination of glutamic acid release from biphenyl **150** by derivatization with OPA reagent and using a HPLC. Analysis was performed on a NUCLEODUR® 300-5 HILIC (4.6 x 250 mm) column, using MeCN and 10mM acetate buffer (pH = 5.0) in an isocratic ratio 70:30 for elution (flow 0.8 mL/min), detection at 365 nm. Only the elution time between 5-10 min is shown.

3.1.4. Summary and outlook of the biphenyl derivatives

Using synthesized DEAMb halides, a small library of biphenyl derivatives was successfully prepared using the Suzuki reaction. The attachment of a second aromatic ring to a DEAMb core does redshift its absorption spectrum. The highest molar absorption coefficients are shown by compounds, which contain an electron withdrawing substituent in the second aromatic ring and have it located *para* to the diethylamino group. *Ortho* positions (relative to NEt_2) are not suitable for attaching a second aromatic ring due to the sterical hindrance. If the second aromatic ring is attached to *meta* position, the sterical hindrance is the smallest. Moreover the largest batochromatic shift is show by compounds which contain strong electron withdrawing groups. But these substituents decrease the electron density in the DEAMb core thus depletion of the photoactivity is observed. This effect could be shown qualitatively by TDDFT computations. From the prepared biphenyl DEAMb derivatives the best photochemical properties are shown by the *meta*-phenyl substituted compound. Upon irradiation at 365 nm it undergoes photoreaction with a 42% quantum yield ($\varepsilon\Phi_{365}$ = 225 M^{-1} cm^{-1}). The parent DEAMb has 12% quantum yield and a slightly smaller

uncaging cross section ($\varepsilon\Phi_{310}$=200 M^{-1} cm^{-1}). This result is comparable to a literature known, similar photocage (3-dimethylamino benzyl), which released acetate with 8% yield (at 254 nm).[74] Thus the spectral properties of the DEAMb photocage have been successfully improved without losing the photoactivity.

The release of glutamic acid could be successfully demonstrated by various methods (TLC and ninhydrin staining, ^{1}H NMR, HPLC). The best direct determination of glutamic acid can be done by ^{1}H NMR spectroscopy but highly concentrated samples have to be used. For determination of glutamic acid by HPLC, the best results are obtained if a HILIC stationary phase is used. Glutamic acid could be detected directly (by absorption at 210 nm) but the low absorption hinders quantification. This problem could potentially be solved if a light scattering detector would be used instead. Detection was possible also by preparing a fluorescent derivative with an *o*-phthaldialdehyde. The available equipment limited the experiments to UV-Vis detection, but potentially better results could be obtained if a fluorescence detector would be used. To circumvent unspecific derivatization of the still photocaged glutamic acid a post-column derivatization combined with fluorescent detection would be favorable.

3.1.5. Introduction to fluorene photocages

One of the most important conclusions drafted from the biphenyl system is the importance of a sterically undisturbed π-orbital conjugation. But free rotational is not good for photocages, since it's an additional relaxation channel of the excited state, thus has a negative impact on the uncaging quantum yield. Thereby, achieving planarity of the two aromatic rings by limiting the rotational freedom would be favorable. Most easily this can be done by a rigid linker. Some examples are shown in Figure 73.

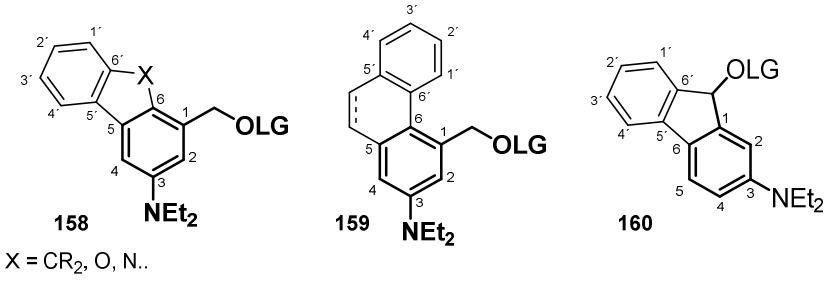

Figure 73: Linkers to limit rotational freedom of the biphenyl compounds.

Introducing a linker X in a *meta*-substituted DEAMb between the carbons 6 and 6´ (**158**) fluorene (X = CH_2), carbazol (X = N) or benzofuran (X = O) would be produced. However, synthesis of these molecules would require large effort due to the complicated substituent pattern.

The same can be said about the molecules based on phenanthrene (**159**). The fluorene derivative **160** differs from the other two compounds by the linker being connected to the benzylic position of the DEAMb, thereby simplifying the substitution pattern (in comparison to compounds **158**-**159**). Accordingly, various fluorene derivatives are commercially available, thus enabling preparation of a small library of compounds in a short time.

Furthermore, the photoactivity of fluorene derivatives is known. For example, the unsubstituted fluorene can release the hydroxy group (**161**)[167] or tertiary amine (**162**)[168] upon irradiation with far UV light (Figure 74). Fluorene derivatives have somewhat been studied as photocages. Lukeman *et al*. have shown the release of acetate and $^{-}$OH group from hydroxy and methoxy substituted fluorene (**163**, R´ = OH, OMe).[169] Amino substituted fluorene derivatives (**163**, R´= NH_2) have been studied in the lab of Wirz.[170] In both cases light under 300 nm was used for uncaging.

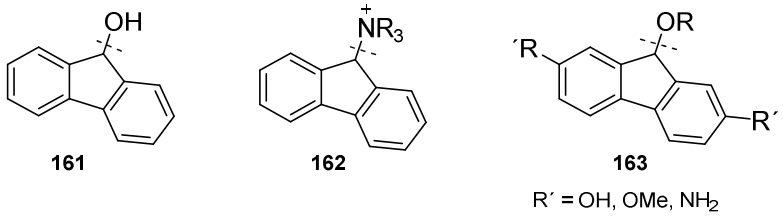

Figure 74: Literature known photoactive fluorene derivatives. The dashed line shows which bond is broken in a photoreaction.

The commercial availability of fluorene derivatives and the literature examples showing their photoactivity was encouraging to further investigate their photochemistry.

3.1.6. Comparison of fluorene and biphenyl derived photocages

The commercially available 2-amino-fluoren-9-one (**164**) was converted to 2-dimethylamino-fluren-9-ol (**165**) in a reductive amination (Figure 75). A glutamic acid leaving group was installed in a Steglich type esterification (**166**), followed by removal of Boc and tBu protecting groups by treatment with TFA to give **167**. Also, fluorene acetate **167** was prepared by treating the alcohol **165** with Ac_2O in pyridine.

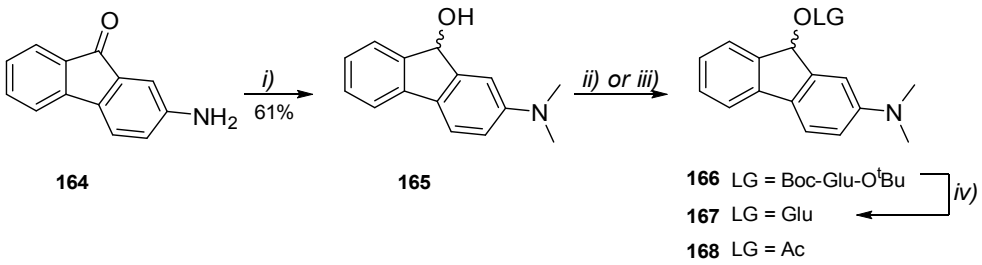

Figure 75: Synthesis of 2-dimethylamino fluorenol derivatives. Reaction conditions: *i*) H_2CO, $NaBH_3CN$, AcOH; *ii*) Ac_2O, pyridine (yield 65%); *iii*) Boc-Glu-OtBu, EDC-HCl, DMAP, CH_2Cl_2 (yield 65%); *iv*) TFA, CH_2Cl_2 (yield 45%);

The absorption spectrum of the newly synthesized fluorenol derivative **167** was compared to the best biphenyl compound **148** (Figure 76). The positive impact of the rigid structure on the spectral properties can be seen immediately – the molar absorption coefficient at 365 nm is two times larger. The quantum yield of uncaging is smaller, but due to improved spectral properties the uncaging cross section is still larger than that of the biphenyl (274 M^{-1} cm^{-1} for **167** and 225 M^{-1} cm^{-1} for **148**).

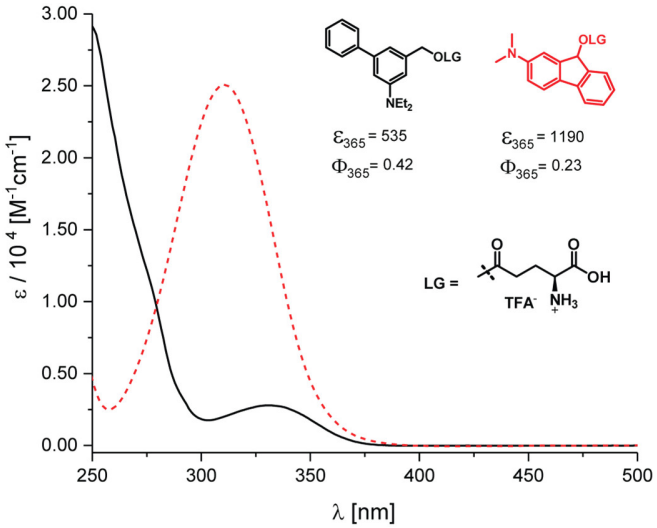

Figure 76: Molar absorption coefficient of the fluorenol derivative **167** (red, dashed) in comparison to biphenyl **148** (black). Measurements were done in 0.1M TEAA buffer (+ 20% MeCN). ***ε*** is given in M^{-1} cm^{-1}. Figure reproduced from Reinfelds, M. *et al*. *Chem. Eur. J.* **2018**, 24 (doi: 10.1002/chem.201802390) with permission; Copyright 2018 Wiley-VCH Verlag GmbH & Co. KGaA, Weinheim.

These results proved the high potential of the fluorene ring system as a basis for a photolabile protecting group. The computational methods proved to be useful in the biphenyl system, so they were also used to predict the best further substituent pattern for fluorene derivatives.

3.1.7. TDDFT computations of fluorene derivatives

To guide the synthetic work in the fluorene systems, the substituent effects were computed using TDDFT methods (see also chapter 3.1.2). The computational work was done by Jan von Cosel, Konstantin Falahati, Carsten Hamerla (group of Irene Burghardt).

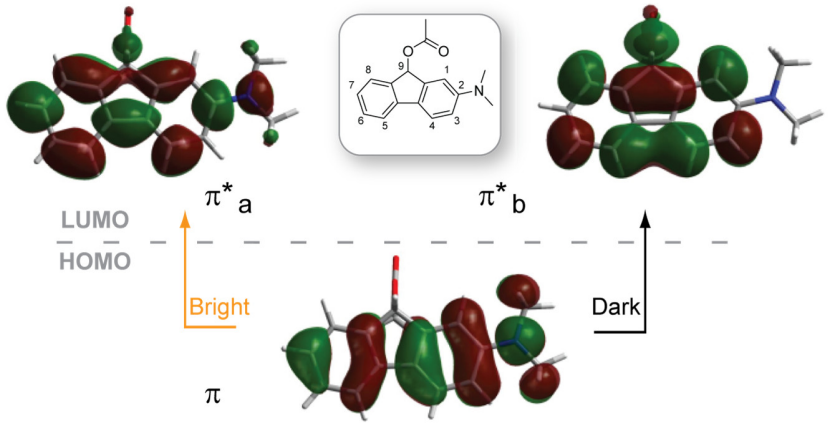

Figure 77: Frontier molecular orbitals as obtained at the TD-PBE0/Def2-TZVP level of theory. Spectroscopically dark and bright state orbital transitions are indicated. Figure reproduced from Reinfelds, M. *et al*. *Chem. Eur. J*. **2018**, 24 (doi: 10.1002/chem.201802390) with permission; Copyright 2018 Wiley-VCH Verlag GmbH & Co. KGaA, Weinheim.

The frontier molecular orbitals of the 2-dimethylamino fluorenol acetate (**168**) are shown in Figure 77. Unlike the biphenyl derivatives, no clearly recognizable meta effect (for meta effect see chapter 1.3.3) can be claimed for the fluorenes. The excited state mainly consists of two types of electronic transitions. The bright state (spectroscopically accessible state) involves orbital transition $\pi \rightarrow \pi_a^*$. The transition $\pi \rightarrow \pi_b^*$ which results in a meta effect-like orbital distribution is associated with a dark state. The energetic sequence of π_a^* and π_b^* varies with the substituent pattern, thereby this nomenclature was introduced.

In both cases a high orbital contribution can be seen on the sp^2 hybridized carbons to which the methylene bridge (C9) is attached. This is a potential prerequisite to facilitate bond cleavage in the excited state between the C9 and leaving group (in Figure 77 – acetate). Introduction of a further electron donating or withdrawing group lowers the excitation energy. However, in case of strong electron withdrawing substituents a significant charge transfer in the bright state can be seen. For example, in the 2-diethylamino-7-nitro fluorenol (Figure 78) the electron density in LUMO is significantly shifted away from the C9 atom if compared to 2-diethylamino fluorenol (Figure 77). Thereby little or no uncaging can be expected (see also Figure 60 and the discussion therein).

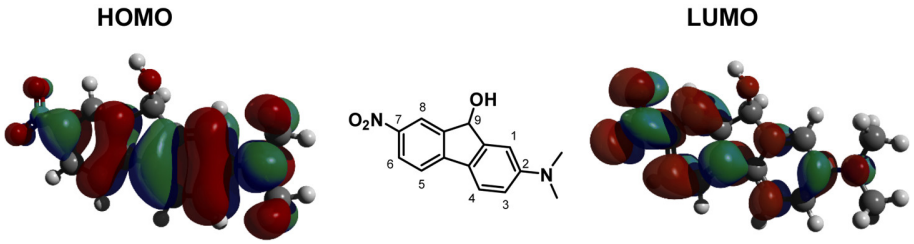

Figure 78: Frontier molecular orbitals as obtained at the TD-PBE0/Def2-TZVP level of theory. Figure produced in a collaboration with Jan von Cosel, Konstantin Falahati, Carsten Hamerla (group of Irene Burghardt).

No clear preference in terms of the favorable position of an additional electron donating group can be extracted from the computational data. Replacing 2-*N*,*N*-dialkylamino with 2-*N*,*N*-diarlyamino keeps the electron donating properties and reduces the excitation energy (for example of the HOMO-LUMO frontier molecular orbitals see appendix, Figure 145). As a result, the compounds which are synthetically easiest to access were prepared and their photochemical properties tested.

3.1.8. Synthesis of fluorene derivatives

The compound **169**, first isolated from anthracene oil in 1867 by French chemist Marcellin Berthelot (1827-1907), was named fluorene (*French*: fluoréne) due to its bright fluorescence (Figure 79). Since then that has become the name of entire class of compounds derived from **169**. The positons 2 and 7 can be directly functionalized in aromatic substitution reactions (like nitration, halogenation),[171] while the methylene bridge (C9) can be easily oxidized to yield fluorenone **170**.[172] Thus, easily commercially available are derivatives of the fluorene **169** and fluorenone **170** with substituents in the positions 2 and/or 7. The fluorenol **161** can be prepared from the keton **170** by reduction.

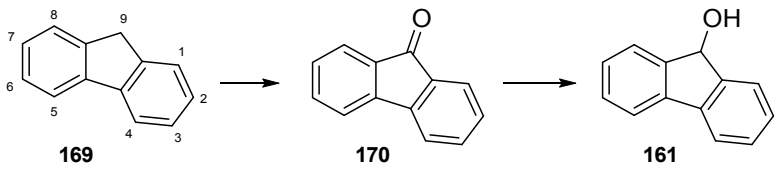

Figure 79: Fluorene **164**, fluorenone **165** and fluorenol **161**.

From the 2-bromofluorenone **171** the *N*,*N*-diarylamino fluorenones **172a-b** were prepared in a Buchwald–Hartwig amination. The yields of this reaction were below average (**172a** 35%, **172b** 22%), but no optimization was performed. The ketons **172a-b** could be reduced by NaBH4 to give alcohols **173a-b**. Upon completion of the reaction, the solution becomes colorless, thus

allowing easy determination of a full conversion. By treating the alcohols **173a-b** with Ac_2O in pyridine, the acetyl esters **174a-b** were obtained in average yields (**174a** 50%, **174b** 85%).

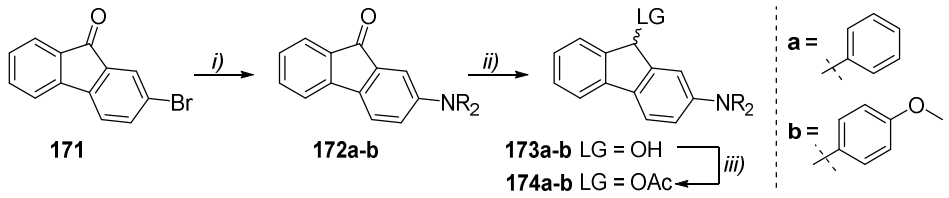

Figure 80: Synthesis of *N*,*N*-diarylamino fluorenols. Reaction conditions: *i*) HNR_2, $Pd(OAc)_2$, P^tBu_3, toluene; *ii*) $NaBH_4$, THF/EtOH *iii*) Ac_2O, pyridine;

Glutamic acid, used in the biphenyl system as a leaving group, was replaced by acetate. This was done because the glutamic acid would have to be installed for each new fluorenol derivative separately, followed by removal of the protecting groups, thus making the synthesis procedure longer.

Preparation of the diamine **176** by reduction of the 2,7-dinitrofluorenon **175** using Fe/HCl or Fe/AcOH gave low yields, in spite of full conversion of the starting material (Figure 81). A possible side reaction could be polymerization due to a condensation of the amino group with the carbonyl group (to give imine). A satisfying yield could be achieved in a Zinin reaction (where Na_2S is used as a reducing agent).[173]

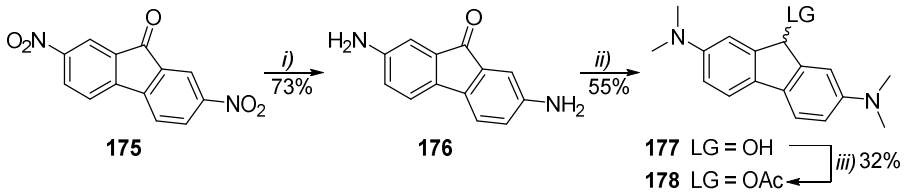

Figure 81: Synthesis of the 2,7-di-*N*,*N*-dimethyl fluorenols **177** and **178**. Reaction conditions: *i*) Na_2S, EtOH; *ii*) H_2CO, $NaBH_3CN$, AcOH; *iii*) AcCl, DIPEA, CH_2Cl_2;

The reductive amination of the keton **176** happened with a rather low yield. The obtained alcohol **177** proved to be particularly difficult to acylate using Ac_2O and pyridine. Formation of the expected product was slow and unknown side products were produced. Better results were achieved using acetyl chloride in CH_2Cl_2 with DIPEA as base. However, also in this case a full conversion could not be reached even after addition of more reagents. Yet, the yield of the compound **178** (32%) was not further optimized.

The commercially available 2,7-dibromofluorenone **179** was converted to the diamine **180** using the Buchwald–Hartwig amination (Figure 82). Also in this case the yield was low (32%).

Reduction of the keton gave the alcohol **187** and subsequent acylation resulted in the product **182** with good yields.

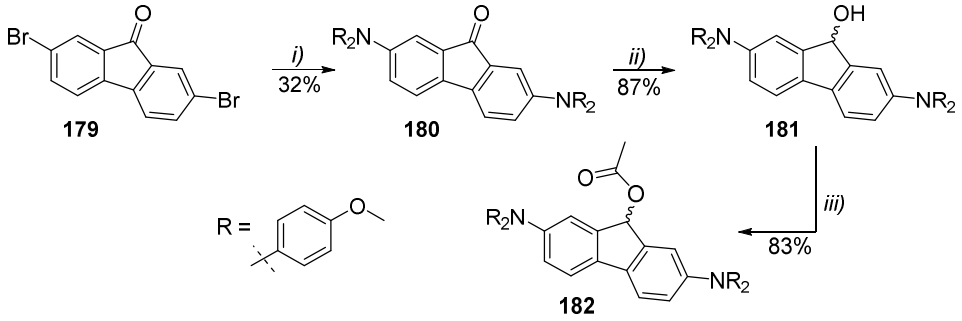

Figure 82: Synthesis of the diarylfluorenol acetate **182**. Reaction conditions: *i*) HNR_2, $Pd(OAc)_2$, P^tBu_3, toluene; *ii*) $NaBH_4$, THF/EtOH *iii*) Ac_2O, pyridine;

The bromide **183** was nitrated using HNO_3/H_2SO_4 (Figure 83). The reaction stoichiometry had to be controlled precisely because a formation of di- and tri-nitrated compound is also possible. Since the starting material has good solubility but the product **184** has low solubility in ethyl acetate, they can be easily separated from each other. Thus, the best results can be achieved by stopping the nitration reaction before the side products are formed while the starting material is still present.

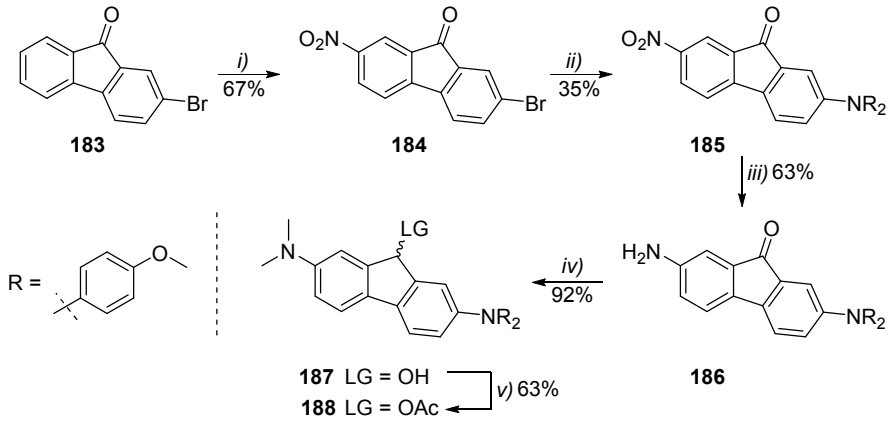

Figure 83: Synthesis of unsymmetrical diamine **188**. Reaction conditions: *i*) HNO_3, H_2SO_4; *ii*) HNR_2, $Pd(OAc)_2$, P^tBu_3, toluene; *iii*) Na_2S, EtOH; *iv*) H_2CO, $NaCNBH_3$, AcOH; *v*) Ac_2O, pyridine;

The following synthesis steps were described for other fluorene derivatives. The compound **185** was produced in a Buchwald–Hartwig amination, then reduced in a Zinin reaction to diamine **186**. In a reductive amination the carbonyl group was reduced and the amino group methylated (**187**), followed by acylation with Ac_2O in pyridine to give unsymmetrical 2,7-diamino fluorenol acetate **188**.

The commercially available bi-fluorenol **189** was converted to the diamine **190** using Buchwald–Hartwig amination (Figure 84). Also in this case the yield was low (27%). The alcohol **191** was obtained by reduction of the keton **190**. Subsequent acylation to give the product **192** proceeded with good yields.

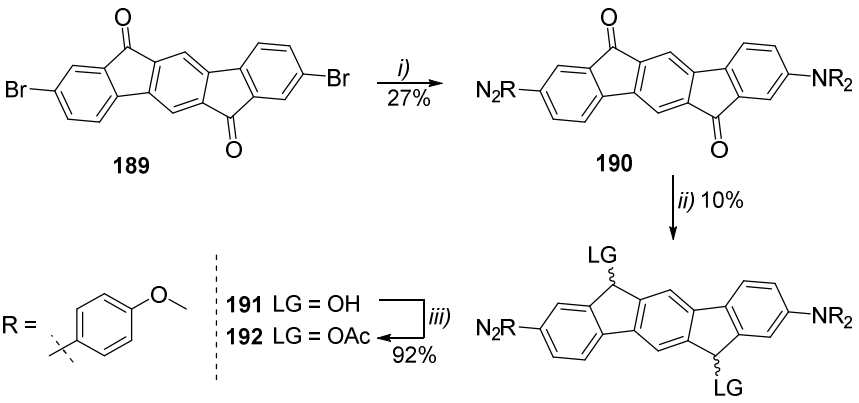

Figure 84: Synthesis of a bi-fluorene derivative **192**. Reaction conditions: *i*) HNR_2, $Pd(OAc)_2$, $PtBu_3$, toluene; *ii*) $NaBH_4$, THF/EtOH *iii*) Ac_2O, pyridine;

Due to non-stereospecific reduction of the carbonyl group by $NaBH_4$, a mixture of diastereomeric **191** (thus, after the acylation also diastereomeric **192**) was obtained. However, both diastereomers were used for photochemical characterization without a separation.

The synthesis of the fluorene derivatives turned out to be straightforward. The yields (also the low ones as in the case of Buchwald-Hartwig amination) were reproducible from compound to compound (from one substituent pattern to another).

3.1.9. Photochemical characterization of fluorene derivatives

3.1.9.1. Absorption spectra and uncaging in aqueous acetonitrile

The UV-Vis absorption spectra of the prepared fluorenol acetates are shown in Figure 85. Upon replacement of the glutamic acid leaving group with acetate, the solubility of the fluorenol photocages in highly aqueous solvents decreases. Thereby the amount of MeCN used for the measurements was increased to 90% (with 10% 0.1M TEAA buffer).

The absorption maximum of the simplest member – 2-dimethylamino fluorenol acetate (**168**) is located at 319 nm (Table 4). When the leaving group was glutamic acid (compound **167**) and the content of MeCN in the solvent only 20%, the absorption maximum was 311 nm (Figure 76). The uncaging quantum yield of acetate **168** is slightly smaller (Φ_{365}=0.15) than that of glutamate **167** (Φ_{365}=0.23), however, since also the solvent composition is different, no conclusions can be made about the influence of the leaving group on quantum yield.

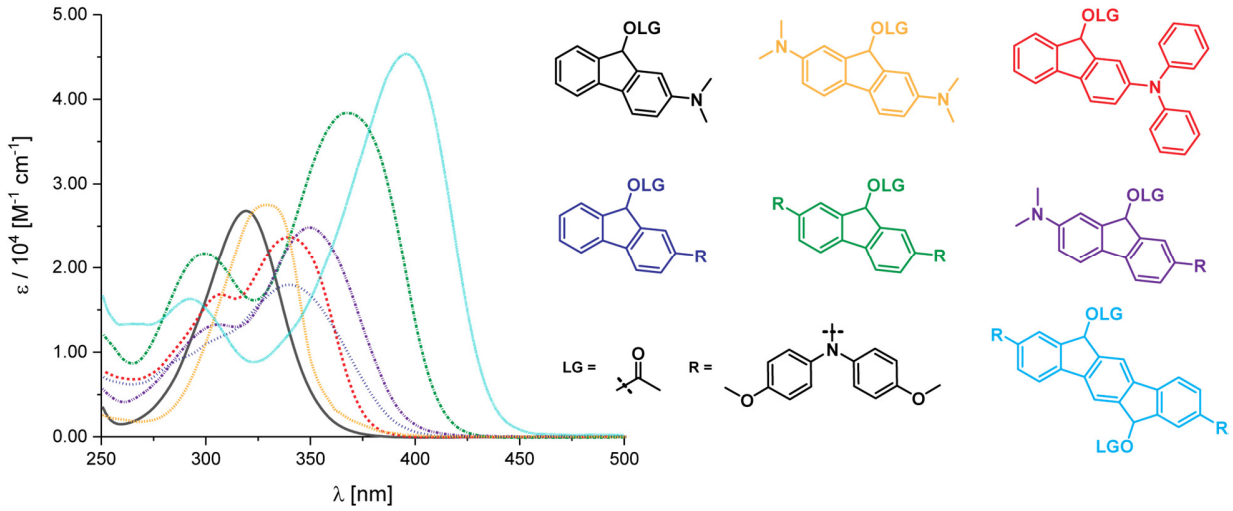

Figure 85: UV-Vis spectra of the fluorenol acetates. Measurement were done in MeCN with 10% 0.1M TEAA buffer.

Changing the methyl substituent on the amino group to phenyl (**174a**) redshifts the absorption maximum to 339 nm, but decreases the molar absorption coefficient at the maximum (Table 4). However, the molar absorption coefficient is 9 times higher at 365 nm (9077 $M^{-1}cm^{-1}$) for **174a** and 1160 $M^{-1}cm^{-1}$for **168**). In spite of a decreased uncaging quantum yield (at 365 nm) when the methyl substituent is changed to phenyl (from 15% to 2.7%), the uncaging cross section of the phenyl compound **174a** is still larger due to q higher molar absorption coefficient at the irradiation wavelength.

Expanding the *N*-aryl substituent π-electron system by additional *para*-methoxy groups (**174b**) changes the absorption maximum only by one nm (to 340 nm) in comparison to the phenyl substituted compound (**174a**). Even though the molar absorption coefficient at absorption maximum is smaller (17974 $M^{-1}cm^{-1}$ for **174b** and 23729 $M^{-1}cm^{-1}$for **174a**), the absorption peak is broader, thus the molar absorption coefficient of the compound **174b** is higher than that of the compound **174a** at 365 nm. More importantly, the uncaging quantum yield increases to 19% (365 nm) resulting in a very good uncaging cross section ($\varepsilon\Phi_{365}$= 2103 $M^{-1}cm^{-1}$). This increase of the uncaging quantum yield can be explained by the two additional methoxy groups, which make the *para*-methoxyphenyl substituent a stronger electron donor than the simple phenyl.[174]

The large influence of the π-electron density in the aromatic ring on the uncaging quantum yield can be seen, when a second diethylamino group is introduced (**178**). The absorption maximum of this compound is shifted by 10 nm (to 329 nm) when compared to the monosubstituted analogue **168**. Thereby also at 365 the molar absorption coefficient is higher (2635 $M^{-1}cm^{-1}$for **178** and 1160 $M^{-1}cm^{-1}$ for **168**) while the uncaging quantum yield is nearly three times higher (42%).

Expanding the π-electron system by replacing the methyl substituents of the amino group in compound **178** with *para*-methoxyphenyl (**182**) shifts the tail of the longest wavelength absorption band to the visible and increases the molar absorption coefficient at 365 nm to 38201 $M^{-1}cm^{-1}$. Thereby, even though the uncaging quantum yield is smaller (10%) than for the similarly substituted compound **178**, the uncaging cross section is three times larger ($\varepsilon\Phi_{365}$= 3820 $M^{-1}cm^{-1}$for **182** and $\varepsilon\Phi_{365}$= 1107 $M^{-1}cm^{-1}$for **178**).

Elongating the aromatic conjugation with one more six membered ring (**192**) shifts the absorption maximum to 396 nm and increases the molar absorption coefficient to 45370 M^{-1} cm^{-1}. The uncaging quantum yield of this compound was 18%.

The unsymmetrical 2-dimethylamino-7-(bis(*para*-methoxyphenyl)amino) fluorenol acetate **188** combines the expanded π-electron system in one side with the stronger electron donating abilities of the dimethylamino group on the other side. This combination indeed is profitable, because the molar absorption coefficient at 365 nm is high (ε_{365}= 19702 $M^{-1}cm^{-1}$) just as the uncaging quantum yield at 365 nm (27%) is. As a result, this compound has the highest uncaging cross section ($\varepsilon\Phi_{365}$= 5320 $M^{-1}cm^{-1}$) of all prepared fluorenol derivatives.

The excitation energy, computed by TDDFT (see chapter 3.1.7) is in a good agreement with the experimental values (Table 4). As previously described, the spectroscopically bright transition is the $\pi \rightarrow \pi_a^*$, thus when this is the dominant transition upon excitation the oscillator strength is large. However, depending on the substituent pattern, this can be $S_0 \rightarrow S_1$or $S_0 \rightarrow S_2$tranistion.

Table 4: The photochemical properties of fluorene derivatives. Table with modifications reproduced from Reinfelds, M. *et al. Chem. Eur. J.* **2018**, 24 (doi: 10.1002/chem.201802390) with permission; Copyright 2018 Wiley-VCH Verlag GmbH & Co. KGaA, Weinheim.

	Computational data[a]						Experimental data[b]				
	S_1			**S_2**							
Compound	Excitation energy (nm)	Oscillator strength	Orbital transition	Excitation energy (nm)	Oscillator Strength	Orbital transition	λ_{max}[c] (nm)	$\varepsilon\lambda_{max}$ ($M^{-1}cm^{-1}$)	ε_{365} ($M^{-1}cm^{-1}$)	Φ_{365} (%)	$\varepsilon\Phi_{365}$[d] ($M^{-1}cm^{-1}$)
167	n.d.[e]	n.d.	n.d.	n.d.	n.d.	n.d.	311[f]	24150[f]	1190[f]	23[f]	274[f]
168	325	0.0076	0.163 $\pi \rightarrow \pi_a^*$ 0.676 $\pi \rightarrow \pi_b^*$	305	0.5862	0.677 $\pi \rightarrow \pi_a^*$ -0.155 $\pi \rightarrow \pi_b^*$	319	26805	1160	15	174
174a	365	0.5438	0.688 $\pi \rightarrow \pi_a^*$ 0.123 $\pi \rightarrow \pi_b^*$	351	0.0337	-0.121 $\pi \rightarrow \pi_a^*$ 0.667 $\pi \rightarrow \pi_b^*$	339	23729	9077	2.7	245
174b	371	0.0358	-0.178 $\pi \rightarrow \pi_a^*$ 0.666 $\pi \rightarrow \pi_b^*$	365	0.5724	0.675 $\pi \rightarrow \pi_a^*$ 0.182 $\pi \rightarrow \pi_b^*$	340	17974	11069	19	2103
178	355	0.0001	0.085 $\pi \rightarrow \pi_a^*$ 0.694 $\pi \rightarrow \pi_b^*$	315	0.8694	0.694 $\pi \rightarrow \pi_a^*$ -0.079 $\pi \rightarrow \pi_b^*$	329	27523	2635	**42**	1107
182	399	0.0185	-0.227 $\pi \rightarrow \pi_a^*$ 0.651 $\pi \rightarrow \pi_b^*$	394	1.1145	0.658 $\pi \rightarrow \pi_a^*$ 0.233 $\pi \rightarrow \pi_b^*$	369	38359	38201	10	3820
188	387	0.0069	0.170 $\pi \rightarrow \pi_a^*$ 0.673 $\pi \rightarrow \pi_b^*$	365	0.8194	0.676 $\pi \rightarrow \pi_a^*$ -0.161 $\pi \rightarrow \pi_b^*$	349	24848	19702	27	**5320**
192	n.d.	n.d.	n.d.	n.d.	n.d.	n.d.	396	45370	25400	18	4572

[a] Obtained TD-PBE0/Def2-TZVP level of theory. [b] Measurements were done in MeCN with 10% 0.1M TEAA buffer. [c] The value of the longest wavelength absorbance band (S_0-S_1 transition). [d] Uncaging cross section. [e] Not determined. [f] Measurements were done in 0.1M TEAA buffer with 20% MeCN.

3.1.9.2. Solvatochromic experiments

A shift of the absorption maximum to longer wavelengths was observed when the glutamic acid leaving group of the fluorenol (**167**) was replaced by acetate (**167**) and the content of MeCN in the solvent system was increased from 20% to 90%. To further investigate the effect of the solvent to the absorption maximum, the fluorenol alcohols **165** and **181** were measured in different solvents (Figure 86).

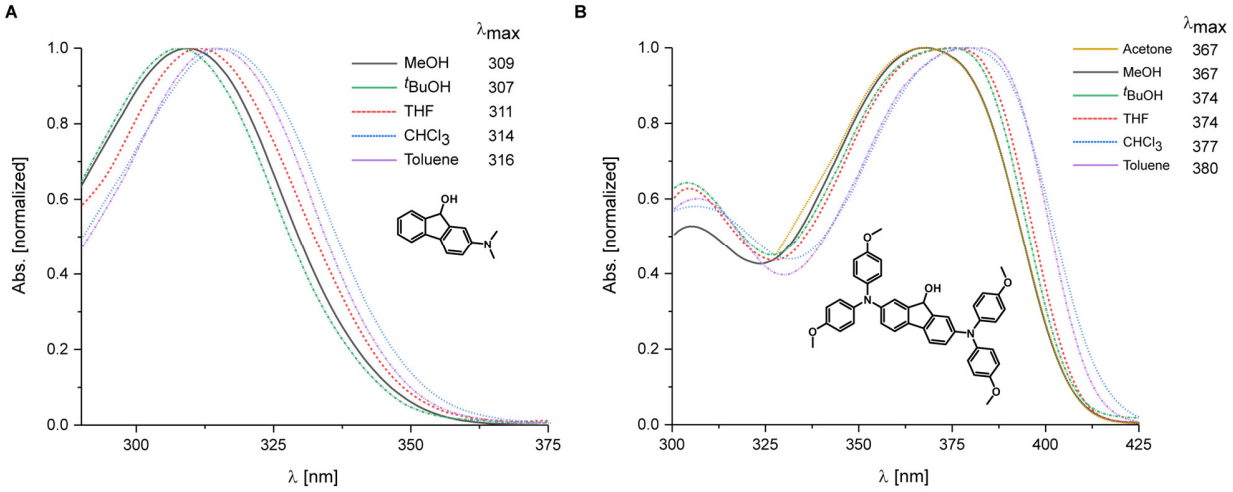

Figure 86: Solvatochromic study of the fluorenol alcohol **165** (panel A) and fluorenol alcohol **181** (panel B).

The absorption maximum of both alcohols is shifted to longer wavelengths in unpolar solvents like toluene or chloroform. Although the absorption shift is not large, a negative solvatochromism can be recognized when polar solvents such as methanol are used. In an H-bond donating solvents a zwitterionic ground state structure of 2-dimethylamino fluorenol **165** with a partially positive charge on the nitrogen atom and negative on the hydroxy group has been suggested.[175] However, the compound **181** has the same absorption maximum in acetone and methanol (367 nm), thus suggesting hydrogen boding to not be the only factor influencing the solvent-solute interactions.

The molar absorption coefficient of the fluorenol acetate **182** in methanol does not differ significantly from the value obtained in MeCN (+10% 0.1M TEAA buffer) as can be seen in Figure 87A. But the molar absorption coefficient value decreases (Figure 87B, green) if the acetate group in the compound **182** is replaced by a hydroxy one (compound **181**). Curiously, the opposite is true for the compound **177**, which has a larger molar absorption coefficient in methanol (Figure 87B, blue) when compared to the corresponding acetate **178** in MeCN with 10% 0.1M TEAA buffer (see Figure 85), while no significant changes can be seen for the monosubstituted fluorenol alcohol

165 (Figure 87B, black) when it is compared to the acetate in MeCN with 10% 0.1M TEAA buffer (see Figure 85). Please see Table 5 in Chapter 3.1.9.3 for the molar absorption coefficient values.

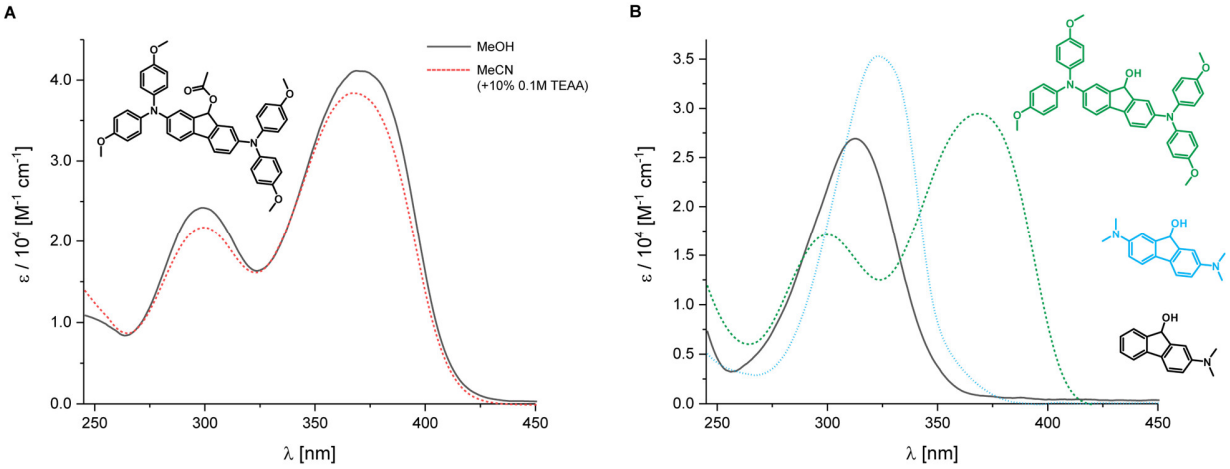

Figure 87: *A* - Molar absorption coefficients of the fluorenol acetate **182** in MeOH and MeCN + 10% 0.1M TEAA buffer; *B* - Molar absorption coefficients of the fluorenols **165**, **177** and **182** in MeOH.

3.1.9.3. The products of the irradiation

It is expected that irradiation of fluorenol esters **167-168** in water containing solvent would yield the fluorenol **165** (Figure 88). And indeed, the irradiation of the fluorenol glutamate **167** results in generation of one photoproduct (Figure 89A). By using ^{1}H NMR spectroscopy this was confirmed to be the fluorenol alcohol **165**. Also the release of the glutamic acid (see appendix, Figure 147) could be shown. The same product is formed when the fluorenol acetate **168** is irradiated (see appendix, Figure 148).

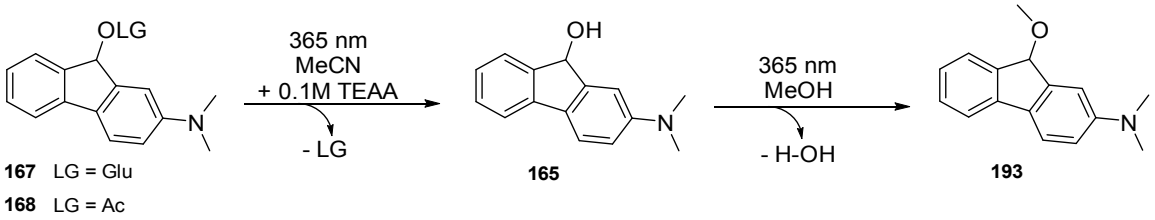

Figure 88: Irradiation reaction of the 2-dimethylaminofluorenol derivatives.

It is known that the fluoren-9-ol (**161**) produces a fluorenyl carbocation upon irradiation (see chapter 3.1.5).[167] In order to test whether the same behavior can be seen also for substituted fluorenols, the compound **165** was irradiated in methanol. Trapping of the photochemically generated fluorenyl carbocation by methanol should result in a generation of the methyl ether **193**.

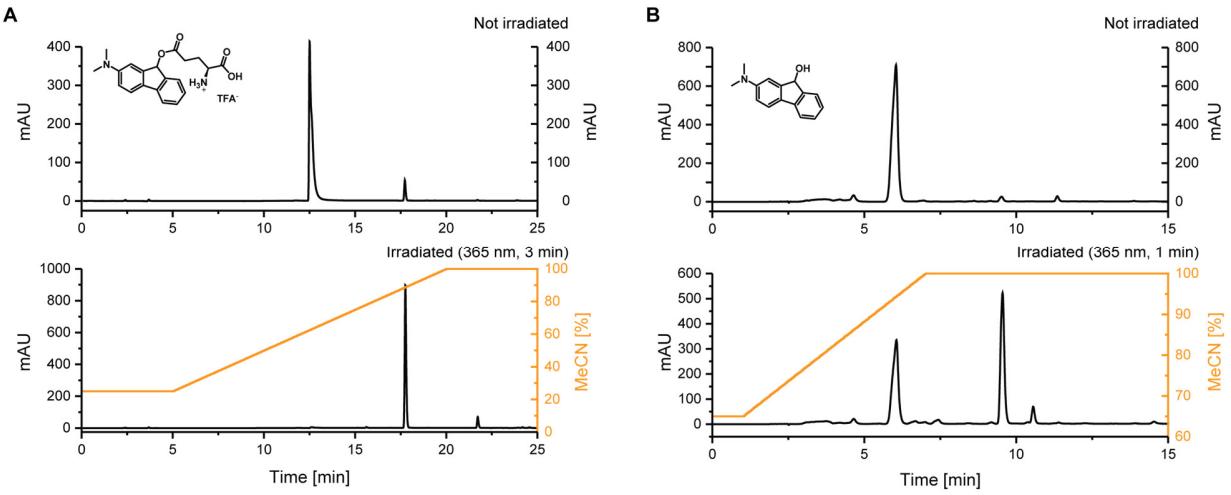

Figure 89: HPLC (traces at 310 nm) before and after irradiation of the fluorenol glutamic ester (**167**) in 0.1M TEAA (+20% MeCN). The irradiation power (LED 365 nm) was ca. 20 mW, solution absorbance ca. 0.04, volume - 1.5 mL and concentration ca. 0.03 mM. Figure' s panel A with modifications reproduced from Reinfelds, M. *et al. Chem. Eur. J.* **2018**, 24 (doi: 10.1002/chem.201802390) with permission; Copyright 2018 Wiley-VCH Verlag GmbH & Co. KGaA, Weinheim.

The irradiation of **165** in MeOH is shown in Figure 89B. Formation of a new product with a later elution time can be seen, suggesting that the methyl ether **193** might indeed have been formed. The quantum yield of this reaction was determined to be 28% (Table 5).

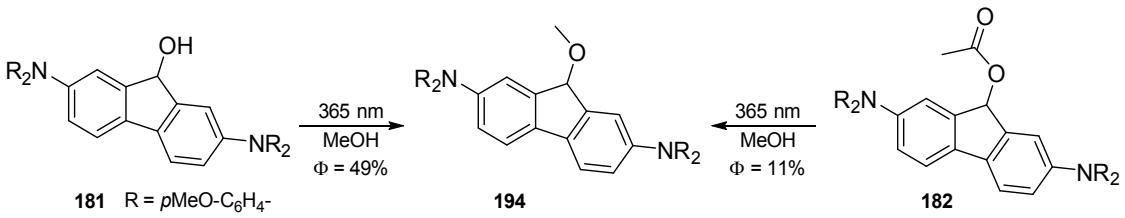

Figure 90: The photoreaction of fluorenol **181** and its acetate **182** in methanol.

Irradiation of fluorenol alcohol **181** in methanol (Figure 90) follows the same behavior, producing a product with a later elution time (Figure 91A-B, blue labeled peak eluting at 14.05 min) with a 49% quantum yield. Irradiation of the acetate **182** in methanol results in a formation of the same product (Figure 91D, blue labeled peak eluting at 14.05) but with a smaller quantum yield (11%). These observations suggest fluorenyl carbocation formation upon irradiation of fluorenol, which then is trapped by a solvent.

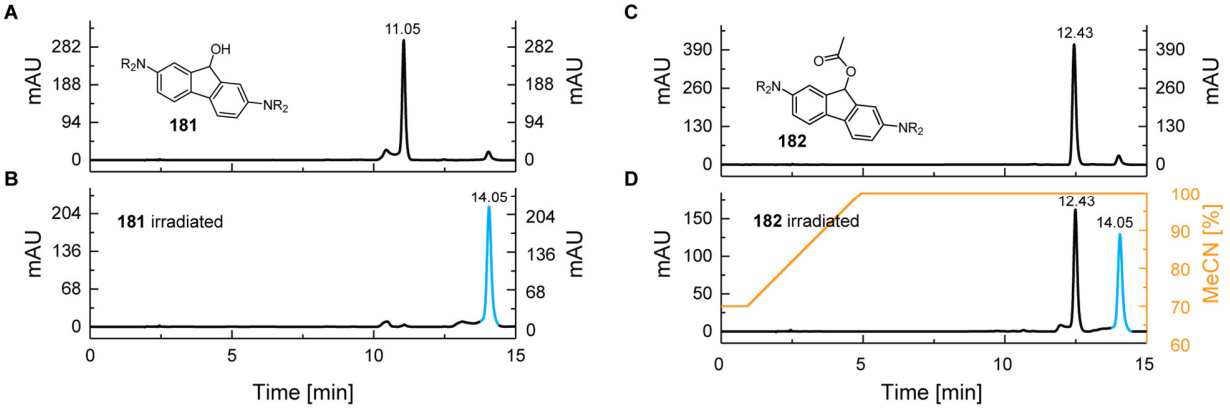

Figure 91: Irradiation of the fluorenol acetate **182** and fluorenol **181** in methanol.

A similar quantum yield was obtained, when compound **182** was irradiated in aqueous MeCN (Table 4), but as the primary photoproduct, the alcohol **181** was produced (see appendix, Figure 149). If the alcohol **181** was irradiated in these conditions, secondary photoproducts were formed, from which only the fluorenone **180** could be assigned.

Table 5: Photochemical properties of fluorene derivatives II.

Compound Nr.	Solvent	λ_{max} (nm)	$\varepsilon\lambda_{max}$ ($M^{-1}cm^{-1}$)	ε_{365} ($M^{-1}cm^{-1}$)	Φ_{365} (%)	$\varepsilon\Phi_{365}$[b] ($M^{-1}cm^{-1}$)
182[a]	MeCN	369	38359	38201	10	3820
182	MeOH	368	41155	40369	11	4440
181	MeOH	368	29462	29322	**49**	**14368**
165	MeOH	312	26913	967	28	270
177	MeOH	322	35310	2491	67	1669

[a] Measurements were done in MeCN (+10% 0.1M TEAA buffer). [b] Uncaging cross section.

Also the fluorenol acetate **192** with the elongated π-system was photoactive in methanol, upon irradiation producing products with later elution time (data not shown), similarly to the compound **57** in methanol.

The photoactivity of the compound **192** was tested also in an aqueous MeCN solution. The compound consists of a mixture of two diastereomers which were analyzed together. The uncaging reaction should first generate a diastereomeric mixture of mono-uncaged compound **195**, which upon longer irradiation should yield the completely uncaged product **196** (Figure 92).

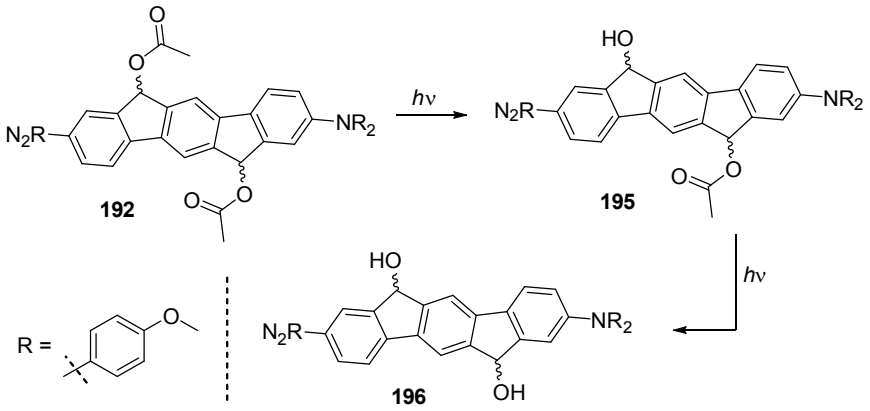

Figure 92: Uncaging reaction of the biflurenonol **192**.

The HPLC analysis of the irradiation is shown in Figure 93. As expected, a set of two signals can be seen at 27 and 29 min, rising from the two diastereomers of the compound **192** (Figure 93A, upper panel). Upon irradiation, new signals with faster elution time (min 16 and 18) are generated (Figure 93A, middle panel, red). Mono-uncaged products **195** also undergoes photoreaction, to give a set of two news peaks (min 9 and 14) which probably are the diastereomers of the compound **196**. The change of the peak area in HPLC during irradiation is shown in Figure 93B. A graph, typical for multi-step reactions ($A \rightarrow B \rightarrow C$) can be seen, thus suggesting that reaction follows the suggested pathway.

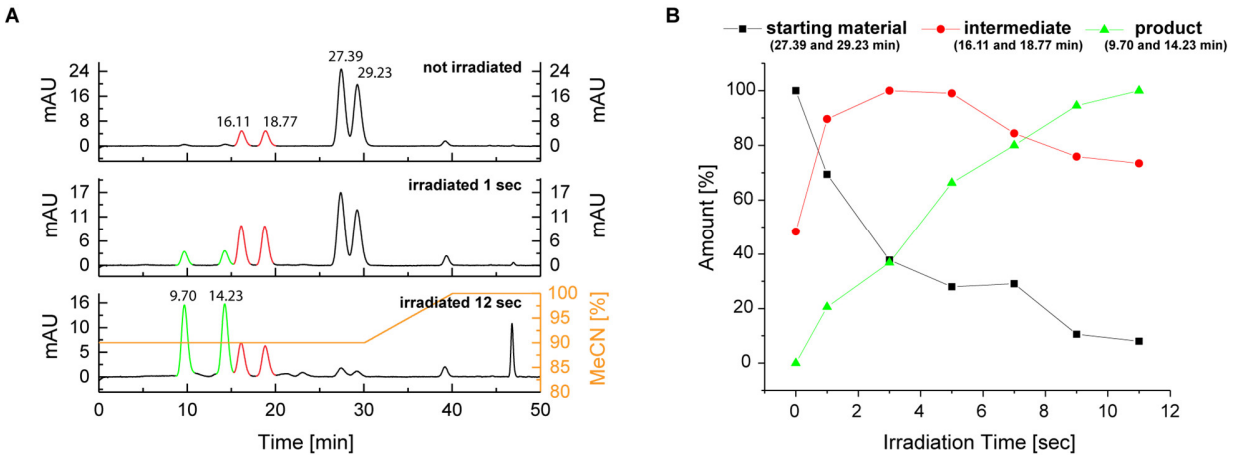

Figure 93: Irradiation of the compound **192**. *A* – HPLC analysis before (top panel) and after irradiation (1 sec – middle panel, 12 sec – lower panel). *B* – The change of the peak area in the HPLC chromatograms during the photoreaction.

During irradiation of compound **181** in methanol, a new absorption band is formed. It absorbs light with longer wavelengths than the starting material (Figure 94). A similar band is formed if a 0.1M HCl is added to the solution of the compound **181** (without irradiation), suggesting formation of a fluorenyl cation.

In ground state the fluorenyl carbocation is antiaromatic and very acidic conditions are necessary for its quantitative generation from the corresponding alcohol.[176] Nevertheless, the production of a fluorenol methyl ether in an acid catalyzed S_N1 reaction between fluorenol and methanol has been shown.[177] The reactions has small rate constants ($10^{-5}\ s^{-1}$), thus the concentration of fluorenyl cation generated per time should be small. These data are in agreement with the small intensity of the new absorption band observed upon addition of an acid to the fluorenol **181**. The absorption intensity of the photochemically generated fluorenyl cation also is small. Thus, either it is generated in a small extend or is fast quenched by methanol. The photoreactions high quantum yield (Φ_{365} = 49%, Table 5) suggests the latter.

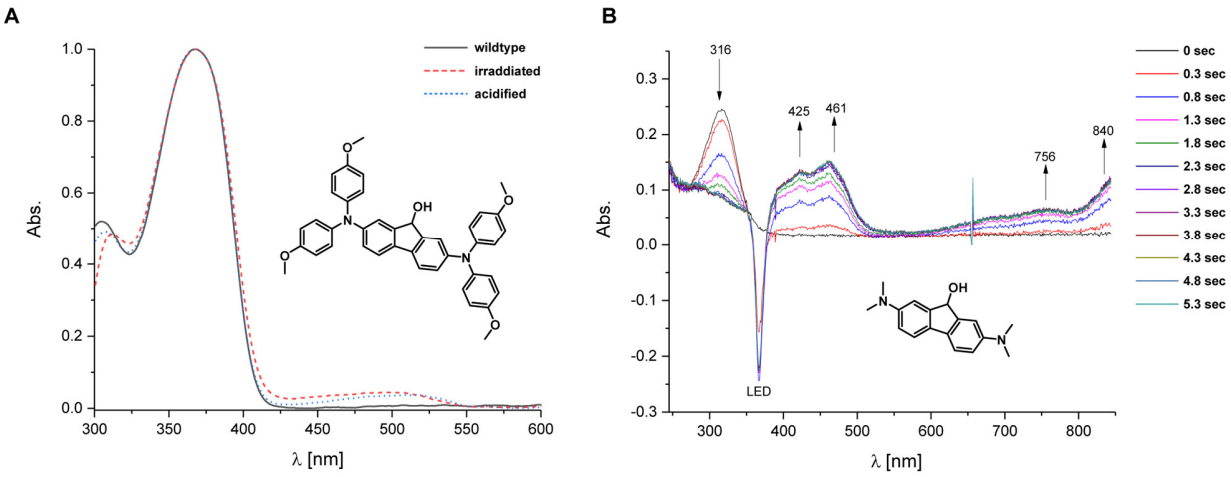

Figure 94: Irradiation of the fluorenol alcohols to give long lived intermediates.

The 2,7-dimethylamino fluorenol **177** in methanol behaves similarly. Upon irradiation a new redshifted absorption band is produced and the product of the photoreaction is fluorenol methyl ether (see appendix, Figure 150). The quantum yield of the reaction was determined to be high (Φ_{365} = 67%, Table 5). Formation of a methyl ether could be shown by mass spectrometry.

If a saturated water solution of the fluorenol **177** is irradiated, multiple new absorption bands are generated (Figure 94B) with wavelengths centered at 425, 461, 756 and 840 nm. All of these bands reach their maximal intensity and also decay with the same rate (see the Figure 95A) indicating that they origin from the same species.

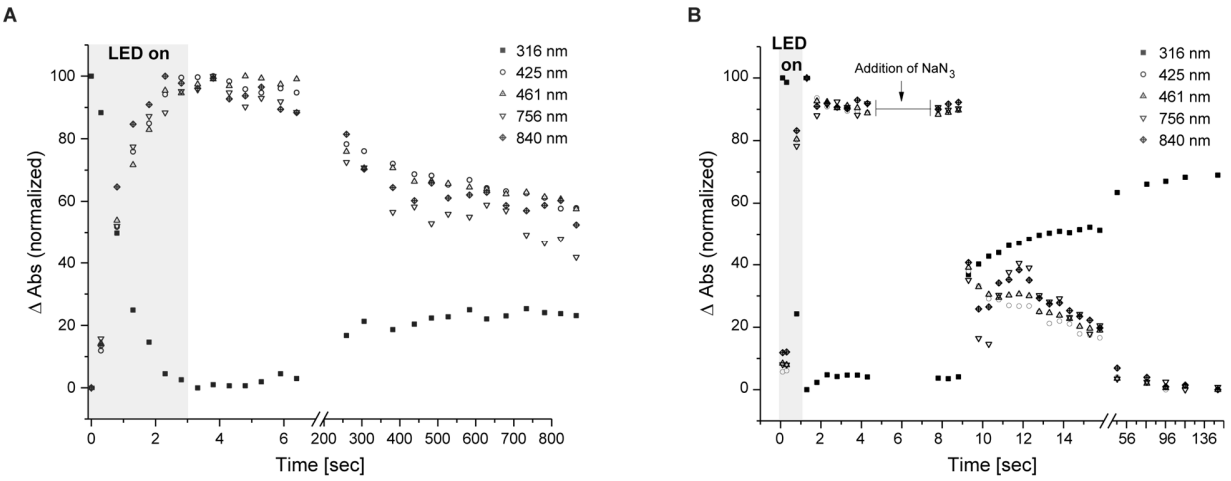

Figure 95: *A* – The absorption change at indicated wavelentghts upon irradiation of the fluorenol **177** in water; *B* – quenching of the irradiated flurenol **177** with sodium azide.

Formation of fluorenyl cation upon irradiation of unsubstituted fluorenol in polar solvents is well studied and the lifetime of this cation was determined to be in a ps time scale.[167,178] But the transition observed after irradiation of the substituted fluorenol **177** is in a minute or possibly even hour range in non-buffered water with 20% MeCN (see Figure 95A). This suggests that the amino substituents in compound **177** have a stabilizing effect on the cationic intermediate, probably by forming a quinone methide-like structure **197** (Figure 96) as has been observed upon irradiation of hydroxy substituted fluorenes.[169,179]

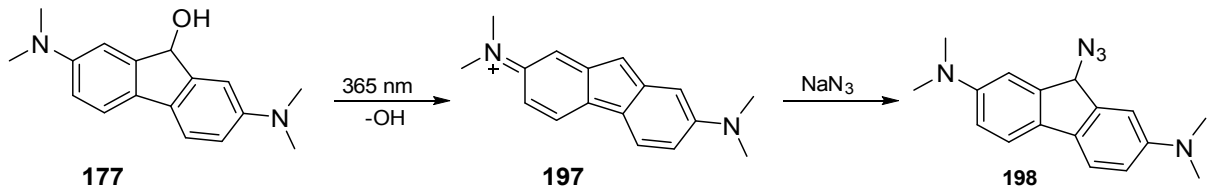

Figure 96: Flurenyl cation stabilization by formaton of a quinone methide-like structure **197** and further quenching of it using NaN_3.

A nucleophilic addition of inorganic anions to the photochemically generated 9-aryl-fluorenyl cation has been demonstrated to have large rate constants,[180] thus a quenching test of the cationic intermediate **197** with a nucleophile was performed. To that end, an irradiated mixture of **177** (in water with 20% MeCN) was mixed with NaX (X = -Cl; -I; $-N_3$). The fastest effect could be seen if sodium azide was added, in agreement with literature.[180] The absorption bands in the visible range decrease their intensity (Figure 95B) while the absorption at 316 nm again increases, however not reaching the intensity before irradiation (see also Figure 97A). Formation of a new

peak could be seen by HPLC analysis (Figure 97B) but the mass spectral analysis of the peak, eluting at 14.91, was not successful.

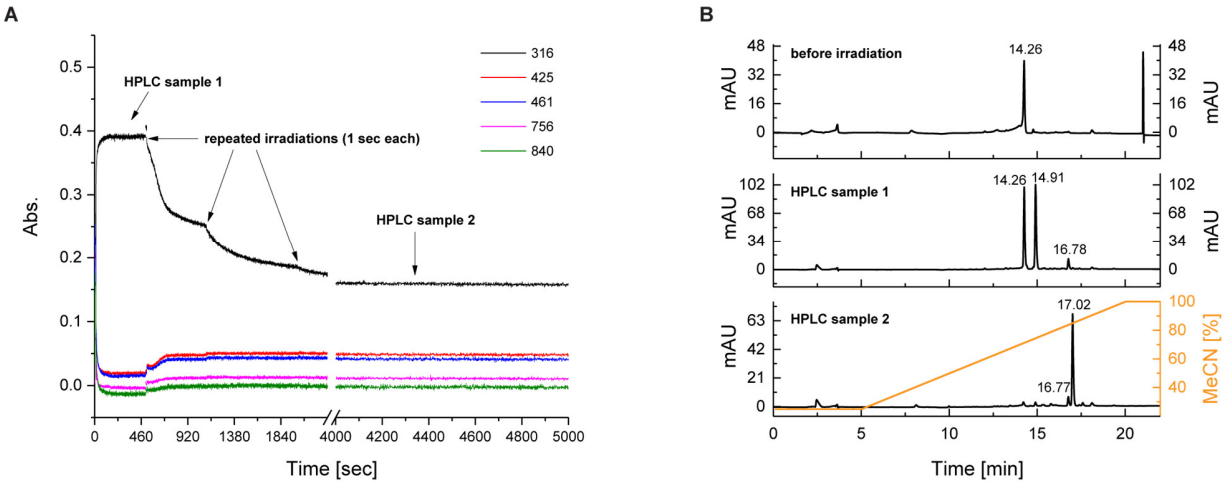

Figure 97: *A* – The absorption intensity change at indicated wavelentghts upon irradiation of the fluorenol **177** (in water) and quenching with sodium azide; *B* – HPLC analysis of the starting material (**177**) and irradiated mixture.

If short irradiation was repeated, the absorption at 316 nm decreased (Figure 97A). Interestingly, the absorption kept decreasing also after the irradiation, thus suggesting a thermal dark-reaction. The HPLC analysis of the three times irradiated sample (each irradiation was 1 s) showed complete transformation of the starting material and also of the primary photoproduct into a secondary photoproduct whose structure was not determined.

The detection of a long-lived intermediate formed upon irradiation of the fluorenol **177** and its successful quenching are very intriguing results and might be used for the photochemical generation of electrophiles. It could have an application, for example, in photoinduced protein labeling.[181]

3.1.10. Origins of the photoactivity observed for fluorenol derivatives, a discussion

Wan and Krogh reported in 1985 the solvolysis of fluren-9-ol in methanolic solution upon irradiation and production of methyl ether. They suggested formation of an aromatic cationic system in the excited state as the driving force of the photoreaction.[182] In a follow up study, it was demonstrated that fluorenol (**161**), which forms a cation with $4n$ π-electrons (**161a**) undergoes efficient photolysis (Figure 98). The compound **199**, which would form a cation with $2+4n$ π-electrons (**199a**) did not photolyse, and neither did the diphenylmethanol **200** which would form the noncyclic but conjugation-stabilized benzyl cation **200a**. However, in the ground state the observed reactivity was opposite - methyl ethers **199b** and **200b** could be produced in an acid

catalyzed reaction while fluorenol **161** in such conditions was stable. The authors concluded that generation of a cation with 4n π-electrons in the excited state promotes the photoreaction. [183]

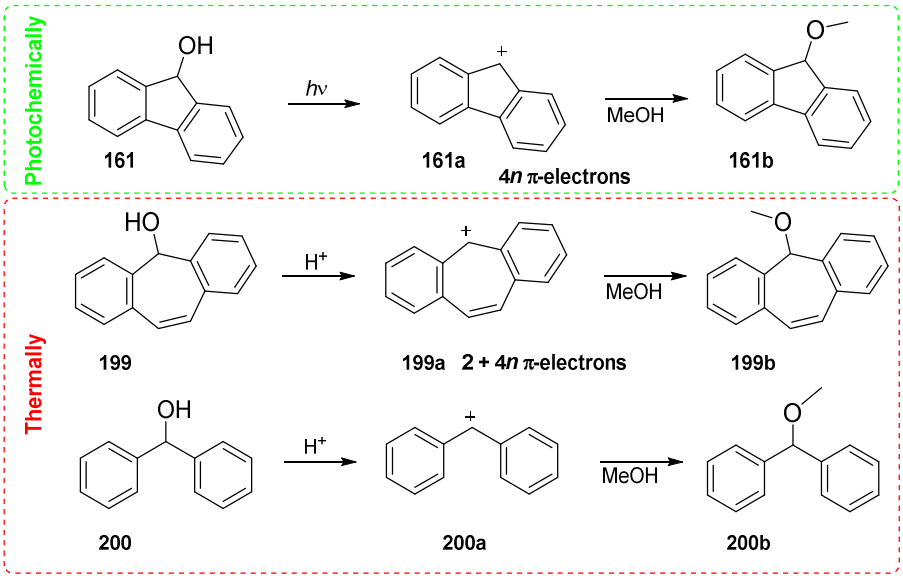

Figure 98: The photochemical and thermal methyl ether generation from structurally similar alcohols **161**, **199** and **200**.

The Hückel molecular orbital theory, which was developed in the 1930s, states that 2+4*n* π-electron annulenes are aromatic (stabilized) in ground state, while 4*n* π-electron annulenes are antiaromatic (destabilized). During the later development of the molecular orbital theory, the mirror-image relationship between the stabilization and destabilization energies of π-electrons in the excited state was shown. This effect is now known as Baird´s rule (originally Baird showed it for $\pi\pi^*$ excited triplet states, however, later it was expanded also for excited singlet states). For a more detailed discussion the reader is directed to literature.[184] The most important is the conclusion that cation **161a** in the excited state is stabilized (aromatic) due to its 4*n* π-electronic structure, thus its formation would be favorable as suggested by Wan and Krogh in 1985.

For the sake of discussion, a very simplified schematic example of the 2D potential energy surfaces for the fluorenol (**Fl-LG**) are shown in Figure 99. Excitation of a molecule leads to its Frank-Condon excited singlet state (**Fl-LG***), from which the molecule will search for a path leading to an excited singlet state energy minimum. The aromatic stabilization of the fluorenyl cation in its excited state (**Fl^{+}***) could potentially favor its generation. The energetic minima of the excited state potential surface can be located close to ground state energetic maxima (the both surfaces can cross or nearly cross). In these places the excited molecule can undergo internal conversion to the ground state *via*, for example, conical intersections.[185] Thus, a ground state

fluorenyl cation (**Fl**$^+$) could be generated in spite of the high energetic barrier of its generation in thermal reactions.

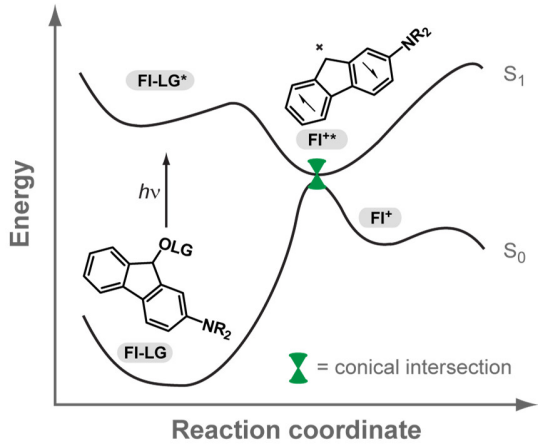

Figure 99: Schematic representation of 2D potential energy surfaces for the photoreaction of 2-amino substituted fluorene derivatrives.

Such nonadiabatic reaction usually happens very fast and no intermediates can be observed.[186] The ultrafast generation of the fluorenyl cation from the fluorenol alcohol upon irradiation in water within the first 10 ps fits to this criteria.[167] Also computational data suggests that the fluorenol cation has a low-energy conical intersection.[76]

In summary, the photoactivity of the fluorenol could be explained as follows: the aromatic stabilization of 4*n* π-electron annulenes in the excited state favor the generation of fluorenyl cation (resulting in a leaving group release), which undergoes rapid intersystem crossing *via* a conical intersection to a high energy ground state cation, which is then available for further reactions with nucleophiles.

3.1.11. Summary and outlook of the fluorene derivatives

The fluorenol derivatives were chosen as the second generation of DEAMb derived photocages because of their structural similarity to biphenyl compounds. However, the linkage of the second aromatic ring to the benzylic carbon by a single bond makes the fluorenes planar. Fluorenol photoactivity has already been demonstrated in literature. The 2-dimethylamino substituted fluorenol had improved spectral properties when compared to the best biphenyl compound, without losing the good uncaging quantum yield for glutamic acid release. The uncaging cross section was slightly better than that of the best biphenyl derivative ($\varepsilon\Phi_{365}$ = 274 $M^{-1}cm^{-1}$). The release of glutamic acid was demonstrated by ^{1}H NMR.

TDDFT computations indicated that further substitution of the fluorenol aromatic ring with electron donating or accepting groups would decrease excitation energy. However, similar to the biphenyls, introduction of a strong electron withdrawing group results in a charge transfer character in the excited state, which is orthogonal to bond cleavage between the atom C(9) and the LG. Thus, only compounds with electron donating substituents were prepared.

Synthesis was done from commercially available starting materials and was straightforward. However, some steps had low yields (especially Buchwald-Hartwig amination). In order to reduce synthesis time, acetate was used as the leaving group.

Due to the unpolar nature of the fluorenols bearing an acetate leaving group, the solvent system used for photochemical characterization was changed to MeCN (with 10% 0.1M TEAA). The molar absorption coefficients of the longest wavelength absorption band of the prepared fluorenol derivatives were significantly higher than those of biphenyl compounds. The uncaging quantum yields of the fluorenol acetates were between 2-42% (at 365 nm). In combination with the high molar absorption coefficients, very good uncaging cross section values were obtained (up to 5300 $M^{-1}cm^{-1}$) while neither of the compounds had an uncaging cross section below 170 $M^{-1}cm^{-1}$.

Fluorenol alcohol was detected as the primary photoproduct when the corresponding acetates were irradiated in aqueous acetonitrile. If the reaction was performed in methanol, another photoproduct was generated. The same photoproduct arises if the corresponding fluorenol alcohol was irradiated in methanol, thus suggesting formation of fluorenol methyl ether. In case of fluorenols, this can be considered as a release of the hydroxy group. Further studies of the uncaging reaction suggested a formation of long-fluorenol cation, which could be trapped not only by solvent, but also by inorganic nucleophiles such as sodium azide. These results open up the road to further explore this interesting reactivity by kinetic, spectroscopic and theoretical studies.

3.2. The vibrationally promoted electronic resonance (VIPER) experiments.

3.2.1. Synthesis of the coumarin derivatives

For the VIPER experiments coumarin and *p*-hydroxyphenyacyl (*p*HP) derived photocages were chosen. The VIPER pulse sequence (see Chapter 1.4) was first demonstrated on coumarin laser dye coumarin-6, thereby structurally similar coumarin photocage – DEACM was selected as a first candidate.[151]

Computational predictions were done (by Jan von Cosel, group of Irene Burghardt and Carsten Neumann, group of Jens Bredenbeck) to determine which vibrational modes are most suitable for pre-excitation in a VIPER pulse sequence. Those bands should be well separated in IR spectra and their absorption cross section should be large. Besides, they should be coupled to the electronic transition of the molecule. For the DEACM photocage the C=O stretch mode and two ring distortion modes have been selected as most suitable, a particularly large effect being shown by the lower frequency ring mode.[187] Thus, two positions of 7-diethylamino coumarin azide were chosen for synthesis - the position 4 and position 2 (**201**-**202**, Figure 100). Besides the ^{13}C labeled molecules, also non-labeled coumarin derivatives bearing IR active leaving groups (**203**-**205**) were designated for synthesis.

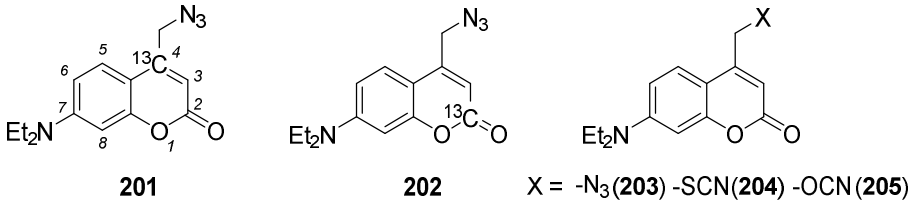

Figure 100: The structures of coumarine derivatives with an IR active leaving group.

The compounds **201**-**205** can be prepared from the coumarin alcohol **206**, which in turn can be prepared by oxidation of the α-methyl group of coumarin **207** (Figure 101) using literature known methods.[188]

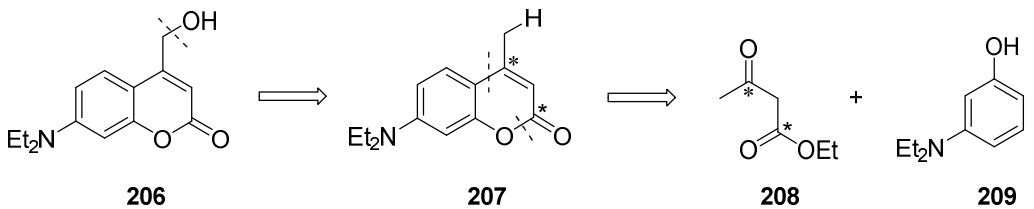

Figure 101: Retrosynthetic analysis of coumarin alcohol **206**.

The coumarin ring system can be built in a well-known Pechmann condensation reaction between ethylacetoacetate (**208**) and 3-diethylamino phenol (**209**). The ^{13}C label can be incorporated in the coumarin ring in this step by using ethylacetoacetate containing ^{13}C label.

It is believed that the first step in the Pechmann condensation reaction is transesterification of the ethyl acetoacetate **208** by phenol **209** to give the β-ketoester **210a** (Figure 102). After an intramolecular conjugated addition the cyclized molecule **210b** is formed which rearomatizes into **210c**. After elimination of water the coumarin **207** is produced. The exact order of the reactions steps stays unknown[189] and probably is substrate and catalyst dependent.[190] But the key steps in this reaction are acid catalyzed, so the choice of an acid is crucial.

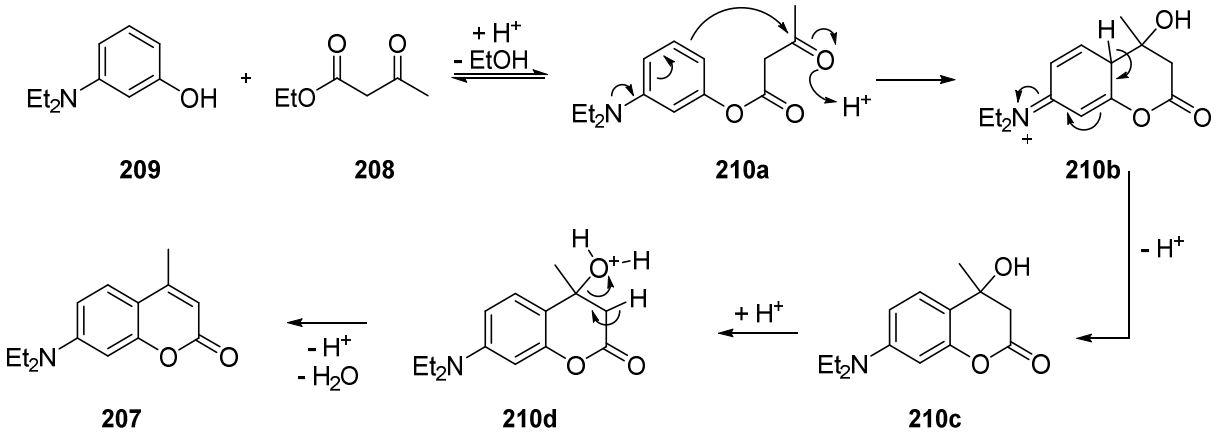

Figure 102: The plausible mechanism of the Pechmann condensation.

Various Brønsted-Lowry and Lewis acids have been tested for this substrate and $ClTi(OiPr)_3$ turned out to be the best.[191,192] Using ^{13}C labeled ethyl acetoacetate (**208a** or **208b**) the coumarins **207a** or **207b** were produced with good yields (Figure 103). For analytical details about the isotopic incorporation see Chapter 3.2.2.

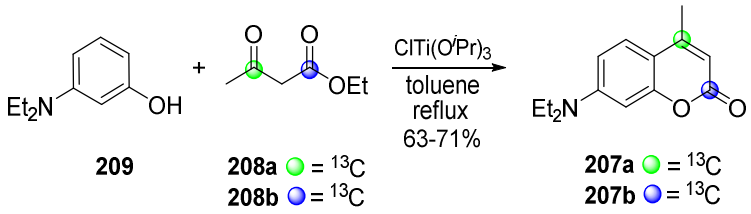

Figure 103: The Pechmann condensation with isotopically labeled ethyl acetoacetate.

The benzylic methyl group at the 4 position of the coumarin molecule was functionalized in a reaction with the *N*,*N*-dimethylformamide dimethylacetal (Figure 104).[188] The double bond of the enamines **211(a-b)** was oxidatively cleaved with $NaIO_4$, to yield aldehydes **212(a-b)**.

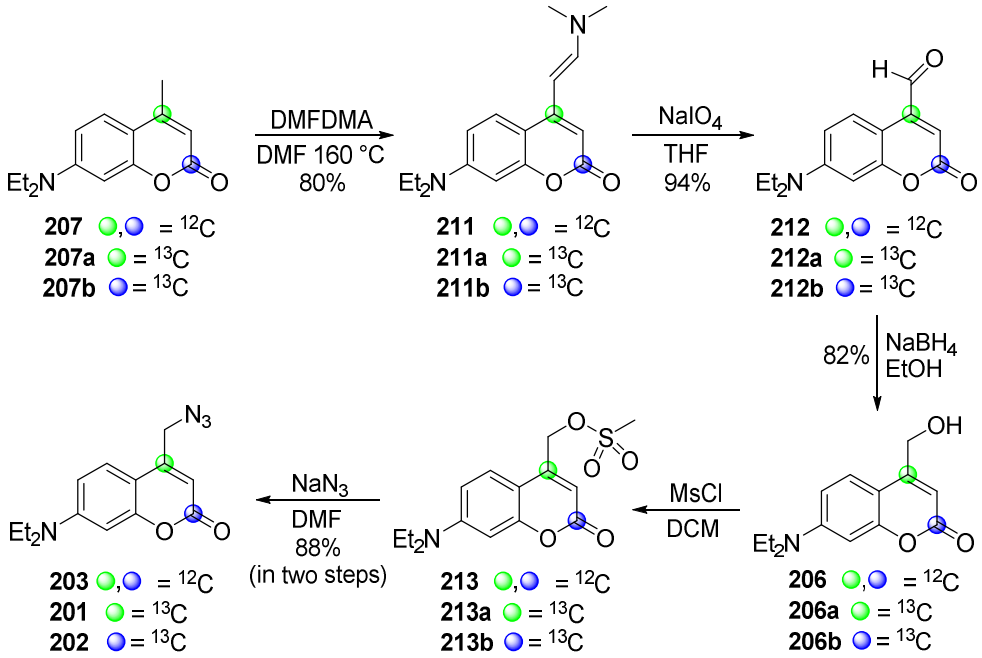

Figure 104: Synthesis of coumarin azide. The average yield of three reactions is given.

Alternatively, SeO_2 could be used to directly oxidize benzylic carbon in molecule **207(a-b)** to aldehyde **212(a-b)**,[193] however, the reported yields are low and selenium oxide is toxic.[21,129] The aldehyde **212(a-b)** was reduced with $NaBH_4$ to give coumarin alcohol **206(a-b)**. The hydroxyl group was mesylated **213(a-b)** and transformed into coumarin azide **201-203** in a reaction with sodium azide. All reactions had good yields. The thiocyanate **204** (Figure 100) was prepared by replacing the NaN_3 with KSCN in the last step of synthesis.

Preparation of the cyanate **205** was attempted by dehydration of the carbamate **214** (Figure 105). The carbamate **214** was prepared by treating coumarin alcohol **206** with trichloroacetyl isocyanate, followed by hydrolysis.[194,195] However, the yield is small (22%) and unreproducible (repeated reaction gave 4% yield).

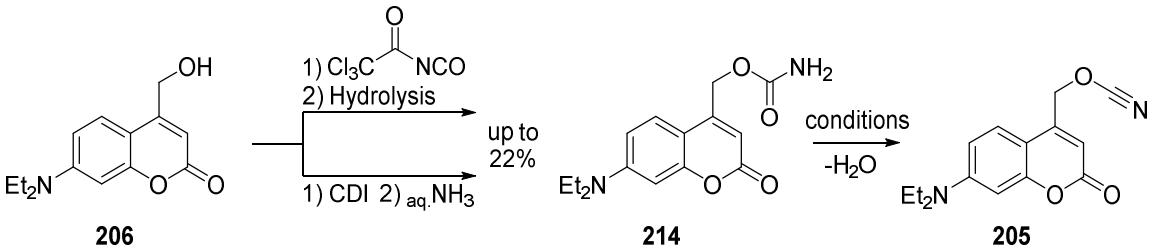

Figure 105: Synthesis of cyanate **205** *via* dehydration (for reaction conditions see the text) of carbamate **214**.

Alternatively carbamate **214** was prepared by activating hydroxyl coumarin with 1,1'-carbonyldiimidazole (CDI) and then treating it with ammonia. Also in this case the yield did not exceed 22%.

For the dehydration step, a literature method[194] (PPh_3 + CBr_4) was tested, as well as other reagents typically used in nitrile preparation from amides ($POCl_3$, $SOCl_3$).[196] None of the conditions yielded the expected product. A complex mixture of various coumarin derivatives was obtained instead. Unsuccessful dehydration has previously been observed for alkyl cyanates.[197]

The phenyl ester of cyano acid has been prepared by reaction of thiophosgene with phenol, followed by addition of sodium azide.[198] These conditions were applied to the coumarin alcohol (**206**), which reacted with thiophosgene to produce the compound **215** (Figure 106). It was then treated with sodium azide, to produce the thiatriazol derivative **216**. Upon heating, sulfur and nitrogen are expected to be eliminated, yielding the cyanate **205**. For a similar reaction, with 5-isobutoxy-1,2,3,4-thiatriazol as a substrate, it has been shown, that the nitrogen molecule is formed from N(2) and N(3).[199] The elimination probably proceeds *via* dinitrogen sulfide N_2S.[200]

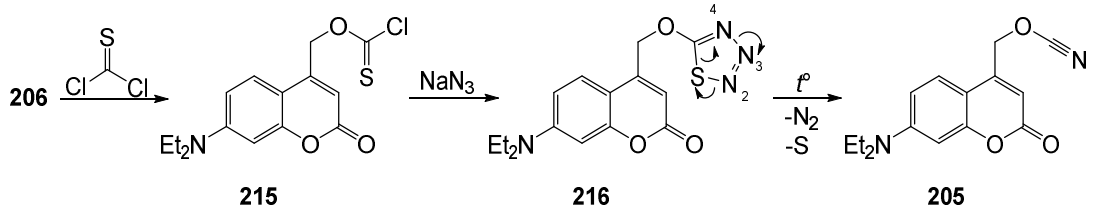

Figure 106: Synthesis of cyanate **205** *via* thiatriazol.

No product was obtained. Instead, a small amount of coumarin azide **203** (ca. 6% calculating from alcohol **206**) was obtained and the coumarin alcohol **206** was recovered (ca. 25% from initial load), together with unidentified side products.

No further attempts to produce the cyanate **205** were carried out. There are not many reports in literature about cyanate preparation.[201] A modified von Braun reaction between alkoxides (*e.g.* deprotonated coumarin alcohol **206**) and cyanogen halides (*e.g.* BrCN) could still be tested[202], however, the cyanogen halides are highly poisonous. There is also lack of information in literature whether such an α-aryl alcohol derived cyanate as the coumarin **205** would be stable enough to be isolated and characterized. It is known that cyanates can undergo isomerization at room temperature to give isocyanates, which are highly reactive to nucleophiles, and trimerize to give cyanuric acid derivatives.[194,203,204] Yet some alkyl and aryl cyanates have been reported and characterized, although their high reactivity/instability was recognized.[202,205–207] Generally, aryl

cyanates are more stable than their alkyl analogues, while the most unstable are short-chain alkyl cyanates.[208]

3.2.2. The analytical data of ^{13}C incorporation in coumarin azides

In order to control the ^{13}C isotope label incorporation in the coumarin molecule, NMR and IR spectroscopy and high resolution mass spectrometry were used. First, the signals in ^{1}H and ^{13}C NMR spectra of commercially available DEACM coumarin (**207**) were assigned using 2D NMR experiments (COSY, HSQC and HMBC). The spectra are shown in appendix (Figure 158 to Figure 161). The correct incorporation of the ^{13}C label in DEACM coumarins **207a** and **207b** could be confirmed by comparing the respective ^{1}H and ^{13}C spectra to the assigned spectra of unlabeled compound **207**. The spectra are shown in appendix (Figure 162 for **207a** and Figure 163 for **207b**). Further confirmation of the correct signal assignment in NMR spectra could be obtained from the $^{1}H^{13}C$ and $^{13}C^{13}C$ couplings observed for the compounds containing the ^{13}C label.

Analogue analysis was done for the coumarin azides **201**-**203**. The assigned spectra of the unlabeled compound are shown in appendix: Figure 164 for ^{1}H and ^{13}C, Figure 165 for COSY, Figure 166 for HSQC and Figure 167 for HMBC. The position of the ^{13}C isotopes in the labeled azides **201** and **202** were confirmed by comparing their ^{1}H and ^{13}C spectra with the assigned spectra of the unlabeled compound **203**. These spectra are shown in appendix (Figure 168 for **201** and Figure 169 for **202**).

Finally, the incorporation of the ^{13}C label and its position in the coumarin azides **201**-**202** was confirmed by IR spectroscopy. The most relevant signals in the IR spectra are shown in Figure 107.

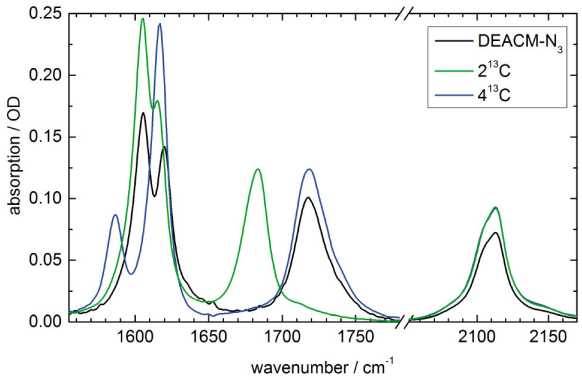

Figure 107: The IR spectra (ring mode, carbonyl and azide region) of the coumarin azides **201** (blue), **202** (green) and **203** (black) in dry MeCN. The IR spectra were measured and the figure prepared by Daniela Kern-Michler, Carsten Neumann, Nicole Mielke and Luuk van Wilderen (group of Jens Bredenbeck). Reprinted with permission from *J. Am. Chem. Soc.* **2018**, 140, 926-931. Copyright 2018 American Chemical Society.

The signal centered at 2110 cm^{-1} (black line) is the azide stretching mode and it is not influenced by the isotopic label in coumarins **201** (blue) and **202** (green). The signal at 1720 cm^{-1} is the C=O stretching mode. This signal is not changed for the compound **201** (which contains ^{13}C label in the position 4 of the coumarin molecule), but is shifted to 1680 cm^{-1} if the ^{13}C label is in the carbonyl group of coumarin (**202**). The signals at approximately 1600 and 1620 cm^{-1} are the ring modes of coumarin. Incorporation of a ^{13}C label in the positon 4 of the coumarin molecule (**201**) has the largest effect on changing these modes (particularly the low frequency ring mode). The IR spectra were measured, assigned and the figure prepared by Daniela Kern-Michler, Carsten Neumann, Nicole Mielke and Luuk van Wilderen (group of Jens Bredenbeck).

3.2.3. The irradiation study of coumarin photocages

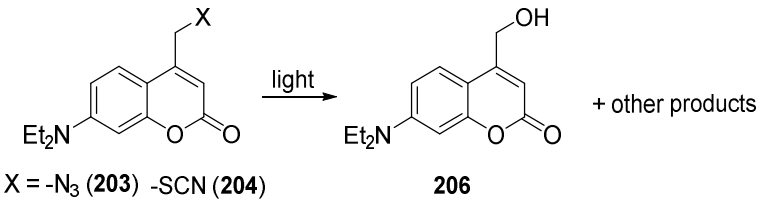

Figure 108: The uncaging of the coumarin pseudohalides.

According to the uncaging mechanism of coumarin photocages (Figure 27), coumarin alcohol is expected as the uncaging product in aqueous solutions.[54] In order to test whether the prepared coumarin azide **203** and thiocyanate **204** (Figure 108) follows this behavior, an irradiation study was done. The photoreaction of prepared coumarin derivatives was studied in steady state and in ultrafast timescale.

A sample of coumarin azide **203** in 0.1M TEAA buffer with 20% MeCN (c = 0.1µM) was analyzed *via* HPLC (Figure 109D). The irradiation was done with 385 nm LED since the absorbance spectrum of the coumarin azide has its maximum at 384 nm (Figure 109A). A complete conversion of starting material was observed and one major photoproduct was produced (Figure 109E). This could be assigned to coumarin alcohol **206** by comparing it to standard substance (Figure 109F, peak at 15.0 min, blue). The irradiated solution acquired red color, which plausibly originates from coumarin aldehyde **212** as can be seen from comparison to the standard compound (Figure 109F, peak at 16.0 min, red).

It is known that in the presence of oxygen a photooxidation of coumarin alcohol is possible and the corresponding aldehyde as well as carboxylic acid is produced.[209] Uncaging of the 3-aryl substituted coumarin photocage produced aldehyde, what authors proposed to origin from the

oxidation of coumarin carbocation by DMSO.[130] In the irradiation experiment shown in Figure 109 no actions to exclude air were taken.

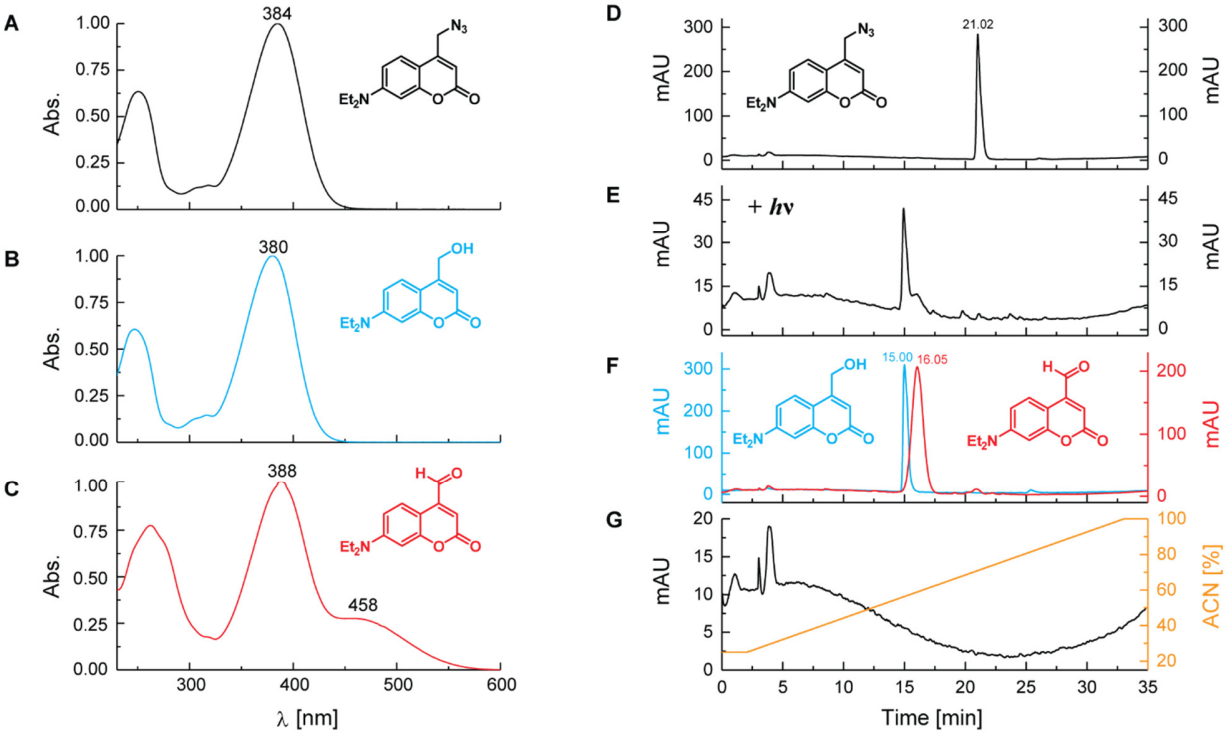

Figure 109: Absorbance spectra of coumarin azide **203** (A), coumarin alcohol **206** (B) and coumarin aldehyde **212** (C). All spectra measured by HPLC. The HPLC (detection at 400 nm) traces shown are those of the coumarin azide **203** before (D) and after irradiation at 385 nm (E), coumarin alcohol **206** and aldehyde **212** (F), the buffer used for sample preparation and the solvent gradient (G).

A further irradiation study was done with NMR. The ^{1}H NMR spectrum (4-11 ppm) of the coumarin azide before and after irradiation is shown in Figure 110. For a comparison, also the spectra of the coumarin alcohol and the coumarin aldehyde are shown. Air was excluded from the irradiated mixture by passing a stream of argon through the solution (MeCN-d_3 with 5% v/v D_2O) for 15 min.

In the irradiated sample, signals of the alcohol and the aldehyde can be found, thus confirming observations from the HPLC analysis. Since the solution was degassed, the formation of oxidation product, aldehyde, was not expected.

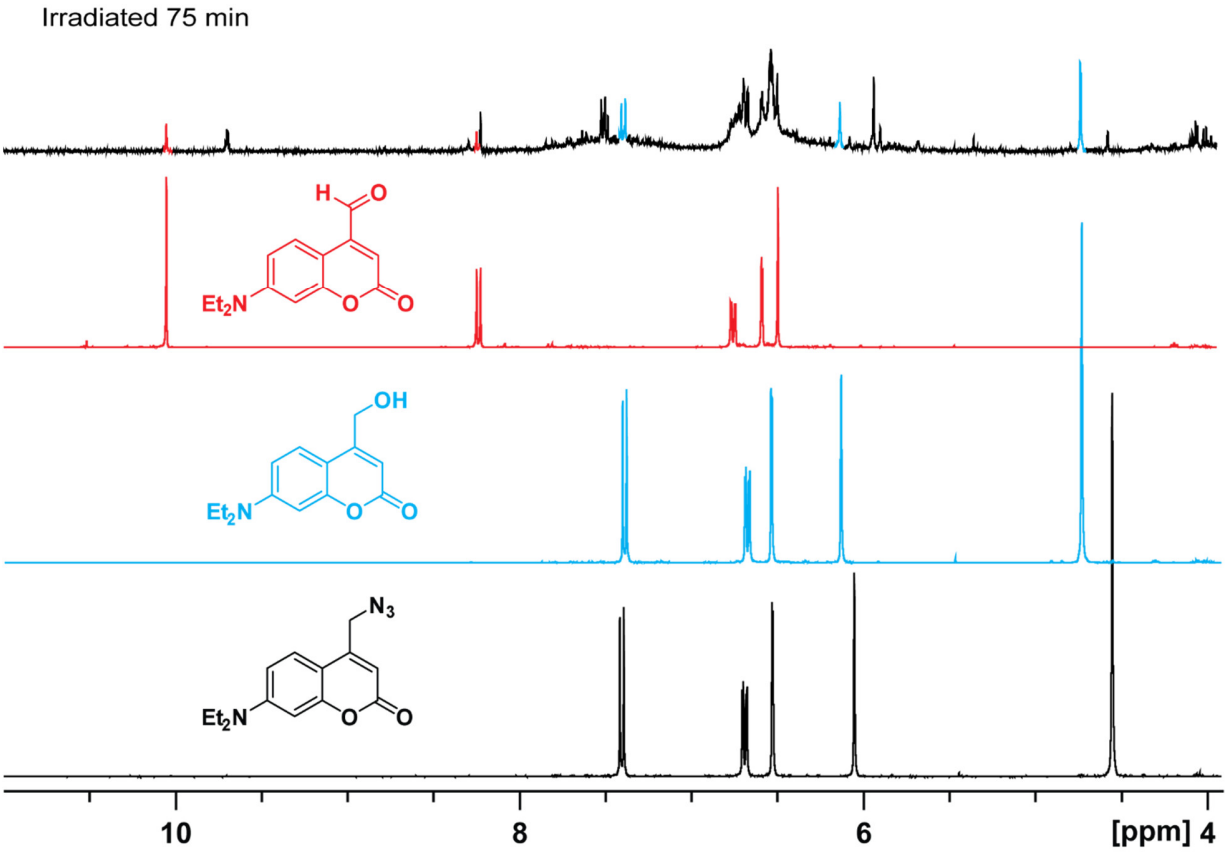

Figure 110: ^{1}H NMR spectra (400 MHz) of the irradiation of the coumarin azide **203** before and after irradiation (75 min) in MeCN-d_3 with 5% v/v D_2O (13 mM). For a comparison, spectra of coumarin alcohol **206** and aldehyde **212** are also given.

On the other hand, it is possible that oxidation happens by other means than in a reaction with O_2. For example, in a study of the 7-diethylamino-4-methylcoumarin (**207**) photodegradation a product with a reduced double bond in the pyrone (lactone) ring of the coumarin was assigned (mass spectral analysis) as one of the products. It was proposed, that in high concentration solutions (1-10 mM) a bimolecular reaction happens involving an excited singlet state coumarin and a ground state coumarin.[210,211] The observation of the coumarin alcohol **206** oxidation even in absence of air could be a result of such a reaction. The concentration of the coumarin azide **203** in the NMR experiment was 13 mM.

Further details about the fate of the coumarin azide upon irradiation can be extracted from the same irradiation experiment if a wider part of the spectrum is analyzed (Figure 111). The signals in the yellow (I) and green rectangles (II) correspond to the benzene ring of the coumarin molecule (*b*, *c* and *d*), the signal *f* (red rectangle, III) comes from the coumarin pyrone ring (signal assignment is shown in the lowest segment of Figure 111). In the gray rectangle (IV) resides the methylene group signal (*e*). The blue rectangle (V) marks the area, where the signals from the coumarin

photodimers would be located.[212,213] The integral values of each spectrum was adjusted to N-**CH₂**-CH₃ signal (*a*). The last signal in the right side of Figure 111 comes from dimethyl sulfone, which was used as an internal standard (*IS*).

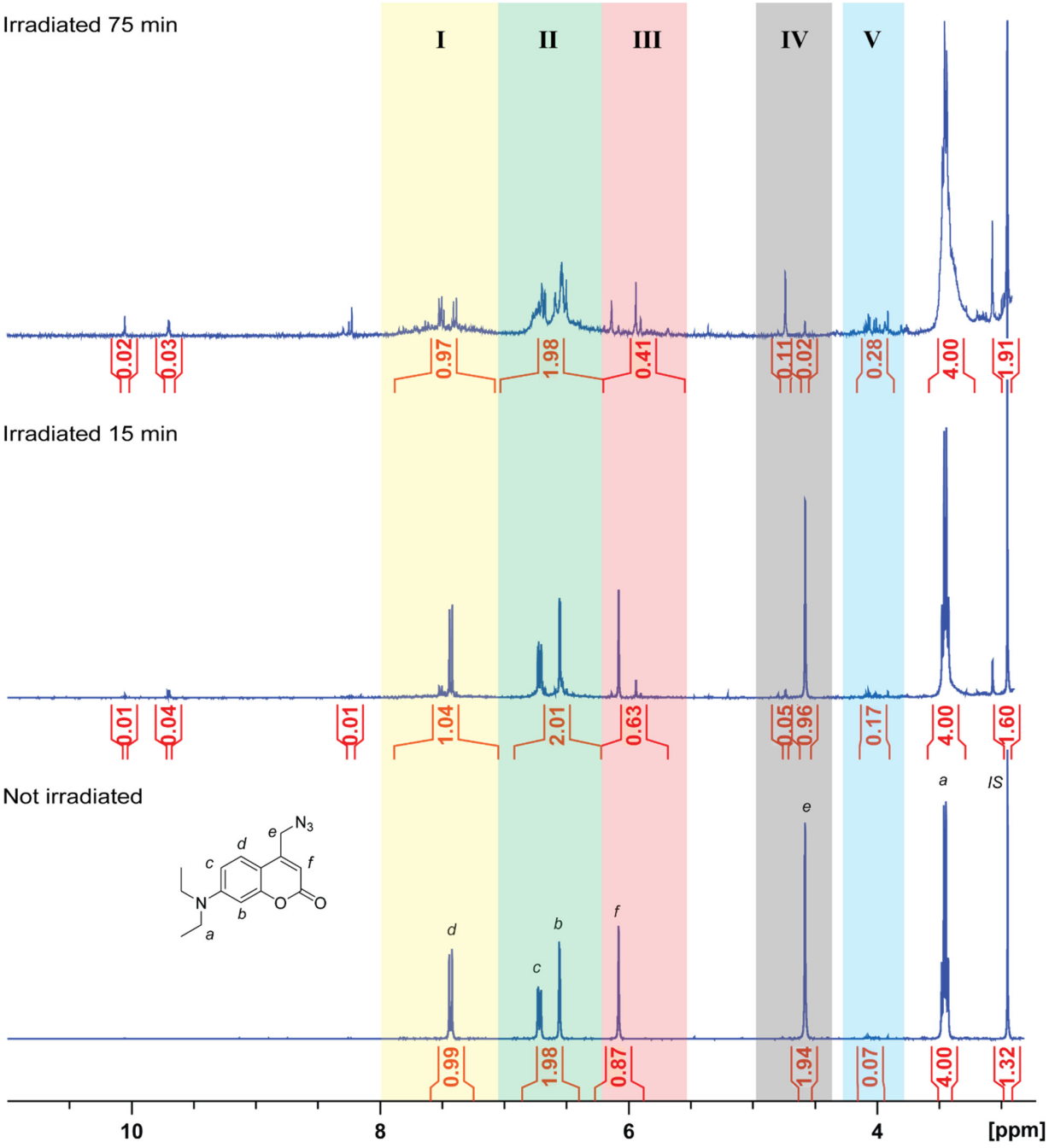

Figure 111: ^{1}H NMR spectra (400 MHz) of the irradiation of the coumarin azide **203** in MeCN-d_3 with 5% v/v D_2O (13 mM).

After 15 minutes of irradiation a change of the integral values can be observed in the gray (IV) and red rectangle (III), while in the yellow (I) and green (II) rectangle the sum of the integral

values remains as it was in the not irradiated sample. The same can be observed after longer irradiation (75 min). The signals of the pyrone ring (f) and methylene group (e) in the red and gray rectangle have significantly decreased without being replaced by new signals in this area, indicating major changes of the pyrone ring and the benzylic position.

The integral values of the signals in the blue rectangle (V) has increased, which might indicate formation of coumarin dimers. Photodimerization of the coumarin pyrone ring [2+2] is a well-known reaction.[214] IR measurements of coumarin azide **203** irradiation under similar conditions also suggested formation of dimers.[114] Other reactions, resulting in coumarin aromatic ring changes, might involve pyrone ring decarboxylation and decarbonylation.[106,215]

The integral value of the internal standard (*IS*) increases and since that is relative to N-**CH_2**-CH_3 signal (*a*), which is used as integration standard, a conclusion can be made that some changes of the amino substituents have occurred.

A dealkylation of the amino group upon irradiation of 7-diethylamino-4-methylcoumarin (**207**) has been observed in a degassed ethanol solution.[209] A bimolecular mechanism was suggested, where the carbonyl group of excited state coumarin homolytically abstracts hydrogen from the ethyl substituent (-NEt_2) of a ground state coumarin molecule, which after subsequent reaction steps results in a dealkylation of the amino group.[216]

In conclusion, the NMR results suggest that irradiation of coumarin azide **203** leads to a complex mixture of products if the solution concentration is high (in mM range). This has already been observed for 7-amino substituted coumarin dyes when the photoreaction was controlled by NMR.[210,211]

Samples of the ^{13}C labeled coumarin (**201** and **202**) after irradiation were also analyzed with HPLC (Figure 112). The irradiation was done by Daniela Kern-Michler, Carsten Neumann and Nicole Mielke (group of Jens Bredenbeck).

The analyzed samples were combined from multiple experiments, where irradiation was done by a high power pulsed laser (including VIPER experiments) as well as from experiments where a high power LED was used. The sample was prepared in MeCN and was in the mM concentration range.

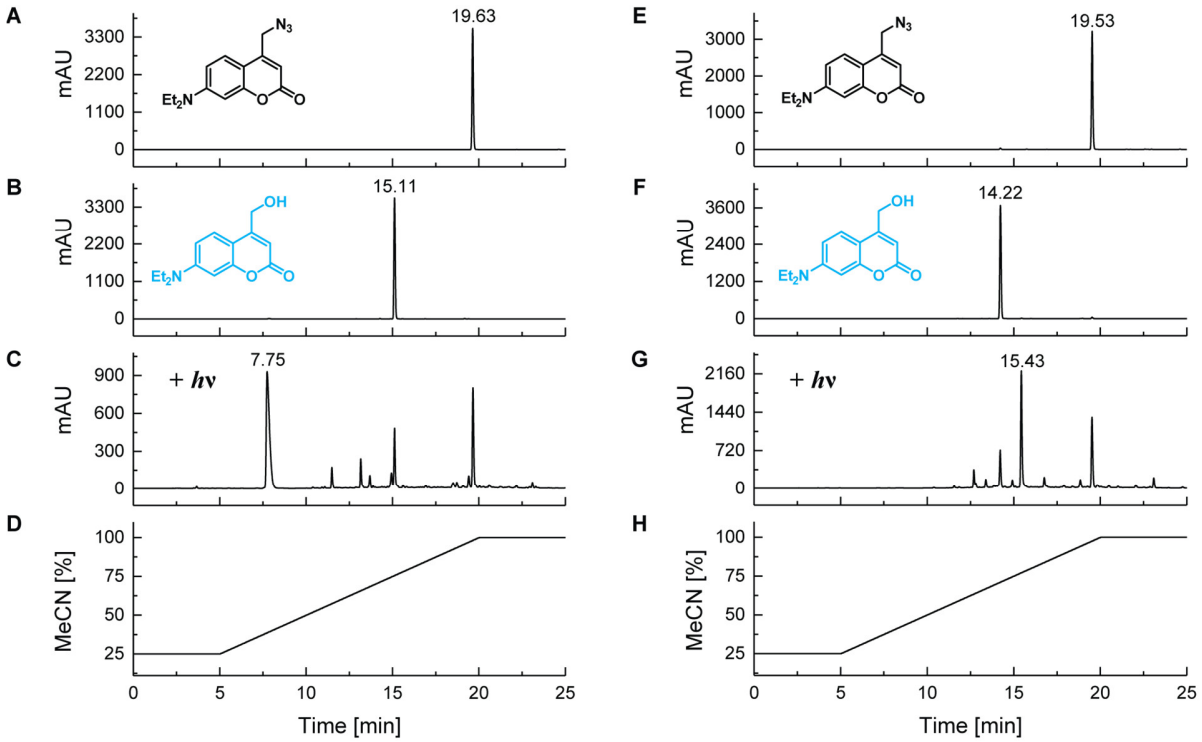

Figure 112: The HPLC traces of the coumarin azide **203** (A, E), coumarin alcohol **206** (B, F) and irradiated samples of coumarin azides **201** and **202** (C, G). The analyses were performed on a reverse phase (C18) column, elution was done by MeCN and 50mM NH_4OAc (*p*H = 5, traces A-C) or 0.05% TFA (*p*H = 2, traces E-G), detection at 400 nm, the solvent composition during analysis is shown in D and H section.

No full conversion of the starting material has been achieved (Figure 112C, G). Similar to the previously described HPLC analysis (Figure 109), also in this case the coumarin alcohol **206** could be found among the photoproducts. Also traces of coumarin aldehyde **212** could be detected. Interestingly, a new signal could be seen among the photoproducts at 7.75 min (Figure 112C). Formation of this photoproduct can be seen also if the irradiation is done in presence of D_2O (data not shown). This peak changes its position to 15.43 min (Figure 112G) if the pH value of the elution buffer is changed from 5 to 2. The retention time shift upon pH change suggests presence of a protolytic group, for example, carboxylic acid.

However, the UV-Vis spectra (Figure 113A) does not support the idea that this unknown product is 7-(diethylamino)coumarin-4-carboxylic acid. The absorbance spectrum of the peak eluting at 7.75 min (Figure 112C) is shown in Figure 113A as a black line, the peak eluting at 15.43 min (Figure 112G) as a black dashed line. Upon change of the pH value from 5 to 2, also the absorbance maximum is bathochromically shifted by 18 nm. The absorbance maximum of the 7-(diethylamino)coumarin-4-carboxylic acid is located at 385 nm (in EtOH),[217] thereby it is

unlikely to be the unknown photoproduct. The identification of this photoproduct was attempted by mass spectrometry, however it was not successful. No further identification attempts were carried out.

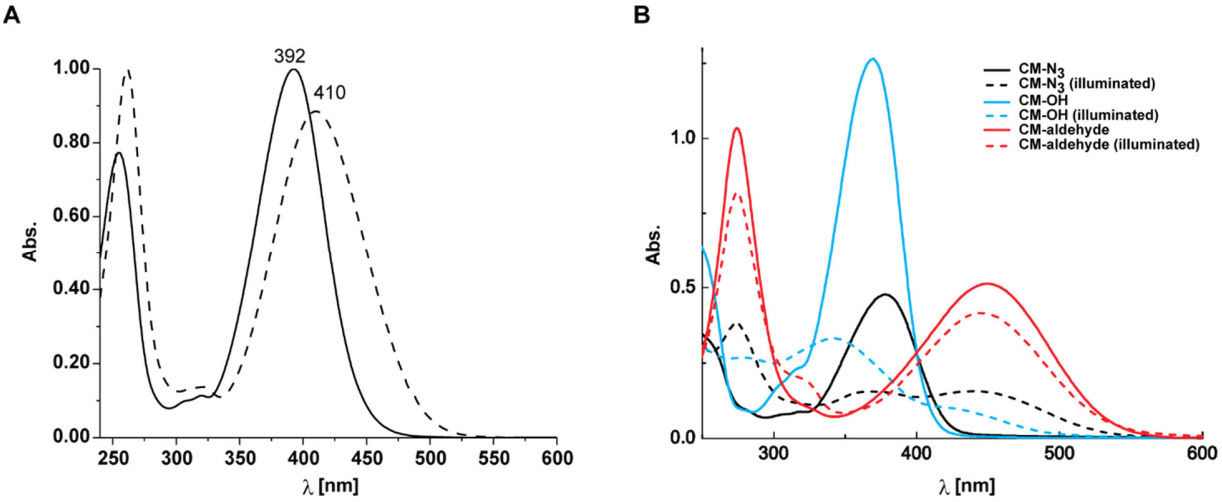

Figure 113: *A* – The solid black line shows the absorbance spectrum of the peak eluted at 7.75 min (Figure 112C), the dashed line – the absorbance spectrum of the peak eluted at 15.43 min (Figure 112G). Spectra measured by HPLC; *B* – Absorbance spectra before and after illumination of the azide **203** (CM-N_3), alcohol **206** (CM-OH) and aldehyde **212** (CM-aldehyde). Irradiation experiments were done and the original figure shown in the B panel was prepared by Daniela Kern-Michler, Carsten Neumann, Nicole Mielke and Luuk van Wilderen (group of Jens Bredenbeck). Used in this work with graphically modified axis and colors. Reproduced from Ref. [114] with permission of the PCCP Owner Societies.

The known photoproducts of coumarin azide photolysis are photoactive (Figure 113B) and prolonged irradiation leads to complete absorbance disappearance above 350 nm as confirmed by the steady state UV-Vis irradiation measurements (done by Daniela Kern-Michler, Carsten Neumann, Nicole Mielke and Luuk van Wilderen from the group of Jens Bredenbeck).[114] These results agree with the observation from the NMR irradiation experiments (Figure 111).

A sample of coumarin thiocyanate **204** in 0.1M TEAA buffer with 20% MeCN (c = 0.4µM) was analyzed with HPLC (Figure 114A). The irradiation was done with 385 nm LED since the absorbance spectrum of the coumarin thiocyanate is nearly identical to coumarin azide **203**, which has its maximum at 384 nm (Figure 109A). The major primary photoproduct (Figure 114B) is also in this case the coumarin alcohol **206** (assigned by comparison to a standard compound, see Figure 109F, peak at 15.0 min, blue). Also production of a coumarin aldehyde **212** can be seen (assigned by comparison to standard compound Figure 109F, peak at 16.0 min, red). If irradiation is continued (Figure 114C), the size of the coumarin alcohol and aldehyde peak decreases while the peak at 8.54 min increases. Identity of this secondary photoproduct was not determined.

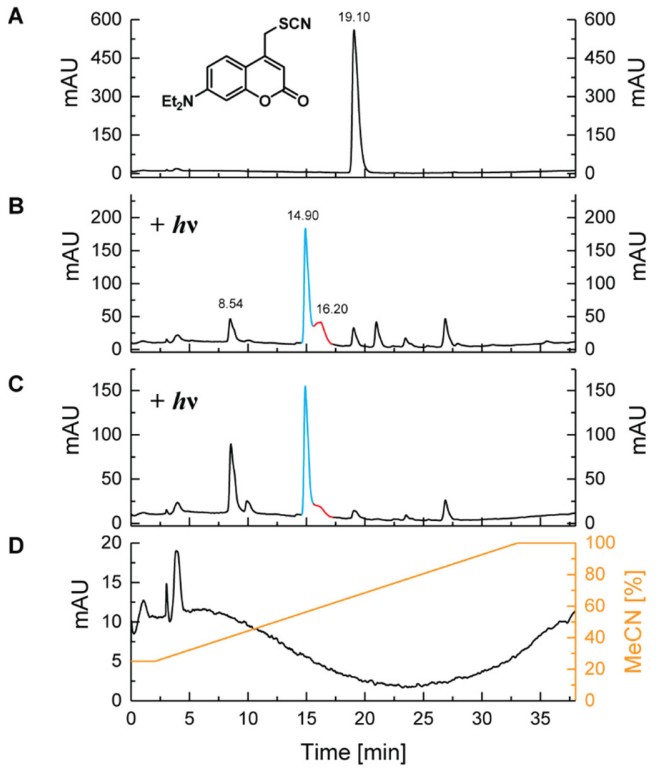

Figure 114: The HPLC traces (detection at 400 nm) of the coumarin thiocyanate **204** before (A) and after irradiation at 385 nm for 30 sec (B) and 10 min (C).

3.2.4. The ultrafast spectroscopy data

The ultrafast uncaging dynamics of coumarin azide **203** were investigated by ultrafast IR spectroscopy and the results have been published.[114] A short summary is given in given chapter. All experiments described here were performed and evaluated by Daniela Kern-Michler, Carsten Neumann, Nicole Mielke and Luuk van Wilderen (group of Jens Bredenbeck).

In Figure 115A the steady state infrared spectra of the coumarin azide **203** is shown. The measurement was done in MeCN with different amounts of D_2O (the legend in panel B shows the ratio in v/v%). The blue circled signal is assigned to the azide stretch mode, the green circled signal to the carbonyl stretch mode and the magenta circled signals to the ring stretching modes (see Figure 107 for a comparison with isotopically labeled coumarin azide). The light-minus-dark difference spectra show bleaches of all these signals (Figure 115B) along with a rise of signals from the photoproducts. New bands appear at both sides of the bleached azide signal, which are assigned to azide anion (around 2015 cm^{-1}) and protonated (deuterated) azide – hydrazoic acid (around 2139 cm^{-1}). The signal at 1769 cm^{-1} was assigned to a coumarin dimer, formed as a result of [2+2] cycloaddition.

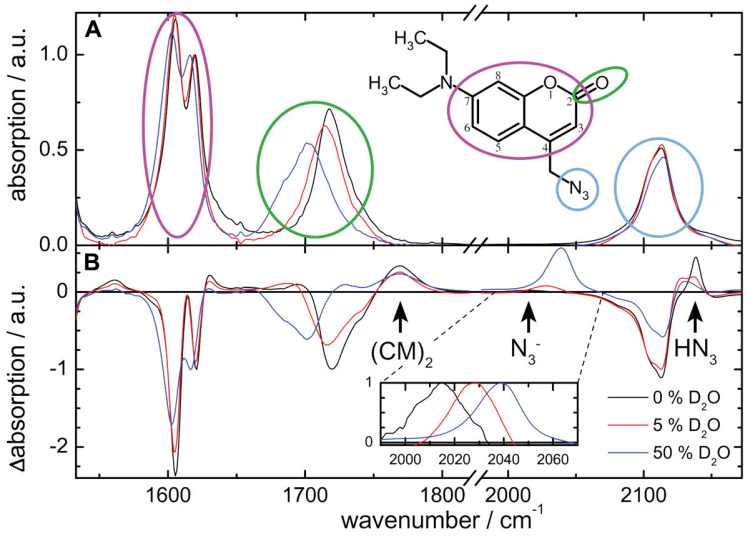

Figure 115: The top panel (A) shows the infrared spectrum (solvent-subtracted) of the coumarin azide **203** in dry MeCN (black) and with added D_2O (v%, 5 - red, 50 - blue). The lower panel (B) shows light minus dark difference spectra after irradiation (24 mM solutions, 50 µm pathlength, 365 nm LED). Experiments were done and the figure was prepared by Daniela Kern-Michler, Carsten Neumann, Nicole Mielke and Luuk van Wilderen (group of Jens Bredenbeck). Reproduced from Ref. [114] with permission of the PCCP Owner Societies.

The overall absorbance of released azide (in both its protonation forms) was smaller than expected (approximately 50%), suggesting a possible N_2 formation. Bubbles could be observed in the irradiated sample, but only CO_2 formation could be proven spectroscopically since the nitrogen cannot be detected by IR spectroscopy (data not shown in Figure 115).

Nitrogen formation is possible from the azide group, which is known to be photoactive upon irradiation with far UV light (<270 nm).[218] However, for irradiation experiments of coumarin azide **203** light of a longer wavelength was used (≥365 nm), making direct excitation of the azide group impossible. Alkyl azides have been cleaved (to give nitrene intermediates and N_2) by sensitized irradiation.[219] Coumarin could act as a triplet sensitizer albeit intersystem crossing yields of 7-aminocoumarin derivatives are small.[106] Alkyl azide derivative sensitization has been possible with sensitizers whose triplet energy is as low as 205 (kJ mol^{-1})[220] despite the high triplet energy of alkyl azides (310-335 kJ mol^{-1}).[219,221] Thereby it would be probable that 7-diethylamino-4-methylcoumarin (its triplet energy is 240 kJ mol^{-1})[222] or its derivatives formed in the uncaging reaction could act as sensitizer of azide group promoting the release of nitrogen.

3.2.5. VIPER uncaging

The vibrationally promoted electronic resonance (VIPER) uncaging of coumarin azides **201-202** has been previously published.[223] Short summary is given in this chapter. All experiments

described here were performed and evaluated by Daniela Kern-Michler, Carsten Neumann, Nicole Mielke and Luuk van Wilderen (group of Jens Bredenbeck). For the theoretical background of VIPER uncaging please see Chapter 1.4.

The IR active leaving groups – azide and thiocyanate, were discovered not to be suitable for reaction monitoring. The azide release turned out to be a complicated process (formation of the N_3^- and DN_3, possible release of the N_2, see chapter 3.2.4). Thereby it is not practical to use the changes of the azide stretch mode in the IR spectra to probe the photoreaction. Furthermore, it bears little information about the fate of the coumarin molecule after the uncaging. The uncaging of the thiocyanate **204** happened cleaner and only a SCN anion was released, but its absorption intensity was low. As a result the VIPER uncaging was probed using the carbonyl group signals.

The UV-Vis absorbance spectra of the ^{13}C labeled isotopomers **201** and **202** (Figure 116A-B) are identical but the infrared absorbance spectra of both molecules are different. Thereby, a spectroscopic discrimination is possible between the two isotopomers in the infrared frequency range. (Figure 116C, for signal assignment and discussion see chapter 3.2.2 and Figure 107).

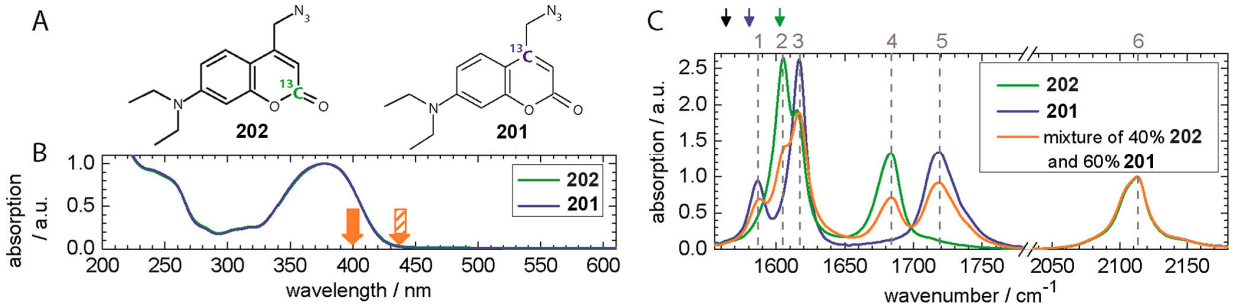

Figure 116: *A* - The structures of isotopically labeled coumarin azides (**201** and **202**); *B* – UV-Vis absorbance spectra of the coumarin azides **201** and **202** in MeCN; *C* – steady state IR spectra of the azide moiety (band 6), carbonyl groups (bands 4 and 5) and ring modes (bands 1, 2, 3) in MeCN. Experiments were done and the original figure was prepared by Daniela Kern-Michler, Carsten Neumann, Nicole Mielke and Luuk van Wilderen (group of Jens Bredenbeck). Adapted with permission from *J. Am. Chem. Soc.* **2018**, 140, 926-931. Copyright 2018 American Chemical Society.

In Figure 117 only the carbonyl region of the IR spectra is shown. Panel A shows the steady state spectra of the individual isotopomers **201** (blue) and **202** (green) as well as the mixture of both compounds (60% **201** and 40% **202**).

Panel B in Figure 117 shows the Vis-pump IR-probe (IR probe delay 2.5 ps) spectra of the carbonyl region. Upon resonant UV (400 nm) irradiation (Figure 116B, filled orange arrow) of the pure isotopomers **201** or **202** a ground state bleach of the corresponding carbonyl groups (labeled by 4 and 5, the green and blue lines) can be seen. If both compounds are irradiated in a mixture

(orange line), the ground state bleaches of the both carbonyl groups can be seen simultaneously (orange line).

For the VIPER irradiation experiment a mixture of both compounds was used. To selectively excite only compound **202**, a narrow band IR-pump pulse, centered at the ring modes of this molecule (Figure 116C, green arrow), is used, followed by an off-resonant Vis-pump pulse (437 nm, Figure 117B striped orange arrow) with a delay of 1.5 ps between the two pulses. The IR probe pulse then arrives with 2.5 ps delay. In this case, only the ground state bleach of the carbonyl group of compound **202** (Figure 117C, green line) can be seen.

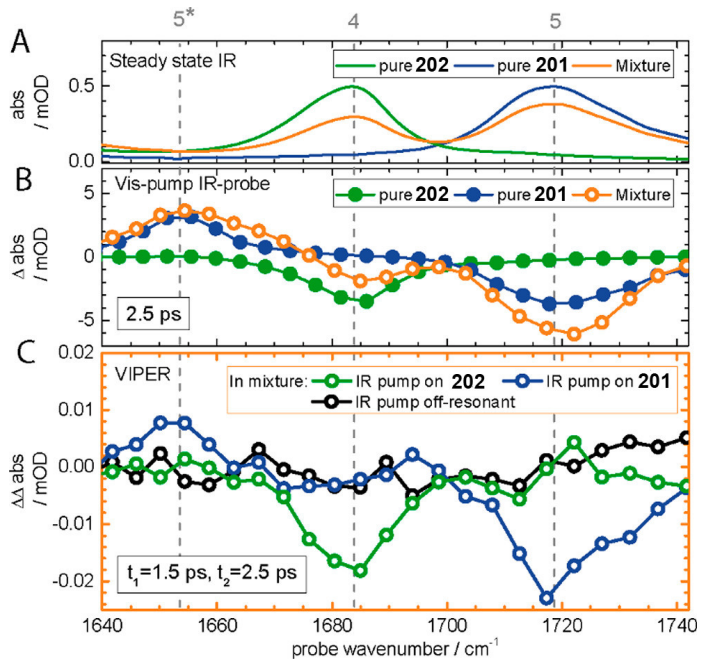

Figure 117: *A* - steady state IR spectra of the carbonyl region (bands 4 and 5) from the azides **201** and **202** in MeCN; *B* – Vis-pump IR-probe spectra of the carbonyl region; *C* – VIPER spectra of the carbonyl region, from a mixture of 60% **201** and 40% **202**. Experiments were done and the original figure was prepared by Daniela Kern-Michler, Carsten Neumann, Nicole Mielke and Luuk van Wilderen (group of Jens Bredenbeck). Adapted with permission from *J. Am. Chem. Soc.* **2018**, 140, 926-931. Copyright 2018 American Chemical Society.

If the IR-pump pulse is centered at the lower frequency ring modes of compound **201** (Figure 116C, blue arrow), only the ground state bleach of the carbonyl group of compound **201** (Figure 117C, blue line) can be seen. The essential role of the IR-pump pulse was additionally demonstrated by setting the IR-pump pulse at an off-resonant (Figure 116C, black arrow). In this case, neither of the carbonyl group ground state bleaches in the mixture of compounds **201** and **202** can be seen (Figure 117C, black line). Thus, selective excitation of one isotopomer in the mixture with another one was achieved.

3.2.6. The synthesis of *para*-hydroxy phenacyl (*p*HP) photolabile protecting group

As the next candidate to further test the scope and limitations of the VIPER method the *p*HP (*para*-hydroxyphenacyl) photocage was selected. Its photochemical reactivity is well studied (see chapter 1.3.1) and its absorbance spectrum has well defined borders at the longest wavelength side (which is an important property for VIPER excitation). Initially, three derivatives had to be prepared (structures are shown in Figure 118) for testing by Vis-pump-IR-probe spectroscopy. Each of them carries a leaving group which should give a characteristic signal in the IR spectra.

Computations showed, that electronic excitation with an off-resonant Vis-pump pulse (in the VIPER pulse sequence) would work the best if the IR-pump pulse would be centered to the ring distortion mode in the IR spectrum. However, also the effect of vibrational excitation of the carbonyl stretch mode is non-negligible.[187] Thereby, for the VIPER experiments on *p*HP photocage the ^{13}C label should be introduced in the carbonyl group and in the aromatic ring.

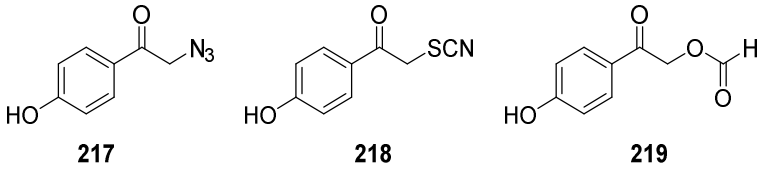

Figure 118: The structures of *p*HP derivatives for Vis-pump-IR-probe spectroscopic experiments.

The *p*HP azide **217** was prepared from the commercially available bromide **220** in a S_N2 reaction, using NaN_3 as source of the azide ion (Figure 119). In the same way the thiocyanate **218** could be prepared using ammonium thiocyanate.

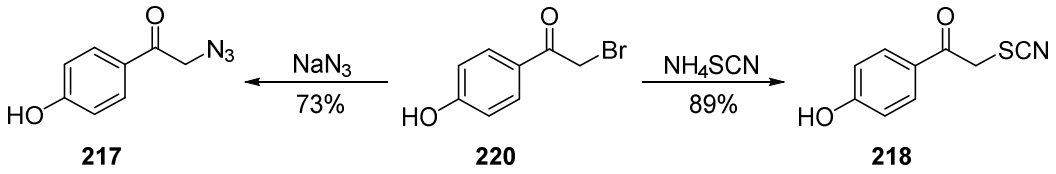

Figure 119: Synthesis of *p*HP azide **217** and thiocyanate **218**.

Treating the bromide **220** with sodium formate did not result in formation of the **219** (Figure 120). Although during the reaction a formation of the expected product could be observed (as detected by TLC-MS), it underwent hydrolysis to give compound **23** in a mixture with starting material **220**.

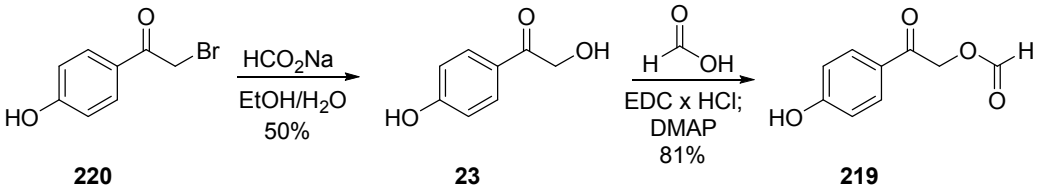

Figure 120: Synthesis of *p*HP formate **219**.

After purification, the compound **23** was used to prepare the formic ester **219** in a Steglich-type esterification (Figure 120). As a condensation reagent 1-Ethyl-3-(3-dimethylaminopropyl)-carbodiimide hydrochloride (EDC x HCl) was used with DMAP as catalyst. The reaction proceeded with good selectivity at the primary alcohol (hydroxyl keton), despite the presence of the unprotected phenol group. For carbodiimide-mediated acylations, selective reactions with aliphatic alcohols in presence of phenols have been reported. However, such a selectivity was possible only with acids capable of forming ketene intermediates. Keeping the pH value low to avoid formation of nucleophilic phenolate also played an important role. However, if a catalysis like DMAP was used, the selectivity was bad.[224] A plausible explanation for the high selectivity observed in the esterification of compound **23** under the used conditions could lie in its resonance forms (Figure 121).

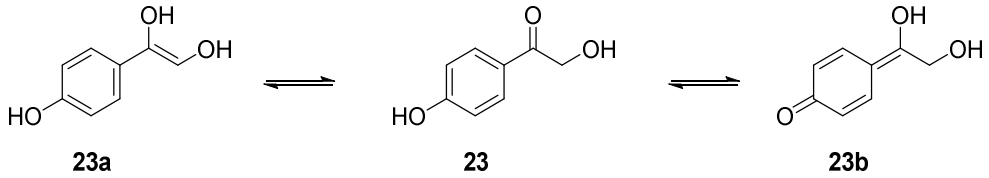

Figure 121: Resonance structures of *p*HP alcohol **23**.

The compound **23** can have two resonance structures, the enol **23a** and quinone-like **23b**. The latter resonance structure (**23b**) makes acylation of the phenolic hydroxyl group less likely. It has been reported that in the DMAP catalyzed esterification reaction the alcohol might be pre-coordinated by hydrogen bonds to the activated DMAP-ester.[225] The diol-like structure of resonance forms **23a** and **23b** could facilitate such pre-coordination to DMAP-formate, and after the formic group transfer from DMAP giving the compound **219**.

All *p*HP derivatives (**217**-**219**) could be successfully prepared from the bromide **220**, thereby it was necessary to develop synthesis of the bromide itself, later to be used for the synthesis of the ^{13}C-labeled compounds. Retrosynthetic analysis is very simple (Figure 122). The bromide **220** could be prepared from the acetophenone **221** which could be prepared from phenol **222** and acetyl synthon **223**.

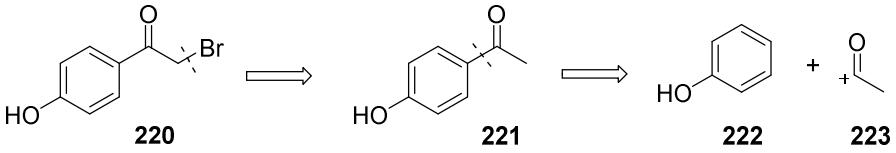

Figure 122: Retrosynthetic analysis of *p*HP bromide **220** synthesis.

A regioselective Friedel-Crafts acylation of the phenol **222** with acetyl chloride in trifluorosulfonic acid (Figure 123) has been reported.[226] In these conditions a quantitative yield of the expected product was achieved.

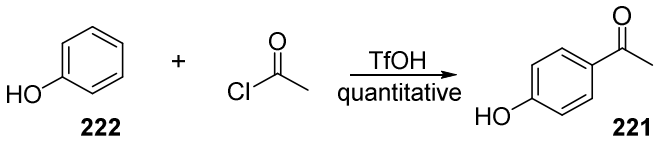

Figure 123: Synthesis of acetophenone **221** by Friedel-Crafts acylation.

The bromination of the acetophenone was tested next (Figure 124). Using molecular brom as the reagent (in Et_2O at room temperature), a mixture of at least 4 products was obtained without reaching full conversion of the starting material **222**. An alternative reaction, using $CuBr_2$ (2 eq) as the source of bromide, in refluxing ethylacetate and chloroform mixture (1:1), was tested.[227] Also this reaction does not lead to full conversion while addition of more $CuBr_2$ leads to formation of side product **223**. This side product was formed also with two equivalents of $CuBr_2$, however, the isolated yield of **220** was 78% (with 9% of starting material left and 16% of sideproduct **223** formed).

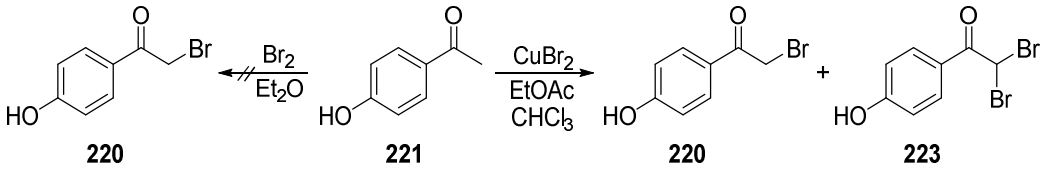

Figure 124: Synthesis of bromide **220** by bromination of the acetophenone.

A similar reaction, using I_2 and CuO, resulted in a lower yield of the expected mono-iodo product (approximately 50%) and a higher amount of **223** iodo analogue.[228]

The Friedel-Crafts acylation of the phenol **222** with 2-bromoacetyl chloride **224** (Figure 125), in conditions used for preparation of acetophenon **221** (Figure 123), was tested. The expected product **220** (65%) was obtained in a mixture with side product **225** (7%). Increasing the amount of acylating agent to 1.2 eq did not increase the yield of **220** (58%), but did increase the amount of **225** detected in the crude reaction mixture (as determined by NMR).

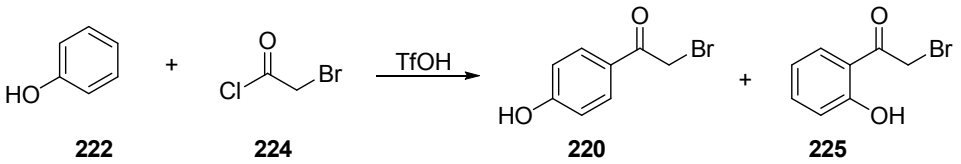

Figure 125: Synthesis of bromide **15** by Friedel-Crafts acylation.

The *ortho*-substituted product (**225**) has better solubility in unpolar solvents (*e.g.* cyclohexane, chloroform) than the *para*-substitued (**220**), which can be used to efficiently separate the two products.[229] However, to remove last traces of the side product **225** from the desired product **220**, a chromatography is also necessary. The different solubility could be attributed to an intramolecular hydrogen bond formation which is possible only for the *ortho*-hydroxy substituted compound (Figure 126).[230]

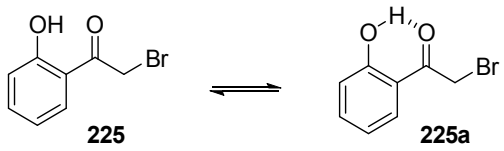

Figure 126: Intramolecular hydrogen bond formation in the *ortho*-hydroxy substituted acetophenone derivative **225**.

The compound **220** showed instability in DMSO-d_6 (Figure 117). Upon storage of the sample for 12 h, a hydrolysis can be observed.

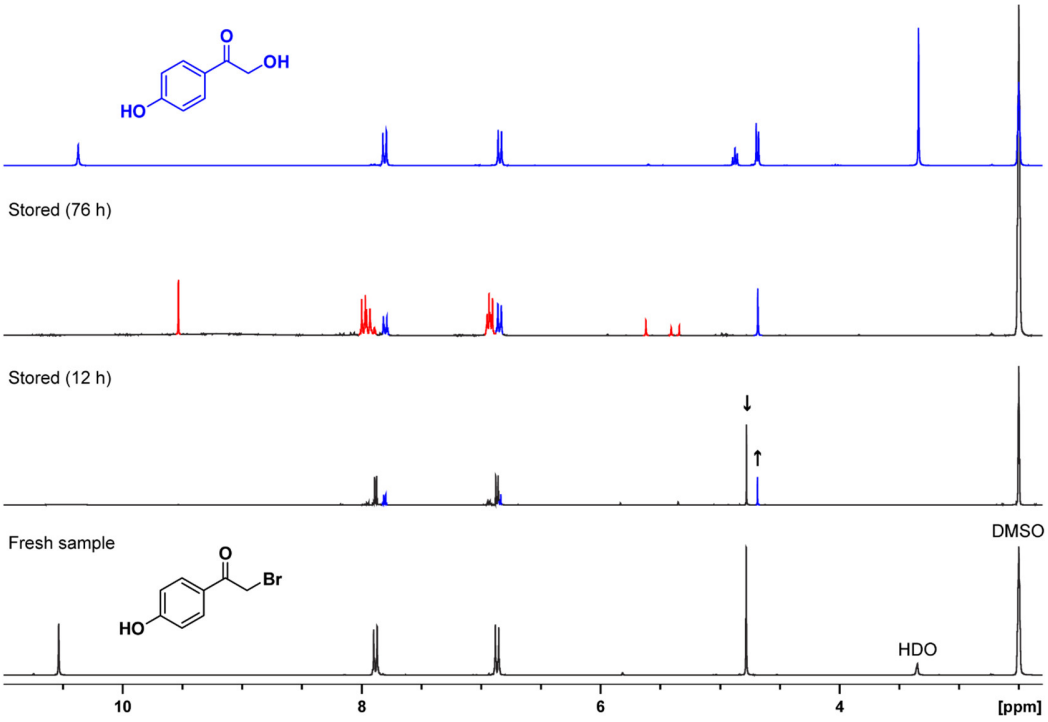

Figure 127: NMR spectra of the decomposition of the compound **220** in DMOS-d_6.

The product identity could be assigned by comparison to a standard sample **23** (upper panel in Figure 127). Prolonged storage (76 h) leads to a complete decomposition of compound **220**, giving the alcohol **23** and other, unidentified products (red color in Figure 127) which maybe results from Kornblum oxidation. No decomposition could be seen in saturated $CDCl_3$ solution.

Vis-pump-IR-probe measurements of the compounds **217**-**219** were done by Daniela Kern-Michler and Carsten Neumann (the data are not shown in this work). It could be seen, that all the samples undergo a photoreaction. The IR signal of the leaving group from the compound **219**, formic acid, was overlaying with other carbonyl group modes in the IR spectrum, thereby it was not selected for VIPER measurements. The irradiation of the azide **217** gave a complex and unreproducible mixture of products. Photolysis of structurally similar α-azido acetophenone also yielded s mixture of multiple photoproducts rising from the formation of benzoyl radicals and triplet alkyl nitrenes as primary photoproducts.[231] The uncaging of the thiocyanate **218** happened cleaner, and the leaving group, thiocyanate anion, was well spectrally separated from other signals in the IR spectrum. Thus, for VIPER experiments the thiocyanate was chosen as the leaving group and the isotopically labeled *p*HP-SCN was prepared.

In the carbonyl group ^{13}C labeled *p*HP thiocyanate **228** (Figure 128) was prepared in a three step synthesis. Friedel-Craft acylation of phenol **222** with isotopically labeled acetyl chloride **226** was done as described in the synthesis of compound **221** (Figure 123). This was followed by bromination with $CuBr_2$ as described for compound **220** (Figure 124) to give compound **227**. It was then transformed to thiocyanate in a reaction with NH_4SCN as described for compound **218** (Figure 119).

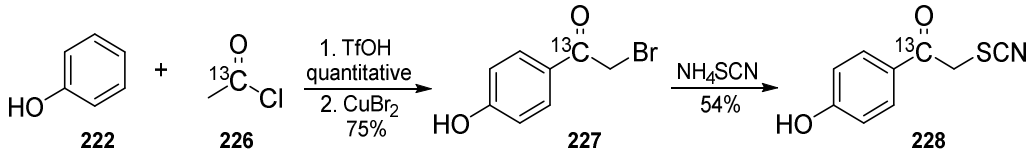

Figure 128: Synthesis of in the carbonyl group ^{13}C labeled *p*HP thiocyanate **228**.

Compound **230** with a ^{13}C label in each position of the aromatic ring (Figure 129) was prepared in a Friedel-Crafts acylation of ^{13}C-labeled phenol **229** with 2-bromoacetyl chloride **224** as previously described for the compound **220** (Figure 125), followed by reaction with a NH_4SCN as described for compound **218** (Figure 119).

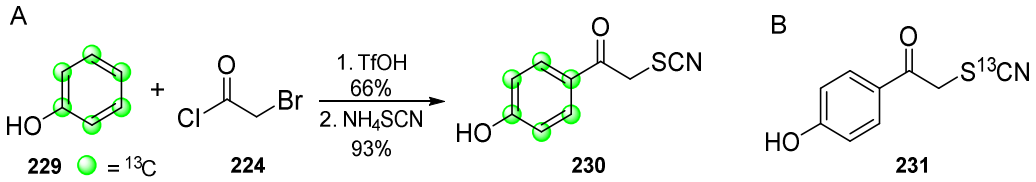

Figure 129: *A* - Synthesis of in the aromatic ring ^{13}C labeled pHP thiocyanate **230**. *B* - Structure of the thiocyanate **231** with a ^{13}C label in the leaving group.

The same reaction was used for the preparation of *p*HP derivative **231** with ^{13}C label in the leaving group, as starting materials using compound **220** and $KS^{13}CN$.

3.2.7. The analytical data of ^{13}C incorporation in *p*HP thiocyanates

In order to control the ^{13}C isotope label incorporation in *p*HP thiocyanates NMR and IR spectroscopy and high resolution mass spectrometry was used. First, the signals in ^{1}H and ^{13}C NMR spectra (Figure 173) of *p*HP thiocyanate **218** were assigned using 2D NMR experiments (COSY - Figure 174, HSQC - Figure 175 and HMBC - Figure 176). The correct incorporation of the ^{13}C label in *p*HP thiocyanates **228** and **230-231** could be confirmed by comparing the respective ^{1}H and ^{13}C spectra to the assigned spectra of unlabeled compound **218**. The spectra are shown in the appendix (Figure 177 for **228**, Figure 178 for **230** and Figure 179 for **231**). Further confirmation of the correct signal assignment in NMR spectra could be obtained from the $^{1}H^{13}C$ and $^{13}C^{13}C$ couplings observed for the compounds containing the ^{13}C label. The HRMS analysis also confirmed the incorporation of the ^{13}C isotopes (for more details please see the experimental part of this work).

Finally, the incorporation of the ^{13}C label and their position in the *p*HP thiocyanates **228**, **230** and **231** were confirmed by IR spectroscopy. The most relevant signals in the IR spectra are shown in Figure 130.

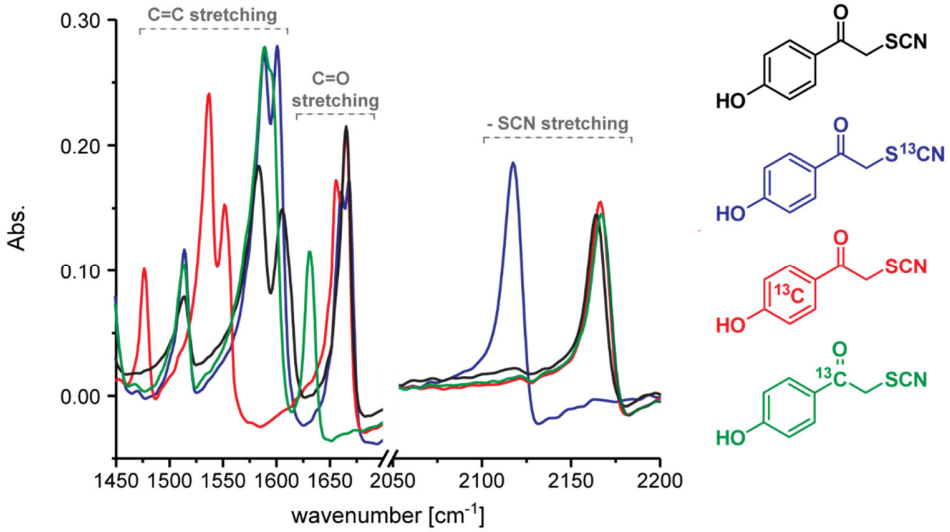

Figure 130: ATR-FTIR spectra of the *p*HP thiocyanate (with and without ^{13}C label).

The –SCN stretching mode is largely unaffected from the ^{13}C label in the aromatic ring (**230**) or carbonyl group (**228**) and is located at the same frequency as for the unlabeled compound. If the ^{13}C label is located in the thiocyanate group (**231**, blue in Figure 130), its stretching vibration shifts down by ~48 cm^{-1} from 2165 cm^{-1} for unlabeled compound (**218**, black in Figure 130) to 2117 cm^{-1} for -S^{13}CN. A ^{13}C label in the carbonyl group has a similar effect on carbonyl mode. The C=O stretching mode for the labeled compound (**228**, green in Figure 130) is shifted down by ~35 cm^{-1} from 1665 cm^{-1} for the unlabeled compound to 1630 cm^{-1} for ^{13}C=O. The higher frequency ring distortion modes for the compounds without ^{13}C label in the aromatic ring are located at 1605 cm^{-1} and 1583 cm^{-1} while for ^{13}C labeled aromatic ring (**230**, red in Figure 130), they are shifted down by ~45-55 cm^{-1} to 1551 cm^{-1} and 1537 cm^{-1}. The lower frequency ring distortion mode for the compounds without ^{13}C label in the aromatic ring is located at 1514 cm^{-1} while for the ^{13}C labeled aromatic ring it is shifted down by ~38 cm^{-1} to 1476 cm^{-1}. The bond assignment is in good agreement with other *p*HP derived photocage (with phosphate as leaving group).[232]

The IR spectra confirmed the correct isotopic label incorporation in the *p*HP-SCN molecules. The ^{13}C labeled modes of variously labeled compounds are well spectrally separated from each other and from the unlabeled compound, thus suitable for VIPER experiments.

3.2.8. The irradiation study of *p*HP photocages

The prepared *p*HP thiocyanate **218** and pHP formate **219** were irradiated in order to test their photoactivity. The *p*HP derived photocages are soluble not only in organic solvents, but also in water, so the photoreaction was tested in both.

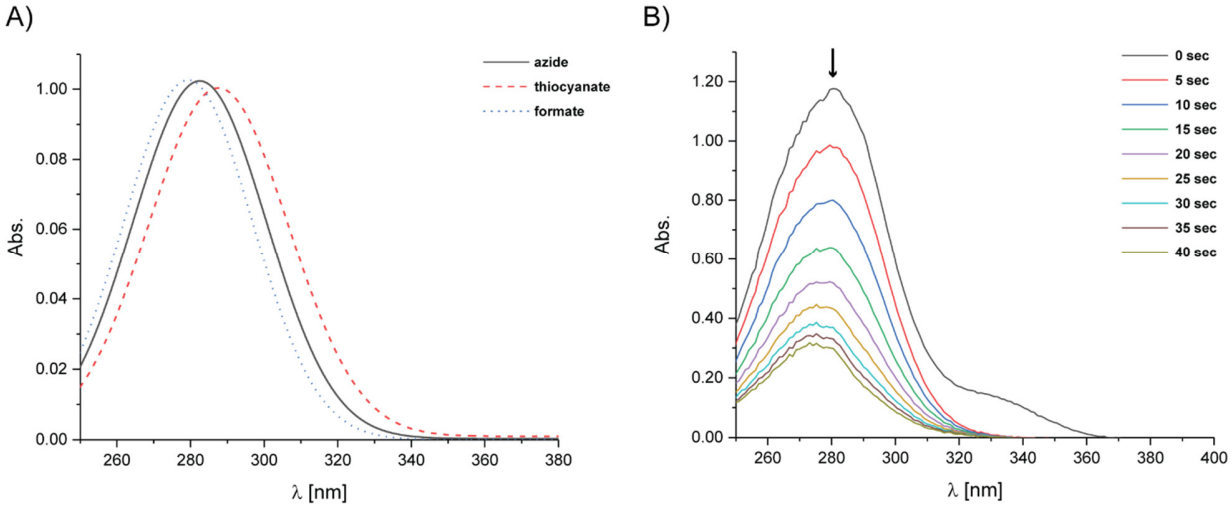

Figure 131: *A* - Normalized UV-Vis absorbance spectra of the *p*HP azide (**217**), thiocyanate (**218**) and formate (**219**) in MeCN. *B* - Irradiation of the formate **219** (ca. 95 µM in H_2O) at 310 nm (volume 2 mL, 1 cm pathlength, the irradiation power was not specified).

The absorbance spectrum maxima of the *p*HP azide (**217**), thiocyanate (**218**) and formate (**219**) lie around 280-290 nm (Figure 131A). Upon irradiation of the *p*HP photocages, the absorbance spectra should change due to lost conjugation between the carbonyl group and the phenyl ring (see uncaging mechanism in chapter 1.3.1). Thereby, a saturated solution of formate **219** in H_2O was irradiated at 310 nm and the reaction was controlled by UV-Vis spectroscopy (Figure 131B). Indeed, as soon as the irradiation was started, the absorbance at 280 nm decreased.

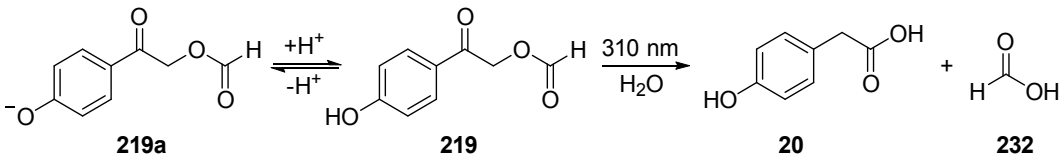

Figure 132: The protolytic equilibrium of phenol **219** and phenolate **219a** and the uncaging reaction.

The pK_a of the phenolic hydroxyl group is 8.0, thereby in unbuffered aqueous solution a small amount of a deprotonated phenol **219a** is present (Figure 132). Its absorbance peak can be seen in the absorbance spectrum before the irradiation (Figure 131B, 0 sec) between 320-360 nm.[13] This signal disappears when the irradiation is started, because from each *p*HP molecule two equivalents of an acid are released (*p*-hydroxyphenyl acetic acid **20** and formic acid **232**). That

lowers the pH value of the solution, shifting the protolytic equilibrium between phenol and phenolate the protonated form **219**.

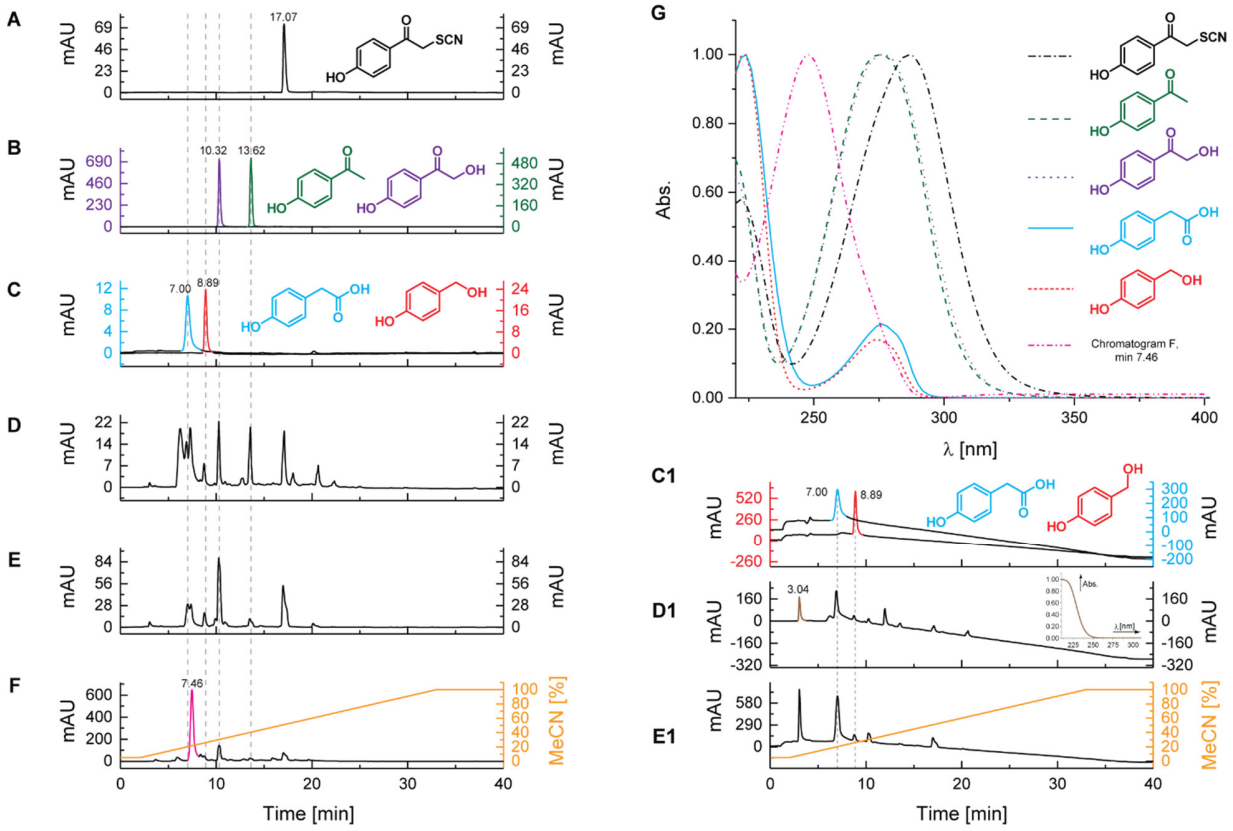

Figure 133: HPLC chromatograms with detection at 254 nm: *A* - *p*HP thiocyanate **218**; *B* - acetophenone **221** (green) and hydroxyl keton **23** (violet); *C* - *p*-hydroxyphenyl acetic acid **20** (blue) and 4-Hydroxybenzyl alcohol **26** (red); *D* – thiocyanate **218** after irradiation by high pressure mercury lamp (in 1:1 MeCN-d_3+D_2O); *E* - thiocyanate **218** after irradiation by low pressure mercury lamp (in 1:1 MeCN-d_3+D_2O); *F* - thiocyanate **218** after irradiation by laser light source in dry MeCN; *G* – normalized absorbance spectra of thiocyanate **218** and known reaction products (measured by HPLC); HPLC chromatograms with detection at 220 nm: *C1* - *p*-hydroxyphenyl acetic acid **20** (blue) and 4-Hydroxybenzyl alcohol **26** (red); *D1* – thiocyanate **218** after irradiation by high pressure mercury lamp (in 1:1 MeCN-d_3+D_2O), the UV-Vis absorbance spectra of the peak at 3.04 min is shown in inlay; *E1* - thiocyanate **218** after irradiation by low pressure mercury lamp (in 1:1 MeCN-d_3+D_2O); The dashed gray lines over chromatograms serve as guides-to-the-eye.

A further irradiation study was performed for the thiocyanate **218**. A sample was prepared in MeCN-d_3 mixed with D_2O (1:1 v/v %) and irradiated using a high pressure mercury arc lamp (no filters were used) or a low pressure mercury arc lamp (254 nm). The irradiated mixtures were analyzed by HPLC and NMR. The HPLC analysis of the starting material is shown in Figure 133 (panel A), along with expected photoproducts (panels B-C). The irradiated mixtures in MeCN-d_3 /D_2O are shown in panels D and E. Panel F shows irradiation, which was performed in dry MeCN.

When the irradiation is performed in presence of water (D_2O), all four known photoproducts can be seen (compare segments D-E with the standard substances shown in segments B-C in Figure 133). In the sample, which was irradiated with a high pressure mercury arc lamp (such a lamp emits a broadband UV-Vis light), a formation of multiple (secondary) photoproducts can be seen (Panel D). A sample, which was irradiated by a low pressure mercury lamp (the main emitted wavelength is 254 nm), has less photoproducts. Irradiation in dry MeCN (laser light source), gives one major photoproduct (Panel F). The UV-Vis spectra of this peak differs from other photoproducts (Figure 133G, magenta). Its identity was not determined.

The main expected photoproduct *p*-hydroxyphenyl acetic acid **20** has a low intensity absorbance peak at 275 nm and an absorbance minimum at 254 nm (Figure 133G, blue). The same can be said about another known photoproduct, the 4-hydroxybenzyl alcohol **26** (Figure 133G, red). Other potential photoproducts have much stronger absorbance intensities at 254 nm (acetophenone **221** and alcohol **20**, Figure 133G, green and violet). These absorption differences might lead to wrong interpretation of product distribution in the irradiated samples if only the HPLC chromatograms recorded at 254 nm (as in Figure 133A-F) are analyzed. Thereby also a 220 nm wavelength was used for the detection since at this wavelength all compounds absorb comparably. At this wavelength *p*-hydroxyphenyl acetic acid **20** was confirmed as the major photoproduct (Figure 133C1-E1). These results fit to the expectations according to the reaction mechanism (see Chapter 1.3.1). In the chromatograms which are recorded at 220 nm another peak can be seen eluting at 3.04 min. The early elution time and absorbance spectrum (see the inlay, Figure 133D1) suggest that it could be the released thiocyanate anion. The extinction coefficient of –SCN at 220 nm is in the same order of magnitude (10^3 M^{-1} cm^{-1}) as it is for phenol, which is in line with the similar peak intensity of the two photoproducts.[233,234]

The NMR study further confirms the conclusions from the HPLC data. After 60 minutes of irradiation the expected product *p*-hydroxyphenyl acetic acid **20** is formed (Figure 134, blue color) as the major photoproduct.

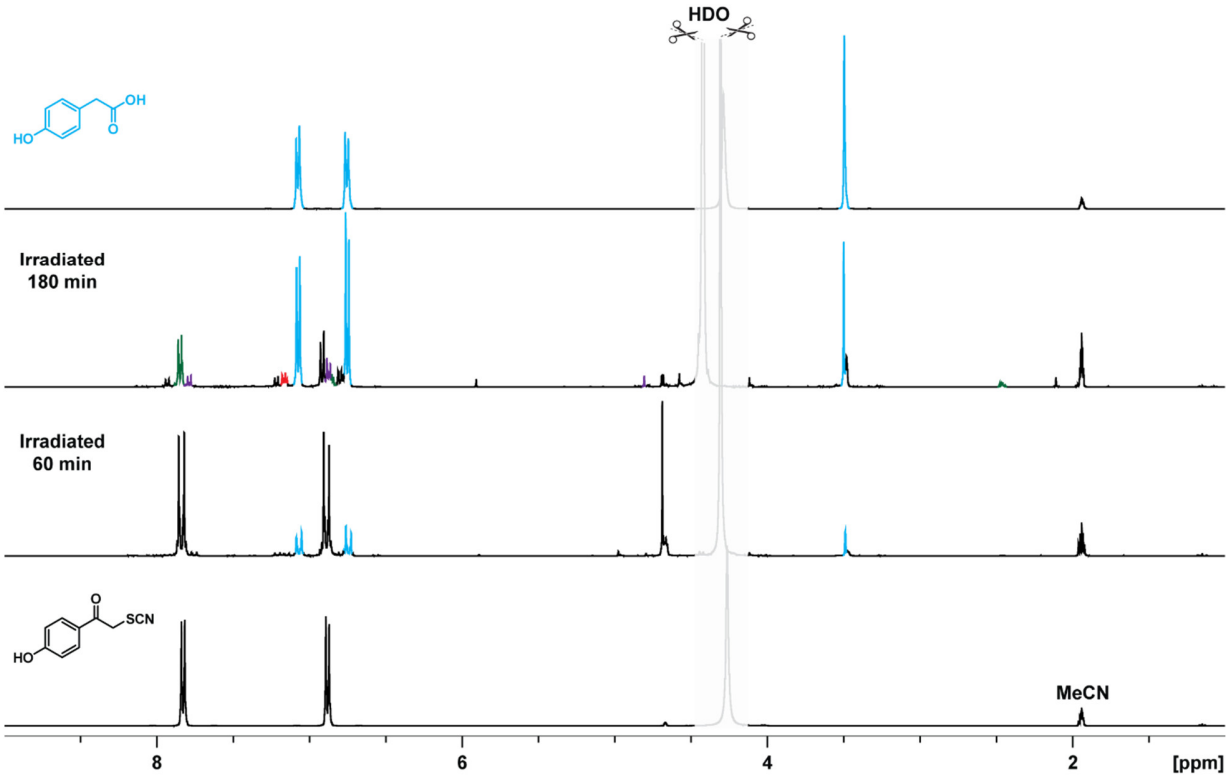

Figure 134: ^{1}H NMR (400 MHz) analysis of the thiocyanate **218** irradiation by high pressure mercury lamp (in 1:1 MeCN-d_3+D_2O) for 60 and 180 min. For a comparison, spectra of expected photoproduct – the *p*-hydroxyphenyl acetic acid **20** (blue) is also given. For clarity the HDO signal is covered by a semitransparent mask.

Upon longer irradiation time, also other photoproducts could be detected (Figure 134, green and violet color). By comparison to standard samples (data not shown) these could be assigned to acetophenone **221** and alcohol **23**, thus confirming observations in the HPLC analysis.

3.2.9. Summary about *p*HP photocages

The synthesis of *p*HP derivatives is not complicated and the individual steps have good to quantitative yields. Thiocyanate demonstrated the best uncaging behavior in Vis-pump-IR-probe experiments of all prepared derivatives bearing IR active leaving groups (azide, formate and thiocyanate). Thus ^{13}C labeled derivatives of thiocyanate were prepared and their IR spectra compared. The ^{13}C labeled vibrational modes were well separated from unlabeled analogues, thereby they are suitable for VIPER experiments. The irradiation experiments revealed that *p*HP thiocyanate uncages efficiently and the produced photoproducts are as reported in literature. At the time of submission of this work, the VIPER experiments are still in course.

4. Summary and Outlook

The objective of this work was the design and synthesis of new photolabile protecting groups. The 3-diethylaminobenzyl (DEAMb) photocage, which is known to release even bad leaving groups with good quantum yields, was selected as the structural base of this work. The main drawback of DEAMb photocage is the need to use far UV light to trigger the photoreaction. It was anticipated that expanding its π-electron system (*e.g.* by further aromatic substituents) would improve its spectral properties.

Results were positive and the spectral properties of the DEAMb photocage has been improved without losing its good photoactivity. Thus, expanding of the aromatic conjugation by introducing a second aromatic ring is a valid approach to improve spectral properties of the DEAMb photocage. The second aromatic ring can be introduced easily by Suzuki coupling. This reaction happens best if the DEAMb-derived aryl halide has minimal sterical hindrance close to the halogen atom (*para*, *meta* positions relative to the amino group). The use of glutamic acid as a leaving group allows to perform the photochemical characterization in a solvent with a high water content.

The best spectral improvement is shown by compounds which have the second aromatic ring in *para* and *meta* positions. Substituents *ortho* to the amino group have low molar absorption coefficients, since the two aromatic rings are forced out of coplanarity due to steric hindrance. Derivatives with a strong electron withdrawing substituent have the most redshifted absorption spectra, but the lowest uncaging quantum yields. Corresponding to Zimmerman's meta effect, this effect can be explained by the decreased electron density in the *meta* position (at the benzylic carbon) of the DEAMb core. TDDFT computations of the frontier molecular orbitals qualitatively confirm this explanation.

Meta-phenyl substituted DEAMb had the highest uncaging quantum yield (42%) which results in an uncaging cross section ($\varepsilon\Phi_{365}$) of 225 M^{-1} cm^{-1}. The release of the glutamic acid can be shown by TLC and ninhydrin staining. The best results for glutamic acid detection by HPLC can be achieved using HILIC stationary phase and detection at 210 nm or by derivatization with *ortho*-phthaldialdehyde. Furthermore, also ^{1}H NMR is suitable for the detection of glutamic acid release.

Blocking of the rotational freedom around the biphenyl bond further improves the spectral properties of the DEAMb photocage. By linking the second aromatic ring to the benzylic carbon,

fluorene derivatives are produced. TDDFT computations of *meta*-electron donor substituted fluorenes reveal an increased electron density in the excited state at the benzylic carbon, which is a potential prerequisite to achieve bond dissociation (uncaging). By changing the substituents at the amino group or by introducing an *m*-amino group in both aromatic rings of the fluorene molecule, the spectral properties can be tuned in a predictable manner. For example, replacing of methyl groups by aryl red-shifts the absorption spectrum maximum, but decreases the molar absorption coefficients due to a more pronounced nature of sp^3 hybridization of the nitrogen atom in case of the bulky aryl substituents.

All prepared fluorenol derivatives were photoactive and the uncaging quantum yields ranged from good to very good. Uncaging cross section values for acetate release were very good ($\varepsilon\Phi_{365}$ up to 5300 M^{-1} cm^{-1}) and neither of the compounds had an uncaging cross section below 170 M^{-1} cm^{-1}.

The results in this work confirm that photolabile protecting groups, which demonstrate photoactivity due to increased electron density at the position where the leaving group is attached, can be optimized by combining computational data with organic synthesis. The frontier molecular orbital shape and the orbital coefficients give already enough information to select the most promising (or the opposite – least promising) derivatives for the synthesis.

In order to avoid decrease in the photoreaction's quantum yield due to internal conversion, it is advisable to decrease rotational freedoms in the molecule maximally. Furthermore, the review of literature and experimental results show, that sterical effects play an important role in the photochemical properties and should be carefully considered when the substituent pattern of a photocage is designed.

Irradiation of some fluorenols in methanol gave corresponding methyl ethers, thus a formal release of hydroxide ion and generation of, presumably, fluorenyl cation is possible photochemically. Also for these photoreactions the quantum yields were high (28-67%) and the uncaging cross section ($\varepsilon\Phi_{365}$) even reached 14300 M^{-1} cm^{-1}. Preliminary work in aqueous conditions shows, that the fluorenyl cation can be quenched by nucleophiles. Thus, the fluorene derivatives described in this work have a high potential not only as photolabile protecting groups, but also as photochemically generated electrophiles.

Fluorenyl cations in ground state are Hückel-antiaromatic, thus should have a high energetic barrier of thermal generation. Consequently, the ease of ground state fluorenyl cation generation by a photochemical reaction is of high theoretical interest. A further exploration of interesting

reactivity, observed in this work, by kinetic, spectroscopic and computational studies should be performed.

The second part of this work describes the custom synthesis of coumarin and *para*-hydroxyphenacyl (*p*HP) derived photocages for the VIPER project. VIPER (VIbrationally Promoted Electronic Resonance) is a mixed pulse sequence (IR-pump, UV-Vis-pump, IR-probe) developed in the lab of Jens Bredenbeck as an analytical tool in 2D IR spectroscopy. It was proposed, that a selective uncaging from one molecule in an ensemble of near-identical ones could be possible using VIPER if this molecule would have distinct IR absorption band (for vibrational pre-excitation). Isotopologues and isotopomers are an extreme case of molecules which are near identical and differ only by isotopic composition or position. As a result in solution and at room temperature they have an identical UV-Vis absorption spectrum but different IR spectrum. To that end, isotopologues and isotopomers of coumarin and *p*HP derived photocages had to be prepared for a proof of principle VIPER-uncaging study.

The synthesis routs of isotopically labeled coumarin and *p*HP derived photocages were based on literature known methods and were successful. Reaction yields were satisfying and reproducible. The spectroscopic experiments done for the coumarin photocage by Daniela Kern-Michler, Carsten Neumann, Nicole Mielke and Luuk van Wilderen (group of Jens Bredenbeck) confirmed that it is possible to achieve selective photoreaction of one coumarin isotopomer in presence of another using the VIPER pulse sequence. Follow up studies with *p*HP photocage should demonstrate a selective release of the leaving group from only those molecules, which have been excited by VIPER pulse sequence.

5. Experimental Part

A large part of Chapter 5 is reproduced from M. Reinfelds, J. von Cosel, K. Falahati, C. Hamerla, T. Slanina, I. Burghardt, A. Heckel, A New Photocage Derived from Fluorene, *Chem. Eur. J.* **2018**, 24 (doi: 10.1002/chem.201802390) with permission; Copyright 2018 Wiley-VCH Verlag GmbH & Co. KGaA, Weinheim. Experimental details reproduced here can be found in the article and its electronic supporting information and will not be referenced separately throughout the chapter.

5.1. General information

Reagents and solvents were purchased from TCI, Acros Organics (Thermo Fisher Scientific), Sigma Aldrich (Merck), Fluorochem and abcr, and were used as received. Carbon ^{13}C-enriched starting materials where purchased from: ethyl acetoacetate-1-^{13}C, acetyl chloride-1-^{13}C and potassium thiocyanate-^{13}C from Sigma Aldrich (Merck), ethyl acetoacetate-3-^{13}C from Eurisotop and phenol-^{13}C6 from Toronto Research Chemicals.

For normal and reverse phase TLC pre-coated ALUGRAM® Xtra SIL aluminum sheets from Macherey-Nagel were used. Visualization was done with UV light (254 and 365 nm). For direct phase column chromatography Macherey-Nagel silica gel 60 (particle size 0.04-0.06 mm) was used, for reverse phase column chromatography Macherey-Nagel prefilled Chromabond® Flash RS200 C18ec. Direct phase purification was done in glass columns or Büchi Sepacore® setup, equipped with a C601 pump, C615 pump manager, C635 detector and C660 fraction collector. Technical grade solvents were used (EtOAc - ethyl acetate, Cy – cyclohexane). Reverse phase purification was exclusively done with Sepacore® setup, using analytical grade solvents (MeCN and ultra-pure water).

NMR spectra were measured on a Bruker DPX 250, AV 300, AV 400, AV 500 MHz or DRX 600 device. Deuterated solvents (purchased at Eurisotop) were used for sample preparation. Spectra were referenced to the solvent peak. The values used therefore were: $CDCl_3$ ^{1}H 7.26, ^{13}C 77.16; DMSO-d_6 ^{1}H 2.50, ^{13}C 39.52; MeCN-d_3 ^{1}H 1.94, ^{13}C 1.32 and 118.2; CD_3OD-d_4 ^{1}H 3.31, ^{13}C 49.00; D_2O ^{1}H 4.79, ^{13}C no reference was done. In those cases when solvent mixtures were used (MeCN-d_3 + D_2O and CD_3OD-d_4 + D_2O), spectra were calibrated to the organic solvent signal. Chemical shifts (δ) are reported on a ppm scale. Following abbreviations (or combinations thereof) were used to describe multiplicities: s = singlet, d = doublet, t = triplet, q = quartet, m = multiplet, br = broad. Coupling constants (*J*) are reported in Hertz (Hz).

Mass spectrometry was performed on ThermoFisher Surveyor MSQ™ (ESI - Electrospray ionization) and MALDI-LTQ Orbitrap XL™ (HRMS - High-Resolution Mass Spectrometry) device from Thermo Fisher Scientific. Measurements were done in Serviceeinheit Massenspektrometrie of Goethe University (Fachbereich 14) by Andreas Münch, Dr. Uwe Hener, and Simon Zenglein (ESI-MS); and Matthias Brandl (HRMS).

UV-Vis spectra were measured in a 1.0 cm quartz fluorescence cuvette (QS) from Hellma-Analytics. Two different spectrometers were used unless otherwise noted: Ocean Optics USB4000 detector connected *via* optical fiber and convex lens, mounted in an adapter, to cuvette holder CVH100 (Thorlabs). On the opposite side of the cuvette holder a DH-mini light source (Ocean Optics) was connected in the same way. The results were evaluated using an in-house programmed software (*PHITS*; Photoswitch Irradiator Test Suite) based on LabVIEW. The second spectrometer was a JASCO-V650. In both cases spectra were measured with 1 nm steps.

Irradiation experiments were done in a 1.0 cm quartz fluorescence cuvette (QS) from Hellma-Analytics equipped with a magnetic stirrer. The light source (365 nm LED M365L2 unless noted otherwise) was operated by DC2100 or DC4100 LED drivers in external trigger mode (both from Thorlabs). An in-house programmed software *PHITS* or arbitrary morphing waveform generator WF-820 (from Mair & Rohner OEG) was used as external trigger.

For high-performance liquid chromatography an Agilent Technologies 1260 Infinity instrument was used, equipped with a quaternary pump, automatic liquid sampler, thermostatted column compartment and diode array detector. Separation was done using MultoKrom® 100-5 C18 column (250 x 4.6 mm) from CS-Chromatographie Service GmbH unless noted otherwise. Binary solvent mixtures were used for elution. Typical gradients used for quantum yield determination are described in Table 6 and shown in Figure 135.

Table 6: HPLC gradients used for quantum yield determination.

Gradient 1		Gradient 2		Gradient 3		Gradient 4	
Time (min)	Solvent A (%)	Time (min)	Solvent A (%)	Time (min)	Solvent A (%)	Time (min)	Solvent A (%)
0 to 5	25	0 to 1	65	0 to 1	70	0 to 1	70
5 to 20	25 to 100	1 to 7	65 to 100	1 to 7	70 to 100	1 to 5	70 to 100
20 to 25	100	7 to 15	100	7 to 15	100	5 to 15	100

Gradient 1: Solvent A – MeCN; solvent B – 50 mM NH_4OAc in ultra-pure water.

Gradients 2-4: Solvent A – MeCN; solvent B – 50 mM NH_4OAc in ultra-pure water premixed with 5 v/v% MeCN.

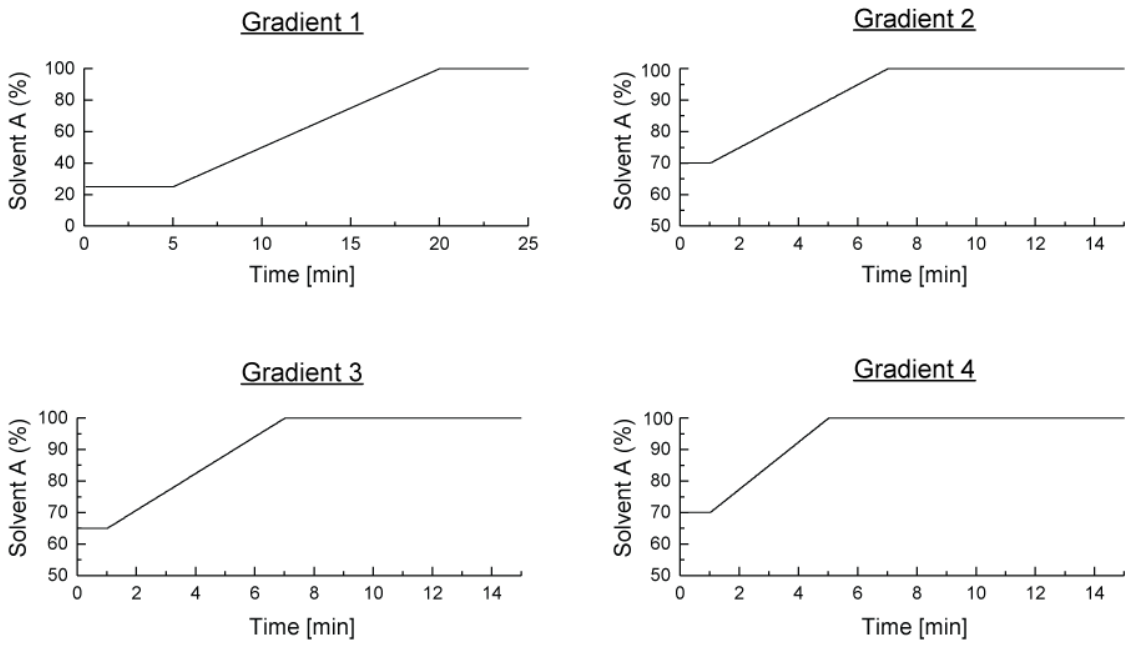

Figure 135: HPLC gradients.

Following gradients have been used for quantum yield determination of the compounds indicated:

Gradient 1: **128**, **127**, **131**, **132**, **137**, **138**, **139**, **142**, **145**, **147**, **148**, **149**, **150**, **167**;

Gradient 2: **174b**, **188**, **165**, **177**;

Gradient 3: **285a**; **168** (with modification of solvent A: 1 to 11 min 70 to 100%, 11 to 15 min 100%);

Gradient 4: **178**, **182**, **181**;

In the appendix of this work, NMR spectra in form of figures are shown for the following key compounds: **128**, **133**, **137**, **141**, **143**, **144**, **146**, **207**, **207a**, **207b**, **201**, **202**, **203**, **204**, **217**, **218**, **219**, **228**, **230**, **231**;

For other key compounds (**117-120**, **123**, **127**, **131**, **132**, **138-140**, **142**, **145**, **147- 150**, **167**, **168**, **174a**, **174b**, **178**, **182**, **188**, **233**) the reader is referred to the electronic supporting information of M. Reinfelds, J. von Cosel, K. Falahati, C. Hamerla, T. Slanina, I. Burghardt, A. Heckel, A New Photocage Derived from Fluorene, *Chem. Eur. J.* **2018**, 24 (doi: 10.1002/chem.201802390).

5.2. Molar absorption coefficient measurements

A stock solution of compound **167** was prepared by weighting small amount of sample (approx. 1.09 mg) in glass vial and dissolving it in 15 mL of 0.1M TEAA (containing 20% MeCN). Then a dilution series from this stock solution was prepared. Absorbance spectra in wavelength range 220-550 nm were measured for all solutions.

The data analysis was started by baseline correction. This was done by subtracting the average value of baseline shift in the wavelength range where sample does not absorb (in this case 450-550 nm) from the entire spectra. Then the linearity of measured data was checked by plotting absorbance vs. concentration (Figure 136).

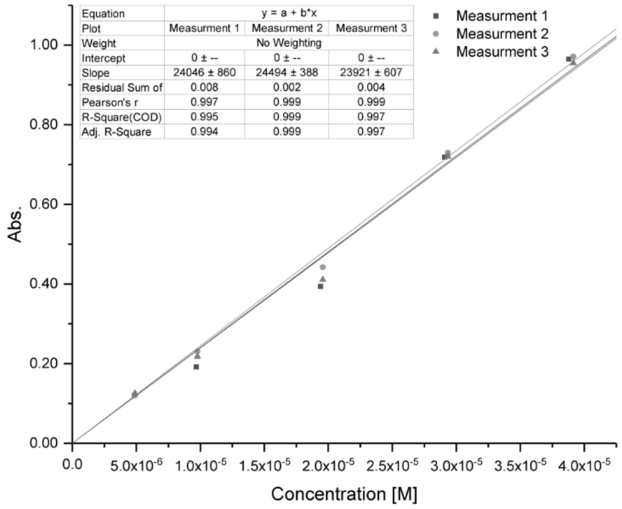

Figure 136: Absorbance against concentration for compound **167** (at 311 nm), fitted using liner regression. Fit parameters are shown in inlay. Measurements were done in 0.1M TEAA + 20% MeCN.

Then the molar absorption coefficient was calculated at each wavelength. The average molar absorption coefficient of three measurements is reported (Figure S17).

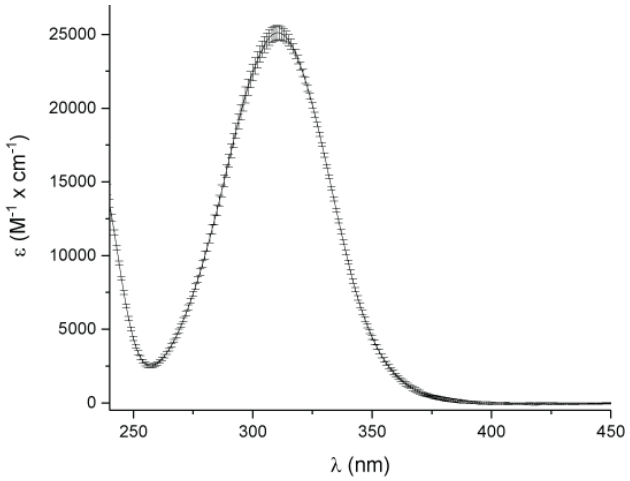

Figure 137: The average molar absorption coefficient of the compound **167**, from three measurements (with error bars). Measurements were done in 0.1M TEAA + 20% MeCN.

5.3. Quantum yield measurements

5.3.1. Actinometry

Iron (III) ferrioxalate actinometry was used to determinate the photon flux of a LED. A modified method of Hatchard and Parker[235] was used:

The necessary solutions:

1. $K_3[Fe(C_2O_4)_3]$ in 50mM H_2SO_4 (c = 0.006 mol·L^{-1})
2. 1,10-phenanthroline 0.12% (in H_2O)
3. Buffer A: 180 mL of 0.5M H_2SO_4 with 300 mL 1M sodium acetate and 20 mL of H_2O
4. Buffer B: 100 mL of buffer A with 160 mL 0.05M H_2SO_4 and 100 mL H_2O

A $K_3[Fe(C_2O_4)_3]$ solution (2 mL) was irradiated for 2 seconds in a 3 mL quartz fluorescence cuvette with a magnetic stirrer. Aliquot of 120 µL was then taken and mixed with 120 µL of 1,10-phenanthroline and 1260 µL buffer B (= the total volume 1.5 mL). The same procedure was repeated for 10, 22 and 30 seconds of irradiation time. The absorbance at 510 nm was measured for all collected samples. This procedure was repeated two times more. Then the average value of absorbance was plotted against irradiation time to confirm linearity (Figure 138).

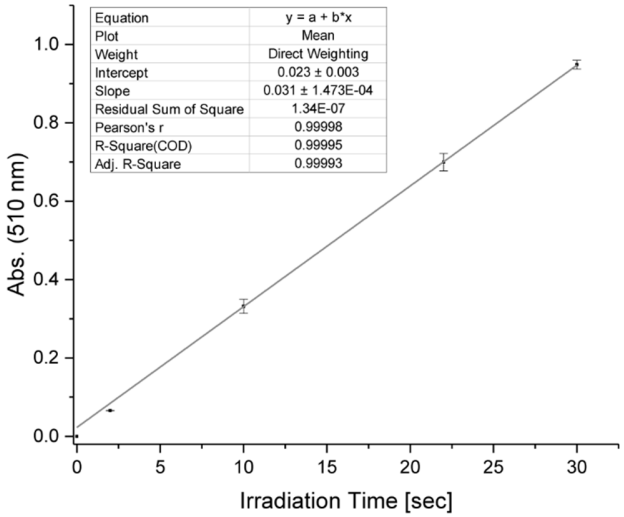

Figure 138: Absorbance against irradiation time fitted using linear regression. Fit parameters are shown in inlay.

To calculate the amount of Fe^{2+} produced after 10 seconds of irradiation Equation 1 was used:

$$n_{Fe^{2+}} = \frac{V_{irr.}}{V_{aliq.}} \cdot \frac{k_1 \cdot t \cdot V_{incub.}}{\varepsilon_{510}} = \frac{2.000\ (mL)}{0.120\ (mL)} \cdot \frac{0.031\ (s^{-1}) \cdot 10(s) \cdot 0.0015\ (L)}{11050(M^{-1} \cdot cm^{-1})} = 7.01 \cdot 10^{-7}(mol) \qquad \text{(Eq. 1)}$$

where $V_{irr.}$ is the irradiated volume (2 mL), $V_{aliq.}$ is the aliquot volume (120 µL), k_1 is the slope from graph ($0.031 s^{-1}$), t is time (here, 10 seconds), $V_{incubated}$ is the volume of the complexed Fe with 1,10-phenanthroline (1.5 mL), ε_{510} is the molar absorption coefficient of $Fe^{2+}(Phe)_3$ complex (ε_{510} = 11 050 M^{-1} cm^{-1}).

To calculate photon flux of the light source used (in this example 365 nm LED) the Equation 2 was then used:

$$n_{photons} = \frac{n_{Fe^{2+}}}{\Phi \cdot t} = \frac{7.01 \cdot 10^{-7}(mol)}{1.21 \cdot 10(s)} = 5.80 \cdot 10^{-8}(mol \cdot s^{-1}) \qquad \text{(Eq. 2)}$$

where $n_{Fe^{2+}}$is the iron produced (as calculated in the equation 4), Φ is the quantum yield of the reaction at the given wavelength (1.21 at 365 nm, 1.24 at 310 nm)[235], t is the irradiation time (here, 10 seconds).

5.3.2. Reaction quantum yields

A solution (approx. 50 mL; 33.8µM) of the compound **167** was prepared. The exact concentration was determined spectroscopically. To this mixture ca. 40 mg of phenylalanine was added which serves as internal standard for HPLC analysis, and does not absorb light in irradiation wavelength (Figure 139). After the phenylalanine had dissolved, the solution was filtrated using paper filter.

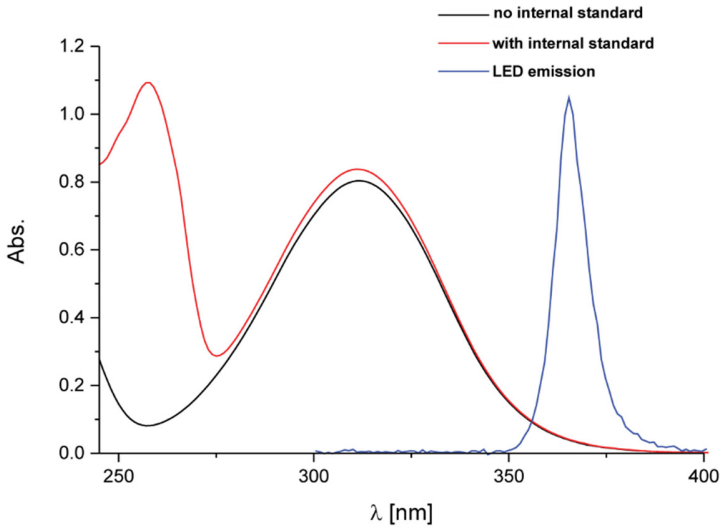

Figure 139: Absorbance of compound **167**, prepared for quantum yield measurements (in 0.1M TEAA + 20% MeCN).

A 1.5 mL aliquot from the prepared solution was irradiated for various times. Each time point was repeated three times. The conversion of the starting material was determined by HPLC as the ratio of the peak areas of the internal standard and the starting material (detection at 254 nm). The disappearance of starting material was plotted as a function of time (Figure 140). Resulting graph is fitted using exponential decay function (Equation 3):

$$y = A_1 e^{\frac{-x}{t_1}} + y_0 \qquad \text{(Eq. 3)}$$

Where x is the time, A_1 and t_1 are fit parameters and y_0 is a constant.

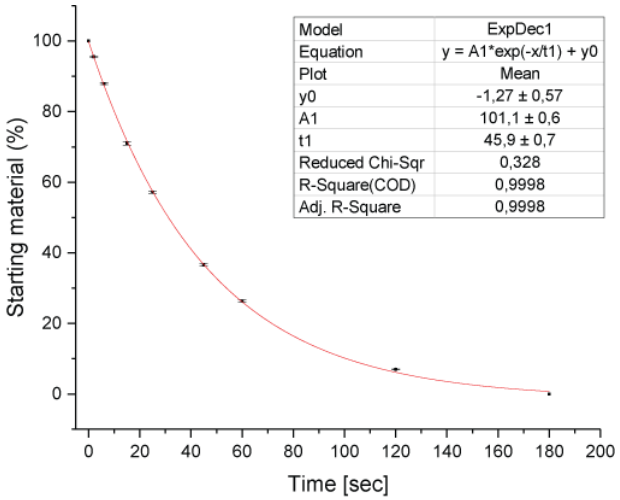

Figure 140: The amount of starting material (%) at different irradiation times, fitted by exponential decay function. Fit parameters are shown in inlay.

To determinate the initial rate of the photoreaction only the beginning of the curve is important. Thereby, the first derivative of the function shown in Equation 3 is calculated (Equation 4):

$$y' = -\frac{A_1 e^{\frac{-x}{t_1}}}{t_1} \quad \text{(Eq. 4)}$$

Placing the values of the fit parameters in this equation (x = 0 s) gives the rate of the concentration change of the starting material in the beginning of the reaction (Equation 4.1):

$$y' = -\frac{101.1\ (\%)}{45.9\ (s)} = -2.20\ (\% \cdot s^{-1}) \quad \text{(Eq. 4.1)}$$

Knowing the concentration of irradiated solution, the irradiated volume, photon flux of the light source and the absorbance of the solution, the quantum yield is calculated using Equation 5:

$$\Phi = \frac{[c] \cdot V \cdot \Delta C}{n_{photons} \cdot (1 - 10^{-A})} \quad \text{(Eq. 5)}$$

Where $[c]$ is the concentration of the solution, V is the irradiated volume, Δc is the change in concentration, determined in the Equation 4.1; n_{photons} is the photon flux at irradiation wavelength, determined previously; A is the absorbance of solution at irradiation wavelength.

$$\Phi = \frac{3.38 \cdot 10^{-5}(mol \cdot L^{-1}) \cdot 0.0015(L) \cdot 0.0220(s^{-1})}{5.80 \cdot 10^{-8}(mol \cdot s^{-1}) \cdot (1 - 10^{-0.0391})} = \frac{1.11 \cdot 10^{-9}(mol \cdot s^{-1})}{4.99 \cdot 10^{-9}(mol \cdot s^{-1})} = 0.22$$

For the cases of low absorbance at irradiation wavelength, absorbed photons over the entire range of LED emission can be calculated by integrating the LED emission spectra. Data are shown in Table 7.

Table 7: Absorbed photons over normalized LED emission range

nm	Absorbance (A)	Absorption factor ($1\text{-}10^{-A}$)	LED emission (mol s^{-1})	Photons absorbed (mol s^{-1})
395	0.0027	0.0063	0.00E+00	0.00E+00
394	0.0028	0.0064	1.58E-11	1.01E-13
393	0.0033	0.0075	5.28E-11	3.99E-13
392	0.0035	0.0079	8.45E-11	6.71E-13
391	0.0038	0.0087	7.92E-11	6.91E-13
390	0.0042	0.0097	6.87E-11	6.65E-13
389	0.0047	0.0108	7.92E-11	8.55E-13
388	0.0049	0.0113	7.92E-11	8.95E-13
387	0.0055	0.0127	1.48E-10	1.87E-12
386	0.0061	0.0140	1.37E-10	1.92E-12
385	0.0068	0.0155	1.64E-10	2.54E-12
384	0.0075	0.0171	1.85E-10	3.16E-12
383	0.0083	0.0190	2.69E-10	5.13E-12
382	0.0093	0.0212	2.75E-10	5.81E-12
381	0.0105	0.0239	3.22E-10	7.69E-12
380	0.0114	0.0258	3.75E-10	9.69E-12
379	0.0125	0.0283	5.23E-10	1.48E-11
378	0.0136	0.0308	5.71E-10	1.76E-11
377	0.0150	0.0339	6.92E-10	2.35E-11
376	0.0160	0.0362	9.09E-10	3.29E-11
375	0.0171	0.0386	1.10E-09	4.26E-11
374	0.0188	0.0424	1.38E-09	5.84E-11
373	0.0207	0.0464	1.91E-09	8.86E-11
372	0.0224	0.0503	2.21E-09	1.11E-10
371	0.0245	0.0548	2.74E-09	1.50E-10
370	0.0277	0.0617	3.37E-09	2.08E-10
369	0.0303	0.0673	3.91E-09	2.63E-10
368	0.0331	0.0733	4.33E-09	3.18E-10
367	0.0360	0.0795	5.03E-09	4.00E-10
366	0.0391	0.0861	5.28E-09	4.55E-10
365	0.0425	0.0933	5.02E-09	4.68E-10
364	0.0469	0.1023	4.36E-09	4.46E-10
363	0.0515	0.1118	3.32E-09	3.71E-10
362	0.0561	0.1213	2.70E-09	3.28E-10
361	0.0614	0.1318	1.93E-09	2.54E-10
360	0.0667	0.1424	1.35E-09	1.92E-10
359	0.0730	0.1548	1.02E-09	1.59E-10
358	0.0796	0.1675	7.03E-10	1.18E-10
357	0.0866	0.1807	4.81E-10	8.69E-11
356	0.0944	0.1954	3.33E-10	6.50E-11
355	0.1027	0.2107	2.38E-10	5.01E-11
354	0.1120	0.2273	1.27E-10	2.88E-11
353	0.1214	0.2439	6.87E-11	1.67E-11
352	0.1319	0.2619	3.70E-11	9.68E-12
351	0.1433	0.2810	2.11E-11	5.94E-12
350	0.1552	0.3004	0.00E+00	0.00E+00
349	0.1679	0.3207	0.00E+00	0.00E+00
		sum:	5.80E-08	**4.82E-09**

Replacing absorbed photon value of $4.99 \cdot 10^{-9}(mol \cdot s^{-1})$ used in the Equation 5, with the value normalized over the entire emission range of LED: $4.82 \cdot 10^{-9}(mol \cdot s^{-1})$, the resulting quantum yield slightly increases to 0.23 (or 23%).

5.4. Synthesis of biphenyl derivatives

5.4.1. General procedure A – esterification of carboxylic acids

Synthesis of the ethyl 3-aminobenzoate hydrochloride (**117**)

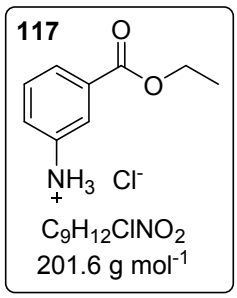

In a round bottom flask the 3-amino benzoic acid **116** (10.0 g, 73 mmol, 1 eq) was dissolved in dry ethanol (100 mL). The mixture was cooled in ice bath before dropwise addition of $SOCl_2$ (26.0 g, 219 mmol, 15.8 mL, 3 eq). When addition was finished, the mixture was refluxed until TLC analysis showed full conversion. The mixture was cooled to room temperature. During cooling precipitate was formed. The mixture was poured in Et_2O, then filtrated and washed on filter with Et_2O, dried in air to give the crude product **117** (13.71 g, 93%) which was used in next step without further purification. ^{1}H NMR (DMSO-d_6, 250 MHz): δ 10.3-8.0 (br, 3H), 7.92-7.78 (m, 2H), 7.63-7.45 (m, 2H), 4.33 (q, 2H, J = 7.1 Hz), 1.32 (t, 3H, J = 7.1 Hz) ppm. NMR data are in agreement with literature.[236]

5.4.2. General procedure B – ethylation of amino group

Synthesis of the ethyl 3-(diethylamino)benzoate (**118**)

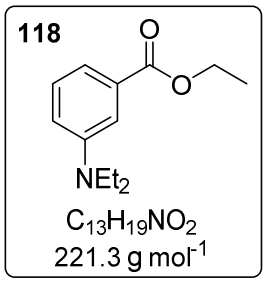

The compound **117** (7.26 g, 36 mmol, 1.0 eq) was suspended in dry DMF (50 mL). Then to the mixture ethyl bromide (24.28 g, 223 mmol, 6.2 eq), KI (12.67 g, 76 mmol, 2.1 eq) and K_2CO_3 (14.92 g, 108 mmol, 3 eq) were added. The reaction mixture was heated (120 °C) until complete conversion could be confirmed by TLC (24 h). The mixture was cooled to room temperature, diluted with EtOAc and water, organic phase separated, aqueous phase extracted two times more with EtOAc, combined organic phase washed 3 x with 50% brine, 1 x brine, dried over Na_2SO_4 and after filtration concentrated in reduced pressure. Crude **118** (7.56 g, 95%) was obtained as brownish oil. It was used in next step without further purification. ^{1}H NMR ($CDCl_3$, 250 MHz): δ 7.38-7.34 (m, 1H), 7.32-7.27 (m, 1H), 7.25-7.20 (m, 1H), 6.88-6.81 (m, 1H), 4.36 (q, 2H, J = 7.1 Hz), 3.38 (q, 4H, J = 7.1 Hz), 1.38 (t, 3H, J = 7.1 Hz), 1.17 (t, 6H, J = 7.1 Hz) ppm. NMR data are in agreement with literature.[237]

5.4.3. General procedure C – reduction of ester with $LiAlH_4$

Synthesis of the (3-(diethylamino)phenyl)methanol (**119**)

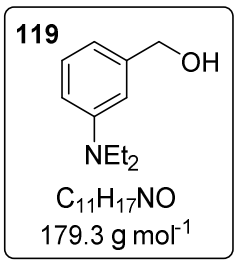

The compound **118** (3.98 g, 18.0 mmol, 1.0 eq) was dissolved in THF (40 mL) and cooled in ice bath before addition of $LiAlH_4$ (818 mg, 21.6 mmol, 1.2 eq) divided in five equal portions. The reaction mixture was stirred for 2 h while cooling in ice bath, then allowed to reach room temperature. When TLC analysis showed full conversion, the mixture was carefully quenched with EtOAc, then diluted with water and filtrated through sand. Organic phase was separated, washed with water, brine, dried over Na_2SO_4 and after filtration concentrated in reduced pressure to give brown oil. After column chromatography (SiO_2, Cy : EtOAc 3:1) product **119** (2.45 g, 69%) was obtained as light brown oil. ^{1}H NMR (300 MHz, $CDCl_3$): δ 7.23-7.17 (m, 1H), 6.72-6.68 (m, 1H), 6.66-6.59 (m, 2H), 4.63 (d, 2H, *J* = 5.7 Hz), 3.37 (q, 4H, *J* = 7.1 Hz), 1.55 (t, 1H, *J* = 5.7 Hz) 1.16 (t, 6H, *J* = 7.1 Hz) ppm. NMR data are in agreement with literature.[85]

Synthesis of the (5-(diethylamino)-2-iodophenyl)methanol (**120**)

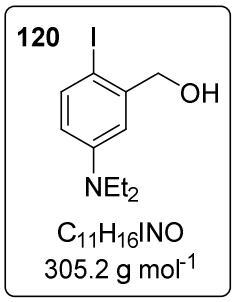

The compound **119** (20.0 g, 112 mmol, 1.0 eq) was dissolved in CH_2Cl_2 (100 mL) mixed with $NaHCO_3$ (16.9 g, 201 mmol, 1.8 eq) in H_2O (110 mL). I_2 (33.6 g, 133 mmol, 1.2 eq) was added to the intensively stirred two phase mixture. The reaction mixture was stirred until TLC analysis showed full conversion (4 h). Organic phase was separated, aqueous phase extracted two times with CH_2Cl_2, combined organic washed with brine, dried over Na_2SO_4 and after filtration concentrated in reduced pressure to give dark brown oil. After column chromatography (SiO_2, Cy : EtOAc 3:1) **120** (23.9 g, 70%) was obtained as yellowish solid. ^{1}H NMR (500 MHz, $CDCl_3$): δ 7.53 (d, 1H, *J* = 8.8 Hz), 6.80 (d, 1H, *J* = 3.1 Hz), 6.35 (dd, 1H, *J* = 8.8, 3.1 Hz), 4.60 (s, 2H), 3.34 (q, 4H, *J* = 7.1 Hz), 1.99 (s, 1H), 1.16 (t, 6H, *J* = 7.1 Hz) ppm. ^{13}C NMR (125 MHz, $CDCl_3$): 148.3, 142.9, 139.5, 113.3, 112.5, 78.7, 69.9, 44.5, 12.6 ppm. HRMS (MALDI) m/z: $[M+H]^+$ Calcd for $C_{11}H_{17}INO$ 306.03493; Found 306.03525.

5.4.4. General procedure D – Steglich-type esterification

Synthesis of (*S*)-1-*tert*-butyl 5-(5-(diethylamino)-2-iodobenzyl) 2-((*tert*-butoxycarbonyl)amino) pentanedioate (**123**)

The compound **120** (10.0 g, 32.8 mmol, 1.0 eq) was dissolved in CH_2Cl_2 (100 mL). To the solution

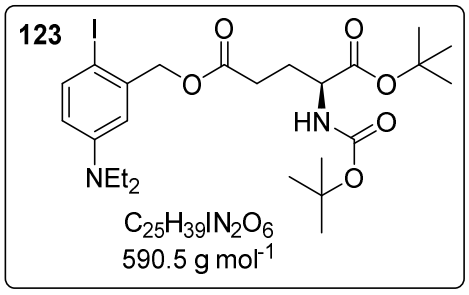

EDC-HCl (10.0 g, 52.3 mmol, 1.6 eq), DIPEA (5.07 g, 39.3 mmol, 1.2 eq), DMAP (0.4 g, 3.3 mmol, 0.1 eq) and *N*-(*tert*-butoxycarbonyl)-*L*-glutamic acid 1-*tert*-butyl ester **121** (15.0 g, 49.5 mmol, 1.5 eq) was added. The reaction mixture was stirred until TLC analysis showed full conversion (20 h). Upon completion, the mixture was washed two times with 0.01M HCl, then twice with saturated $NaHCO_3$ and twice with brine. Organic layer dried over Na_2SO_4 and after filtration concentrated in reduced pressure to give slightly brown oil. After column chromatography (SiO_2, Cy : EtOAc 5:1) the product (16.0 g, 83%) was obtained as light brown oil which upon storage becomes solid. ^{1}H NMR (500 MHz, $CDCl_3$): δ 7.56 (d, 1H, *J* = 8.8 Hz), 6.69 (d, 1H, *J* = 3.1 Hz), 6.37 (dd, 1H, *J* = 8.8, 3.1 Hz), 5.12-5.03 (m, 2.9H, major rotamer), 4.86-4.73 (m, 0.1H, minor rotamer), 4.26-4.17 (m, 0.9H, major rotamer), 4.12-4.01 (m, 0.1H, minor rotamer), 3.32 (q, 4H, *J* = 7.1 Hz), 2.55-2.38 (m, 2H), 2.24-2.14 (m, 1H), 2.01-1.90 (m, 1H), 1.45 (9H, s), 1.43 (9H, s), 1.14 (t, 6H, *J* = 7.1 Hz) ppm. ^{13}C NMR (125 MHz, $CDCl_3$): δ 172.6, 171.5, 155.5, 148.0, 139.8, 138.4, 113.8, 113.8, 82.3, 79.9, 79.8, 70.9, 53.5, 44.5, 30.5, 28.5, 28.3, 28.1, 12.5 ppm. HRMS (MALDI) m/z: $[M]^{\cdot+}$ Calcd for $C_{25}H_{39}IN_2O_6$ 590.18473; Found 590.18292.

5.4.5. General procedure E – Suzuki coupling

Synthesis of the (*S*)-1-*tert*-butyl 5-((4'-cyano-4-(diethylamino)-[1,1'-biphenyl]-2-yl)methyl) 2-((*tert*-butoxy carbonyl)amino)pentanedioate (**233**)

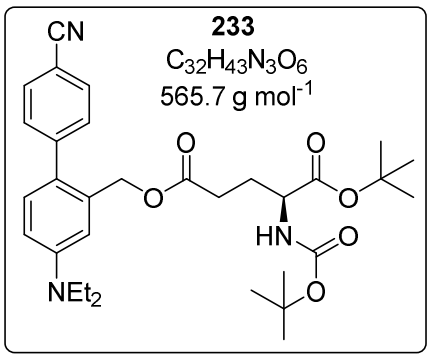

The reaction conditions were adopted from the literature.[39] The compound **123** (400 mg, 0.68 mmol, 1.0 eq) was dissolved in toluene (10 mL). Then 2M Na_2CO_3 (1.2 mL) was added and solution degassed by passing through argon stream for 10 min. Then $Pd(PPh_3)_4$ (47mg, 0.04 mmol, 0.06eq) was added and degassing with argon stream was repeated. In a separate flask 4-cyanobenzeneboronic acid (208 mg, 1.42 mmol, 2.1 eq) was dissolved in EtOH and degassed with argon stream before adding it to the

toluene solution. The reaction mixture was then refluxed under argon atmosphere until TLC analysis showed full conversion (5 h). Upon completion the mixture was diluted with ethyl acetate and H_2O, organic phase separated, aqueous phase washed twice with EtOAc. The combined organic phase was washed with brine, dried over Na_2SO_4 and after filtration concentrated in reduced pressure to give slightly yellow oil. Purification was done by column chromatography (SiO_2, Cy : EtOAc 9:1 to 3:1). However, it was not possible to separate side products (boronic acid homocoupling) in direct phase chromatography. To obtain analytically pure sample also reverse phase (C18) column chromatography was performed (MeCN : H_2O 70:30 to 100%). However, it is important to note that for next synthetic step (deprotection of *tert*-butyl and Boc esters) this impurity does not disturb and can be easily removed by filtration afterward. The product was obtained as oil (230 mg, 60%). ^{1}H NMR (500 MHz, $CDCl_3$): δ 7.68-7.64 (m, 2H), 7.45-7.42 (m, 2H), 7.13 (d, 1H, J = 8.6 Hz), 6.76 (d, 1H, J = 2.5 Hz), 6.70 (dd, 1H, J = 8.6, 2.5 Hz), 5.10-5.04 (m, 0.9H, major rotamer), 4.99 (s, 2H), 4.84-4.73 (m, 0.1H, minor rotamer), 4.23-4.15 (m, 0.9H, major rotamer), 4.08-3.99 (m, 0.1H, minor rotamer), 3.40 (q, 4H, J = 7.1 Hz), 2.47-2.30 (m, 2H), 2.18-2.08 (m, 1H), 1.92-1.83 (m, 1H), 1.45 (9H, s), 1.42 (9H, s), 1.19 (t, 6H, J = 7.1 Hz) ppm. ^{13}C NMR (125 MHz, $CDCl_3$): δ 172.6, 171.4, 155.5, 147.9, 145.9, 133.8, 132.1, 131.3, 130.1, 127.3, 119.2, 113.1, 111.8, 110.1, 82.4, 79.9, 65.2, 53.4, 44.5, 30.5, 28.4, 28.3, 28.1, 12.7 ppm. HRMS (MALDI) m/z: $[M^-]^+$ Calcd for $C_{32}H_{43}N_3O_6$ 565.31464; Found 565.31301.

5.4.6. General procedure F – protecting group cleavage with TFA

Synthesis of the (*S*)-1-carboxy-4-((4'-cyano-4-(diethylamino)-[1,1'-biphenyl]-2-yl)methoxy)-4-oxobutan-1-amin- ium 2,2,2-trifluoroacetate (**132**)

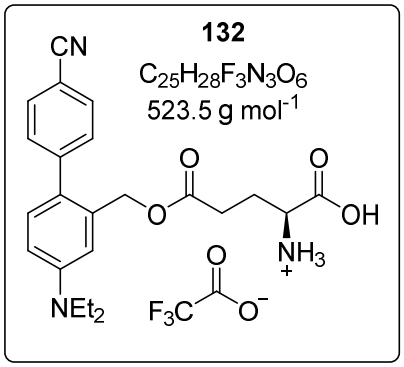

The compound **233** (70 mg, 0.12 mmol) was dissolved in dry CH_2Cl_2 (4 mL). To the solution TFA (4 mL) was added. Resulting mixture was stirred overnight (20 h), then evaporated. Additional co-evaporation with MeCN and toluene was done to ensure that all the TFA is removed. The oily product was purified using reverse phase (C18) column chromatography (MeCN : H_2O 20:80 to 100%). After removal of the solvent, product **132** was obtained as solid (46 mg, 73%). ^{1}H NMR (300 MHz, D_2O): δ 7.89-7.81 (m, 2H), 7.66 (d, 1H, J = 1.8 Hz), 7.60-7.50 (m, 4H), 5.11 (d, 2H, J = 2.3 Hz), 3.90 (t, 1H, J = 6.7 Hz), 3.67 (q, 4H, J = 7.2 Hz), 2.52-2.43 (m, 2H), 2.10-1.99 (m, 2H), 1.11 (t, 6H, J = 7.2 Hz) ppm. ^{13}C NMR (75 MHz, D_2O): δ 173.4, 171.9, 143.6, 142.6, 136.5, 135.5, 132.6, 132.2, 129.6, 123.4, 122.6,

119.3, 110.8, 64.4, 53.8, 52.3, 29.3, 24.8, 9.6 ppm. HRMS (MALDI) m/z: $[M]^+$ Calcd for $C_{23}H_{28}N_3O_4$ 410.20743; Found 410.20692.

Synthesis of the (*S*)-1-tert-butyl 5-(5-(diethylamino)-2-((4-(trifluoromethyl)phenyl)ethynyl) benzyl) 2-((*tert*-butoxycarbonyl)amino) pentanedioate (**126**)

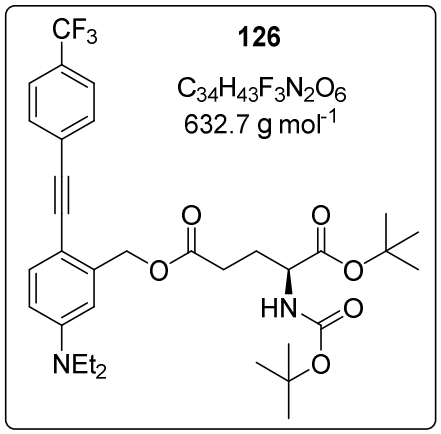

Compound **123** (530 mg, 0.89 mmol, 1 eq) was dissolved in Et_2O. To the solution piperidin (6 mL), CuI (1.7 mg, 1 mol%) and $Pd(PPh_3)_4$ (25 mg, 2.5 mol%) was added and the solution was degassed by passing through argon stream for 10 min. The mixture was cooled in ice bath before addition of 4-ethynyl-α,α,α-trifluorotoluene (168 mg, 0.98 mmol, 1.1 eq) over period of 10 min. The reaction mixture was allowed to reach the room temperature and it was stirred overnight. The mixture was diluted with Et_2O and saturated NH_4Cl, organic phase separated, aqueous phase washed twice with Et_2O. The combined organic phase was washed with 1M HCl, brine, dried over Na_2SO_4 and after filtration concentrated in reduced pressure. Purification was done by column chromatography (SiO_2, Cy : EtOAc 9:1 to 5:1) to yield 253 mg (45%) of the product. ^{1}H NMR (500 MHz, $CDCl_3$): δ 7.57-7.55 (m, 4H), 7.39 (d, 1H, J= 8.7 Hz), 6.67 (d, 1H, J= 2.4 Hz), 6.59 (dd, 1H, J= 8.7, 2.4 Hz), 5.33-5.26 (m, 2H), 5.09-4.98 (m, 0.85H, major rotamer), 4.86-4.71 (m, 0.15H, minor rotamer), 4.24 – 4.10 (m, 0.85H, major rotamer), 4.10-3.95 (m, 0.15H, minor rotamer), 3.39 (q, 4H, J= 7.1 Hz), 2.53– 2.38 (m, 2H), 2.21 – 2.10 (m, 1H), 1.97 - 1.87 (m, 1H), 1.42 (s, 18H), 1.18 (t, 6H, J= 7.1 Hz) ppm. ^{13}C NMR (125 MHz, $CDCl_3$): δ 172.8, 171.4, 155.5, 148.2, 138.9, 134.0, 131.3, 129.1 (q, $^2J_{CF}$ = 32 Hz), 128.1, 125.3 (q, $^3J_{CF}$ = 3.6 Hz), 124.2 (q, $^1J_{CF}$ = 272 Hz), 111.7, 111.1, 107.7, 91.0, 90.6, 82.3, 79.9, 65.8, 53.5, 44.5, 30.5, 28.4, 28.0, 27.0, 12.7 ppm. HRMS (MALDI) m/z: $[M+H]^+$ Calcd for $C_{34}H_{43}F_3N_2O_6$ 632.30677; Found 632.30511.

Synthesis of the (*S*)-1-*tert*-butyl 5-((4-(diethylamino)-4'-nitro-[1,1'-biphenyl]-2-yl)methyl) 2-((*tert*-butoxycarbonyl)amino)pentanedioate (**234**)

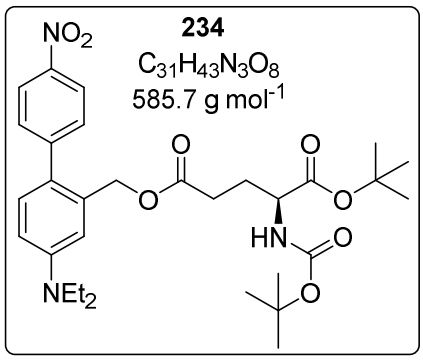

Compound **234** was synthesized from 400 mg (0.68 mmol) of **123**, following the general procedure E, to give 180 mg (45%) of product. ^{1}H NMR (500 MHz, $CDCl_3$): δ 8.26-8.22 (m, 2H), 7.51-7.47 (m, 2H), 7.17 (d, 1H, *J* = 8.5 Hz), 6.78 (s, 1H), 6.71 (d, 1H, *J* = 8.5 Hz), 5.12-5.04 (m, 0.85H, major rotamer), 5.01 (s, 2H), 4.93-4.77 (m, 0.15H, minor rotamer), 4.24-4.15 (m, 1H), 3.41 (q, 4H, *J* = 7.1 Hz), 2.48-2.30 (m, 2H), 2.19-2.08 (m, 1H), 1.95-1.83 (m, 1H), 1.45 (s, 9H), 1.43 (s, 9H), 1.20 (t, 6H, *J* = 7.1 Hz) ppm. ^{13}C NMR (125 MHz, $CDCl_3$): δ 172.6, 171.4, 155.5, 148.0, 146.5, 133.9, 131.4, 130.3, 130.1, 126.9, 123.6, 113.2, 111.8, 82.4, 80.0, 65.2, 53.4, 44.5, 30.5, 28.4, 28.3, 28.1, 12.7 ppm. HRMS (MALDI) m/z: $[M^-]^+$ Calcd for $C_{31}H_{43}N_3O_8$ 585.30447; Found 585.30199.

Synthesis of the (*S*)-1-carboxy-4-((4-(diethylamino)-4'-nitro-[1,1'-biphenyl]-2-yl)methoxy)-4-oxo-butan-1-aminium 2,2,2-trifluoroacetate (**133**)

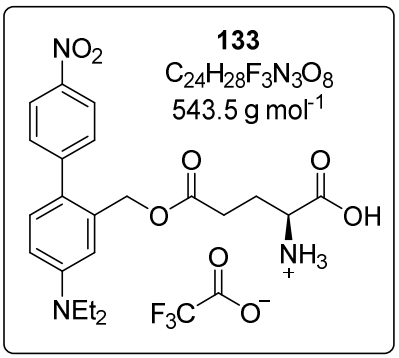

Compound **133** was synthesized from **234** (65 mg, 0.11 mmol) following the general procedure F, to give 55 mg (91%) of product. ^{1}H NMR (500 MHz, D_2O): δ 8.34-8.26 (m, 2H), 7.69-7.64 (m, 1H), 7.64-7.52 (m, 4H), 5.12 (d, 2H, *J* = 3.3 Hz), 3.93 (t, 1H, *J* = 6.7 Hz), 3.68 (q, 4H, *J* = 7.1 Hz), 2.54-2.44 (m, 2H), 2.12-1.99 (m, 2H), 1.12 (t, 6H, *J* = 7.1 Hz) ppm. ^{13}C NMR (125 MHz, D_2O): δ 173.3, 171.6, 147.3, 145.4, 142.2, 136.6, 135.6, 132.2, 130.0, 123.7, 123.5, 122.6, 64.4, 53.8, 52.0, 29.3, 24.7, 9.6 ppm. HRMS (MALDI) m/z: $[M+Na]^+$ Calcd for $C_{22}H_{27}N_3O_6Na$ 452.17921; Found 452.17953.

Synthesis of the (*S*)-1-*tert*-butyl 5-((4-(diethylamino)-4'-methoxy-[1,1'-biphenyl]-2-yl)methyl) 2-((*tert*-butoxycarbonyl)amino)pentanedioate (**235**)

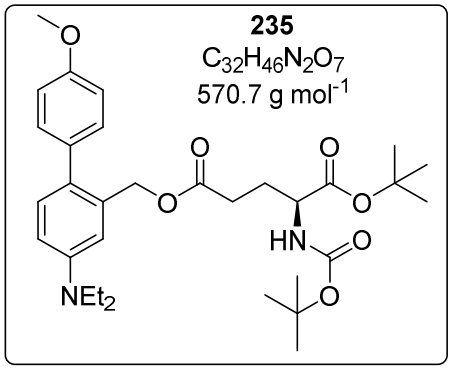

Compound **235** was synthesized from 465 mg (0.79 mmol) of **123**, following the general procedure E, to give 380 mg (84%) of product. ^{1}H NMR (500 MHz, $CDCl_3$): δ 7.25-7.21 (m, 2H), 7.14 (d, 1H, *J* = 8.5 Hz), 6.94-6.89 (m, 2H), 6.74 (d, 1H, *J* = 2.5 Hz), 6.69 (dd, 1H, *J* = 8.5, 2.5 Hz), 5.12-4.98 (m, 3H), 4.24-4.15 (m, 1H), 3.83 (s, 3H), 3.38 (q, 4H, *J* = 7.1 Hz), 2.48-2.30 (m, 2H), 2.19-2.08 (m, 1H), 1.95-1.83 (m, 1H), 1.45 (s, 9H), 1.43 (s, 9H), 1.19 (t, 6H, *J* = 7.1 Hz) ppm. ^{13}C NMR (125 MHz, $CDCl_3$): δ 172.8, 171.5, 158.5, 155.5, 147.1, 133.8, 133.3, 131.4, 130.6, 129.3, 113.7, 112.8, 111.9, 82.3, 79.9, 65.7, 55.4, 53.5, 44.5, 30.6, 28.4, 28.3, 28.1, 12.8 ppm. HRMS (MALDI) m/z: $[M+H]^+$ Calcd for $C_{32}H_{47}N_2O_7$ 571.33778; Found 571.33569.

Synthesis of the (*S*)-1-carboxy-4-((4-(diethylamino)-4'-methoxy-[1,1'-biphenyl]-2-yl)methoxy)-4-oxo-butan-1-aminium 2,2,2-trifluoroacetate (**131**)

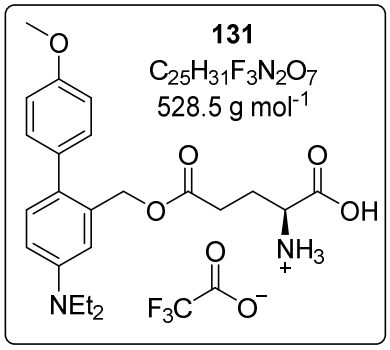

Compound **131** was synthesized from **235** (370 mg, 0.65 mmol) following the general procedure F, to give 165 mg (48%) of product. ^{1}H NMR (500 MHz, CD_3OD-d_4 + D_2O): δ 7.23-7.19 (m, 2H), 7.08 (d, 1H, *J* = 8.4 Hz), 6.95-6.91 (m, 2H), 6.79 (d, 1H, *J* = 2.6 Hz), 6.73 (dd, 1H, *J* = 8.4, 2.6 Hz), 5.00 (s, 2H), 3.82 (s, 3H), 3.57 (t, 1H, *J* = 6.3 Hz), 3.40 (q, 4H, *J* = 7.1 Hz), 2.60-2.49 (m, 2H), 2.17-2.02 (m, 2H), 1.66 (t, 6H, *J* = 7.1 Hz) ppm. ^{13}C NMR (125 MHz, MeCN-d_3 + D_2O): δ 173.6, 172.9, 158.4, 147.2, 133.6, 133.2, 131.2, 130.5, 129.1, 113.8, 113.4, 112.5, 65.7, 55.2, 54.1, 44.3, 30.2, 25.9, 11.9 ppm. HRMS (MALDI) m/z: $[M]^+$ Calcd for $C_{23}H_{31}N_2O_5$ 415.22275; Found 415.22219.

Synthesis of the (*S*)-1-*tert*-butyl 5-((4-(diethylamino)- 4'-(trifluoromethyl)-[1,1'-biphenyl]-2-yl)methyl) 2-((*tert*-butoxycarbonyl)amino)pentanedioate (**124**)

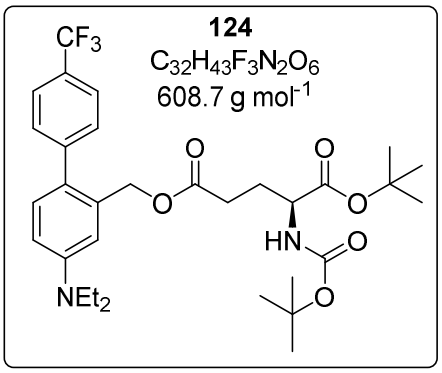

Compound **124** was synthesized from 400 mg (0.68 mmol) of **123**, following the general procedure E, to give 297 mg (72%) of product. ^{1}H NMR (500 MHz, $CDCl_3$): δ 7.65-7.60 (m, 2H), 7.47-7.42 (m, 2H), 7.15 (d, 1H, *J* = 8.6 Hz), 6.76 (d, 1H, *J* = 2.6 Hz), 6.71 (d, 1H, *J* = 8.6, 2.6 Hz), 5.11-5.03 (m, 0.85H, major rotamer), 5.01 (s, 2H), 4.84-4.73 (m, 0.15H, minor rotamer), 4.24-4.15 (m, 0.85H, major rotamer), 4.09-3.99 (m, 0.15H, minor rotamer), 3.40 (q, 4H, *J* = 7.1 Hz), 2.48-2.31 (m, 2H), 2.19-2.07 (m, 1H), 1.93-1.83 (m, 1H), 1.45 (s, 9H), 1.43 (s, 9H), 1.20 (t, 6H, *J* = 7.1 Hz) ppm. ^{13}C NMR (125 MHz, $CDCl_3$): δ 172.7, 171.4, 155.5, 147.7, 144.7, 133.8, 131.4, 129.8, 128.6 (q, $^2J_{CF}$ = 32 Hz), 124.5 (q, $^1J_{CF}$ = 272 Hz), 127.9, 125.2 (q, $^3J_{CF}$ = 3.6 Hz), 112.9, 111.8, 82.4, 79.9, 65.3, 53.5, 44.5, 30.5, 28.4, 28.3, 28.1, 12.7 ppm. HRMS (MALDI) m/z: $[M+H]^+$ Calcd for $C_{32}H_{44}F_3N_2O_6$ 609.31460; Found 609.31271.

Synthesis of the (*S*)-1-carboxy-4-((4-(diethylamino)- 4'-(trifluoromethyl)-[,1'-biphenyl]-2-yl)methoxy)-4-oxo-butan-1-aminium 2,2,2-trifluoroacetate (**128**)

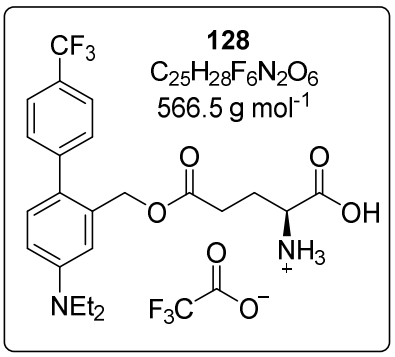

Compound **128** was synthesized from **124** (68 mg, 0.11 mmol) following the general procedure F, to give 38 mg (60%) of product. ^{1}H NMR (400 MHz, CD_3OD-d_4 + D_2O): δ 7.72-7.67 (m, 2H), 7.49-7.45 (m, 2H), 7.15 (d, 1H, *J* = 8.5 Hz), 6.85 (d, 1H, *J* = 2.5 Hz), 6.81 (dd, 1H, *J* = 8.5, 2.5 Hz), 5.01 (s, 2H), 3.64 (t, 1H, *J* = 6.3 Hz), 3.40 (q, 4H, *J* = 7.1 Hz), 2.60-2.46 (m, 2H), 2.17-2.02 (m, 2H), 1.15 (t, 6H, *J* = 7.1 Hz) ppm. ^{13}C NMR (125 MHz, CD_3OD-d_4 + D_2O): δ 174.6, 174.0, 148.9, 146.0, 134.5, 132.0, 130.8, 129.5, 129.3 (q, $^2J_{CF}$ = 32 Hz), 127.8 (q, $^1J_{CF}$ = 272 Hz), 126.0 (q, $^3J_{CF}$ = 3.6 Hz), 115.0, 114.1, 66.5, 55.1, 45.5, 31.0, 27.0, 12.6 ppm. HRMS (MALDI) m/z: $[M]^+$ Calcd for $C_{23}H_{28}F_3N_2O_4$ 453.19957; Found 453.19780.

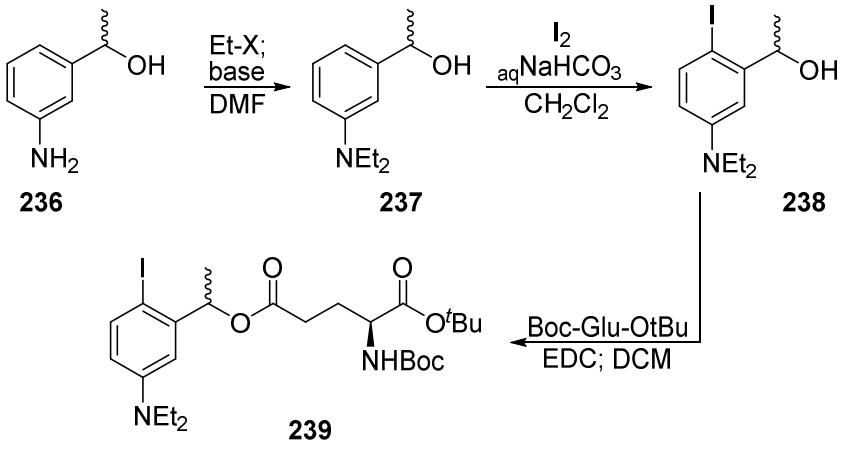

Figure 141: Synthesis scheme of compound **239**.

Synthesis of the 1-(3-(diethylamino)phenyl)ethanol (**237**)

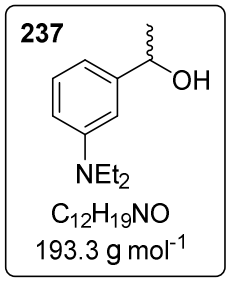

Synthesis was done following general procedure B with small adaptations *e.g.* alkylation reagent and base. 1-(3-Aminophenly)ethanol (4.987 g, 36.3 mmol, 1 eq) was dissolved in dry DMF (40 mL). Then ethyl iodide (9.49 g, 87.1 mmol, 2.4 eq) and DIPEA (22.51 g, 174 mmol, 4.8 eq) was added and further operations were as described in the general procedure B. The crude **237** (6.498 g, 92%) was obtained as brownish oil. It was used in next step without further purification. ^{1}H NMR ($CDCl_3$, 250 MHz): δ 7.23-7.13 (m, 1H), 6.74-6.55 (m, 3H), 4.90-4.76 (m, 1H), 3.36 (q, 4H, *J* = 7.1 Hz), 1.75 (d, 1H, *J* = 3.4 Hz), 1.49 (d, 3H, *J* = 6.4 Hz), 1.16 (t, 6H, *J* = 7.1 Hz) ppm. HRMS (MALDI-LTQ Orbitrap) m/z: $[M+H]^+$ Calcd for $C_{12}H_{20}NO$ 194.15394; found: 194.15415.

Synthesis of the 1-(5-(diethylamino)-2-iodophenyl)ethanol (**238**)

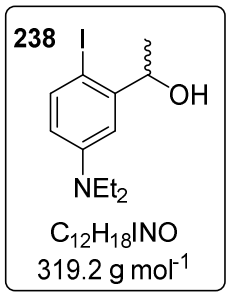

The compound **237** (6.15 g, 30 mmol, 1.0 eq) was dissolved in CH_2Cl_2 (30 mL) mixed with saturated $NaHCO_3$ in H_2O (30 mL). I_2 (11.71 g, 46 mmol, 1.4 eq) was added to the intensively stirred two phase mixture. The reaction mixture was stirred until TLC analysis showed full conversion (48 h). Organic phase was separated, organic phase diluted with CH_2Cl_2 and washed with 50% $Na_2S_2O_3$ and brine. The organic phase was dried over Na_2SO_4 and after filtration concentrated in reduced pressure to give dark brown oil. After column chromatography (SiO_2, Cy : EtOAc 9:1 to 1:3) compound **238** (5.137 g, 50%) was obtained as yellowish solid. ^{1}H NMR (500 MHz, $CDCl_3$): δ 7.52 (d, 1H, *J* = 8.6 Hz), 6.92 (d, 1H, *J* = 3.0 Hz), 6.34 (dd, 1H, *J* =

8.6, 3.0 Hz), 4.99 (dd, 1H, *J* = 6.4, 3.0 Hz), 3.34 (q, 4H, *J* = 7.1 Hz), 1.92 (d, 1H, *J* = 2.6 Hz), 1.45 (d, 3H, *J* = 6.4 Hz), 1.15 (t, 6H, *J* = 7.1 Hz) ppm. ^{13}C NMR (125 MHz, $CDCl_3$): 148.4, 147.9, 139.6, 113.4, 109.7, 78.8, 73.9, 44.5, 23.8, 12.6 ppm. HRMS (MALDI) m/z: $[M+H]^+$ Calcd for $C_{12}H_{19}INO$ 320.05058; Found 320.05031.

Synthesis of the (2*S*)-1-*tert*-butyl 5-(1-(5-(diethylamino)-2-iodophenyl)ethyl) 2-((*tert*-butoxycarbonyl) amino)pentanedioate (**239**)

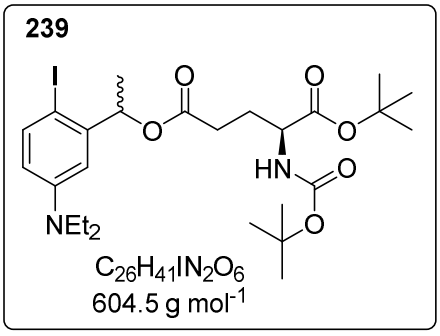

Compound **239** was synthesized from 4.09 g (12.8 mmol) of **238**, following the general procedure D, to give 6.20 g (80%) of product. ^{1}H NMR (500 MHz, $CDCl_3$): δ 7.52 (d, 1H, *J* = 8.8 Hz), 6.68 (m, 1H), 6.34 (dd, 1H, *J* = 8.8, 2.0 Hz), 5.95-5.89 (m, 1H), 5.15-4.98 (m, 0.9H, major rotamer), 4.85-4.68 (m, 0.1H, minor rotamer), 4.25-3.99 (m, 0.9H and 0.1H, major and minor rotamer), 3.38-3.28 (m, 4H), 2.54-2.32 (m, 2H), 2.22-2.09 (m, 1H), 1.98-1.86 (m, 1H), 1.48 (dd, 3H, *J* = 6.5, 3.4 Hz), 1.45 (s, 9H), 1.43 (s, 9H), 1.17-1.11 (t, 6H, *J* = 7.1 Hz) ppm. ^{13}C NMR (125 MHz, $CDCl_3$): δ 171.9, 171.8, 171.5, 155.6, 148.2, 144.3, 139.8, 113.7, 109.9, 82.3, 82.3, 79.9, 78.6, 76.5, 53.7, 53.5, 44.6, 30.8, 30.7, 28.5, 28.3, 28.2, 28.1, 21.5, 21.5, 12.6 ppm. HRMS (MALDI) m/z: $[M+H]^+$ Calcd for $C_{26}H_{41}N_2O_6Na$ 627.19015; Found 627.19102.

Synthesis of the (1*S*)-1-carboxy-4-(1-(4'-cyano-4-(diethylamino)-[1,1'-biphenyl]-2-yl)ethoxy)-4-oxobutan-1-aminium 2,2,2-trifluoroacetate (**137**)

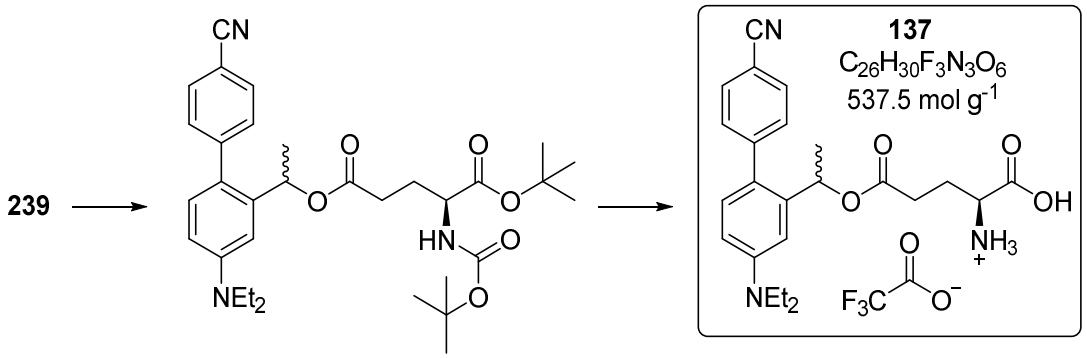

The compound **137** was synthesized in two steps from compound **239** (700 mg, 1.19 mmol) following the general procedure E (Suzuki coupling). The reaction mixture was purified *via* column chromatography. The product was obtained in a mixture with unidentified side product. It was used in the next step without further purification. ^{1}H NMR (500 MHz, $CDCl_3$): δ 7.69-7.65 (m, 2H), 7.49-7.45 (m, 2H), 7.00 (d, 1H, *J* = 8.6 Hz), 6.76-7.73 (m, 1H), 6.64 (d, 1H, *J* = 8.6, 2.0 Hz), 5.90-

5.82 (m, 1H), 5.13-4.99 (m, 0.90H, major rotamer), 4.84-4.69 (m, 0.1H, minor rotamer), 4.23-4.11 (m, 0.9H, major rotamer), 4.08-3.97 (m, 0.1H, minor rotamer), 3.45-3.36 (m, 4H), 2.48-2.26 (m, 2H), 2.16-2.04 (m, 1H), 1.92-1.80 (m, 1H), 1.44 (s, 9H), 1.42 (s, 9H), 1.40-1.36 (m, 3H), 1.23-1.17 (m, 6H) ppm. ^{13}C NMR (125 MHz, $CDCl_3$): δ 172.1, 172.0, 171.4, 155.6, 155.5, 148.0, 146.3, 140.4, 132.2, 131.0, 130.5, 125.7, 119.3, 111.2, 110.2, 108.0, 82.4, 82.3, 79.9, 70.1, 70.1, 53.6, 53.4, 44.5, 30.8, 30.7, 28.4, 28.3, 28.2, 28.1, 22.8 ppm. HRMS (MALDI) m/z: $[M^{\cdot}]^+$ Calcd for $C_{33}H_{45}N_3O_6$ 579.33029; Found 579.32855. The protecting group cleavage was done following the general procedure F. The product was purified *via* RP column chromatography to give 95 mg (15% in two steps) of compound **137** as white solid. ^{1}H NMR (600 MHz, MeCN-d_3 + D_2O): δ 7.74-7.72 (m, 2H), 7.44-7.40 (m, 2H), 6.98 (d, 1H, J = 8.6 Hz), 6.76 (d, 1H, J = 2.6 Hz), 6.68 (dd, 1H, J = 8.6, 2.6 Hz), 5.73-5.68 (m, 1H), 3.55-3.51 (m, 1H), 3.34 (q, 4H, J = 7.1 Hz), 2.49-2.33 (m, 2H), 2.02-1.88 (m, 2H), 1.36-1.34 (m, 3H), 1.07 (t, 6H, J = 7.1 Hz) ppm. ^{13}C NMR (150 MHz, MeCN-d_3 + D_2O): δ 174.0, 173.9, 173.7, 173.7, 149.0, 147.2, 141.0, 133.2, 131.8, 131.3, 126.9, 120.3, 112.9, 110.2, 109.7, 71.6, 54.9, 45.2, 31.2, 31.1, 26.6, 26.5, 22.4, 12.6 ppm. HRMS (MALDI) m/z: $[M+H]^+$ Calcd for $C_{24}H_{29}N_3O_4$ 424.22308; Found 424.22243.

Synthesis of the (*S*)-1-*tert*-butyl 5-(3-(diethylamino)benzyl) 2-((*tert*-butoxycarbonyl)amino) pentanedioate (**122**)

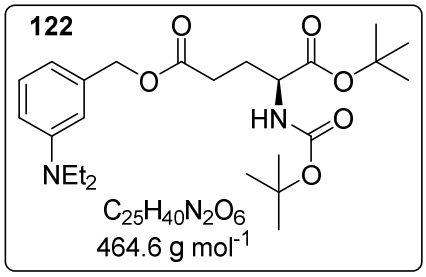

The compound **122** was synthesized from compound **119** (100 mg, 0.56 mmol) following the general procedure D. Oily product (193 mg, 74%) was obtained. ^{1}H NMR (300 MHz, $CDCl_3$): δ 7.23-7.14 (m, 1H), 6.67-6.59 (m, 3H), 5.13-4.99 (m, 2.9H, major rotamer), 4.90-4.68 (m, 0.1H, minor rotamer), 4.29-3.96 (m, 0.9H and 0.1H, major and minor rotamer), 3.35 (q, 4H, J = 7.1 Hz), 2.55-2.33 (m, 2H), 2.25-2.09 (m, 1H), 2.01-1.85 (m, 1H), 1.46 (s, 9H), 1.43 (s, 9H), 1.16 (t, 6H, J = 7.1 Hz) ppm. ^{13}C NMR (75 MHz, $CDCl_3$): δ 172.9, 171.5, 155.5, 148.1, 136.9, 129.6, 115.4, 111.8, 111.7, 82.3, 77.4, 67.4, 53.6, 44.5, 30.6, 28.5, 28.3, 28.1, 12.7 ppm. HRMS (MALDI) m/z: $[M+H]^+$ Calcd for $C_{25}H_{41}N_2O_6$ 465.29591; Found 465.29487.

Synthesis of the (*S*)-1-carboxy-4-((3-(diethylamino)benzyl)oxy)-4-oxobutan-1-aminium 2,2,2-trifluoro acetate (**127**)

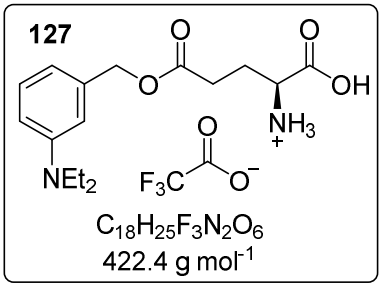

The compound **127** was synthesized from compound **122** (411 mg, 0.88 mmol) following general procedure F. White powder (330 mg, 88%) was obtained. ^{1}H NMR (500 MHz, D_2O): δ 7.67-7.59 (m, 2H), 7.54 (s, 1H), 7.51-7.47 (m, 1H), 5.23 (s, 2H), 3.87 (t, 1H, *J* = 6.5 Hz), 3.64 (q, 4H, *J* = 7.1 Hz), 2.72-2.59 (m, 2H), 2.25-2.13 (m, 2H), 1.09 (t, 6H, *J* = 7.1 Hz) ppm. ^{13}C NMR (125 MHz, D_2O): δ 174.1, 173.0, 138.5, 136.8, 130.9, 130.0, 122.2, 121.6, 66.0, 53.7, 53.2, 29.7, 25.2, 9.6 ppm. HRMS (MALDI) m/z: $[M]^+$ Calcd for $C_{16}H_{25}N_2O_4$ 309.18088; Found 309.18083.

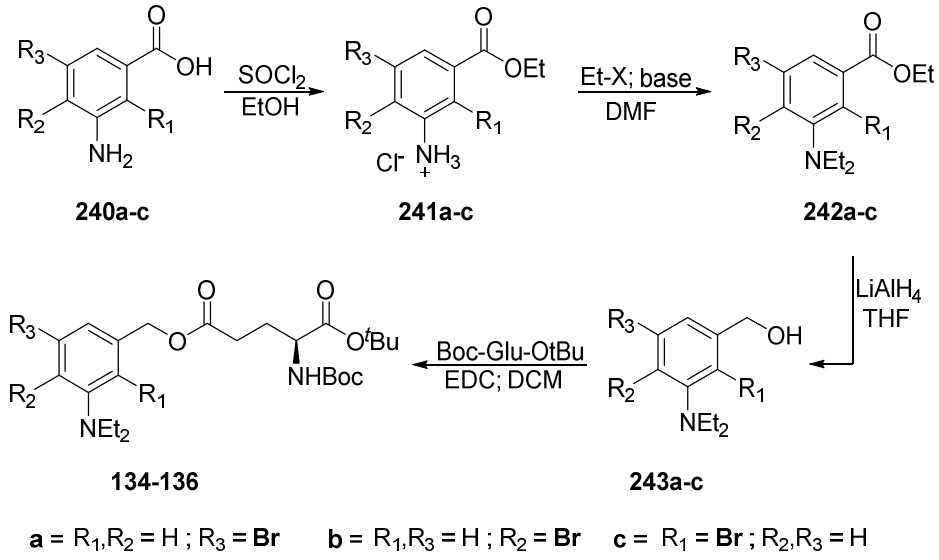

Figure 142: Synthesis of the aryl halides **134-136**.

Synthesis of the ethyl 3-amino-5-bromobenzoate hydrochloride (**241a**)

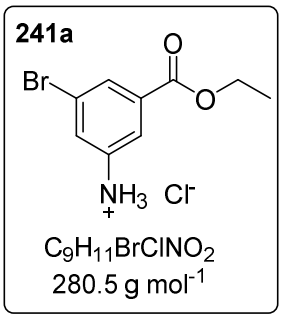

Synthesis was done following general procedure A. From 3-amino-5-brombenzoic acid (5.0 g, 23 mmol, 1 eq) and $SOCl_2$ (22.0 g, 185 mmol, 13.4 mL, 8 eq) in EtOH (85 mL) the product **241a** (5.57 g, 86%) was obtained. It was used in next step without further purification. Analytical sample was prepared by neutralization with saturated $NaHCO_3$ and extraction with EtOAc. ^{1}H NMR ($CDCl_3$, 300 MHz): δ 7.55-7.51 (m, 1H), 7.28-7.26 (m, 1H), 7.00-6.97 (m, 1H), 4.35 (q, 2H, *J* = 7.1 Hz), 4.0-3.3 (br s, 2H), 1.37 (t, 3H, *J* = 7.1 Hz) ppm. NMR data are in agreement with literature.[238]

Synthesis of the ethyl 3-bromo-5-(diethylamino)benzoate (**242a**)

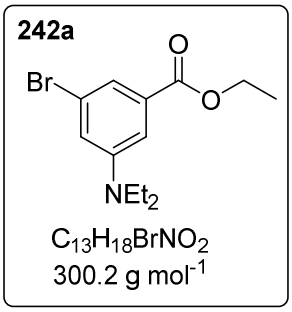

Synthesis was done following general procedure B with small adaptations *e.g.* alkylation reagent and base. Compound **241a** (5.57 g, 20 mmol, 1 eq) was suspended in dry DMF (50 mL). Then ethyl iodide (37.29 g, 238 mmol, 12 eq) and DIPEA (18.00 g, 139 mmol, 7 eq) was added and further operations were as described in the general procedure B. The crude **242a** (5.75 g, 96%) was obtained as brownish oil. It was used in next step without further purification. ^{1}H NMR (300 MHz, $CDCl_3$): δ 7.41-7.37 (m, 1H), 7.26-7.24 (m, 1H), 6.94-6.89 (m, 1H), 4.35 (q, 2H, *J* = 7.1 Hz), 3.36 (q, 4H, *J* = 7.1 Hz), 1.37 (t, 3H, *J* = 7.1 Hz), 1.17 (t, 6H, *J* = 7.1 Hz) ppm. ^{13}C NMR (75 MHz, $CDCl_3$): δ 166.3, 148.8, 132.9, 123.9, 118.8, 118.1, 111.6, 61.3, 44.6, 14.4, 12.5 ppm. HRMS (MALDI-LTQ Orbitrap) m/z: $[M+H]^+$ Calcd for $C_{13}H_{19}{}^{79}BrNO_2$ 300.05937; found: 300.05881; Calcd for $C_{13}H_{19}{}^{81}BrNO_2$ 302.05732; found: 302.05743.

Synthesis of the ethyl (3-bromo-5-(diethylamino)phenyl)methanol (**243a**)

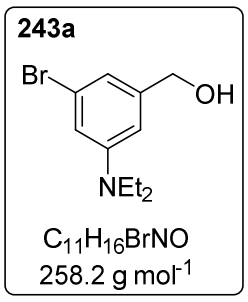

From compound **242a** (5.70 g, 19 mmol), following the general procedure C, the product **243a** (4.57 g, 93%) was obtained as oil. ^{1}H NMR (300 MHz, $CDCl_3$): δ 6.77-6.73 (s, 1H), 6.71-6.67 (m, 1H), 6.58-6.55 (m, 1H), 4.58 (d, 2H, *J* = 5.7 Hz), 3.33 (q, 4H, *J* = 7.1 Hz,), 1.62 (t, 1H, *J* = 5.9 Hz), 1.15 (t, 6H, *J* = 7.1 Hz) ppm. ^{13}C NMR (75 MHz, $CDCl_3$): δ 149.3, 143.8, 123.9, 116.6, 113.6, 108.7, 65.5, 44.5, 12.6 ppm. HRMS (MALDI-LTQ Orbitrap) m/z: $[M+H]^+$ Calcd for $C_{11}H_{17}{}^{79}BrNO$ 258.04880; Found: 258.04960; Calcd for $C_{11}H_{17}{}^{81}BrNO$ 260.04676; Found: 260.04726.

Synthesis of the (*S*)-5-(3-bromo-5-(diethylamino)benzyl) 1-*tert*-butyl 2-((*tert*-butoxycarbonyl) amino) pentanedioate (**134**)

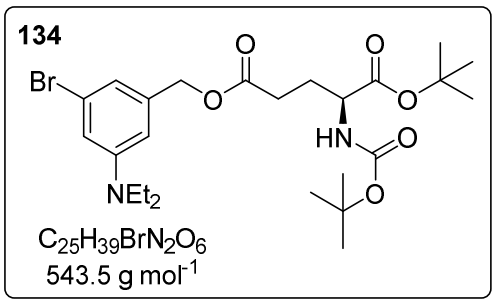

From compound **243a** (4.57 g, 19 mmol), following slightly modified general procedure D (no DIPEA was used; extraction step with 0.01M HCl was skipped; saturated $NaHCO_3$ replaced with water), the product **134** (4.74 g, 50%) was obtained as oil. ^{1}H NMR (300 MHz, $CDCl_3$): δ 6.77-6.69 (m, 2H), 6.51 (s, 1H), 5.14-4.94 (m, 2.9 H, major rotamer), 4.89-4.70 (m, 0.1H, minor rotamer), 4.29-4.00 (m, 0.9H + 0.1H, major and

minor rotamer), 3.32 (q, 4H, *J* = 7.1 Hz), 2.55-2.34 (m, 2H), 2.24-2.08 (m, 1H), 1.99-1.85 (m, 1H), 1.46 (s, 9H), 1.43 (s, 9H), 1.16 (t, 6H, *J* = 7.1 Hz) ppm. ^{13}C NMR (125 MHz, $CDCl_3$): δ 172.7, 171.4, 155.5, 149.1, 138.5, 123.8, 117.7, 114.1, 110.0, 82.4, 79.9, 66.4, 53.5, 44.5, 30.5, 28.5, 28.3, 28.1, 12.5 ppm. HRMS (MALDI-LTQ Orbitrap) m/z: $[M+Na]^+$ Calcd for $C_{25}H_{39}{}^{79}BrN_2NaO_6$ 565.18837; Found: 565.18766; Calcd for $C_{25}H_{39}{}^{81}BrN_2NaO_6$ 567.18632; Found: 567.18865.

Synthesis of the (*S*)-1-carboxy-4-((5-(diethylamino)-[1,1'-biphenyl]-3-yl)methoxy)-4-oxobutan-1-aminium 2,2,2-trifluoroacetate (**148**)

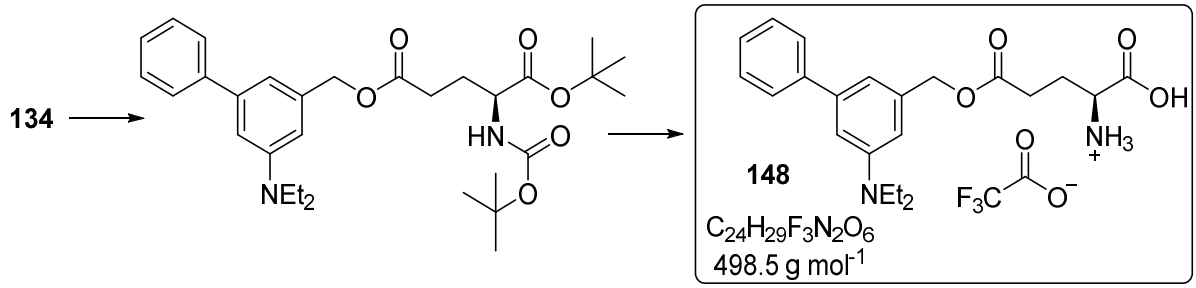

The compound **148** was synthesized in two steps from compound **134** (273 mg, 0.50 mmol) following the general procedure E (Suzuki coupling). The reaction mixture was purified *via* column chromatography. The product was obtained in a mixture with unidentified side product. It was used in the next step without further purification. The protecting group cleavage was done following the general procedure F. The product was purified *via* RP column chromatography to give 50 mg (20% in two steps) of **148** as white solid. ^{1}H NMR (500 MHz, CD_3OD-d_4 + D_2O): δ 7.57-7.53 (m, 2H), 7.45-7.40 (m, 2H), 7.36-7.31 (m, 1H), 6.86-6.83 (m, 2H), 6.72-6.71 (m, 1H), 5.13 (s, 2H), 3.66 (t, 1H, *J* = 6.3 Hz), 3.41 (q, 4H, *J* = 7.1 Hz), 2.69-2.56 (m, 2H), 2.22-2.08 (m, 2H), 1.16 (t, 6H, *J* = 7.1 Hz) ppm. ^{13}C NMR (125 MHz, CD_3OD-d_4 + D_2O): δ 174.8, 174.0, 149.7, 143.8, 142.9, 138.5, 129.8, 128.4, 127.9, 115.8, 112.8, 112.3, 68.5, 55.2, 45.7, 31.2, 27.2, 12.7 ppm. HRMS (MALDI) m/z: $[M]^+$ Calcd for $C_{22}H_{29}N_2O_4$ 385.21218; Found 385.21147.

Synthesis of the (*S*)-1-carboxy-4-((3-(diethylamino)-5-(naphthalen-1-yl)benzyl)oxy)-4-oxobutan-1-aminium 2,2,2-trifluoroacetate (**147**)

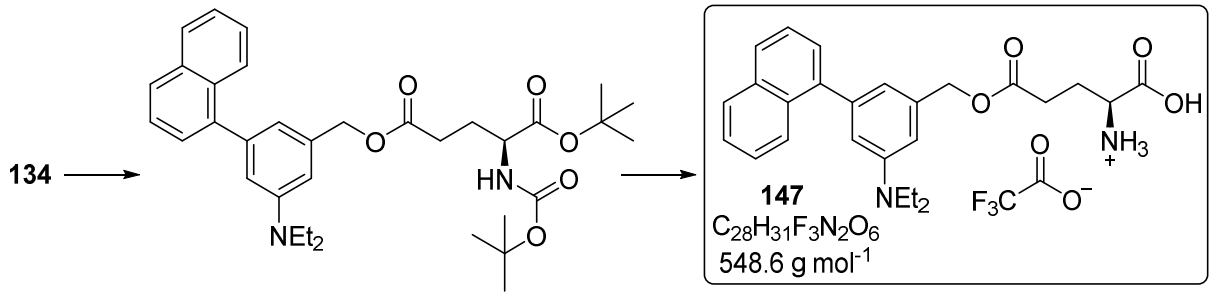

The compound **147** was synthesized in two steps from compound **134** (328 mg, 0.60 mmol) following the general procedure E (Suzuki coupling). The reaction mixture was purified *via* column chromatography. The product was obtained in a mixture with unidentified side product. It was used in the next step without further purification. The protecting group cleavage was done following the general procedure F. The product was purified *via* RP column chromatography to give 57 mg (17% in two steps) of **147** as white solid. ^{1}H NMR (500 MHz, CD_3OD-d_4 + D_2O): δ 7.92-7.89 (m, 1H), 7.88-7.84 (m, 2H), 7.53-7.46 (m, 2H), 7.44-7.39 (m, 1H), 7.39-7.36 (m, 1H), 6.79-6.76 (m, 1H), 6.70-6.68 (m, 2H), 5.16 (s, 2H), 3.62 (t, 1H, J = 6.3 Hz), 3.39 (q, 4H, J = 7.1 Hz), 2.68-2.55 (m, 2H), 2.22-2.08 (m, 2H), 1.16 (t, 6H, J = 7.1 Hz) ppm. ^{13}C NMR (125 MHz, CD_3OD-d_4 + D_2O): δ 174.7, 174.2, 149.2, 143.2, 142.0, 138.2, 135.3, 132.8, 129.3, 128.5, 127.5, 126.9, 126.8, 126.8, 126.4, 118.2, 115.0, 112.2, 68.4, 55.3, 45.6, 31.2, 27.4, 12.8 ppm. HRMS (MALDI) m/z: $[M]^+$ Calcd for $C_{26}H_{31}N_2O_4$ 435.22783; Found 435.22720.

Synthesis of the (*S*)-1-carboxy-4-((5-(diethylamino)-4'-methoxy-[1,1'-biphenyl]-3-yl)methoxy)-4-oxo butan-1-aminium 2,2,2-trifluoroacetate (**138**)

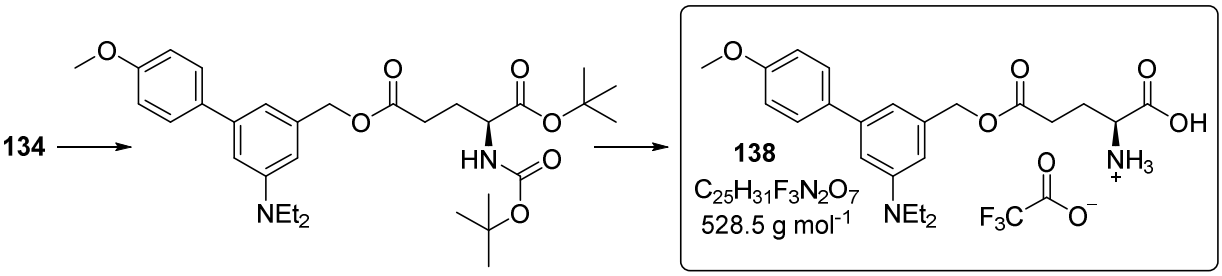

The compound **138** was synthesized in two steps from compound **134** (433 mg, 0.80 mmol) following the general procedure E (Suzuki coupling). The product was obtained in a mixture with side product. It was used in the next step without further purification. The protecting group cleavage was done following the general procedure F. The crude material was purified *via* RP

column chromatography to give 75 mg (18% in two steps) of **138** as white solid. ^{1}H NMR (500 MHz, CD_3OD-d_4 + D_2O): δ 7.53-7.48 (m, 2H), 7.02-6.98 (m, 2H), 6.83-6.80 (m, 2H), 6.69-6.66 (m, 1H), 5.12 (s, 2H), 3.84 (s, 3H), 3.64 (t, 1H, J = 6.3 Hz), 3.40 (q, 4H, J = 7.1 Hz), 2.68-2.55 (m, 2H), 2.22-2.08 (m, 2H), 1.16 (t, 6H, J = 7.1 Hz) ppm. ^{13}C NMR (125 MHz, CD_3OD-d_4 + D_2O): δ 174.8, 174.3, 160.4, 149.7, 143.3, 138.4, 135.5, 129.0, 115.6, 115.2, 112.3, 112.0, 68.5, 56.0, 55.3, 45.7, 31.2, 27.4, 12.7 ppm. HRMS (MALDI) m/z: $[M]^+$ Calcd for $C_{23}H_{31}N_2O_5$ 415.22275; Found 415.22218.

Synthesis of the (*S*)-1-*tert*-butyl 5-((5-(diethylamino)-4'-(trifluoromethyl)-[1,1'-biphenyl]-3-yl) methyl) 2-((*tert*-butoxycarbonyl)amino)pentanedioate (**245**)

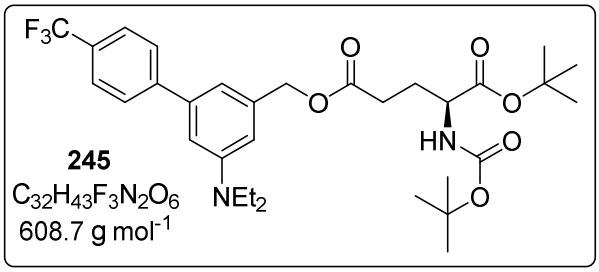

Compound **245** was synthesized from **134** (206 mg, 0.38 mmol) following the general procedure E. 160 mg (69%) was obtained. ^{1}H NMR (300 MHz, $CDCl_3$): δ 7.70-7.63 (m, 4H), 6.83-6.80 (m, 1H), 6.79-6.75 (m, 1H), 6.69-6.66 (m, 1H), 5.17-5.02 (m, 3H), 4.28-4.14 (m, 0.9H, major rotamer), 4.11-4.00 (m, 0.1H, minor rotamer), 3.41 (q, 4H, J = 7.1 Hz), 2.57-2.33 (m, 2H), 2.25-2.10 (m, 1H), 2.01-1.86 (m, 1H), 1.45 (s, 9H), 1.42 (s, 9H), 1.20 (t, 6H, J = 7.1 Hz) ppm. ^{13}C NMR (75 MHz, $CDCl_3$): δ 172.9, 171.4, 155.5, 148.5, 141.6, 137.7, 129.4 (q, ^{2}J = 32 Hz), 127.7, 127.0 (q, ^{1}J = 272 Hz), 125.7 (q, ^{3}J = 3.8 Hz), 115.6, 114.5, 111.3, 110.6, 82.4, 79.9, 67.2, 53.5, 44.6, 30.5, 28.4, 28.3, 28.1, 12.7 ppm. HRMS (MALDI) m/z: $[M+H]^+$ Calcd for $C_{32}H_{44}F_3N_2O_6$ 609.31460; Found 609.31197.

Synthesis of the (*S*)-1-carboxy-4-((5-(diethylamino)-4'-(trifluoromethyl)-[1,1'-biphenyl]-3-yl) methoxy)-4-oxobutan-1-aminium 2,2,2-trifluoroacetate (**150**)

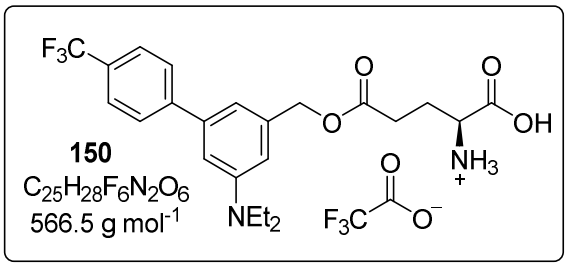

The compound was synthesized from **245** (160 mg, 0.26 mmol), following the general procedure F. Product **150** (41 mg, 27%) was obtained as off white powder. ^{1}H NMR (500 MHz, MeCN-d_3 + D_2O): δ 7.79-7.74 (m, 2H), 7.73-7.69 (m, 2H), 6.86-6.82 (m, 2H), 6.74-6.71 (m, 1H), 5.08 (s, 2H), 3.59 (t, 1H, J = 6.3 Hz), 3.39 (q, 4H, J = 7.1 Hz), 2.61-2.48 (m, 2H), 2.16-2.07 (m, 1H), 2.06-1.98 (m, 1H), 1.11 (t, 6H, J = 7.1 Hz) ppm. ^{13}C NMR (125 MHz, MeCN-d_3 + D_2O): δ 174.1, 172.8, 148.9, 148.5 (d, ^{5}J = 1.4 Hz), 141.1, 138.2, 128.9 (q, ^{2}J = 32 Hz), 128.0, 125.9 (q, ^{3}J = 3.8 Hz), 124.9 (q, ^{1}J = 272 Hz), 114.3, 112.0, 110.6,

67.4, 54.4, 44.5, 30.5, 26.1, 12.1 ppm. HRMS (MALDI) m/z: $[M]^+$ Calcd for $C_{23}H_{28}F_3N_2O_4$ 453.19957; Found 453.19862.

Synthesis of the (*S*)-1-*tert*-butyl 5-((4'-cyano-5-(diethylamino)-[1,1'-biphenyl]-3-yl)methyl) 2-((*tert*-butoxycarbonyl)amino)pentanedioate (**246**)

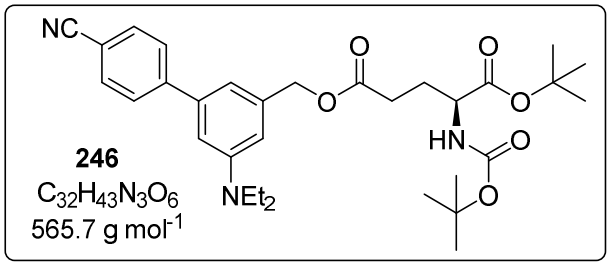

246
$C_{32}H_{43}N_3O_6$
565.7 g mol^{-1}

Compound **246** was synthesized from **134** (222 mg, 0.41 mmol) following the general procedure E. 165 mg (71%) was obtained. ^{1}H NMR (500 MHz, $CDCl_3$): δ 7.74-7.69 (m, 2H), 7.68-7.63 (m, 2H), 6.80 (s, 1H), 6.75 (s, 1H), 6.68 (s, 1H), 5.17-5.02 (m, 2.9H, major rotamer), 4.88-4.70 (m, 0.1H, minor rotamer), 4.27-4.15 (m, 0.9H, major rotamer), 4.13-4.00 (m, 0.1H, minor rotamer), 3.41 (q, 4H, J = 7.1 Hz), 2.55-2.37 (m, 2H), 2.24-2.12 (m, 1H), 1.98-1.88 (m, 1H), 1.45 (s, 9H), 1.43 (s, 9H), 1.20 (t, 6H, J = 7.1 Hz) ppm. ^{13}C NMR (125 MHz, $CDCl_3$): δ 172.9, 171.4, 155.6, 148.6, 146.7, 141.0, 137.9, 132.6, 128.1, 119.2, 114.4, 111.7, 110.4, 82.4, 79.9, 67.1, 53.5, 44.6, 30.5, 28.5, 28.3, 28.1, 12.7 ppm. HRMS (MALDI) m/z: $[M+H]^+$ Calcd for $C_{32}H_{44}N_3O_6$ 566.32246; Found 566.32165.

Synthesis of the (*S*)-1-carboxy-4-((4'-cyano-5-(diethylamino)-[1,1'-biphenyl]-3-yl)methoxy)-4-oxobutan-1-aminium 2,2,2-trifluoroacetate (**139**)

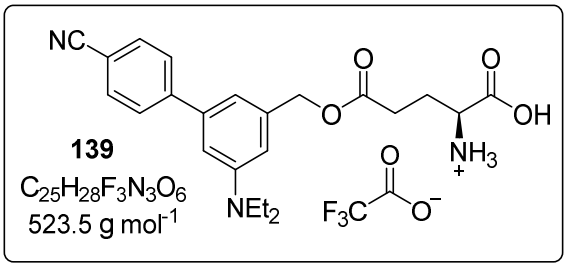

139
$C_{25}H_{28}F_3N_3O_6$
523.5 g mol^{-1}

The compound **139** was synthesized from **246** (165 mg, 0.29 mmol) following the general procedure F. Product (28 mg, 18%) was obtained as off white powder. ^{1}H NMR (300 MHz, MeCN-d_3 + D_2O): δ 7.82-7.72 (m, 4H), 6.89-6.81 (m, 2H), 6.78-6.72 (m, 1H), 5.08 (s, 2H), 3.59 (t, 1H, J = 6.3 Hz), 3.39 (q, 4H, J = 7.1 Hz), 2.60-2.50 (m, 2H), 2.19-2.01 (m, 2H), 1.11 (t, 6H, J = 7.1 Hz) ppm. ^{13}C NMR (125 MHz, MeCN-d_3 + D_2O): δ 174.1, 172.7, 148.9, 146.6, 140.8, 138.4, 133.1, 128.3, 119.5, 114.2, 112.2, 110.7, 110.5, 67.3, 54.5, 44.5, 30.6, 26.1, 12.2 ppm. HRMS (MALDI) m/z: $[M^{\cdot}]^+$ Calcd for $C_{23}H_{28}N_3O_4$ 410.20743; Found 410.20712.

Synthesis of the (S)-1-carboxy-4-((3-(diethylamino)-5-(pyridin-4-yl)benzyl)oxy)-4-oxobutan-1-aminium 2,2,2-trifluoroacetate (**149**)

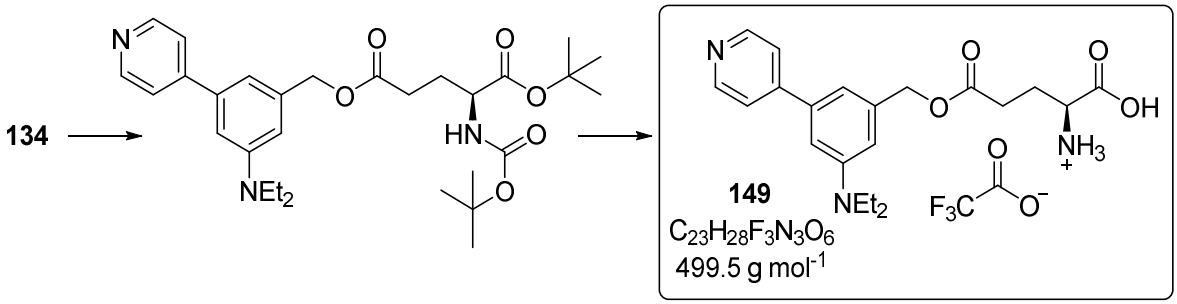

The compound **149** was synthesized in two steps from compound **134** (228 mg, 0.53 mmol) following the general procedure E (Suzuki coupling). The reaction mixture was purified *via* column chromatography. The product was obtained in a mixture with side product. It was used in the next step without further purification. The protecting group cleavage was done following the general procedure F. The product was purified *via* RP column chromatography to give 60 mg (23% in two steps) of the **149** as white solid. ^{1}H NMR (400 MHz, CD_3OD-d_4 + D_2O): δ 8.58-8.52 (m, 2H), 7.69-7.64 (m, 2H), 6.96-6.94 (m, 1H), 6.92-6.90 (m, 1H), 6.82-6.79 (m, 1H), 5.15 (s, 2H), 3.60 (t, 1H, J = 6.3 Hz), 3.44 (q, 4H, J = 7.1 Hz), 2.69-2.55 (m, 2H), 2.22-2.08 (m, 2H), 1.19 (t, 6H, J = 7.1 Hz) ppm. ^{13}C NMR (125 MHz, CD_3OD-d_4 + D_2O): δ 174.8, 174.5, 151.4, 150.3, 149.9, 140.2, 139.2, 123.2, 115.1, 114.1, 111.4, 68.2, 55.3, 45.5, 31.2, 27.4, 12.7 ppm. HRMS (MALDI) m/z: $[M]^+$ Calcd for $C_{21}H_{28}N_3O_4$ 386.20743; Found 386.20704.

Synthesis of the (*S*)-1-*tert*-butyl 5-((5-(diethylamino)-4'-nitro-[1,1'-biphenyl]-3-yl)methyl) 2-((*tert*-butoxycarbonyl)amino)pentanedioate (**247**)

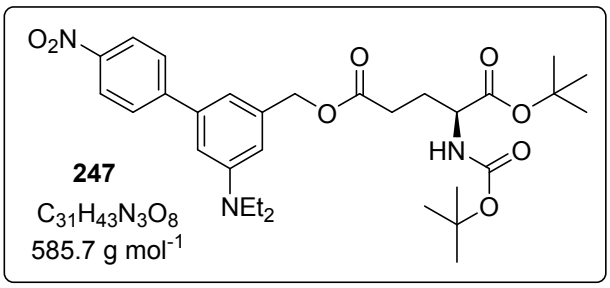

Compound **247** was synthesized from **134** (222 mg, 0.41 mmol) following the general procedure E. Product (169 mg, 70%) was obtained as yellow oil. ^{1}H NMR (500 MHz, $CDCl_3$): δ 8.33-8.23 (m, 2H), 7.76-7.67 (m, 2H), 6.84 (s, 1H), 6.78 (s, 1H), 6.70 (s, 1H), 5.17-5.04 (m, 2.9H, major rotamer), 4.87-4.72 (m, 0.1H, minor rotamer), 4.27-4.15 (m, 0.9H, major rotamer), 4.13-4.00 (m, 0.1H, minor rotamer), 3.42 (q, 4H, J = 6.5 Hz), 2.56-2.37 (m, 2H), 2.24-2.12 (m, 1H), 1.99-1.88 (m, 1H), 1.45 (s, 9H), 1.42 (s, 9H), 1.21 (t, 6H, J = 6.5 Hz) ppm. ^{13}C NMR (125 MHz, $CDCl_3$): δ 172.9, 171.4, 155.5, 148.7, 148.6, 147.2, 140.6, 137.9, 128.1, 124.1, 114.5,

112.0, 110.5, 82.4, 80.0, 67.1, 53.5, 44.6, 30.5, 28.5, 28.3, 28.1, 12.7 ppm. HRMS (MALDI) m/z: $[M+H]^+$ Calcd for $C_{31}H_{44}N_3O_8$ 586.31229; Found 586.31106.

Synthesis of the (*S*)-1-carboxy-4-((5-(diethylamino)-4'-nitro-[1,1'-biphenyl]-3-yl)methoxy)-4-oxobutan-1-aminium 2,2,2-trifluoroacetate (**140**)

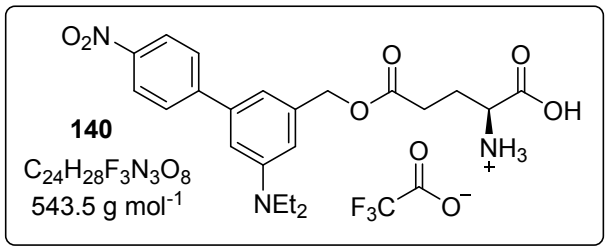

The compound **140** was synthesized from **247** (100 mg, 0.17 mmol) following the general procedure F. Product (46 mg, 50%) was obtained as yellow powder. ^{1}H NMR (500 MHz, MeCN-d_3 + D_2O): δ 8.27-8.22 (m, 2H), 7.83-7.78 (m, 2H), 6.90-6.88 (m, 1H), 6.87-6.85 (m, 1H), 6.77-6.74 (m, 1H), 5.08 (s, 2H), 3.57 (t, 1H, J = 6.3 Hz), 3.39 (q, 4H, J = 7.1 Hz), 2.59-2.47 (m, 2H), 2.14-2.05 (m, 1H), 2.05-1.97 (m, 1H), 1.11 (t, 6H, J = 7.1 Hz) ppm. ^{13}C NMR (125 MHz, MeCN-d_3 + D_2O): δ 174.0, 173.1, 148.7, 148.3, 147.2, 140.1, 138.1, 128.2, 124.1, 114.2, 112.3, 110.5, 67.1, 54.2, 44.3, 30.3, 26.0, 11.9 ppm. HRMS (MALDI) m/z: $[M]^+$ Calcd for $C_{22}H_{28}N_3O_6$ 430.19726; Found 430.19671.

Synthesis of the ethyl 3-amino-4-bromobenzoate hydrochloride (**241b**)

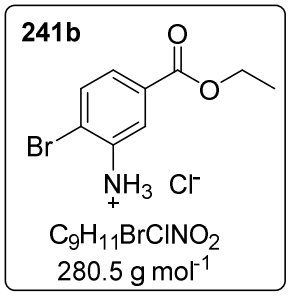

Synthesis was done following the general procedure A. From 3-amino-4-brombenzoic acid (9.0 g, 42mmol, 1 eq) and $SOCl_2$ (39.7 g, 208 mmol, 24.1 mL, 8 eq) in EtOH (75 mL) product **241b** (10.1 g, 86%) was obtained. It was used in next step without further purification. ^{1}H NMR (300 MHz, DMSO-d_6): δ 8.6-7.2 (br, 3H), 7.53-7.45 (m, 2H), 7.07 (dd, 1H, J= 8.2, 2.0 Hz), 4.27 (q, 2H, J = 7.1 Hz), 1.29 (t, 3H, J= 7.1 Hz) ppm. ^{13}C NMR (75 MHz, DMSO-d_6): δ 165.5, 145.2, 132.7, 130.0, 118.3, 116.2, 113.1, 60.8, 14.2 ppm. HRMS (MALDI-LTQ Orbitrap) m/z: $[M]^+$ Calcd for $C_9H_{11}{}^{79}BrNO_2$ 243.99677; Found: 243.99706; Calcd for $C_9H_{11}{}^{81}BrNO_2$ 245.99472; Found: 245.99496.

Synthesis of the ethyl 4-bromo-3-(diethylamino)benzoate (**242b**)

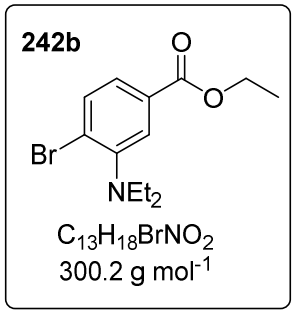

Synthesis was done following the general procedure B. From **241b** (10.0 g, 36 mmol, 1 eq) in a reaction with ethyl iodide (61.2 g, 392 mmol, 10.9 eq) and DIPEA (32.3 g, 250 mmol, 7 eq) product **242b** (10.6 g, quantitative yield) was obtained. It was used in next step without further purification. ^{1}H NMR (300 MHz, $CDCl_3$): δ 7.73 (d, 1H, J = 1.9 Hz), 7.64 (d, 1H, J = 8.3 Hz), 7.55 (dd, 1H, J = 8.3, 1.9 Hz), 4.37 (q, 2H, J =

7.1 Hz), 3.14 (q, 4H, *J* = 7.1 Hz), 1.39 (t, 3H, *J* = 7.1 Hz), 1.03 (t, 6H, *J* = 7.1 Hz) ppm. ^{13}C NMR (75 MHz, $CDCl_3$): δ 166.4, 149.5, 133.9, 130.2, 128.1, 125.3, 125.0, 61.3, 47.1, 14.5, 12.4 ppm. HRMS (MALDI-LTQ Orbitrap) m/z: $[M+H]^+$ Calcd for $C_{13}H_{19}{}^{79}BrNO_2$ 300.05937; Found: 300.06003; Calcd for $C_{13}H_{19}{}^{81}BrNO_2$ 302.05732; Found: 302.05774.

Synthesis of the (4-bromo-3-(diethylamino)phenyl)methanol (**243b**)

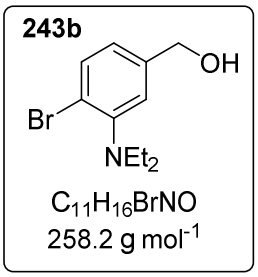

From compound **242b** (10.5 g, 35 mmol), following the general procedure C, the **243b** (8.92 g, 98%) was obtained as oil. ^{1}H NMR (300 MHz, $CDCl_3$): δ 7.55 (d, 1H, *J* = 8.1 Hz), 7.10 (d, 1H, *J* = 1.9 Hz), 6.90 (dd, 1H, *J* = 8.1, 1.9 Hz), 4.64 (d, 2H, *J* = 4.4 Hz), 3.11 (q, 4H, *J* = 7.1 Hz), 1.72-1.63 (m, 1H), 1.03 (t, 6H, *J* = 7.1 Hz) ppm. ^{13}C NMR (75 MHz, $CDCl_3$): δ 149.4, 140.7, 133.9, 123.0, 122.6, 121.5, 65.0, 47.2, 12.4 ppm. HRMS (MALDI-LTQ Orbitrap) m/z: $[M+H]^+$ Calcd for $C_{11}H_{17}{}^{79}BrNO$ 258.04880; Found: 258.04969; Calcd for $C_{11}H_{17}{}^{81}BrNO$ 260.04676; Found: 260.04734.

Synthesis of the (*S*)-5-(4-bromo-3-(diethylamino)benzyl) 1-*tert*-butyl 2-((*tert*-butoxycarbonyl) amino)pentanedioate (**135**)

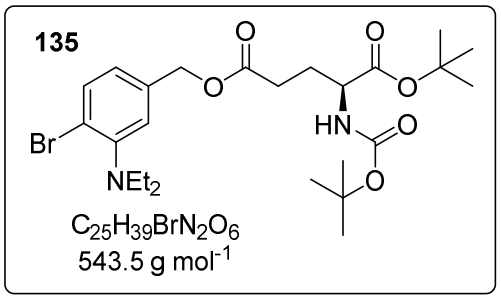

From compound **243b** (4.52 g, 18 mmol), following slightly modified general procedure D (no DIPEA was used), the product **135** (4.87 g, 51%) was obtained as oil. ^{1}H NMR (500 MHz, $CDCl_3$): δ 7.55 (d, 1H, *J* = 8.1 Hz), 7.03 (d, 1H, *J* = 1.8 Hz), 6.89 (dd, 1H, *J* = 8.1, 1.8 Hz), 5.13-5.00 (m, 2.9H, major rotamer), 4.85-4.72 (m, 0.1H, minor rotamer), 4.26-4.57 (m, 0.9H, major rotamer), 4.11-3.98 (m, 0.1H, minor rotamer), 3.10 (q, 4H, J = 7.1 Hz), 2.52-2.35 (m, 2H), 2.22-2.11 (m, 1H), 1.96-1.86 (m, 1H), 1.45 (s, 9H), 1.43 (s, 9H), 1.02 (t, 6H, *J* = 7.1 Hz) ppm. ^{13}C NMR (125 MHz, $CDCl_3$): δ 172.7, 171.4, 155.5, 149.4, 135.6, 134.0, 124.2, 123.9, 122.2, 82.4, 80.0, 66.0, 53.4, 47.1, 30.5, 28.4, 28.3, 28.1, 12.4 ppm. HRMS (MALDI-LTQ Orbitrap) m/z: $[M+Na]^+$ Calcd for $C_{25}H_{39}{}^{79}BrN_2NaO_6$ 565.18837; Found: 565.18730; Calcd for $C_{25}H_{39}{}^{81}BrN_2NaO_6$ 567.18632; Found: 567.18856.

Synthesis of the (*S*)-1-carboxy-4-((4'-methoxy-2-(diethylamino)-[1,1'-biphenyl]-4-yl)methoxy)-4-oxobutan-1-aminium 2,2,2-trifluoroacetate (**141**)

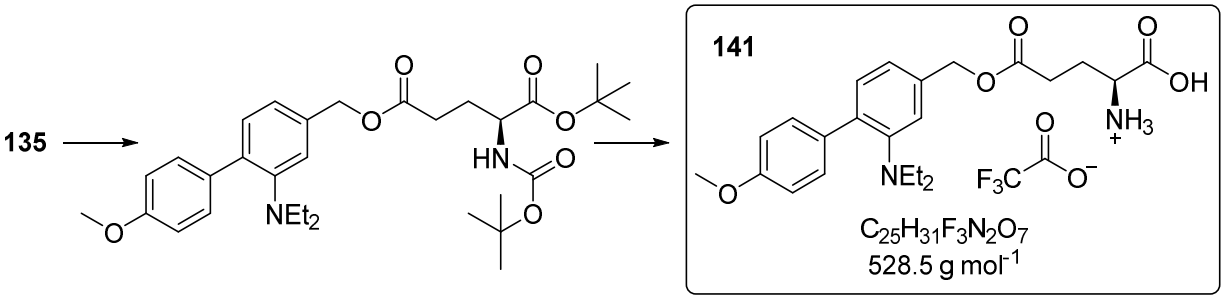

The compound **141** was synthesized in two steps from compound **135** (333 mg, 0.61 mmol) following the general procedure E (Suzuki coupling). The reaction mixture was purified *via* column chromatography. The product was obtained in a mixture with side product. ^{1}H NMR (250 MHz, $CDCl_3$): δ 7.51-7.43 (m, 2H), 7.21-7.15 (m, 1H), 7.02 (m, 2H), 6.94-6.87 (m, 2H), 5.13-5.03 (m, 3H), 4.29-4.13 (m, 1H), 3.83 (s, 3H), 2.88 (q, 4H, *J* = 7.1 Hz), 2.55-2.35 (m, 2H), 2.26-2.08 (m, 1H), 2.03-1.86 (m, 1H), 1.46 (s, 9H), 1.44 (s, 9H), 0.89 (t, 6H, *J* = 7.1 Hz) ppm. HRMS (MALDI) m/z: $[M+H]^+$ Calcd for $C_{32}H_{47}N_2O_7$ 571.33778; Found 571.33890. It was used in the next step without further purification. The protecting group cleavage was done following the general procedure F. The product was purified *via* RP column chromatography to give **141** as light solid which upon storage partly degraded before NMR spectra was measured. However, the relevant signals could be detected. ^{1}H NMR (400 MHz, CD_3OD-d_4 + D_2O): δ 7.52-7.22 (m, 5H), 7.10-7.00 (m, 2H), 5.22 (s, 2H), 3.86 (s, 3H), 3.73-3.68 (m, 1H), 3.19 (q, 4H, *J* = 7.1 Hz), 2.72-2.59 (m, 2H, 2.24-2.12 (m, 2H), 1.02-0.93 (m, 6H) ppm. ^{13}C NMR (500 MHz, CD_3OD-d_4 + D_2O): δ 174.8, 174.2, 131.7, 115.3 ,67.2 ,56.1, 55.1, 47.9, 31.0, 26.9, 11.4 ppm (as extracted from $^{1}H^{13}C$ HSQC spectra). At the time of photochemical characterization the compound was of a better quality as indicated by HPLC analysis (see Figure 154C).

Synthesis of the (*S*)-1-carboxy-4-((4'-cyano-2-(diethylamino)-[1,1'-biphenyl]-4-yl)methoxy)-4-oxobutan-1-aminium 2,2,2-trifluoroacetate (**142**)

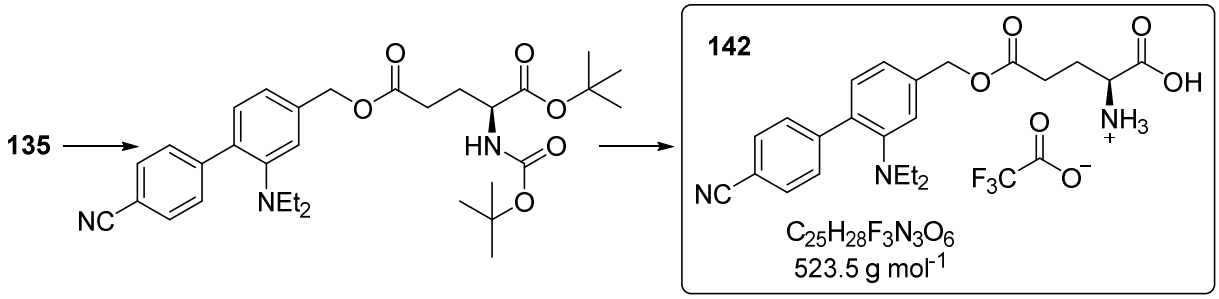

The compound **142** was synthesized in two steps from compound **135** (750 mg, 1.38 mmol) following the general procedure E (Suzuki coupling). The reaction mixture was purified *via* column chromatography. The product was obtained in a mixture with side product. It was used in the next step without further purification. The protecting group cleavage was done following the general procedure F. The product was purified *via* RP column chromatography to give 201 mg (28% in two steps) of **142** as light yellow solid. ^{1}H NMR (500 MHz, MeCN-d_3 + D_2O): δ 7.77-7.68 (m, 4H), 7.23-7.19 (m, 1H), 7.16-7.14 (m, 1H), 7.09-7.06 (m, 1H), 5.11 (s, 2H), 3.67 (t, 1H, J = 6.3 Hz), 2.83 (q, 4H, J = 7.1 Hz), 2.66-2.52 (m, 2H), 2.22-2.12 (m, 1H), 2.10-2.01 (m, 1H), 0.84 (t, 6H, J = 7.1 Hz) ppm. ^{13}C NMR (125 MHz, MeCN-d_3 + D_2O): δ 174.0, 173.7, 149.3, 146.7, 137.2, 135.0, 132.5, 131.7, 130.2, 122.5, 121.7, 119.5, 110.0, 66.7, 54.3, 46.4, 30.5, 26.0, 11.7 ppm. HRMS (MALDI) m/z: $[M]^+$ Calcd for $C_{23}H_{28}N_3O_4$ 410.20743; Found 410.20718.

Synthesis of the (*S*)-1-carboxy-4-((4'-nitro-2-(diethylamino)-[1,1'-biphenyl]-4-yl)methoxy)-4-oxobutan-1-aminium 2,2,2-trifluoroacetate (**143**)

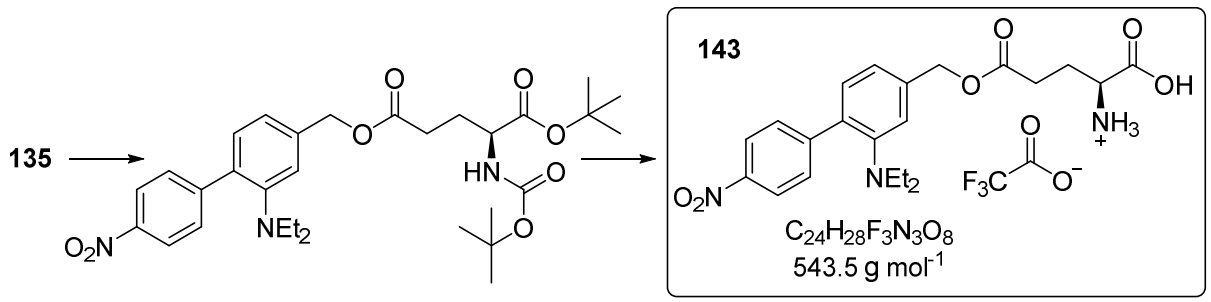

The compound **143** was synthesized in two steps from compound **135** (242 mg, 0.44 mmol) following the general procedure E (Suzuki coupling). The reaction mixture was purified *via* column chromatography. The product was obtained in a mixture with side product. It was used in the next step without further purification. ^{1}H NMR (500 MHz, $CDCl_3$): δ 8.26-8.21 (m, 2H), 7.75-7.70 (m, 2H), 7.21 (d, 1H, J = 7.7 Hz), 7.09-7.04 (m, 2H), 5.16-5.03 (m, 2.9H, major rotamer), 4.88-4.74 (m, 0.1H, minor rotamer), 4.26-4.17 (m, 0.9H, major rotamer), 4.12-4.01 (m, 0.1H, minor rotamer),

2.87 (q, 4H, *J* = 7.1 Hz), 2.55-2.38 (m, 2H), 2.24-2.12 (m, 1H), 1.99-1.89 (m, 1H), 1.46 (s, 9H), 1.44 (s, 9H), 0.91 (t, 6H, *J* = 7.1 Hz) ppm. HRMS (MALDI) m/z: $[M+H]^+$ Calcd for $C_{31}H_{44}N_3O_8$ 586.31229; Found 586.31140. The protecting group cleavage was done following the general procedure F. The product was purified *via* RP column chromatography to give 32 mg (13% in two steps) of **143** as orange solid. ^{1}H NMR (500 MHz, CD_3OD-d_4 + D_2O): δ 8.31-8.26 (m, 2H), 7.82-7.77 (m, 2H), 7.29 (d, 1H, *J* = 7.8 Hz), 7.21-7.20 (m, 1H), 7.16-7.13 (m, 1H), 5.19 (s, 2H), 3.70 (t, 1H, *J* = 6.3 Hz), 2.89 (q, 4H, *J* = 7.1 Hz), 2.72-2.60 (m, 2H), 2.25-2.13 (m, 2H), 0.90 (t, 6H, *J* = 7.1 Hz) ppm. ^{13}C NMR (125 MHz, CD_3OD-d_4 + D_2O): δ 174.9, 174.1, 150.0, 149.8, 147.5, 138.1, 135.8, 132.4, 131.0, 124.4, 122.6, 121.3, 67.6, 55.1, 47.4, 31.1, 27.0, 12.2 ppm. HRMS (MALDI) m/z: $[M]^+$ Calcd for $C_{22}H_{28}N_3O_6$ 430.19726; Found 430.19681.

Synthesis of the ethyl 3-amino-2-bromobenzoate hydrochloride (**241c**)

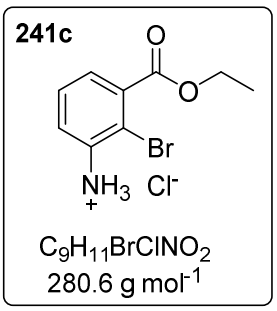

Synthesis was done following the general procedure A. From 3-amino-2-brombenzoic acid (10.0 g, 46 mmol, 1 eq) and $SOCl_2$ (43.8 g, 368 mmol, 26.8 mL, 8 eq) in EtOH (75 mL) product **241c** (8.61 g, 67%) was obtained. It was used in next step without further purification. ^{1}H NMR (500 MHz, CD_3OD-d_4): δ 7.74-7.66 (m, 1H), 7.62-7.52 (m, 2H), 4.41 (q, 2H, *J* = 7.1 Hz), 1.40 (t, 3H, *J* = 7.1 Hz) ppm. ^{13}C NMR (125 MHz, CD_3OD-d_4): δ 167.1, 136.9, 135.1, 130.3, 130.1, 126.9, 115.9, 63.3, 14.4 ppm. HRMS (MALDI-LTQ Orbitrap) m/z: $[M^{\cdot}]^+$ Calcd for $C_9H_{10}{}^{79}BrNO_2$ 242.98894; Found: 242.98912; Calcd for $C_9H_{10}{}^{81}BrNO_2$ 244.98690; Found: 244.98701.

Synthesis of the ethyl 2-bromo-3-(diethylamino)benzoate (**242c**)

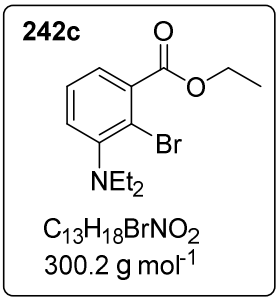

Synthesis was done following the general procedure B. From 3-amonium-2-brombenzoic acid ethyl ester hydrochloride **241c** (4.07 g, 14.5 mmol, 1 eq) in reaction with ethyl iodide (28.7 g, 180 mmol, 12.4 eq) and DIPEA (15.5 g, 120 mmol, 8.2 eq) product **242c** (4.35 g, quantitative) was obtained as oil. It was used in next step without further purification. ^{1}H NMR (500 MHZ, DMSO-d_6): δ 7.42-7.38 (m, 1H), 7.33 (dd, 1H, *J* = 8.0, 1.6 Hz), 7.23 (dd, 1H, *J* = 7.4, 1.6 Hz), 4.30 (q, 2H, *J* = 7.1 Hz), 3.05 (q, 4H, *J* = 7.1 Hz), 1.30 (t, 3H, *J* = 7.1 Hz), 0.94 (t, 6H, *J* = 7.1 Hz) ppm. ^{13}C NMR (100 MHz, DMSO-d_6): δ 166.9, 149.5, 136.4, 127.9, 126.3, 123.8, 119.1, 61.4, 46.4, 14.0, 12.0 ppm. HRMS (MALDI-LTQ Orbitrap) m/z:

$[M+H]^+$ Calcd for $C_{13}H_{19}{}^{79}BrNO_2$ 300.05937; Found: 300.05765; Calcd for $C_{13}H_{19}{}^{81}BrNO_2$ 302.05732; Found: 302.05561.

Synthesis of the (2-bromo-3-(diethylamino)phenyl)methanol (**243c**)

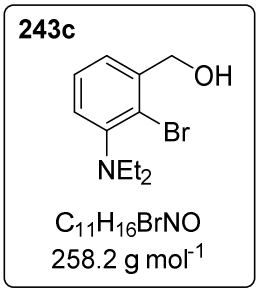

From compound **242c** (4.25 g, 14.1 mmol), following the general procedure C, the product **242c** (2.50 g, 69%) was obtained as oil. ^{1}H NMR (400 MHZ, DMSO-d_6): δ 7.34-7.30 (m, 1H), 7.27-7.23 (m, 1H), 7.10 (dd, 1H, J = 7.8, 1.6 Hz), 5.35 (t, 1H, J = 5.7 Hz), 4.51 (d, 2H, J = 5.7 Hz), 3.00 (q, 4H, J = 7.1 Hz), 0.92 (t, 6H, J = 7.1 Hz) ppm. ^{13}C NMR (125 MHz, DMSO-d_6): δ 148.4, 142.6, 127.2, 122.8, 122.7, 121.5, 63.4, 46.7, 12.1 ppm. HRMS (MALDI-LTQ Orbitrap) m/z: $[M+H]^+$ Calcd for $C_{11}H_{17}{}^{79}BrNO$ 258.04880; Found: 258.04845; Calc. for $C_{11}H_{17}{}^{81}BrNO$ 260.04676; Found: 260.04697.

Synthesis of the (*S*)-5-(2-bromo-3-(diethylamino)benzyl) 1-*tert*-butyl 2-((*tert*-butoxycarbonyl) amino)pentanedioate (**136**)

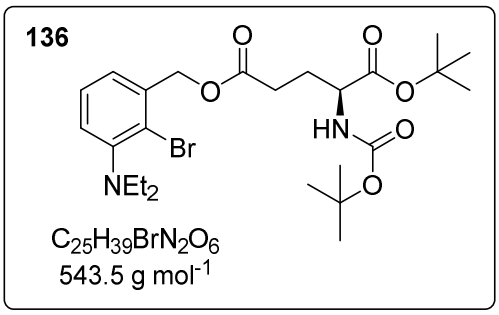

From compound **243c** (2.46 g, 9.52 mmol), following slightly modified general procedure D (no DIPEA was used; extraction step with 0.01M HCl was skipped; saturated $NaHCO_3$ replaced with water), the product **136** (3.44 g, 66%) was obtained as oil. ^{1}H NMR (500 MHz, $CDCl_3$): δ 7.27-7.23 (m, 1H), 7.12-7.05 (m, 2H), 5.25-5.22 (m, 2H), 5.15-5.03 (m, 0.85H, major rotamer), 4.9-4.7 (br s, 0.15H, minor rotamer), 4.28-4.18 (m, 0.85H, major rotamer), 4.14-4.00 (m, 0.15H, minor rotamer), 3.08 (q, 4H, J = 7.1 Hz), 2.57-2.40 (m, 2H), 2.26-2.15 (m, 1H), 2.00-1.90 (m, 1H), 1.46 (s, 9H) 1.43 (s, 9H), 1.01 (t, 6H, J = 7.1 Hz) ppm. ^{13}C NMR (125 MHz, $CDCl_3$): δ 172.7, 171.5, 155.5, 149.8, 136.9, 127.3, 124.5, 124.1, 124.0, 82.4, 79.9, 67.0, 53.5, 47.4, 30.5, 28.5, 28.3, 28.1, 12.3 ppm. HRMS (MALDI-LTQ Orbitrap) m/z: $[M+K]^+$ Calcd for $C_{25}H_{39}{}^{79}BrN_2O_6K$ 581.16231; Found: 581.16031; Calcd for $C_{25}H_{39}{}^{81}BrN_2O_6K$ 583.16026; Found: 583.15813.

Synthesis of the (*S*)-1-carboxy-4-((4'-methoxy-6-(diethylamino)-[1,1'-biphenyl]-2-yl)methoxy)-4-oxobutan-1-aminium 2,2,2-trifluoroacetate (**144**)

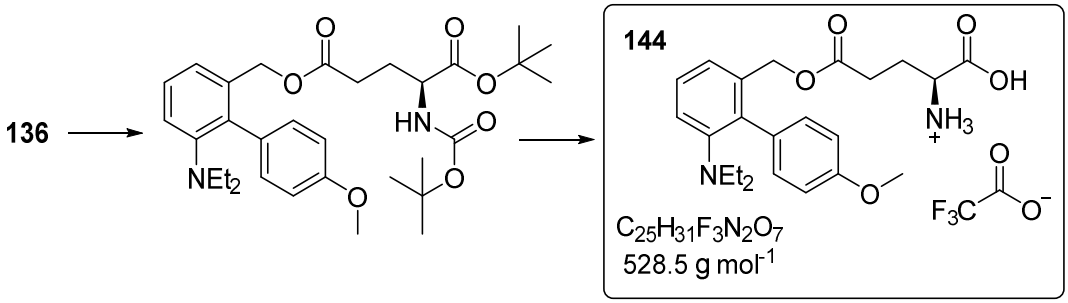

The compound **144** was synthesized in two steps from compound **136** (481 mg, 0.89 mmol, 1.0 eq) following the general procedure E (Suzuki coupling). The reaction was interrupted before it reached full conversion, the product was purified *via* column. However, it was obtained in a mixture with starting material and other, unidentified side products. It was used in the next step without further purification. HRMS (MALDI) m/z: $[M+H]^+$ Calcd for $C_{32}H_{47}N_2O_7$ 571.33778; Found 571.33634. The protecting group cleavage was done following the general procedure F. The product was purified *via* RP column chromatography to give less than 10 mg as a white solid. ^{1}H NMR (400 MHz, MeCN-d_3 + D_2O): δ 7.32-7.26 (m, 1H), 7.17-7.11 (m, 2H), 7.11-7.06 (m, 2H), 6.96-6.91 (m, 2H), 4.73 (s, 2H), 3.78 (s, 3H), 3.56-3.49 (m, 1H), 2.73 (q, 4H, J = 7.1 Hz), 2.46-2.38 (m, 2H), 1.98-1.85 (m, 2H, signal overlaying with MeCN), 0.72 (t, 6H, J = 7.1 Hz) ppm. HSQC (^{1}H-^{13}C) NMR (^{1}H 400 MHz, ^{13}C 100 MHz, MeCN-d_3 + D_2O): δ 132.6, 129.1, 124.8, 123.8, 114.3, 66.5, 56.2, 55.2, 48.1, 31.4, 27.1, 12.6 ppm. HRMS (MALDI) m/z: $[M]^+$ Calcd for $C_{23}H_{31}N_2O_5$ 415.22275; Found 415.22231.

Synthesis of the (*S*)-1-carboxy-4-((4'-cyano-6-(diethylamino)-[1,1'-biphenyl]-2-yl)methoxy)-4-oxobutan-1-aminium 2,2,2-trifluoroacetate (**145**)

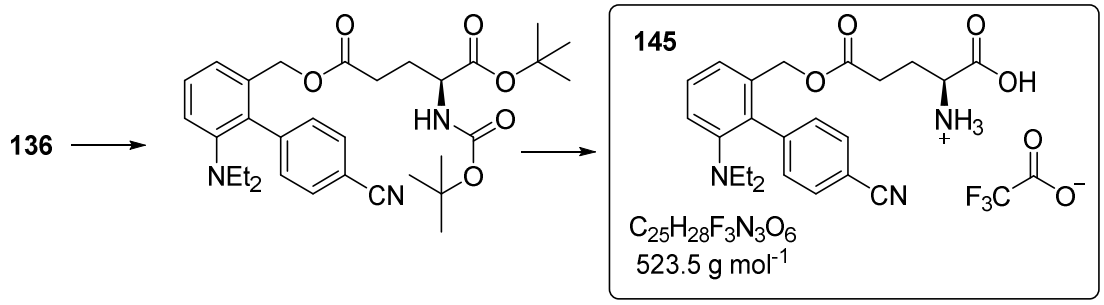

The compound **145** was synthesized in two steps from compound **136** (200 mg, 0.37 mmol, 1.0 eq) following the general procedure E (Suzuki coupling). The product was purified *via* column. However, it was obtained in 2:1 mixture with dehalogenated starting material. It was used in the

next step without further purification. The protecting group cleavage was done following the general procedure F. The product was purified *via* RP column chromatography to give 45 mg (23% in two steps) of **145** as white solid. ^{1}H NMR (600 MHz, CD_3OD-d_4): δ 7.80-7.75 (m, 2H), 7.46-7.42 (m, 2H), 7.39-7.35 (m, 1H), 7.24 (d, 1H, J = 8.1 Hz), 7.21 (d, 1H, J = 7.6 Hz), 4.81 (s, 2H), 3.57 (t, 1H, J = 6.3 Hz), 2.79 (q, 4H, J = 7.1 Hz), 2.55-2.44 (m, 2H), 2.11-2.01 (m, 2H), 0.79 (t, 6H, J = 7.1 Hz) ppm. ^{13}C NMR (150 MHz, CD_3OD-d_4): δ 173.7, 173.6, 150.9, 145.6, 139.0, 135.9, 132.9, 132.8, 129.8, 125.6, 123.8, 119.9, 111.5, 65.9, 55.3, 48.3, 31.0, 27.3, 12.7 ppm. HRMS (MALDI) m/z: $[M]^+$ Calcd for $C_{23}H_{28}N_3O_4$ 410.20743; Found 410.20737.

Synthesis of the (*S*)-1-carboxy-4-((4'-nitro-6-(diethylamino)-[1,1'-biphenyl]-2-yl)methoxy)-4-oxobutan-1-aminium 2,2,2-trifluoroacetate (**146**)

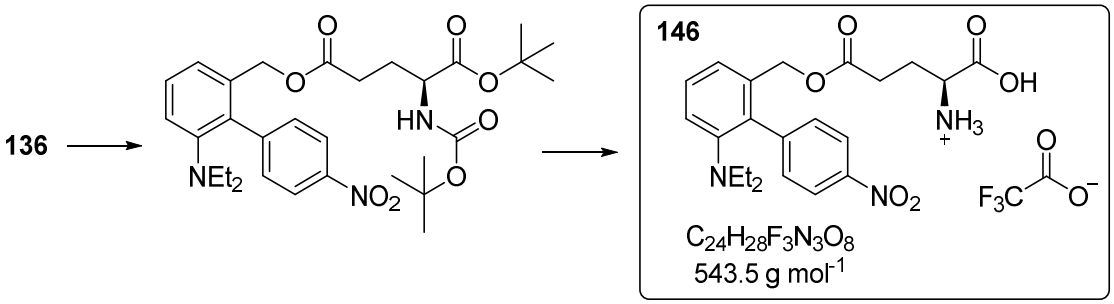

The compound **146** was synthesized in two steps from compound **136** (475 mg, 0.87 mmol) following the general procedure E (Suzuki coupling). The product was purified *via* column but was not obtained pure. It was used in the next step without further purification. The protecting group cleavage was done following the general procedure F. The product was purified *via* RP column chromatography to give less than 20 mg of the product (<4% in two steps) as orange solid. ^{1}H NMR (500 MHz, CD_3OD-d_4 + D_2O): δ 8.32-8.28 (m, 2H), 7.50-7.46 (m, 2H), 7.45-7.40 (m, 1H), 7.29 (d, 1H, J = 8.1 Hz), 7.25 (d, 1H, J = 7.6 Hz), 4.83 (s, 2H), 3.61 (t, 1H, J = 6.3 Hz), 2.79 (q, 4H, J = 7.1 Hz), 2.56-2.43 (m, 2H), 2.11-2.00 (m, 2H), 0.79 (t, 6H, J = 7.1 Hz) ppm. ^{13}C NMR (125 MHz, CD_3OD-d_4 + D_2O): δ 174.2, 174.0, 150.6, 147.9, 147.4, 138.6, 135.5, 132.9, 130.0, 125.9, 124.1, 124.0, 66.0, 55.1, 48.7, 30.9, 27.0, 12.6 ppm. HRMS (MALDI) m/z: $[M]^+$ Calcd for $C_{22}H_{28}N_3O_6$ 430.19726; Found 430.19659.

5.5. Synthesis of fluorene derivatives

5.5.1. General procedure G – reductive amination:

Synthesis of the 2-(dimethylamino)-9H-fluoren-9-ol (**165**)

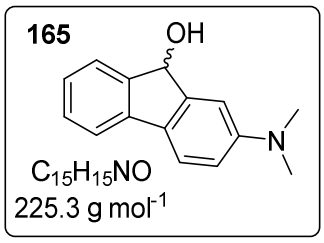

2-Amino-fluoren-9-one **164** (932 mg, 4.78 mmol, 1 eq) was dissolved in AcOH (20 mL). To this mixture paraformaldehyde (890 mg, 29.6 mmol, 6.2 eq) and $NaBH_3CN$ (879 mg, 14.0 mmol, 2.9 eq) was added. The mixture was stirred overnight (18 h), then diluted with water and extracted three times with EtOAc. The combined organic phase washed with water, saturated $NaHCO_3$ and brine, dried over Na_2SO_4 and filtrated. The solvent was removed under reduced pressure to give light brown powder. This was crystalized from EtOAc and Cy to give 658 mg (61%) of a slightly brown solid. ^{1}H NMR (400 MHz, $CDCl_3$): δ 7.59-7.55 (m, 1H), 7.51-7.47 (m, 2H), 7.34-7.29 (m, 1H), 7.18 (td, 1H, *J* = 7.4, 1.0 Hz), 7.04 (d, 1H, *J* = 2.4 Hz), 6.73 (dd, 1H, *J* = 8.4, 2.4 Hz), 5.51 (s, 1H), 3.02 (s, 6H) ppm. ^{13}C NMR (100 MHz, $CDCl_3$): δ 151.1, 147.5, 145.0, 141.0, 129.1, 128.7, 125.9, 125.0, 120.8, 118.7, 113.1, 109.4, 75.6, 41.0 ppm. HRMS (MALDI-LTQ Orbitrap) m/z: $[M^{\cdot}]^+$ Calcd for $C_{15}H_{15}N_1O_1$ 225.11482; Found: 225.11492.

Synthesis of the (2S)-1-tert-butyl 5-(2-(dimethylamino)-9H-fluoren-9-yl) 2-((tert-butoxycarbonyl) amino)pentanedioate (**166**)

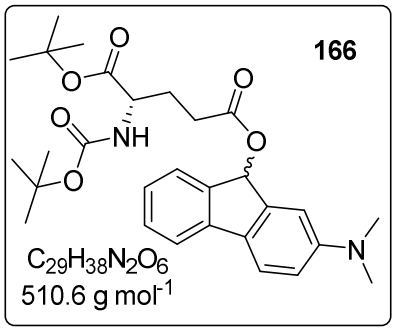

The synthesis was done according to general procedure D with small variations. Compound **165** (388 mg, 1.72 mmol, 1.0 eq) was dissolved in CH_2Cl_2 (10 mL). To the solution EDC-HCl (658 mg, 3.44 mmol, 2 eq), DMAP (21 mg, 0.17 mmol, 0.1 eq) and *N*-(*tert*-butoxycarbonyl)-*L*-glutamic acid 1-*tert*-butyl ester **121** (522 mg, 1.72 mmol, 1 eq) was added. The reaction mixture was stirred until TLC analysis showed full conversion (20 h). Upon completion the mixture was diluted with CH_2Cl_2 and washed with water. The water layer was extracted two times with CH_2Cl_2. Combined organic phase was washed with brine and dried over Na_2SO_4, concentrated in reduced pressure to give slightly brown oil. After column chromatography (SiO_2, Cy : EtOAc 9:1 to 1:1) product **165** (570 mg, 65%) was obtained as light brown oil (mixture of diastereomers). ^{1}H NMR (500 MHz, $CDCl_3$): δ 7.53-7.44 (m, 3H), 7.36-7.30 (m, 1H), 7.18-7.12 (m, 1H), 6.92 (s, 1H), 6.78-6.70 (m, 2H), 5.18-5.04 (0.9H, major rotamer), 4.90-4.75 (0.1H, minor rotamer), 4.30-4.20 (0.9H, major rotamer), 4.15-4.02 (0.1H, minor rotamer),

3.01 (s, 6H), 2.60-2.44 (m, 2H), 2.30-2.18 (m, 1H), 2.05-1.92 (m, 1H), 1.46-1.44 (m, 9H), 1.44-1.42 (m, 9H) ppm. ^{13}C NMR (125 MHz, $CDCl_3$): δ 173.9, 173.8, 171.5, 155.5, 151.0, 143.7, 143.6, 142.0, 141.3, 141.2, 129.6, 125.9, 125.8, 125.8, 120.8, 118.7, 113.3, 110.1, 82.4, 80.0, 75.7, 53.6, 53.5, 41.0, 30.7, 28.5, 28.3, 28.1 ppm. HRMS (MALDI-LTQ Orbitrap) m/z: $[M^{\cdot}]^+$ Calcd for $C_{29}H_{38}N_2O_6$ 510.27244; Found: 510.27131.

Synthesis of (1S)-1-carboxy-4-((2-(dimethylamino)-9H-fluoren-9-yl)oxy)-4-oxobutan-1-aminium 2,2,2-trifluoroacetate (**167**)

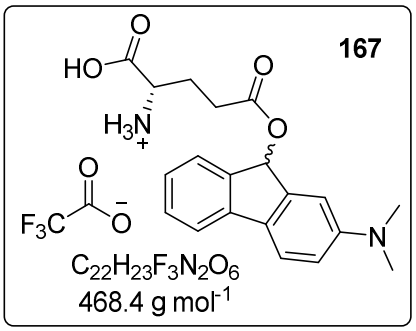

The synthesis was done according to general procedure F. From compound **166** (510 mg, 1.0 mmol, 1 eq), the product **167** (209 mg, 45%) was obtained as white powder (mixture of diastereomers). ^{1}H NMR (400 MHz, CD_3OD-d_4 + D_2O): δ 7.53-7.49 (m, 2H), 7.44 (d, 1H, *J* = 7.5 Hz), 7.34-7.29 (m, 1H), 7.15-7.09 (m, 1H), 6.97-6.94 (m, 1H), 6.79 (dd, 1H, *J* = 8.4, 2.5 Hz), 6.68 (s, 1H), 3.64 (dt, 1H, *J* = 6.3, 2.9 Hz), 2.97 (s, 6H), 2.72-2.64 (m, 2H), 2.28-2.14 (m, 2H) ppm. ^{13}C NMR (100 MHz, CD_3OD+D_2O): δ 175.0, 173.8, 152.5, 144.8, 144.7, 143.3, 143.2, 142.5, 142.5, 131.0, 130.9, 130.5, 126.8, 126.6, 121.6, 119.5, 114.7, 111.2, 76.9, 55.4, 55.4, 41.1, 31.5, 31.4, 27.7, 27.6 ppm. HRMS (MALDI-LTQ Orbitrap) m/z: $[M]^+$ Calcd for $C_{20}H_{22}N_2O_4$ 354.15796; Found: 354.15730.

5.5.2. General procedure H – acylation with Ac_2O

Synthesis of 2-(dimethylamino)-9H-fluoren-9-yl acetate (**168**)

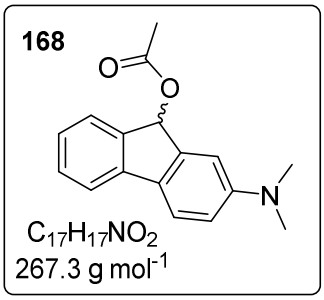

2-Dimethylamino-9-fluorenol **165** (63 mg, 0.28 mmol, 1 eq) was dissolved in pyridine (6 mL). To the solution Ac_2O (1.08 g, 10.5 mmol, 38 eq) was added and mixture was stirred overnight. Upon completion the solution was evaporated until dryness, then purified *via* column chromatography (SiO_2, Cy : EtOAc 9:1) to give 49 mg (65%) of product **168** as off white foam. ^{1}H NMR (500 MHz, $CDCl_3$): δ 7.53-7.49 (m, 2H), 7.47 (d, 1H, *J* = 7.4 Hz), 7.36-7.31 (m, 1H), 7.18-7.13 (m, 1H), 7.0-6.9 (br s, 1H), 6.81-6.69 (m, 2H), 3.01 (s, 6H), 2.19 (s, 3H) ppm. ^{13}C NMR (125 MHz, $CDCl_3$): δ 172.1, 151.0, 143.8, 142.0, 141.3, 129.8, 129.6, 125.9, 125.7, 120.9, 118.8, 113.4, 110.1, 75.5, 41.0, 21.5 ppm. HRMS (MALDI-LTQ Orbitrap) m/z: $[M^{\cdot}]^+$ Calcd for $C_{17}H_{17}NO_2$ 267.12538; Found: 267.12552.

5.5.3. General procedure I – Buchwald–Hartwig amination

Synthesis of the 2-(bis(4-methoxyphenyl)methyl)-9H-fluoren-9-ol (**172b**)

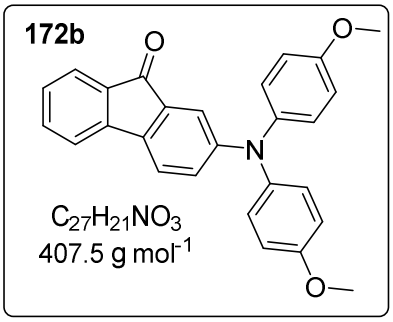

2-bromo-9-fluorenone **171** (569 mg, 2.19 mmol, 1 eq) and 4,4′-dimethoxydiphenylamine (503 mg, 2.19 mmol, 1 eq) was dissolved in dry toluene (10 mL). To the solution was added NaO^{t}Bu (632 mg, 6.59 mmol, 3 eq) and $Pd(OAc)_2$ (24 mg, 0.11 mmol, 0.05 eq). The solution was degassed by argon stream (15 min) before addition of P(^{t}Bu)$_3$ (44 mg, 0.21 mmol, 0.1 eq). The dark colored solution was refluxed under argon atmosphere. During reaction the mixture changes colour to red. When TLC shows complete disappearance of starting material (the fluorenone), solvent was evaporated, the solid leftover dissolved in EtOAc and extracted with water twice. The organic layer was washed with brine, dried over Na_2SO_4, filtrated and solvent was removed under reduced pressure. Purified *via* column chromatography (SiO_2, Cy : EtOAc 19:1 to 9:1 to 3:1) to collect product as dark foam (200 mg, 22%). ^{1}H NMR (400 MHz, DMSO-d_6): δ 7.60-7.57 (m, 1H), 7.56-7.48 (m, 3H), 7.25-7.20 (m, 1H), 7.14-7.07 (m, 4H), 6.99-6.94 (m, 4H), 6.90-6.83 (m, 2H), 3.76 (s, 6H) ppm. NMR data are in agreement with literature.[239]

5.5.4. General procedure J – reduction of carbonyl group with $NaBH_4$

Synthesis of the 2-(bis(4-methoxyphenyl)amino)-9H-fluoren-9-ol (**173b**)

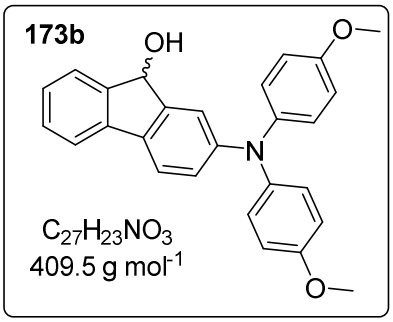

Compound **172b** (200 mg, 0.49 mmol, 1 eq) was dissolved in THF/EtOH 1:1 mixture (5 mL) and cooled in ice bath. Then $NaBH_4$ (28 mg, 0.74 mmol, 1,5 eq) was added and the cooling bath removed. Within 20 minutes reaction mixture changes color to slightly yellow. TLC accordingly confirms complete reduction of starting material. The reaction was quenched with small amount NH_4Cl (aq. solution), solvent was evaporated, solid residue dissolved in EtOAc and extracted with water. The organic layer was washed with brine, dried over Na_2SO_4, filtrated and solvent was evaporated under reduced pressure. Purified *via* column chromatography (SiO_2, Cy : EtOAc 19:1 to 9:1 to 3:1) to collect product **173b** as light yellow foam (98 mg, 49%). ^{1}H NMR (400 MHz, DMSO-d_6): δ 7.59 (d, 1H, J = 7.5 Hz), 7.54 (d, 1H, J = 8.2 Hz), 7.48 (d, 1H, J = 7.4 Hz), 7.33-7.28 (m, 1H), 7.21-7.6 (m 1H), 7.06-7.02 (m, 4H),

7.00 (d, 1H, *J* = 2.2 Hz), 6.95-6.90 (m, 4H), 6.79 (dd, 1H, *J* = 8.2, 2.2 Hz), 5.72 (d, 1H, *J* = 7.3 Hz), 5.33 (d, 1H, *J* = 7.3 Hz), 3.75 (s, 6H) ppm. ^{13}C NMR (100 MHz, DMSO-d_6): δ 155.7, 148.4, 148.3, 146.4, 140.3, 139.6, 131.7, 128.3, 126.6, 126.0, 124.8, 120.5, 119.7, 118.8, 116.3, 115.0, 73.4, 55.2 ppm. HRMS (MALDI-LTQ Orbitrap) m/z: $[M^{\cdot}]^+$ Calcd for $C_{27}H_{23}NO_3$ 409.16725; Found: 409.16638.

Synthesis of the 2-(bis(4-methoxyphenyl)amino)-9H-fluoren-9-yl acetate (**174b**)

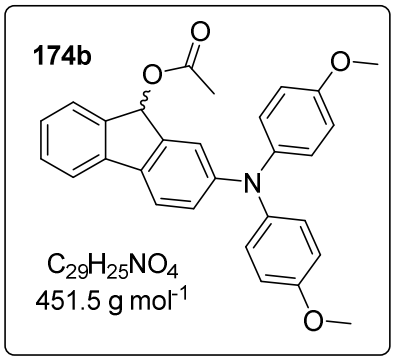

Compound **174b** was prepared as described in general procedure H, using **173b** (78 mg, 0.19 mmol) as starting material. After purification (SiO_2, Cy : EtOAc 9:1 to 3:1) 74 mg (85%) of product **174b** was obtained as a foam. ^{1}H NMR (500 MHz, DMSO-d_6): δ 7.65 (d, 1H, *J* = 7.5 Hz), 7.60 (d, 1H, *J* = 8.3 Hz), 7.45 (d, 1H, *J* = 7.5 Hz), 7.40-7.36 (m, 1H), 7.23-7.19 (m, 1H), 7.05-7.01 (m, 4H), 7.00 (d, 1H, *J* = 2.1 Hz), 6.94-6.90 (m, 4H), 6.81 (1H, dd, *J* = 8.3, 2.1 Hz), 6.57 (s, 1H), 3.74 (s, 6H), 2.07 (s, 3H) ppm. ^{13}C NMR (125 MHz, $DMSO_{D6}$): δ 171.1, 155.8, 148.6, 143.1, 141.4, 140.6, 140.1, 132.6, 129.6, 126.6, 126.6, 125.7, 121.0, 120.7, 119.3, 116.9, 115.0, 74.3, 55.2, 20.9 ppm. HRMS (MALDI-LTQ Orbitrap) m/z: $[M^{\cdot}]^+$ Calcd for $C_{29}H_{25}NO_4$ 451.17781; Found: 451.17881.

Synthesis of the 2-(diphenylamino)-9H-fluoren-9-one (**172a**)

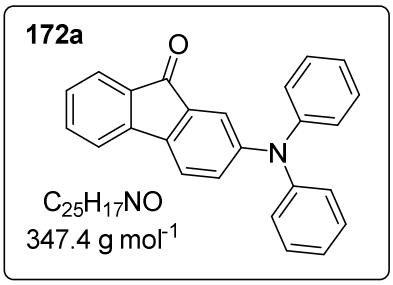

Synthesis was done as described in general procedure I. Starting from 2-bromo-9-fluorenone **171** (318 mg, 1.23 mmol), 149 mg (35%) of product **172a** was obtained as a red solid. ^{1}H NMR (400 MHz, DMSO-d_6): δ 7.69-7.63 (m, 2H), 7.59-7.53 (m, 2H), 7.40-7.33 (m, 4H), 7.31-7.26 (m, 1H), 7.16-7.07 (m, 7H), 7.03 (d, 1H, *J* = 2.1 Hz) ppm. NMR data are in agreement with literature.[240]

Synthesis of the 2-(diphenylamino)-9H-fluoren-9-ol (**173a**)

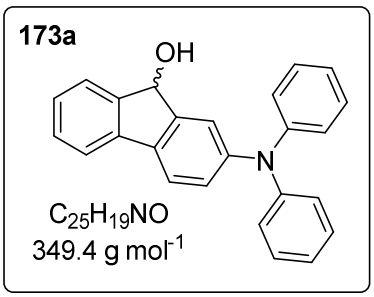

Synthesis was done as described in general procedure J. Starting from compound **172a** (142 mg, 0.41 mmol), 113 mg (79%) of product **173a** was obtained as off-white foam. ^{1}H NMR (400 MHz, $CDCl_3$): δ 7.61-7.58 (m, 1H), 7.56 (d, 1H, *J* = 7.5 Hz), 7.50 (d, 1H, *J* = 8.2 Hz), 7.38-7.34 (m, 2H), 7.29-7.23 (m, 5H), 7.14-7.08 (m, 5H), 7.06-7.00 (m, 2H), 5.49 (s, 1H) ppm. ^{13}C NMR (75 MHz, $CDCl_3$): δ 148.2, 147.9, 147.2, 145.6, 140.1, 134.5, 129.5, 129.3, 127.1, 125.1, 124.7, 124.6, 123.1, 120.8, 120.8, 119.5, 75.3 ppm. HRMS (MALDI-LTQ Orbitrap) m/z: $[M^{\cdot}]^{+}$ Calcd for $C_{25}H_{19}NO$ 349.14612; Found: 349.14593.

Synthesis of the 2-(diphenylamino)-9H-fluoren-9-yl acetate (**174a**)

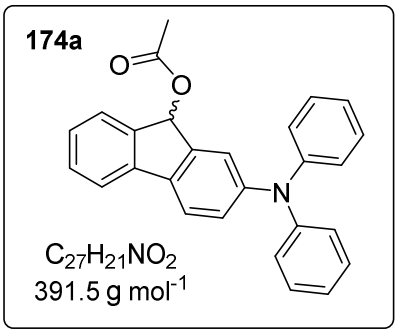

Compound **174a** was prepared as described in general procedure H using **173a** (71 mg, 0.20 mmol, 1 eq) as starting material. A 40 mg (50%) of product **174a** was obtained as off-white foam. ^{1}H NMR (500 MHz, $CDCl_3$): δ 7.58-7.55 (m, 1H), 7.52-7.49 (m, 2H), 7.39-7.35 (m, 1H), 7.28-7.21 (m, 6H), 7.14-7.08 (m, 5H), 7.06-7.00 (m, 2H), 6.70 (s, 1H), 2.13 (s, 3H) ppm. ^{13}C NMR (125 MHz, $CDCl_3$): δ 171.8, 148.1, 147.8, 143.4, 142.2, 141.0, 135.6, 129.7, 129.5, 127.1, 126.0, 125.3, 124.4, 123.1, 121.4, 120.9, 119.6, 75.0, 21.4 ppm. HRMS (MALDI-LTQ Orbitrap) m/z: $[M^{\cdot}]^{+}$ Calcd for $C_{27}H_{21}NO_2$ 391.15668; Found: 391.15638.

Synthesis of the 2,7-diamino-9H-fluoren-9-one (**176**)

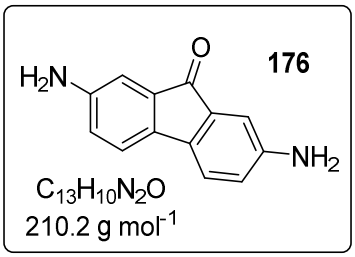

2,7-Dinitrofluoren-9-one **175** (2.16 g, 8.0 mmol, 1 eq) was dissolved in EtOH (40 mL). A solution of Na_2S (2.80 g, 36 mmol, 4.5 eq) in water, containing NaOH (3.20 g, 80 mmol, 10 eq) was added. Mixture was refluxed for 6 h, then cooled to room temperature and filtrated. The crude mixture was purified *via* column (SiO_2, Cy : EtOAc 1:1). Product **176** (1.22 g, 73%) was obtained as dark solid. ^{1}H NMR (400 MHz, DMSO-d_6): δ 7.09 (d, 2H, *J* = 7.9 Hz), 6.70 (d, 2H, *J* = 2.2 Hz), 6.58 (dd, 2H, *J* = 7.9, 2.2 Hz), 5.29 (s, 4H) ppm. NMR data are in agreement with literature.[241]

Synthesis of the 2,7-bis(dimethylamino)-9H-fluoren-9-ol (**177**)

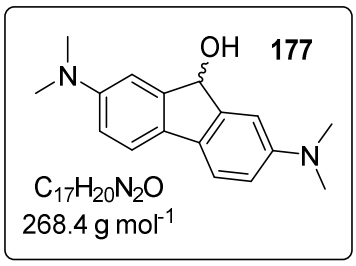

Compound **177** was prepared according to general procedure G, starting from **176** (148 mg, 0.7 mmol). Product **177** (105 mg, 55%) was obtained as off-white solid. ^{1}H NMR (500 MHz, DMSO-d_6): δ 7.35 (d, 2H, J = 8.3 Hz), 6.93 (d, 2H, J = 2.2 Hz), 6.66 (dd, 2H, J = 8.3, 2.2 Hz), 5.60 (d, 1H, J = 7.3 Hz), 5.29 (d, 1H, J = 7.3 Hz), 2.91 (s, 12H) ppm. ^{13}C NMR (125 MHz, DMSO-d_6): δ 149.3, 147.5, 129.1, 118.8, 112.4, 109.6, 73.9, 40.7 ppm. HRMS (MALDI-LTQ Orbitrap) m/z: $[M^{\cdot}]^{+}$ Calcd for $C_{17}H_{20}N_2O_1$ 268.15701; Found: 268.15734.

Synthesis of the 2,7-bis(dimethylamino)-9H-fluoren-9-yl acetate **(178)**

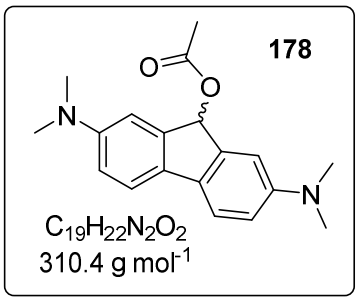

Compound **177** (75 mg, 0.28 mmol, 1 eq) was dissolved in CH_2Cl_2 (20 mL). Acetyl chloride (114 mg, 1.45 mmol, 5.2 eq) and DIPEA (198 mg, 1.54 mmol, 5.5 eq) was added and the mixture was stirred in room temperature. It was quenched by dilution with water before conversion was complete because there was no progress observed for more than 24 h. Organic phase was separated, washed with brine, dried over Na_2SO_4, and filtrated. Solvent was removed under reduced pressure. Purification was done by column chromatography (SiO_2, Cy : EtOAc 9:1). Product **178** (40 mg, 32%) was obtained as off-white solid. ^{1}H NMR (500 MHz, DMSO-d_6): δ 7.40 (d, 2H, J = 8.4 Hz), 6.85 (d, 2H, J = 2.1 Hz), 6.71 (dd, 2H, J = 8.4, 2.1 Hz), 6.54 (s, 1H), 2.90 (s, 12H), 2.15 (s, 3H) ppm. ^{13}C NMR (75 MHz, DMSO-d_6): δ 171.3, 149.4, 142.4, 129.9, 119.2, 113.2, 110.1, 74.8, 40.5, 21.1 ppm. HRMS (MALDI-LTQ Orbitrap) m/z: $[M^{\cdot}]^{+}$ Calcd for $C_{19}H_{22}N_2O_2$ 310.16758; Found: 310.16809.

Synthesis of the 2,7-bis(bis(4-methoxyphenyl)amino)-9H-fluoren-9-one **(180)**

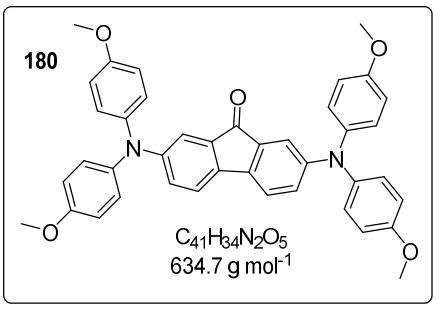

Compound **180** was prepared according to general procedure I, starting from commercially available 2,7-dibromo-9-fluorenone **183** (1.00 g, 2.95 mmol, 1 eq) and 4,4′-dimethoxydiphenylamine (1.35 g, 5.9 mmol, 2 eq). Product **180** (593 mg, 32%) was obtained as green solid. ^{1}H NMR (400 MHz, $CDCl_3$): δ 7.19-7.15 (m, 2H), 7.13 (d, 2H, J = 8.1 Hz), 7.06-6.99 (m, 8H), 6.97-6.91 (m, 2H), 6.85-6.80 (m, 8H), 3.80 (s, 12H) ppm. ^{13}C NMR (100

MHz, $CDCl_3$): δ 194.3, 156.3, 149.0, 140.6, 136.8, 135.8, 126.8, 125.7, 120.1, 116.8, 115.0, 55.7 ppm. HRMS (MALDI-LTQ Orbitrap) m/z: $[M^{\cdot}]^+$ Calcd for $C_{41}H_{34}N_2O_5$ 634.24622; Found: 634.24585.

Synthesis of the 2,7-bis(bis(4-methoxyphenyl)amino)-9H-fluoren-9-ol **(181)**

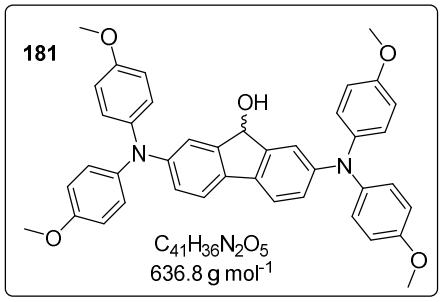

Compound **181** was prepared according to general procedure J, starting from compound **180** (556 mg, 0.88 mmol). Product was obtained in a form of yellow solid (489 mg, 87%). ^{1}H NMR (500 MHz, DMSO-d_6): δ 7.39 (d, 2H, J = 8.2 Hz), 7.02-6.97 (m, 8H), 6.95 (d, 2H, J = 2.1 Hz), 6.92-6.88 (m, 8H), 6.75 (dd, 2H, J = 8.2, 2.1 Hz), 5.69 (d, 1H, J = 6.4 Hz), 5.21 (d, 1H, J = 5.7 Hz), 3.73 (s, 12H) ppm. ^{13}C NMR (125 MHz, DMSO-d_6): δ 155.5, 147.9, 147.2, 140.6, 132.2, 126.4, 120.2, 119.5, 116.9, 115.0, 73.3, 55.3 ppm. HRMS (MALDI-LTQ Orbitrap) m/z: $[M^{\cdot}]^+$ Calcd for $C_{41}H_{36}N_2O_5$ 636.26187; Found: 636.26088.

Synthesis of the 2,7-bis(bis(4-methoxyphenyl)amino)-9H-fluoren-9-yl acetate **(182)**

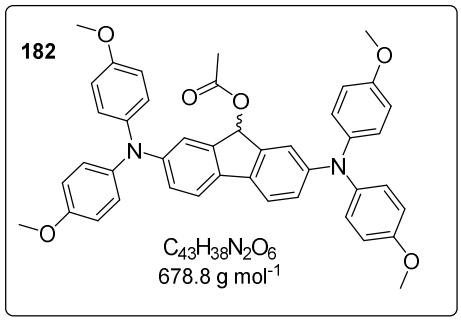

Compound **181** was prepared according to general procedure H, starting from compound **181** (100 mg, 0.16 mmol). Product was obtained as yellow solid (89 mg, 83%). ^{1}H NMR (500 MHz, DMSO-d_6): δ 7.44 (d, 2H, J = 8.3 Hz), 7.00-6.97 (m, 8H), 6.96 (d, 2H, J = 2.2 Hz), 6.92-6.87 (m, 8H), 6.78 (dd, 2H, J = 8.3, 2.2 Hz), 6.42 (s, 1H), 3.73 (s, 12H), 2.00 (s, 3H) ppm. ^{13}C NMR (125 MHz, DMSO-d_6): δ 171.1, 155.6, 147.5, 142.7, 140.3, 133.2, 126.3, 121.3, 120.0, 117.6, 115.0, 74.3, 55.2, 20.8 ppm. HRMS (MALDI-LTQ Orbitrap) m/z: $[M^{\cdot}]^+$ Calcd for $C_{43}H_{38}N_2O_6$ 678.27244; Found: 678.27197.

Synthesis of the 2-bromo-7-nitro-9H-fluoren-9-one (**184**)

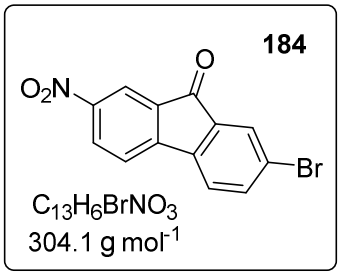

2-Bromo-9-fluorenone **183** (3.54 g, 13.67 mmol, 1 eq) was suspended in water (12 mL) before addition of nitration mixture consisting of conc. HNO_3 (16.8 g, 11.1 mL) and conc. H_2SO_4 (34.20 g, 18.6 mL). The mixture was refluxed for 5 h, the progress monitored *via* NMR. Additional 3.7 mL of conc. HNO_3 and 6,1 mL conc. H_2SO_4 was added and mixture refluxed for 5 h more. The mixture was then cooled to room temperature, diluted with water, filtrated. The yellow powder was

washed with water until the filtrate was neutral. Then the solid was transferred to Erlenmeyer flask, washed with EtOAc and decanted (by doing this procedure one can efficiently separate sparingly soluble product from well soluble starting material). The yellow colored 2-nitro-7-bromo-9-fluorenone **184** was air dried to give 2.80 g (67%). ^{1}H NMR (250 MHz, $CDCl_3$): δ 8.49 (dd, 1H, *J* = 2.1, 0.5 Hz), 8.44 (dd, 1H, *J* = 8.1, 2.1 Hz), 7.89 (dd, 1H, *J* = 1.8, 0.4 Hz), 7.74 (dd, 1H, *J* = 8.0, 1.8 Hz), 7.70 (dd, 1H, *J* = 8.1, 0.5 Hz), 7.55 (dd, 1H, *J* = 8.0, 0.4 Hz) ppm. NMR data are in agreement with literature.[242]

Synthesis of the 2-(bis(4-methoxyphenyl)amino)-7-nitro-9H-fluoren-9-one (**185**)

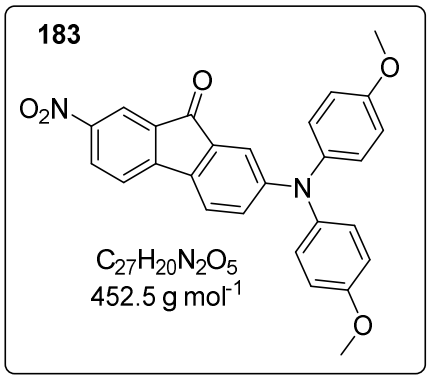

Molecule **185** was prepared as described in general procedure I, starting from **184** (230 mg, 0.75 mmol). Dark colored product (121 mg, 35%) was obtained. ^{1}H NMR (500 MHz, $CDCl_3$): δ 8.35 (d, 1H, *J* =2.1 Hz), 8.32 (dd, 1H, *J* = 8.2, 2.1 Hz), 7.45 (d, 1H, *J* = 8.2 Hz), 7.35 (d, 1H, *J* = 8.3 Hz), 7.21 (d, 1H, *J* = 2.3 Hz), 7.11-7.07 (m, 4H), 6.98 (dd, 1H, *J* = 8.3, 2.3 Hz), 6.90-6.86 (m, 4H), 3.82 (s, 6H) ppm. ^{13}C NMR (125 MHz, $CDCl_3$): δ 191.6, 157.2, 152.0, 151.0, 147.3, 139.3, 136.8, 135.0, 132.4, 130.5, 127.7, 123.6, 122.8, 119.6, 119.3, 115.3, 114.9, 55.7 ppm. HRMS (MALDI-LTQ Orbitrap) m/z: $[M^-]^+$ Calcd for $C_{27}H_{20}N_2O_5$ 452.13667; Found: 452.13610.

Synthesis of the 2-amino-7-(bis(4-methoxyphenyl)amino)-9H-fluoren-9-one (**186**)

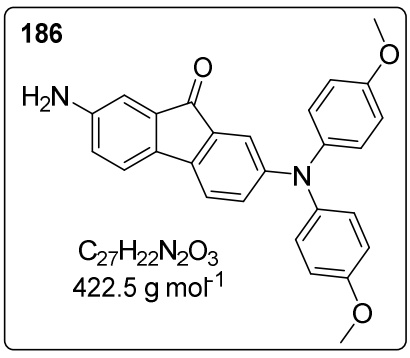

Molecule **185** (120 mg, 0.26 mmol, 1 eq) was dissolved in EtOH (10 mL). A solution of Na_2S (99.3 mg, 1.27 mmol, 4.8 eq) in water, containing NaOH (53 mg, 1.33 mmol, 5 eq) was added. Mixture was refluxed for 3 h. Then EtOH was removed, solid residue dissolved in EtOAc (30 mL), extracted with water (2 x 25 mL), washed with brine, dried over Na_2SO_4 and filtrated. Solvent was removed under reduced pressure. Crude product was purified *via* column chromatography (SiO_2, Cy : EtOAc 19:1 to 1:1). Solvent was removed to give 69 mg (63%) of product **186**. ^{1}H NMR (500 MHz, DMSO-d_6): δ 7.25 (d, 1H, *J* = 8.1 Hz), 7.22 (d, 1H, *J* = 8.0 Hz), 7.06-7.00 (m, 4H), 6.95-6.90 (m, 4H), 6.83 (dd, 1H, *J* = 8.1, 2.3 Hz), 6.79 (d, 1H, *J* = 2.3 Hz), 6.74 (d, 1H, *J* = 2.2 Hz), 6.64 (dd, 1H, *J* = 8.0, 2.2 Hz), 5.49 (s, 2H), 3.75 (s, 6H) ppm. ^{13}C NMR (125 MHz, DMSO-d_6): δ 194.0, 155.9, 149.2, 147.7, 139.8, 137.3,

135.0, 134.3, 131.8, 126.6, 124.9, 121.0, 119.9, 118.7, 115.1, 114.7, 109.6, 55.3 ppm. HRMS (MALDI-LTQ Orbitrap) m/z: $[M^{\cdot}]^+$ Calcd for $C_{27}H_{22}N_2O_3$ 422.16249; Found: 422.16214.

Synthesis of the 2-(bis(4-methoxyphenyl)amino)-7-(dimethylamino)-9H-fluoren-9-ol (**187**)

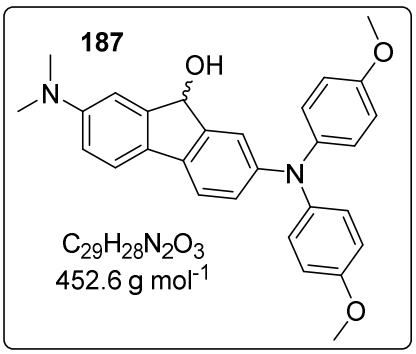

Synthesis was done as described in general procedure G, starting from molecule **186** (60 mg, 0.14 mmol). After purification (SiO_2, Cy : EtOAc 9:1 to 1:1) product **187** (59 mg, 92%) was obtained. ^{1}H NMR (500 MHz, DMSO-d_6): δ 7.40 (d, 1H, J = 8.3 Hz), 7.36 (d, 1H, J = 8.2 Hz), 7.00-6.95 (m, 5H), 6.91-6.87 (m, 5H), 6.76 (dd, 1H, J = 8.2, 2.1 Hz), 6.67 (dd, 1H, J = 8.3, 2.3 Hz), 5.68 (d, 1H, J = 7.1 Hz), 5.25 (d, 1H, J = 7.1 Hz), 3.73 (s, 6H), 2.92 (s, 6H) ppm. ^{13}C NMR (125 MHz, DMSO-d_6): δ 155.4, 149.8, 148.0, 147.4, 146.5, 140.9, 133.5, 128.2, 126.1, 120.9, 119.7, 118.9, 117.7, 115.0, 112.4, 109.4, 73.7, 55.3, 40.6 ppm. HRMS (MALDI-LTQ Orbitrap) m/z: $[M^{\cdot}]^+$ Calcd for $C_{29}H_{28}N_2O_3$ 452.20944; Found: 452.20867.

Synthesis of the 2-(bis(4-methoxyphenyl)amino)-7-(dimethylamino)-9H-fluoren-9-yl acetate (**188**)

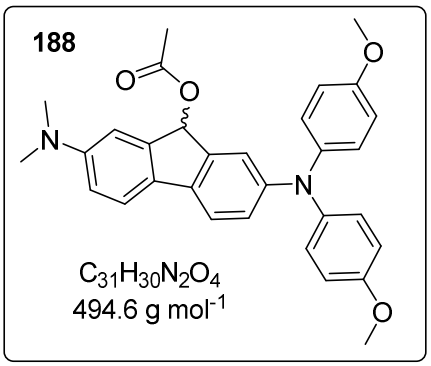

Synthesis was done as described in general procedure H, starting from molecule **187** (28 mg, 0.06 mmol). Product **188** was obtained as off white foam (19 mg, 63%). ^{1}H NMR (500 MHz, DMSO-d_6): δ 7.45 (d, 1H, J = 8.4 Hz), 7.41 (d, 1H, J = 8.2 Hz), 6.99-6.95 (m, 5H), 6.91-6.87 (m, 4H), 6.85 (d, 1H, J = 2.1 Hz), 6.78 (1H, dd, J = 8.3, 2.1 Hz), 6.73 (dd, 1H, J = 8.4, 2.4 Hz), 6.48 (s, 1H), 3.73 (s, 6H), 2.92 (s, 6H), 2.08 (s, 3H) ppm. ^{13}C NMR (125 MHz, DMSO-d_6): δ 171.7, 155.8, 150.3, 147.1, 143.4, 142.7, 141.0, 134.9, 129.2, 126.3, 122.4, 120.4, 119.7, 118.8, 115.3, 113.6, 110.2, 74.9, 55.7, 40.8, 21.4 ppm. HRMS (MALDI-LTQ Orbitrap) m/z: $[M^{\cdot}]^+$ Calcd for $C_{31}H_{30}N_2O_4$ 494.22001; Found: 494.21850.

Synthesis of the 2,8-bis(bis(4-methoxyphenyl)amino)indeno[1,2-b]fluorene-6,12-dione **(190)**

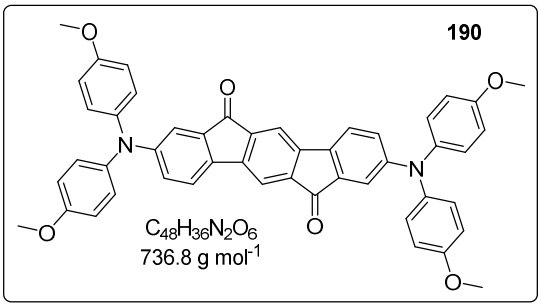

Compound **190** was prepared according to general procedure I, starting from commercially available 2,8-Dibromoindeno[1,2-b]fluorene-6,12-dione **189** (350 mg, 0.79 mmol, 1 eq) and 4,4′-dimethoxydiphenylamine (365 mg, 1.59 mmol, 2 eq). Product (160 mg, 27%) was obtained as dark solid. ^{1}H NMR (500 MHz, $CDCl_3$): δ 7.55 (s, 2H), 7.23 (d, 2H, J = 8.3 Hz), 7.20 (d, 2H, J = 2.3 Hz), 7.07-7.04 (m, 8H), 6.98 (dd, 2H, J = 8.3, 2.3 Hz), 6.87-6.83 (m, 8H), 3.81 (s, 12H) ppm. ^{13}C NMR (125 MHz, $CDCl_3$): δ 193.6, 156.7, 150.4, 145.3, 140.0, 139.6, 135.4, 134.8, 127.2, 124.8, 121.1, 115.9, 115.1, 115.0, 55.7 ppm.

Synthesis of the 2,8-bis(bis(4-methoxyphenyl)amino)-6,12-dihydroindeno[1,2-b]fluorene-6,12-diol (**191**)

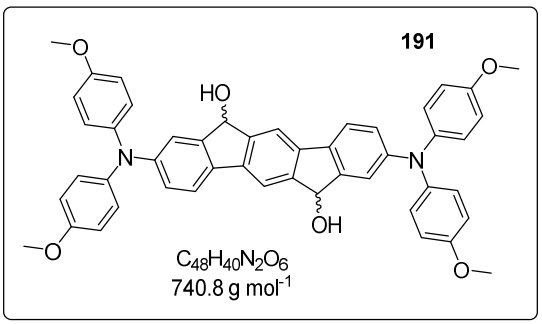

Compound **191** was prepared according to general procedure J, starting from compound **190** (160 mg, 0.22 mmol). Product was obtained in a form of yellow solid (17 mg, 10%). ^{1}H NMR (500 MHz, DMSO-d_6): δ 7.69 (d, 2H, J = 1.6 Hz), 7.55 (d, 2H, J = 8.3 Hz), 7.06-7.02 (m, 8H), 7.01-7.00 (m, 2H), 6.95-6.91 (m, 8H), 6.77 (dd, 2H, J = 8.3, 1.6 Hz), 5.79-5.74 (m, 2H), 5.36-5.32 (m, 2H), 3.75 (s, 12H) ppm. ^{13}C NMR (125 MHz, DMSO-d_6): 155.7, 148.6, 147.9, 147.2, 147.2, 140.4, 138.0, 132.0, 126.6, 120.1, 119.8, 116.3, 115.6, 115.0, 73.3, 55.3 ppm. HRMS (MALDI-LTQ Orbitrap) m/z: $[M^{\cdot}]^{+}$ Calcd for $C_{48}H_{40}N_2O_6$ 740.28809; Found: 740.28782.

Synthesis of the 2,8-bis(bis(4-methoxyphenyl)amino)-6,12-dihydroindeno[1,2-b]fluorene-6,12-diyl diacetate **(192)**

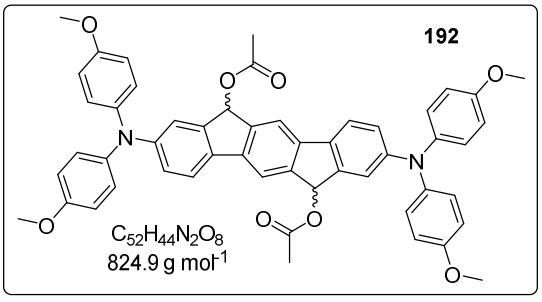

Compound **192** was prepared according to general procedure H, starting from compound **191** (16 mg, 0.021 mmol). Product was obtained as yellow solid (16 mg, 92%). ^{1}H NMR (500 MHz, DMSO-d_6): δ 7.70 (s, 2H), 7.59-7.55 (m, 2H), 7.05-7.00 (m, 8H), 6.98 (s, 2H), 6.94-6.90 (m, 8H), 6.78 (dd, 2H, J = 8.3,

2.2 Hz), 6.62-6.59 (m, 2H), 3.74 (s, 12H), 2.12-2.09 (m, 6H) ppm. ^{13}C NMR (125 MHz, DMSO-d_6): δ 171.1, 155.8, 148.4, 143.4, 143.2, 140.0, 139.4, 132.3, 126.7, 120.8, 120.6, 116.7, 116.6, 115.0, 74.0, 55.3, 20.9 ppm. HRMS (MALDI-LTQ Orbitrap) m/z: $[M^{\cdot}]^+$ Calcd for $C_{52}H_{44}N_2O_8$ 824.30922; Found: 824.30949.

5.6. Synthesis of coumarin derivatives

Synthesis of 7-(diethylamino)-4-methyl-2*H*-chromen-2-one (**207**)

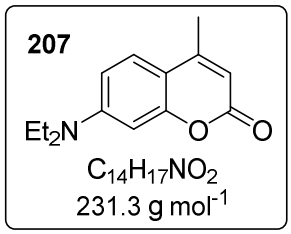

To a solution of 3-diethylaminophenol **209** (762 mg, 4.61 mmol, 1.2 eq) in 8 mL of dry toluene, ethyl acetoacetate **208** (500 mg, 3.84 mmol, 1 eq) was added, followed by 1M chlorotriisopropoxytitanium (IV) in hexanes (7.68 mL, 7.88 mmol, 1 eq) which causes precipitation. The resulting mixture was refluxed for 9h, then cooled to room temperature and stirred overnight. The mixture was quenched with half saturated Rochelle salt and filtrated through a layer of celite and sand. The filtrate was extracted with CH_2Cl_2 (3 x 30 mL), the combined organic phases was washed with brine, dried over Na_2SO_4 and concentrated in reduced pressure to give crude, oily product. It was purified by a column chromatography (SiO_2, CH_2Cl_2 to CH_2Cl_2 : acetone 19:1 + 1 % NEt_3) to give 719 mg (81%) of the product **207** as dark solid. ^{1}H NMR (300 MHz, $CDCl_3$): δ 7.37 (d, 1H, J = 8.9 Hz), 6.57 (dd, 1H, J = 8.9, 2.6 Hz), 6.48 (d, 1H, J = 2.6 Hz), 5.92 (d, 1H, J = 0.9 Hz), 3.40 (q, 4H, J = 7.1 Hz), 2.32 (d, 3H, J = 0.9 Hz), 1.20 (t, 6H, J = 7.1 Hz) ppm. ^{13}C NMR (75 MHz, $CDCl_3$): δ 162.3, 156.2, 153.0, 150.7, 125.6, 109.2, 108.9, 108.5, 97.8, 44.9, 18.5, 12.6 ppm. Carbon NMR data are in agreement with literature.[243]

Synthesis of 7-(diethylamino)-4-methyl-2*H*-chromen-2-one-4^{13}C (**207a**)

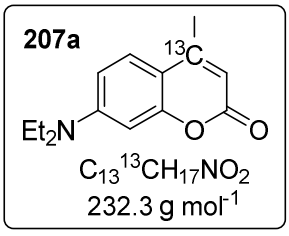

Compound was prepared from 692 mg (4.2 mmol) 3-diethylaminophenol **209** and 500 mg (3.8 mmol) ethyl acetoacetate-3-^{13}C (**208a**) following the procedure described for the synthesis of **207**. The product **207a** (555 mg, 63%) was isolated as brown solid. ^{1}H NMR (500 MHz, $CDCl_3$): δ 7.37 (dd, 1H, J = 9.0 Hz, J_{1H13C} = 3.8 Hz), 6.58 (dd, 1H, J = 9.0, 2.6 Hz), 6.49 (d, 1H, J = 2.6 Hz), 5.93 (d, 1H, J = 1.0 Hz), 3.41 (q, 4H, J = 7.1 Hz), 2.33 (dd, 3H, J_{1H13C} = 6.0 Hz, J = 1.0 Hz), 1.20 (t, 6H, J = 7.1 Hz) ppm. ^{13}C NMR (125 MHz, $CDCl_3$): δ 162.4, 156.1, 153.0 (^{13}C), 150.7, 125.6 (d, $^2J_{cc}$ = 1.4 Hz), 109.2 (d, $^1J_{cc}$ = 54.5 Hz), 108.8 (d, $^1J_{cc}$ = 63.1 Hz), 108.5 (d,

$^{3}J_{cc}$ = 4.0 Hz), 97.8 (d, $^{3}J_{cc}$ = 2.4 Hz), 44.9, 18.5 (d, $^{1}J_{cc}$ = 42.1 Hz), 12.6 ppm. HRMS (MALDI-LTQ Orbitrap) m/z: $[M+H]^+$ Calcd for $C_{13}{}^{13}CH_{18}NO_2$ 233.13656; Found 233.13719.

Synthesis of 7-(diethylamino)-4-methyl-2*H*-chromen-2-one-2^{13}C (**207b**)

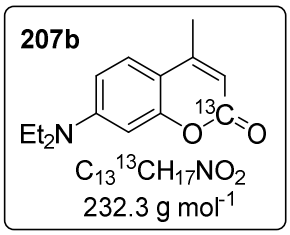

Compound was prepared from 1.13 g (6.8 mmol) 3-diethylaminophenol **209** and 750 mg (5.7 mmol) ethyl acetoacetate-1-^{13}C (**208b**) following the procedure described for the synthesis of **207**. The product **207b** (944 mg, 71%) was isolated as brown solid. ^{1}H NMR (500 MHz, $CDCl_3$): δ 7.37 (d, 1H, *J* = 9.0 Hz), 6.58 (dd, 1H, *J* = 9.0, 2.6 Hz), 6.49 (d, 1H, *J* = 2.6 Hz), 5.94 (dd, 1H, J_{1H13C} = 4.3, *J* = 1.0 Hz), 3.41 (q, 4H, *J* = 7.1 Hz), 2.33 (d, 3H, *J* = 1.0 Hz), 1.20 (t, 6H, *J* = 7.1 Hz) ppm. ^{13}C NMR (125 MHz, $CDCl_3$): δ 162.3 (^{13}C), 156.1 (d, $^{2}J_{cc}$ = 2.3 Hz), 153.0, 150.5, 125.6, 109.3, 108.7, 97.9, 45.0, 18.6 (d, $^{3}J_{cc}$ = 5.9 Hz), 12.6 ppm. HRMS (MALDI-LTQ Orbitrap) m/z: $[M+H]^+$ Calcd for $C_{13}{}^{13}CH_{18}NO_2$ 233.13656; Found 233.13701.

Synthesis of (E)-7-(diethylamino)-4-(2-(dimethylamino)vinyl)-2*H*-chromen-2-one (**211**)

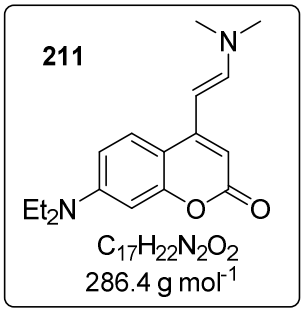

7-(diethylamino)-4-methyl-2H-chromen-2-one **207** (700 mg, 3.0 mmol, 1 eq) was mixed with 0.6 mL (6.0 mmol, 1.5 eq) *N,N*-dimethylformamide dimethyl acetal and 8 mL of dry DMF. The reaction mixture was refluxed for 10 h, then cooled to a room temperature, diluted with water and extracted with EtOAc (3 x 30 mL). The combined organic phase was washed with brine, dried over Na_2SO_4 and concentrated under reduced pressure to give oily, dark product. This was washed twice with cyclohexane and once with Et_2O to give 663 mg (76%) of a crude, solid material which was used in next step without additional purification. ^{1}H NMR (500 MHz, $CDCl_3$): δ 7.52 (d, 1H, *J* = 9.0 Hz), 7.21 (d, 1H, *J* = 13.0 Hz), 6.54 (dd, 1H, *J* = 9.0, 2.6 Hz), 6.49-6.47 (m, 1H), 5.85 (s, 1H), 5.22 (d, 1H, *J* = 13.0 Hz), 3.39 (q, 4H, *J* = 7.1 Hz), 2.99 (s, 6H), 1.19 (t, 6H, *J* = 7.1 Hz) ppm. ^{13}C NMR (125 MHz, $CDCl_3$): δ 163.6, 156.5, 152.4, 150.2, 146.7, 124.9, 108.2, 108.0, 98.2, 93.5, 87.6, 44.8, 41.0, 12.6 ppm. The NMR data are in agreement with literature.[188]

Synthesis of (E)-7-(diethylamino)-4-(2-(dimethylamino)vinyl)-2*H*-chromen-2-one-4^{13}C (**211a**)

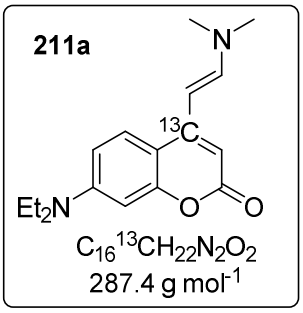

Compound was prepared from **207a** (555 mg, 2.4 mmol) following the procedure described for the synthesis of **211**. The product **211a** (618 mg, 90%) was isolated as brown solid. ^{1}H NMR (500 MHz, $CDCl_3$): δ 7.52 (dd, 1H, J = 9.0, J_{1H13C} = 3.4 Hz), 7.21 (dd, 1H, J = 13.0, J_{1H13C} = 4.0 Hz), 6.54 (dd, 1H, J = 9.0, 2.6 Hz), 6.48 (d, 1H, J = 2.6 Hz), 5.85 (s, 1H), 5.22 (d, 1H, J = 13.0 Hz), 3.39 (q, 4H, J = 7.1 Hz), 2.99 (s, 6H), 1.19 (t, 6H, J = 7.1 Hz) ppm. ^{13}C NMR (125 MHz, $CDCl_3$): δ 163.5 (d, $^2J_{cc}$ = 1.0 Hz), 156.5, 152.4 (^{13}C), 150.2, 146.6 (d, $^2J_{cc}$ = 4.2 Hz), 124.9 (d, $^2J_{cc}$ = 1.0 Hz), 108.2 (d, $^1J_{cc}$ = 54.0 Hz), 108.0 (d, $^3J_{cc}$ = 3.8 Hz), 98.2 (d, $^3J_{cc}$ = 2.4 Hz), 93.6 (d, $^1J_{cc}$ = 62.2 Hz), 87.6 (d, $^1J_{cc}$ = 61.2 Hz), 44.8, 41.0, 12.6 ppm. HRMS (MALDI-LTQ Orbitrap) m/z: $[M+H]^+$ Calcd for $C_{16}{}^{13}CH_{23}N_2O_2$ 288.17876; Found 288.17943.

Synthesis of (E)-7-(diethylamino)-4-(2-(dimethylamino)vinyl)-2*H*-chromen-2-one-2^{13}C (**211b**)

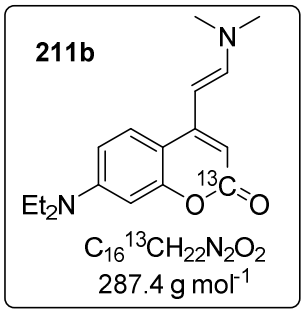

Compound was prepared from **207b** (944 mg, 4.0 mmol) following the procedure described for the synthesis of **211**. The product **211b** (850 mg, 73%) was isolated as brown solid. ^{1}H NMR (500 MHz, $CDCl_3$): δ 7.52 (d, 1H, J = 9.0 Hz), 7.21 (d, 1H, J = 13.0 Hz), 6.54 (dd, 1H, J = 9.0, 2.6 Hz), 6.48 (d, 1H, J = 2.6 Hz), 5.85 (d, 1H, J_{1H13C} = 3.3 Hz), 5.22 (d, 1H, J = 13.0 Hz), 3.39 (q, 4H, J = 7.1 Hz), 2.99 (s, 6H), 1.19 (t, 6H, J = 7.1 Hz) ppm. ^{13}C NMR (125 MHz, $CDCl_3$): δ 163.6 (^{13}C), 156.5 (d, $^2J_{cc}$ = 1.9 Hz), 152.4 (d, $^2J_{cc}$ = 1.0 Hz), 150.2, 146.7, 124.9, 108.2 (d, $^3J_{cc}$ = 6.2 Hz), 108.0, 98.2 (d, $^3J_{cc}$ = 3.1 Hz), 93.6 (d, $^1J_{cc}$ = 78.1 Hz), 87.6 (d, $^3J_{cc}$ = 5.2 Hz), 44.8, 41.0, 12.6 ppm. HRMS (MALDI-LTQ Orbitrap) m/z: $[M+H]^+$ Calcd for $C_{16}{}^{13}CH_{23}N_2O_2$ 288.17876; Found 288.17906.

Synthesis of 7-(diethylamino)-2-oxo-2*H*-chromene-4-carbaldehyde (**212**)

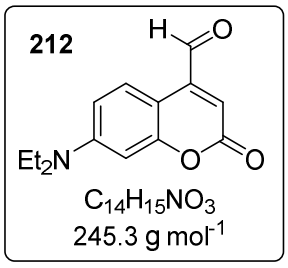

The compound **211** (663 mg, 2.31 mmol, 1 eq) was dissolved in 10 mL of H_2O and THF (1:1). To this solution $NaIO_4$ (1.48 g, 6.94 mmol, 3 eq) was added. The mixture was stirred at room temperature for two hours (color changed to deep red, small amount of a precipitate was formed). The mixture was diluted with EtOAc and H_2O, filtrated through a SiO_2 plug. The organic phase was separated, washed with brine, dried over Na_2SO_4 and concentrated under reduced pressure to yield **212** (509 mg, 90%) as dark red oil which was used in the next step

without additional purification. ^{1}H NMR (500 MHz, $CDCl_3$): δ 10.02 (s, 1H), 8.30 (d, 1H, J = 9.2 Hz), 6.62 (dd, 1H, J = 9.2, 2.6 Hz), 6.52 (d, 1H, J = 2.6 Hz), 6.45 (s, 1H), 3.43 (q, 4H, J = 7.1 Hz), 1.22 (t, 6H, J = 7.1 Hz) ppm. ^{13}C NMR (125 MHz, $CDCl_3$): δ 192.7, 162.0, 157.5, 151.1, 144.0, 127.2, 117.5, 109.6, 103.8, 97.7, 44.9, 12.6 ppm. The NMR data are in agreement with literature.[188]

Synthesis of 7-(diethylamino)-2-oxo-2*H*-chromene-4-carbaldehyde-4-^{13}C (**212a**)

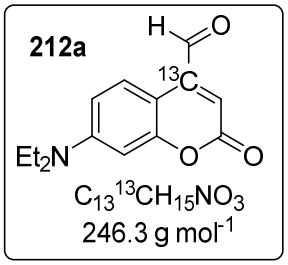

Compound was prepared from **211a** (596 mg, 2.1 mmol) following the procedure described for the synthesis of **212**. The product **212a** (510 mg, 98%; purity less than 90%) was isolated as red solid. ^{1}H NMR (500 MHz, $CDCl_3$): δ 10.03 (d, 1H, J_{1H13C} = 25.9 Hz), 8.31 (dd, 1H, J = 9.1, J_{1H13C} = 3.0 Hz), 6.63 (dd, 1H, J = 9.1, 2.6 Hz), 6.52 (d, 1H, J = 2.6 Hz), 6.45 (d, 1H, J_{1H13C} = 0.7 Hz), 3.43 (q, 4H, J = 7.1 Hz), 1.22 (t, 6H, J = 7.1 Hz) ppm. ^{13}C NMR (125 MHz, $CDCl_3$): δ 192.6 (d, $^{1}J_{cc}$ = 50.0 Hz), 162.0, 157.5, 151.1, 144.1 (^{13}C), 127.2, 117.7 (d, $^{1}J_{cc}$ = 62.8 Hz), 109.7 (d, $^{3}J_{cc}$ = 3.6 Hz), 103.8 (d, $^{1}J_{cc}$ = 58.0 Hz), 97.7 (d, $^{3}J_{cc}$ = 2.6 Hz), 44.9, 12.6 ppm. MS (ESI): m/z = 279.2 $[M + H + MeOH]^+$.

Synthesis of 7-(diethylamino)-2-oxo-2*H*-chromene-4-carbaldehyde-2-^{13}C (**212b**)

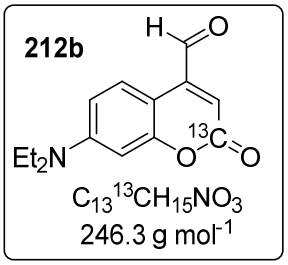

Compound was prepared from **211b** (840 mg, 2.9 mmol) following the procedure described for the synthesis of **212**. The product **212b** (676 mg, 94%) was isolated as red solid. ^{1}H NMR (300 MHz, $CDCl_3$): δ 10.03 (s, 1H), 8.30 (d, 1H, J = 9.2 Hz), 6.63 (dd, 1H, J = 9.2, 2.6 Hz), 6.52 (d, 1H, J = 2.6 Hz), 6.45 (d, 1H, J_{1H13C} = 3.2 Hz), 3.43 (q, 4H, J = 7.1 Hz), 1.22 (t, 6H, J = 7.1 Hz) ppm. ^{13}C NMR (75 MHz, $CDCl_3$): δ 192.6 (d, $^{3}J_{cc}$ = 7.7 Hz), 162.0 (^{13}C), 157.5 (d, $^{2}J_{cc}$ = 2.3 Hz), 151.2, 144.1, 127.2, 117.5 (d, $^{1}J_{cc}$ = 73.5 Hz), 109.7, 103.8 (d, $^{3}J_{cc}$ = 6.2 Hz), 97.8 (d, $^{3}J_{cc}$ = 3.2 Hz), 44.9, 12.6 ppm. MS (ESI): m/z = 279.2 $[M + H + MeOH]^+$.

Synthesis of 7-(diethylamino)-4-(hydroxymethyl)-2*H*-chromen-2-one (**206**)

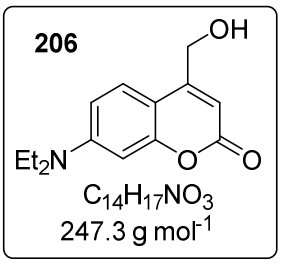

A solution of the compound **212** (508 mg, 2.1 mmol, 1 eq) in EtOH (10 mL) was cooled in an ice bath before addition of $NaBH_4$ (39 mg, 1.0 mmol, 0.5 eq). After 10 minutes the cooling bath was removed and the mixture was stirred 3 h in room temperature before it was quenched with saturated NH_4Cl solution. The mixture was extracted with CH_2Cl_2 (3 x 30 mL), combined organic phase washed with brine, dried over Na_2SO_4 and concentrated in reduced pressure to yield 530 mg of the crude product. This was purified by column chromatography (SiO_2, CH_2Cl_2 to CH_2Cl_2 : acetone 19:1 with 1 % Et_3N as an additive). The product **206** (410 mg, 80%) was obtained as yellow solid. ^{1}H NMR ($CDCl_3$, 300 MHz): δ 7.31 (d, 1H, J = 9.0 Hz), 6.55 (dd, 1H, J = 9.0, 2.6 Hz), 6.49 (d, 1H, J = 2.6 Hz), 6.26 (t, 1H, J = 1.2 Hz), 4.82 (d, 2H, J = 4.0 Hz), 3.40 (q, 4H, J = 7.1 Hz), 2.42 (t, 1H, J = 5.3 Hz), 1.19 (t, 6H, J = 7.1 Hz) ppm. ^{13}C NMR (75 MHz, $CDCl_3$): δ 162.7, 156.3, 154.8, 150.7, 124.5, 108.7, 106.5, 105.6, 97.9, 61.1, 44.9, 12.6 ppm. NMR data are in agreement with literature.[244]

Synthesis of 7-(diethylamino)-4-(hydroxymethyl)-2*H*-chromen-2-one-4-^{13}C (**206a**)

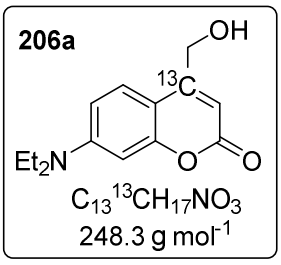

Compound was prepared from **212a** (510 mg, 2.0 mmol) following the procedure described for the synthesis of **206**. The product **206a** (430mg, 87%) was isolated as yellow-brown solid. ^{1}H NMR (400 MHz, $CDCl_3$): δ 7.32 (dd, 1H, J = 9.0, J_{1H13C} = 3.2 Hz), 6.57 (dd, 1H, J = 9.0, 2.6 Hz), 6.52 (d, 1H, J = 2.6 Hz), 6.25-6.24 (m, 1H), 4.83 (d, 2H, J = 3.8 Hz), 3.41 (q, 4H, J = 7.1 Hz), 2.6-2.4 (br s, 1H), 1.21 (t, 6H, J = 7.1 Hz) ppm. ^{13}C NMR (125 MHz, $CDCl_3$): δ 162.7, 156.3, 154.9 (^{13}C), 150.5, 124.5, 108.8, 106.5 (d, $^1J_{cc}$ = 52.5 Hz), 105.9 (d, $^1J_{cc}$ = 65.0 Hz), 98.0, 61.0 (d, $^1J_{cc}$ = 44.5 Hz), 44.9, 12.5 ppm. HRMS (MALDI-LTQ Orbitrap) m/z: $[M+H]^+$ Calcd for $C_{13}{}^{13}CH_{18}NO_3$ 249.13147; Found 249.13216.

Synthesis of 7-(diethylamino)-4-(hydroxymethyl)-2*H*-chromen-2-one-2-^{13}C (**206b**)

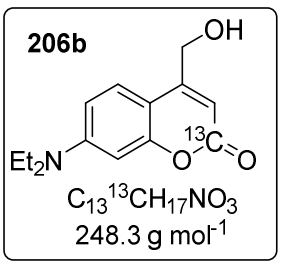

Compound was prepared from **212b** (676 mg, 2.7 mmol) following the procedure described for the synthesis of **206**. The product **206b** (537 mg, 79%) was isolated as yellow-brown solid. ^{1}H NMR (300 MHz, $CDCl_3$): δ 7.32 (d, 1H, J = 9.0 Hz), 6.56 (dd, 1H, J = 9.0, 2.6 Hz), 6.51 (d, 1H, J = 2.6 Hz), 6.25 (td, 1H, J_{1H13C} = 4.2, J = 1.3 Hz), 4.83 (s, 2H), 3.41 (q, 4H, J = 7.1 Hz), 1.9-1.8 (br s, 1H), 1.20 (t, 6H, J = 7.1 Hz) ppm. ^{13}C NMR (75

MHz, $CDCl_3$): δ 162.7 (^{13}C), 156.3 (d, $^2J_{cc}$ = 2.2 Hz), 154.8, 150.6, 124.5, 108.8, 106.5, 105.6 (d, $^1J_{cc}$ = 73.7 Hz), 98.0 (d, $^3J_{cc}$ = 3.3 Hz), 61.1 (d, $^3J_{cc}$ = 5.1 Hz), 44.9, 12.6 ppm. HRMS (MALDI-LTQ Orbitrap) m/z: $[M+H]^+$ Calcd for $C_{13}{}^{13}CH_{18}NO_3$ 249.13147; Found 249.13196.

Synthesis of 4-(azidomethyl)-7-(diethylamino)-2*H*-chromen-2-one (**203**).

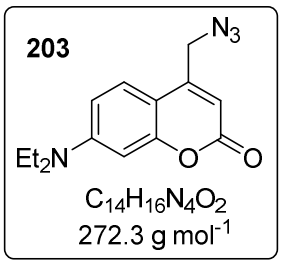

Compound **206** (725 mg, 2.9 mmol, 1 eq) was dissolved in dry CH_2Cl_2 (10 mL) and mixed with Et_3N (594 mg, 5.8 mmol, 2 eq). The solution was cooled in an ice bath before dropwise addition of methanesulfonyl chloride (504 mg, 4.4 mmol, 1.5 eq). After stirring for 1.5 h the mixture was diluted with CH_2Cl_2, washed with saturated $NaHCO_3$ solution and brine, dried over Na_2SO_4 and concentrated under reduced pressure to yield mesylated product (**213**) which had following analytical data: ^1H NMR 250 MHz, $CDCl_3$): δ 7.32 (d, 1H, *J* = 9.0 Hz), 6.60 (dd, 1H, *J* = 9.0, 2.6 Hz), 6.52 (d, 1H, *J* = 2.6 Hz), 6.18-6.15 (m, 1H), 5.29 (d, 2H, *J* = 1.0 Hz), 3.41 (q, 4H, *J* = 7.1 Hz), 3.10 (s, 3H), 1.21 (t, 6H, *J* = 7.1 Hz) ppm. One half of the crude **213** (362 mg, 1.4 mmol) was dissolved in dry DMF (7 mL), NaN_3 (381 mg, 5.8 mmol, 4 eq) was added and the mixture was stirred overnight at room temperature. Upon completion the mixture was diluted with EtOAc, extracted with half-saturated NaCl solution (3 x 30 mL), washed with brine, dried over Na_2SO_4 and concentrated under reduced pressure. The product was purified by a column chromatography (SiO_2, Cy : EtOAc 3:1) to yield 290 mg (93%) of yellow powder. ^1H NMR (500 MHz, $CDCl_3$): δ 7.32 (d, 1H, *J* = 9.0 Hz), 6.59 (dd, 1H, *J* = 9.0, 2.6 Hz), 6.51 (d, 1H, *J* = 2.6 Hz), 6.13 (t, 1H, *J* = 1.0 Hz), 4.43 (d, 2H, *J* = 1.0 Hz), 3.41 (q, 4H, *J* = 7.1 Hz), 1.21 (t, 6H, *J* = 7.1 Hz) ppm. ^{13}C NMR (125 MHz): δ 161.8, 156.6, 150.9, 148.9, 124.9, 108.8, 108.2, 106.4, 98.0, 51.0, 44.9, 12.6 ppm. HRMS (MALDI) m/z: $[M+H]^+$ Calc. for $C_{14}H_{17}N_4O_2$ 273.13460; Found 273.13457.

Synthesis of 4-(azidomethyl)-7-(diethylamino)-2*H*-chromen-2-one 4-^{13}C (**201**).

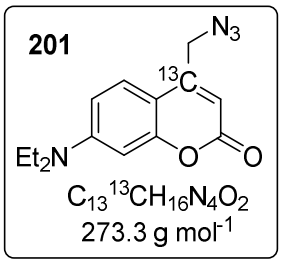

Compound was prepared from **206a** (190 mg, 0.8 mmol) following the procedure described for the synthesis of **203**. Crude, mesylated compound **213a** (239 mg) had the following analytical data: ^1H NMR (500 MHz, $CDCl_3$): δ 7.32 (dd, 1H, J = 9.0, J_{1H13C} = 3.6 Hz), 6.60 (dd, 1H, *J* = 9.0, 2.6 Hz), 6.52 (d, 1H, *J* = 2.6 Hz), 6.18-6.16 (m, 1H), 5.29 (dd, 2H, J_{1H13C} = 4.2, *J* = 1.0 Hz), 3.42 (q, 4H, *J* = 7.1 Hz), 3.10 (s, 3H), 1.21 (t, 6H, *J* = 7.1 Hz) ppm. ^{13}C NMR (75 MHz, $CDCl_3$): δ 161.5, 156.6, 151.0, 147.0 (^{13}C), 124.6, 109.0 (d, $^3J_{cc}$

= 4.0 Hz), 108.0 (d, $^{1}J_{cc}$ = 65.0 Hz), 98.0 (d, $^{2}J_{cc}$ = 2.5 Hz), 65.8 (d, $^{1}J_{cc}$ = 47.4 Hz), 44.9, 38.5, 12.6 ppm. The product **201** (170 mg, 81%) was isolated as yellow solid. ^{1}H NMR (500 MHz, $CDCl_3$): δ 7.32 (dd, 1H, *J* = 9.0, J_{1H13C} = 3.6 Hz), 6.59 (dd, 1H, *J* = 9.0, 2.6 Hz), 6.52 (d, 1H, *J* = 2.6 Hz), 6.13 (d, 1H, *J* = 0.8 Hz), 4.43 (dd, 2H, J_{1H13C} = 4.9, *J* = 0.8 Hz), 3.41 (q, 4H, *J* = 7.1 Hz), 1.21 (t, 6H, *J* = 7.1 Hz) ppm. ^{13}C NMR (125 MHz, $CDCl_3$): δ 161.8, 156.6, 150.9, 148.8 (^{13}C), 124.9 (d, $^{2}J_{cc}$ = 1.0 Hz), 108.8 (d, $^{3}J_{cc}$ = 3.9 Hz), 108.2 (d, $^{1}J_{cc}$ = 64.6 Hz), 106.4 (d, $^{1}J_{cc}$ = 56.1 Hz), 98.0 (d, $^{3}J_{cc}$ = 2.4 Hz), 51.0 (d, $^{1}J_{cc}$ = 44.7 Hz), 44.9, 12.6 ppm. HRMS (MALDI) m/z: $[M+H]^+$ Calc. for $C_{13}{}^{13}CH_{17}N_4O_2$ 274.13796; Found 274.13789.

Synthesis of 4-(azidomethyl)-7-(diethylamino)-2*H*-chromen-2-one 2-^{13}C (**202**)

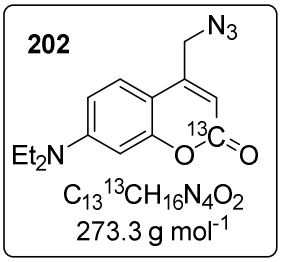

Compound was prepared from **206b** (248 mg, 1.0 mmol) following the procedure described for the synthesis of **203**. Crude, mesylated compound **213b** (366 mg) had the following analytical data: ^{1}H NMR (500 MHz, $CDCl_3$): δ 7.32 (d, 1H, *J* = 9.0 Hz), 6.60 (dd, 1H, *J* = 9.0, 2.6 Hz), 6.52 (d, 1H, *J* = 2.6 Hz), 6.17 (td, 1H, J_{1H13C} = 3.7, *J* = 1.0 Hz), 5.29 (d, 2H, *J* = 1.0 Hz), 3.42 (q, 4H, *J* = 7.1 Hz), 3.10 (s, 3H), 1.21 (t, 6H, *J* = 7.1 Hz) ppm. ^{13}C NMR (125 MHz, $CDCl_3$): δ 161.5 ($^{13}C_q$), 156.6 (d, $^{2}J_{cc}$ = 2.2 Hz), 151.0, 147.0, 124.6, 109.3, 108.0 (d, $^{1}J_{cc}$ = 74.0 Hz), 105.6 (d, $^{3}J_{cc}$ = 6.4 Hz), 98.0 (d, $^{2}J_{cc}$ = 3.2 Hz), 65.8 (d, $^{3}J_{cc}$ = 5.9 Hz), 44.9, 38.5, 12.6 ppm. The product **202** (245 mg, 90%) was isolated as yellow solid. ^{1}H NMR (500 MHz, $CDCl_3$): δ 7.32 (d, 1H, *J* = 9.0 Hz), 6.59 (dd, 1H, *J* = 9.0, 2.6 Hz), 6.52 (d, 1H, *J* = 2.6 Hz), 6.13 (td, 1H, J_{1H13C} = 3.7 Hz, *J* = 1.0 Hz), 4.43 (d, 2H, *J* = 1.0 Hz), 3.41 (q, 4H, *J* = 7.1 Hz), 1.21 (t, 6H, *J* = 7.1 Hz) ppm. ^{13}C NMR (125 MHz, $CDCl_3$): δ 161.8 (^{13}C), 156.6 (d, $^{2}J_{cc}$ = 2.2 Hz), 151.0, 148.8, 124.9, 108.8, 108.2 (d, $^{1}J_{cc}$ = 73.6 Hz), 106.4 (d, $^{3}J_{cc}$ = 6.3 Hz), 98.0 (d, $^{3}J_{cc}$ = 3.2 Hz), 51.0 (d, $^{3}J_{cc}$ = 5.7 Hz), 44.9, 12.6 ppm. HRMS (MALDI) m/z: $[M+H]^+$ Calc. for $C_{13}{}^{13}CH_{17}N_4O_2$ 274.13796; Found 274.13801.

Synthesis of 4-(thiocyanomethyl)-7-(diethylamino)-2*H*-chromen-2-one (**204**)

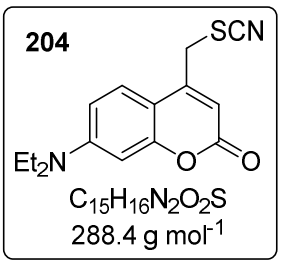

Compound was prepared as described for **203**, using the second half of the crude **213** (362 mg, 1.4 mmol) and KSCN (568 mg, 5.8 mmol, 4.0 eq). The product **204** (368 mg, 87%) was obtained as orange solid. ^{1}H NMR (500 MHz, $CDCl_3$): δ 7.32 (d, 1H, *J* = 9.0 Hz), 6.61 (dd, 1H, *J* = 9.0, 2.6 Hz), 6.53 (d, 1H, *J* = 2.6 Hz), 6.12 (s, 1H), 4.15 (s, 2H), 3.43 (q, 4H, *J* = 7.1 Hz), 1.22 (t, 6H, *J* = 7.1 Hz) ppm. ^{13}C NMR (125 MHz, $CDCl_3$): δ

161.1, 156.9, 151.2, 147.4, 124.8, 110.7, 110.2, 108.9, 105.8, 98.3, 45.0, 33.9, 12.6 ppm. HRMS (MALDI) m/z: $[M+H]^+$ Calc. for $C_{15}H_{17}N_2O_2S$ 289.10053; Found 289.10054.

5.7. Synthesis of *p*HP derivatives

Synthesis of acetophenone (**221**)

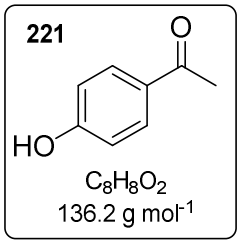

Phenol **222** (333 mg, 3.54 mmol, 1.00 eq) was dissolved in trifluoromethanesulfonic acid and cooled in ice bath. After addition of acetyl chloride (278 mg, 3.54 mmol, 1.00 eq) cooling bath was removed and the mixture was stirred in room temperature. After 5 h, one more equivalent of acetyl chloride (278 mg, 3.54 mmol) was added and 30 min later the mixture was quenched by adding EtOAc and pouring the solution on ice. The aqueous layer was extracted 3 times with EtOAc, the combined organic phase was washed with saturated $NaHCO_3$, brine, dried over Na_2SO_4 and concentrated under reduced pressure to yield off-white solid (487 mg, quantitative). ^1H (250 MHz, $CDCl_3$): δ 7.96-7.87 (m, 2H), 6.96-6.88 (m, 2H), 6.8-6.6 (br s, 1H), 2.57 (s, 3H) ppm. The NMR data are in agreement with the commercially available standard substance.

Synthesis of acetophenone-1-^{13}C (**248**)

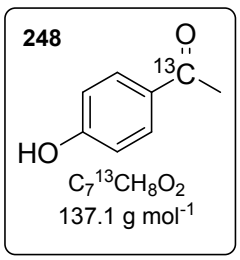

Synthesis was done as described for acetophenone **221**. From phenol **222** (1.30 g, 13.8 mmol, 1.1 eq) and acetyl chloride-1-^{13}C **226** (1.0 g, 12.6 mmol, 1.0 eq) quantitative yield of the product was obtained (1.98 g). ^1H (400 MHz, $CDCl_3$): δ 7.94-7.88 (m, 2H), 6.92-6.86 (m, 2H), 5.69 (s, 1H), 2.57 (s, 3H, J_{1H13C} = 5.8 Hz) ppm. ^{13}C (75 MHz, $CDCl_3$): δ 197.3 (^{13}C), 160.3, 131.1 (d, ^2Jcc = 3.3 Hz), 130.6 (d, $^1J_{cc}$ = 55.0 Hz), 115.4 (d, $^3J_{cc}$ = 4.3 Hz), 26.5 (d, $^1J_{CC}$ = 42.7 Hz) ppm. MS (ESI): m/z = 138.1 $[M + H]^+$.

The optimization of the 4-hydroxyacetophenone halogenation

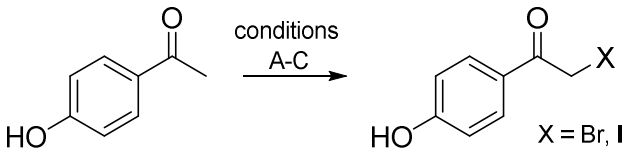

A) 4-hydroxyacetophenone **221** (481 mg, 3.5 mmol, 1.00 eq) was dissolved in 10 mL of dry Et_2O and Br_2 was added dropwise to this mixture (160 mg, 3.5 mmol, 1.00 eq). The reaction happens

immediately (within 1 min). The mixture was quenched with H_2O and Et_2O, extracted with $Na_2S_2O_3$ solution. The organic phase was washed with brine, dried over Na_2SO_4 and concentrated under reduced pressure to give the pink crude product (803 mg). This was analyzed by NMR. In a mixture of four products the desired 2-bromo-4'-hydroxyacetophenone **220** could be detected along with the 2,2-dibromo-4'-hydroxyacetophenone **223** and two unidentified side products in a ratio 1.00 : 0.51 : 0.37 : 0.15. No further purification was done.

B) 4-hydroxyacetophenone **221** (1.00 g, 7.3 mmol, 1.00 eq) was dissolved in 10 mL of dry MeOH. To this mixture, I_2 (2.24 g, 8.82 mmol, 1.20 eq) together with CuO (697 mg, 8.82 mmol, 1.20 eq) was added. After stirring at room temperature for 5 min the reaction was refluxed for 8 h (under argon atmosphere). As the starting material (acetophenone) was consumed (determined by ^{1}H NMR), the reaction mixture was diluted with EtOAc and filtrated through celite. The filtrate was washed with $Na_2S_2O_3$ solution, brine, dried over Na_2SO_4 and concentrated under reduced pressure. Purification was done by a column chromatography (SiO_2, CH_2Cl_2 to CH_2Cl_2 + 3% MeOH) and an analytical sample of the desired 2-iodo-4'-hydroxyacetophenone could be isolated. ^{1}H (300 MHz, DMSO-d_6): δ 10.51 (s, 1H), 7.92-7.85 (m, 2H), 6.88-6.81 (m, 2H), 4.47 (s, 2H) ppm. Estimated yield is around 40-50% (calculating from the crude reaction products ^{1}H NMR spectra). Also this compound is unstable in DMSO producing the same side product as the brominated analogue.

C) These conditions were the best for preparation of <u>2-bromo-4'-hydroxyacetophenone (**220**)</u>

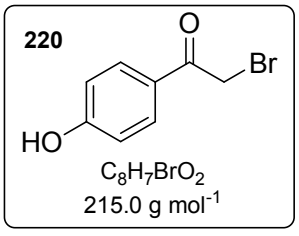

In a round bottom flask, equipped with a reflux condenser and $CaCl_2$ drying tube, 4-hydroxyacetophenone **221** (2.00 g, 14.7 mmol, 1.00 eq) was dissolved in 80 mL of EtOAc and $CHCl_3$ (1:1). Then copper (II) bromide (6.73 g, 30.1 mmol, 2.05 eq) was added and the mixture refluxed for 9 h (however no further change of the reaction mixtures composition was observed already after 1 h of refluxing). The green colored reaction mixture's was filtrated through celite and the solvents were removed under reduced pressure. The dark green crude material was purified by column chromatography (SiO_2, Cy : EtOAc 3:1) to give two fractions, both of which contains the expected product. The mass of the first fraction was 2.07 g and it contains the 2,2-dibromo-4'-hydroxyacetophenone **223** (9%) as side product. The mass of the second fraction was 790 mg and it contain 22% of the starting material. The estimated mass of the desired product from both fractions is 2.45 g (78%). ^{1}H (300 MHz, DMSO-d_6): δ 10.54 (s, 1H),

7.92-7.85 (m, 2H), 6.89-6.84 (m, 2H), 4.78 (s, 2H) ppm. The NMR spectrum is identical to the commercially available compound. The compound is unstable in DMSO (see Figure 127).

Synthesis of 2-bromo-4'-hydroxyacetophenone-1-^{13}C (**227**)

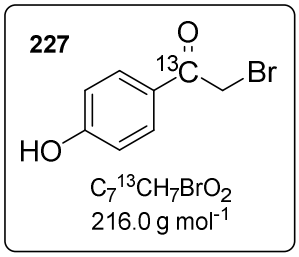

Synthesis was done as described in the optimization of the reaction conditions for synthesis of 2-bromo-4'-hydroxyacetophenone by halogenation of 4-hydroxyacetophenone (conditions C). For synthesis 4-hydroxyacetophenone-1-^{13}C **248** (1.72 g, 12.1 mmol, 1.00 eq) and $CuBr_2$ (5.57 g, 24.9 mmol, 2.05 eq) were used. After purification, three fractions were obtained. The first fraction (277 mg) contains 2,2-dibromo-4'-hydroxyacetophenone-1-^{13}C. ^{1}H (500 MHz, DMSO-d_6): δ 10.77 (s, 1H), 7.99-7.95 (m, 2H), 7.78 (s, 1H), 6.91-6.88 (m, 2H) ppm. ^{13}C (125 MHz, DMSO-d_6): δ 185.2 (^{13}C), 163.4 (d, $^4J_{cc}$ = 0.7 Hz), 123.3 (d, $^2J_{cc}$ = 3.2 Hz), 121.6 (d, $^1J_{cc}$ = 61.4 Hz), 115.8 (d, $^3J_{cc}$ = 4.5 Hz), 43.3 (d, $^1J_{cc}$ = 41.7 Hz) ppm. The second fraction (2.14 g) contains the desired 2-bromo-4'-hydroxyacetophenone-1-^{13}C **227** along with 2,2-dibromo-4'-hydroxyacetophenone and 4'-hydroxyacetophenone **248** (ratio 1.00 : 0.08 : 0.06). The analytical data of 2-bromo-4'-hydroxyacetophenone are as follows: ^{1}H (500 MHz, DMSO-d_6): δ 10.54 (s, 1H), 7.91-7.86 (m, 2H), 6.89-6.84 (m, 2H), 4.78 (d, 2H, J_{1H13C} = 3.4 Hz) ppm. ^{13}C (125 MHz, DMSO-d_6): δ 190.4 (^{13}C), 163.1, 131.9 (d, $^2J_{cc}$ = 3.3 Hz), 125.8 (d, $^1J_{cc}$ = 58.2 Hz), 115.9 (d, $^3J_{cc}$ = 4.5 Hz), 34.0 (d, $^1J_{cc}$ = 42.8 Hz) ppm. The third fraction (249 mg) contains the desired product and starting material (ratio 1 : 0.75). The combined mass from first and second fractions of the side product 2,2-dibromo-4'-hydroxyacetophenone-1-^{13}C is 520 mg (15%), the combined mass from the second and third fraction of the product is 1.95 g (75%).

Synthesis of 2-bromo-4'-hydroxyacetophenone **220** by Friedel-Crafts acylation of phenol

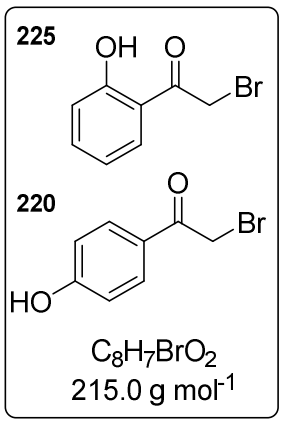

Synthesis was done as described for **221** using phenol (1.0 g, 10.6 mmol, 1.00 eq) and bromoacetyl chloride **224** (1.67 g, 10.6 mmol, 1.00 eq). Purification was done by column chromatography (SiO_2, Cy : EtOAc 3:1 to 1:1 to 1:2) and two fractions were collected. First fraction was the *ortho* isomer **225** (170 mg, 7%). ^{1}H (500 MHz, $CDCl_3$): δ 11.74 (s, 1H), 7.75 (dd, 1H, J = 8.0, 1.5 Hz), 7.56-7.49 (m, 1H), 7.03 (dd, 1H, J = 8.5, 0.8 Hz), 6.98-6.91 (m, 1H), 4.45 (s, 2H) ppm. The NMR spectra are in agreement with literature.[245] Second fraction was the expected product

220 (1.49 g, 66%). ^{1}H (500 MHz, $CDCl_3$): δ 7.97-7.91 (m, 1H), 6.93-6.88 (m, 2H), 5.62 (s, 1H), 4.40 (s, 2H) ppm. ^{1}H NMR spectra of the second fraction is identical to the commercially available compound which was used to measure carbon NMR spectra: ^{13}C (125 MHz, $CDCl_3$): δ 190.2, 160.7, 131.9, 127.4, 115.8, 30.8 ppm. The spectra in DMSO-d_6 is identical with the sample obtained by bromination of 4-hydroxyacetophenone.

Synthesis of 2-bromo-4'-hydroxyacetophenone by Friedel-Crafts acylation of phenol-$^{13}C_6$

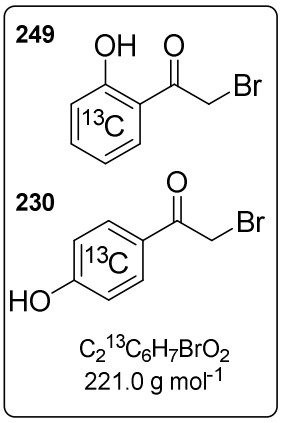

Synthesis was done as described for ^{13}C not labeled compound **220**, using phenol-$^{13}C_6$ **229** (235 mg, 2.35 mmol, 1.00 eq) and bromoacetyl chloride **224** (388 mg, 2.46 mmol, 1.05 eq). The purification was done with a modified procedure. The reaction was quenched by pouring it in ice water, then filtrated. The white solid on the filter was washed with cyclohexane (which predominantly dissolves side product). The aqueous layer was washed 2 x with cyclohexane and combined with cyclohexane from washing of the solid product on the filter. The aqueous layer was washed also 2 x with ethyl acetate. The white residue on filter was dissolved in ethyl acetate, and combined with the ethyl acetate from extraction. From this point each solvent was treated separately. They were washed with saturated $NaHCO_3$, two times with brine, dried over Na_2SO_4 and the solvent was removed under reduced pressure. From cyclohexane extraction 68 mg of crude material was obtained, which was practically pure side product **249** (13%). From ethyl acetate layer 344 mg of crude material was obtained, which was practically pure product **230** (66%). However, to obtain an analytically pure sample, column chromatography was used (SiO_2, eluent for product **249** Cy : EtOAc 5:1, eluent for product **230** Cy : EtoAC 3:1). The NMR sample was prepared directly before measurement to avoid spectra contaminations by signals resulting from the compound degradation in the NMR solvent.

Compound **249**: ^{1}H (500 MHz, $CDCl_3$): δ 11.76-11.71 (m, 1H), 7.95-7.87 (m, 0.5H), 7.73-7.64 (m, 0.5H), 7.63-7.55 (m, 0.5H), 7.41-7.32 (m, 0.5H), 7.22-7.15 (m, 0.5H), 7.15-7.07 (m, 0.5H), 6.90-6.83 (m, 0.5H), 6.82-6.73 (m, 0.5H), 4.45 (s, 2H) ppm. ^{13}C (125 MHz, $CDCl_3$): δ 197.4-196.8 (m), 163.9-162.7 (m, ^{13}C), 138.2-136.9 (m, ^{13}C), 131.1-129.9 (m, ^{13}C), 120.0-118.4 (m, ^{13}C), 117.7-116.5 (m, ^{13}C), 30.0 (d, $^{3}J_{CC}$ = 13.7 Hz) ppm.

Compound **230**: ^{1}H (500 MHz, $CDCl_3$): δ 8.13-8.06 (m, 1H), 7.81-7.74 (m, 1H), 7.10-7.03 (m, 1H), 6.78-6.71 (m, 1H), 5.40-5.34 (m, 1H), 4.39 (s, 2H) ppm. ^{13}C (125 MHz, $CDCl_3$): δ 191.0-

188.7 (m), 161.2-160.0 (m, ^{13}C), 132.4-131.3 (m, ^{13}C), 127.9-126.8 (m, ^{13}C), 116.3-115.2 (m, ^{13}C), 30.8 (d, $^{3}J_{CC}$ = 17.1 Hz) ppm.

Compound **230**: ^{1}H (500 MHz, DMSO-d_6): δ 10.55-10.51 (m, 1H), 8.08-8.00 (m, 1H), 7.76-7.68 (m, 1H), 7.06-6.99 (m, 1H), 6.73-6.67 (m, 1H), 4.78 (s, 2H) ppm. ^{13}C (125 MHz, DMSO-d_6): δ 190.3-189.6 (m), 163.2-162.0 (m, ^{13}C), 132.0-130.9 (m, ^{13}C), 125.9-124.8 (m, ^{13}C), 116.0-114.8 (m, ^{13}C), 33.6 (d, $^{3}J_{CC}$ = 17.7 Hz) ppm.

Synthesis of 2-hydroxy-4'-hydroxyacetophenone (**23**)

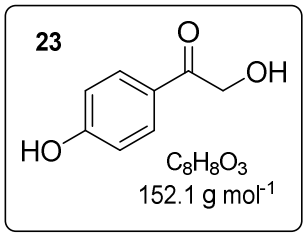

2-bromo-4´-hydroxyacetophenone **220** (428 mg, 2.00 mmol, 1.00 eq) and HCO_2Na (2.04 g, 30.00 mmol, 15.00 eq) were dissolved in a mixture of EtOH and H_2O (2 mL, 2:1) and stirred at room temperature for 96 h. The mixture was diluted with EtOAc and water, the organic phase separated, aqueous phase extracted with EtOAc. The combined organic phase was washed with brine, dried over Na_2SO_4 and the solvent was removed under reduced pressure. The crude product (289 mg) was crystalized from EtOAc/Cy. Product **23** (150 mg, 49%) was obtained as off white solid. ^{1}H (500 MHz, DMSO-d_6): δ 10.37 (s, 1H), 7.83-7.78 (m, 2H), 6.87-6.82 (m, 2H), 4.87 (t, 1H, J = 5.8 Hz), 4.69 (d, 2H, J = 5.8 Hz) ppm. ^{13}C (125 MHz, DMSO-d_6): δ 197.1, 162.2, 130.1, 126.0, 115.3, 64.8 ppm.

Synthesis of 2-formyl-4'-hydroxyacetophenone (**219**)

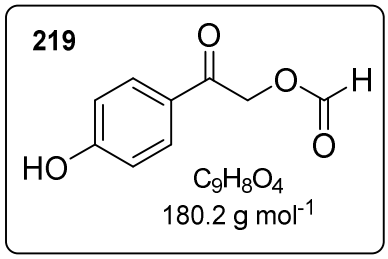

2-hydroxy-4´-hydroxyacetophenone **223** (100 mg, 0.66 mmol, 1.0 eq) was mixed with EDC-HCl (138 mg, 0.72 mmol, 1.1 eq), DMAP (7.3 mg, 0.06 mmol, 0.1 eq) and suspended in dry THF (3 mL). The mixture was cooled in ice bath before addition of formic acid (33.1 mg 0.72 mmol, 1.1 eq). After 5 min the cooling bath was removed and the mixture was stirred for two hours in room temperature. Upon completion the mixture was diluted with EtOAc and water, the organic phase was separated and the aqueous phase extracted with EtOAc. The combined organic phase was extracted twice with 0.1M AcOH, twice with brine, dried over Na_2SO_4 and the solvent was removed under reduced pressure. The crude compound was crystalized from ethyl acetate. ^{1}H (500 MHz, DMSO-d_6): δ 10.51 (s, 1H), 8.40 (s, 1H), 7.87-7.83 (m, 2H), 6.89-6.86 (m, 2H), 5.48 (s, 2H) ppm. ^{13}C (125 MHz, DMSO-d_6): δ 190.2, 162.7, 161.7, 130.4, 125.3, 115.5, 65.6 ppm. MS (ESI): m/z = 179.0 $[M - H]^-$.

Synthesis of 2-azido-4'-hydroxyacetophenone (**217**)

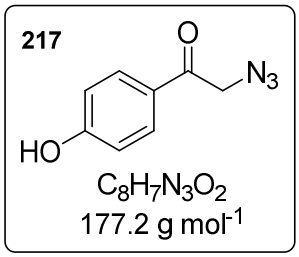

2-bromo-4´-hydroxyacetophenone **220** (428 mg, 2.00 mmol, 1.00 eq) and NaN_3 (260 mg, 4.00 mmol, 2.00 eq) were dissolved in a mixture of EtOH and H_2O (2 mL, 2:1) and stirred at room temperature overnight. The mixture was poured on ice and filtrated to give 253 mg (71%) of the product **217** as white solid. ^{1}H (500 MHz, DMSO-d_6): δ 10.50 (s, 1H), 7.84-7.80 (m, 2H), 6.89-6.85 (m, 2H), 4.76 (s, 2H) ppm. ^{13}C (125 MHz, DMSO-d_6): δ 192.4, 162.7, 130.6, 125.8, 115.4, 54.2 ppm. HRMS (MALDI) m/z: $[M+Na]^+$ Calc. for $C_8H_7N_3NaO_2$ 200.04305; Found 200.04336.

Synthesis of 2-thiocyano-4'-hydroxyacetophenone (**218**)

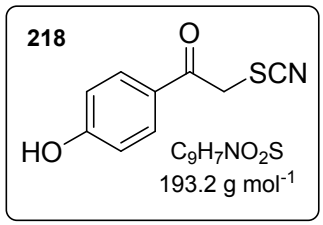

2-bromo-4´-hydroxyacetophenone **220** (428 mg, 2.00 mmol, 1.00 eq) and NH_4SCN (304 mg, 4.00 mmol, 2.00 eq) were dissolved in a mixture of EtOH and H_2O (2 mL, 2:1) and stirred at room temperature overnight. The mixture was poured on ice and filtrated to give 344 mg (89%) of the product as white solid. ^{1}H (500 MHz, $CDCl_3$): δ 7.90-7.87 (m, 2H), 6.95-6.91 (m, 2H), 5.47 (s, 1H), 4.70 (s, 2H) ppm. NMR spectra is in agreement with literature.[246] ^{1}H (500 MHz, DMSO-d_6): δ 10.61 (s, 1H), 7.91-7.87 (m, 2H), 6.90-6.86 (m, 2H), 5.02 (s, 2H) ppm. ^{13}C (125 MHz, DMSO-d_6): δ 190.3, 163.1, 131.4, 125.8, 115.5, 113.1, 41.7 ppm. HRMS (MALDI) m/z: $[M+H]^+$ Calc. for $C_9H_8N_1O_2S_1$ 194.02703; Found 194.02690.

Synthesis of 2-thiocyano-4'-hydroxyacetophenone-1-^{13}C (**228**)

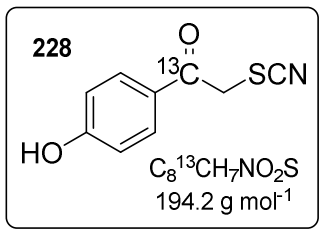

Synthesis was done from bromide **227** (900 mg, 4.19 mmol) and NH_4SCN (637 mg, 8.38 mmol) following the procedure as described for **218**. The crude product (761 mg) was crystalized from EtOAC/Cy to give 445 mg (54%) of pure **228**. ^{1}H (500 MHz, DMSO-d_6): δ 10.61 (s, 1H), 7.91-7.86 (m, 2H), 6.90-6.86 (m, 2H), 5.02 (d, 1H, J_{1H13C} = 4.3 Hz) ppm. ^{13}C (125 MHz, DMSO-d_6): δ 190.3 (^{13}C), 163.1, 131.4 (d, $^2J_{CC}$ = 3.4 Hz), 125.8 (d, $^1J_{CC}$ = 58.6 Hz), 115.5 (d, $^3J_{CC}$ = 4.5 Hz), 113.1 (d, $^3J_{CC}$ = 2.6 Hz), 41.7 (d, $^2J_{CC}$ = 39.9 Hz) ppm. HRMS (MALDI) m/z: $[M+H]^+$ Calc. for $C_8{}^{13}C_1H_8N_1O_2S_1$ 195.03038; Found 195.03008.

Synthesis of 2-thiocyano(-^{13}C)-4'-hydroxyacetophenone-1 (**231**)

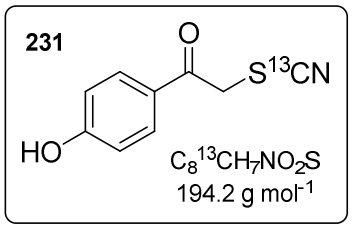

Synthesis was done as described for **218**, using 2-bromo-4´-hydroxyacetophenone **220** (571 mg, 2.67 mmol, 1.05 eq) and KS^{13}CN (250 mg, 2.54 mmol, 1.00 eq). The crude product (538 mg) was crystalized from EtOAc/Cy to give 317 mg (64%) of pure product. ^{1}H (500 MHz, DMSO-d_6): δ 10.61 (s, 1H), 7.91-7.86 (m, 2H), 6.90-6.86 (m, 2H), 5.02 (d, 1H, J_{1H13C} = 4.6 Hz) ppm. ^{13}C (125 MHz, DMSO-d_6): δ 190.3 (d, $^{3}J_{CC}$ = 2.6 Hz), 163.1, 131.4, 125.8, 115.5, 113.1 (^{13}C), 41.7 ppm. HRMS (MALDI) m/z: $[M+H]^+$ Calc. for $C_8{}^{13}C_1H_8N_1O_2S_1$ 195.03038; Found 195.03006.

Synthesis of 2-thiocyano-4'-hydroxyacetophenone-$^{13}C_6$ (**230**)

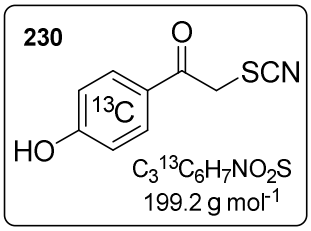

Synthesis was done from bromide **230** (190 mg, 0.86 mmol) and NH_4SCN (131 mg, 1.72 mmol) following the procedure as described for **218**. The crude product was crystalized from EtOAC/Cy to give 101 mg of product, the filtrate was purified by column chromatography (SiO_2, Cy:EtOAc 3:1) to give 58 mg of the product. The combined mass of the product **230** was 159 mg (93%). ^{1}H (500 MHz, DMSO-d_6): δ 10.63-10.58 (m, 1H), 8.08-8.00 (m, 1H), 7.76-7.69 (m, 1H), 7.08-7.00 (m, 1H), 6.76-6.68 (m, 1H), 5.02 (s, 2H) ppm. ^{13}C (125 MHz, DMSO-d_6): δ 190.6-186.9 (m), 163.6-162.5 (m, ^{13}C), 131.9-130.8 (m, ^{13}C), 126.2-125.2 (m, ^{13}C), 116.0-114.9 (m, ^{13}C), 113.0, 41.7 (d, $^{2}J_{CC}$ = 16.6 Hz) ppm. HRMS (MALDI) m/z: $[M+H]^+$ Calc. for $C_3{}^{13}C_6H_7N_1O_2S_1$ 200.04715; Found 200.04718.

6. Appendix

6.1. Supplementary figures

Figure 143, Figure 144 and Figure 149 (with modifications) and Figure 146 - Figure 148 are reprinted from M. Reinfelds, J. von Cosel, K. Falahati, C. Hamerla, T. Slanina, I. Burghardt, A. Heckel, A New Photocage Derived from Fluorene, *Chem. Eur. J.* **2018**, 24 (doi: 10.1002/chem.201802390) with permission; Copyright 2018 Wiley-VCH Verlag GmbH & Co. KGaA, Weinheim.

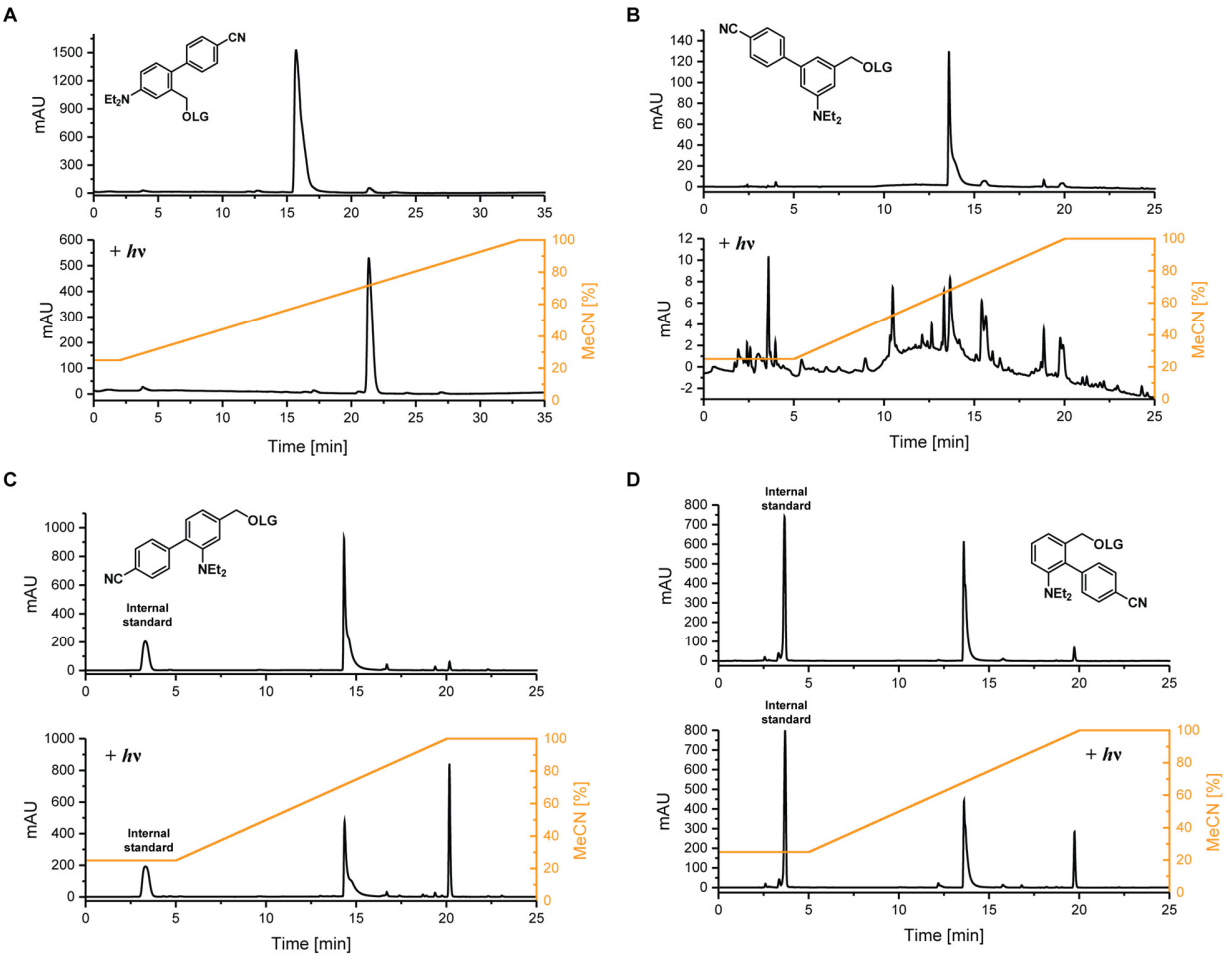

Figure 143: The HPLC analysis of compounds **132** (panel A), **139** (panel B), **142** (panel C), **145** (panel D) before and after irradiation (at 365 nm).

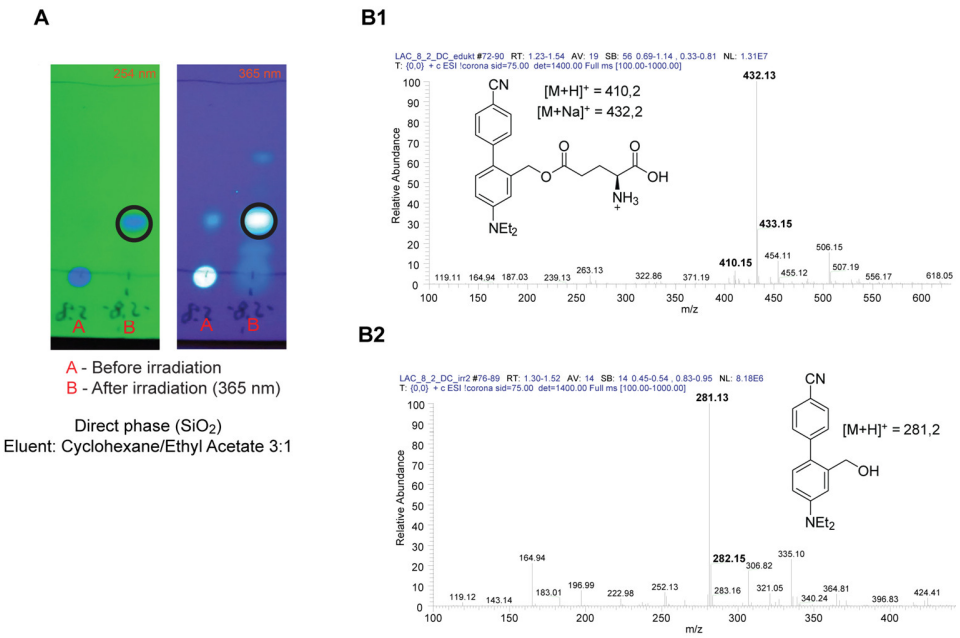

Figure 144: Mass spectral analysis of the irradiation reaction of the compound **132**.

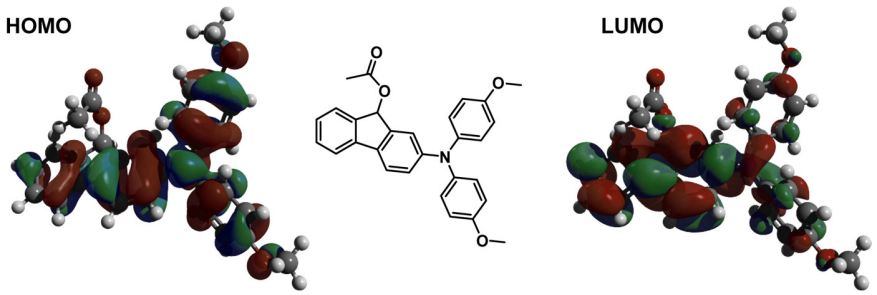

Figure 145: Frontier molecular orbitals of compound **174b** as obtained at the TD-PBE0/Def2-TZVP level of theory. Figure produced in a collaboration with Jan von Cosel, Konstantin Falahati, Carsten Hamerla (group of Irene Burghardt).

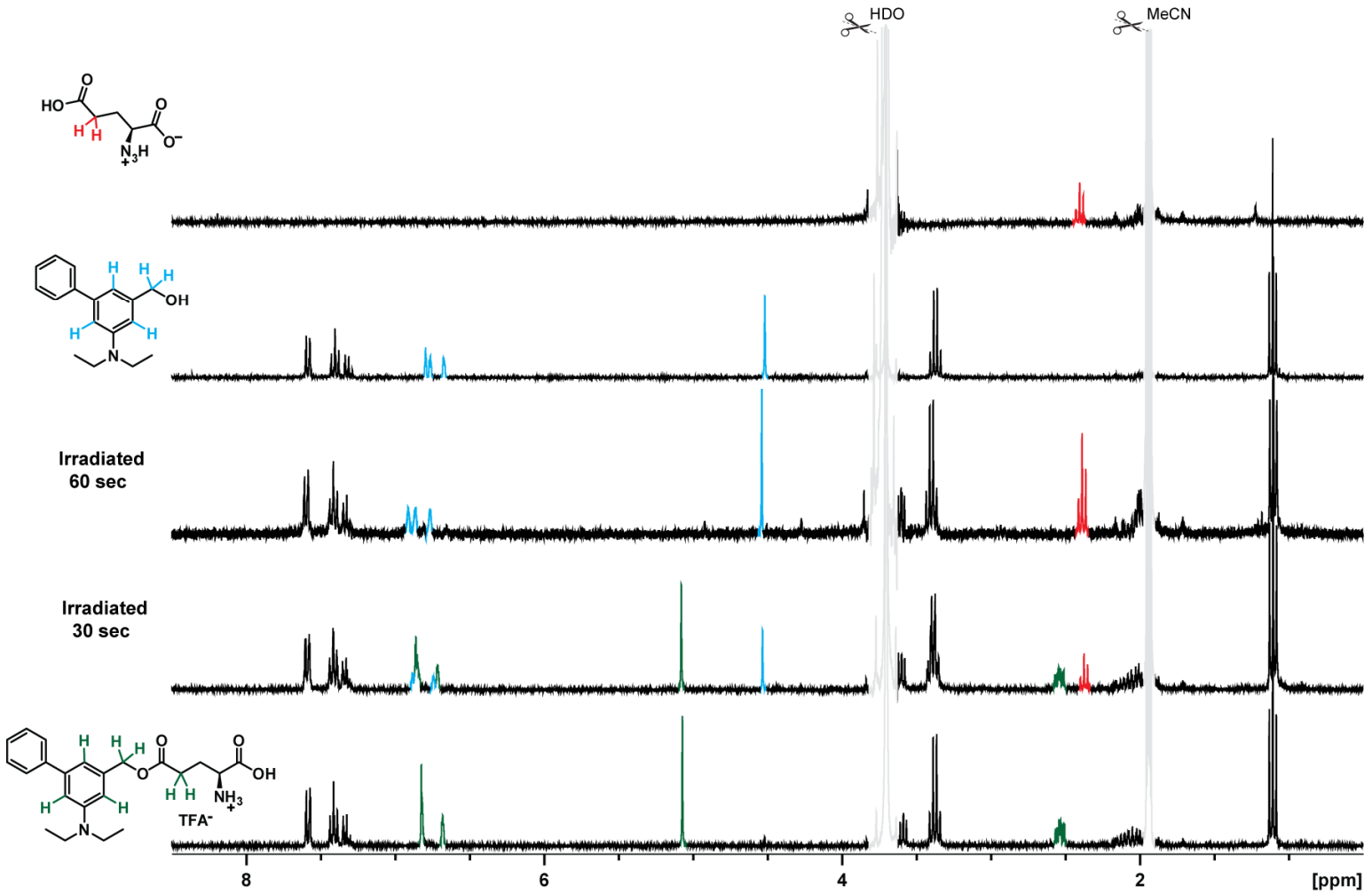

Figure 146: ^{1}H NMR (300 MHz) spectra before and after irradiation of **148** (ca. 10 mM). For comparison, the spectra of the expected photoproducts are shown. All samples were prepared in MeCN-d_3 + D_2O (20% v/v) and did not contain any buffer. The irradiation power (LED 365 nm) was close to 165 µW, volume – ca. 600 µL. For clarity, the signals of D_2O and MeCN-d_3 are covered by a semitransparent mask.

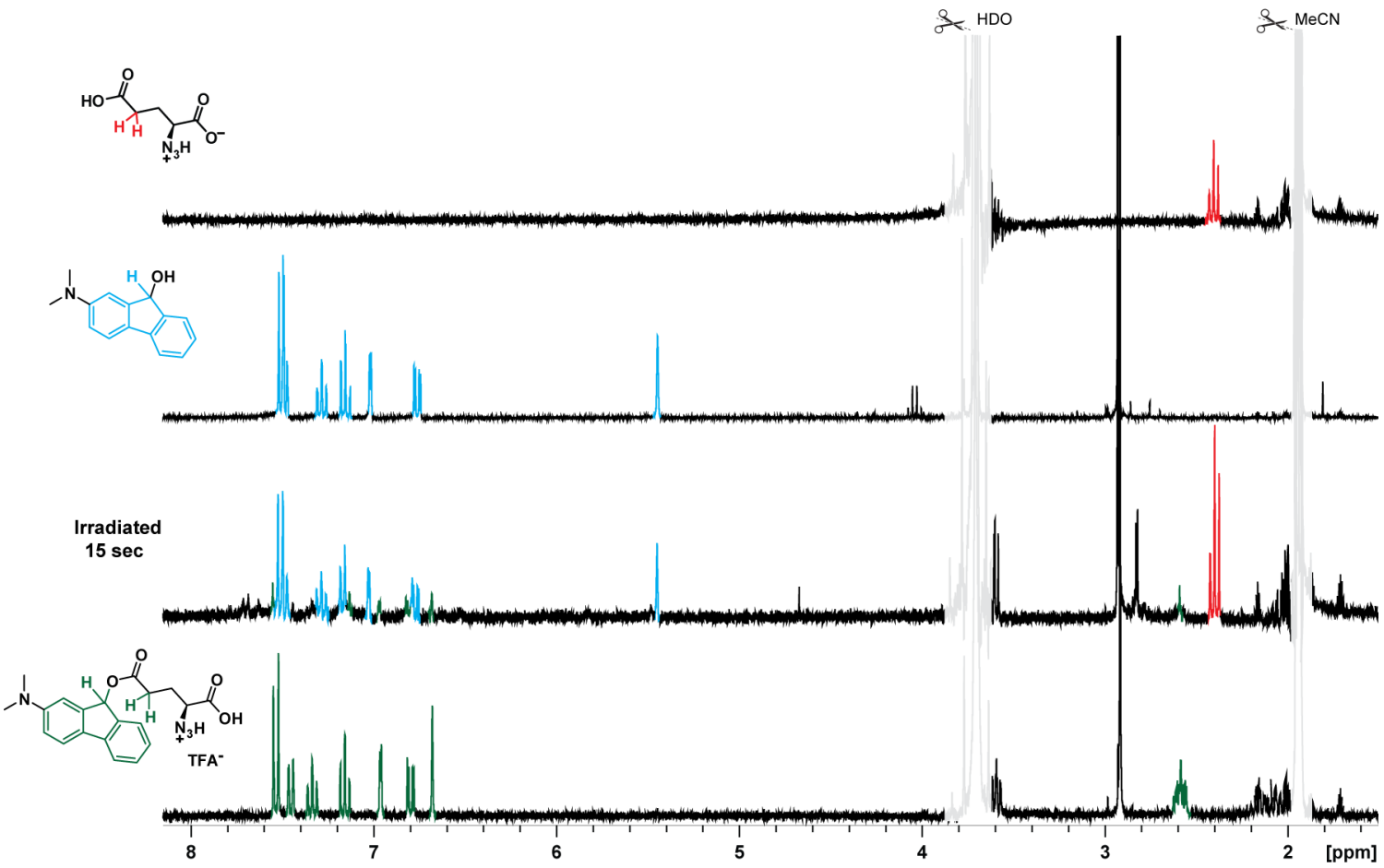

Figure 147: ^{1}H NMR (300 MHz) spectra before and after irradiation of **167** (ca. 4 mM). For comparison, the spectra of the expected photoproducts are shown. All samples were prepared in MeCN-d_3 + D_2O (20 D_2O (20% v/v) and did not contain any buffer. The irradiation power (LED 365 nm) was close to 165 µW, volume – ca. 600 µL. For clarity, the signals of D_2O and MeCN-d_3 are covered by a semitransparent mask.

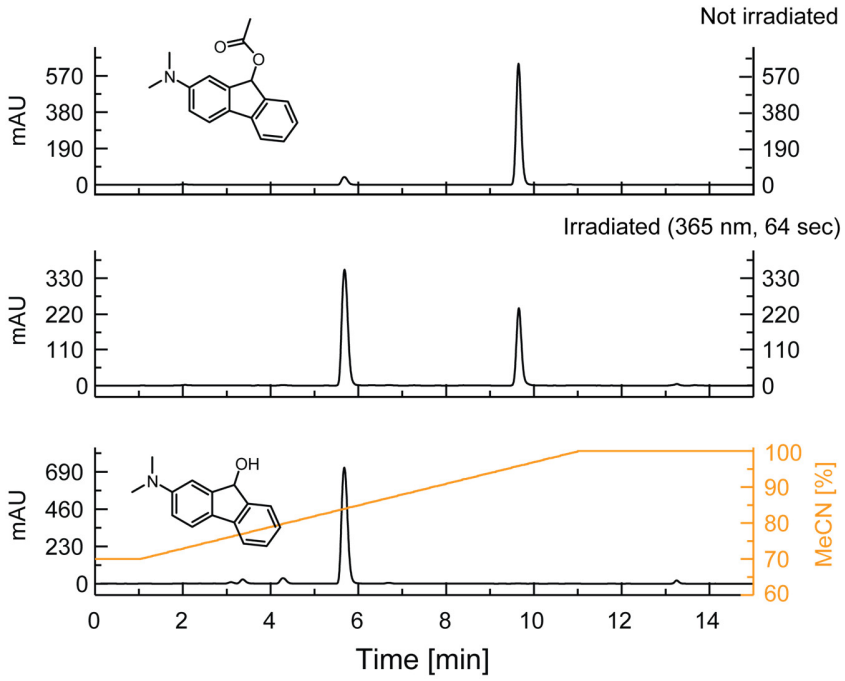

Figure 148: HPLC (traces at 310 nm) before and after irradiation (64 sec) of the fluorenol acetate **168** and comparison to expected photoproduct **165**. The irradiation power (LED 365 nm) was ca. 20 µW, solution absorbance ca. 0.07, volume - 1.5 mL and concentration ca. 0.05 mM.

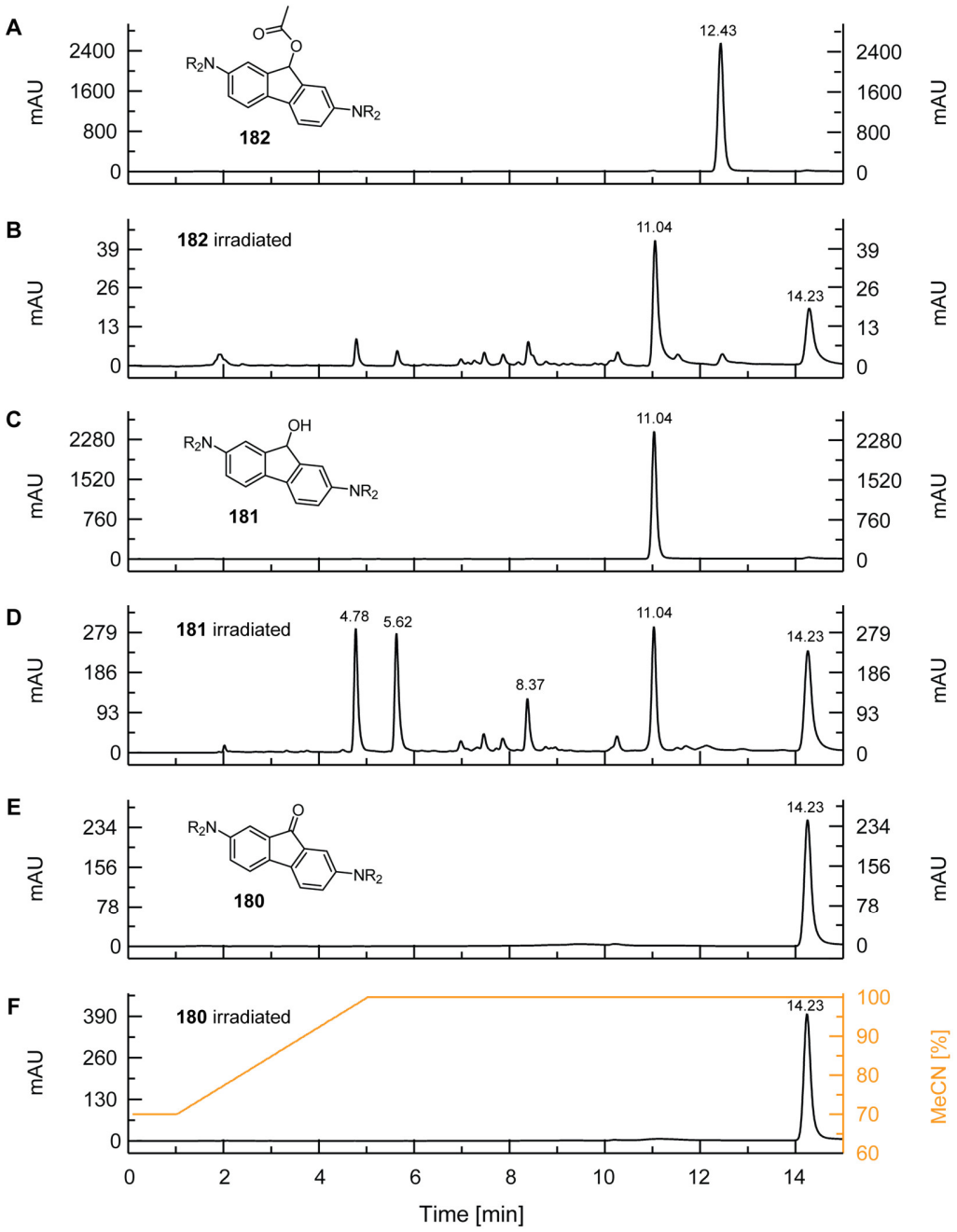

Figure 149: The HPLC analysis for the irradiation of the compound **182**, photoproduct comparison with synthetic standards, photo stability of the primary photoproducts. Irradiation was done at 365 nm, samples prepared in MeCN (with 10% of 0.1M TEAA buffer).

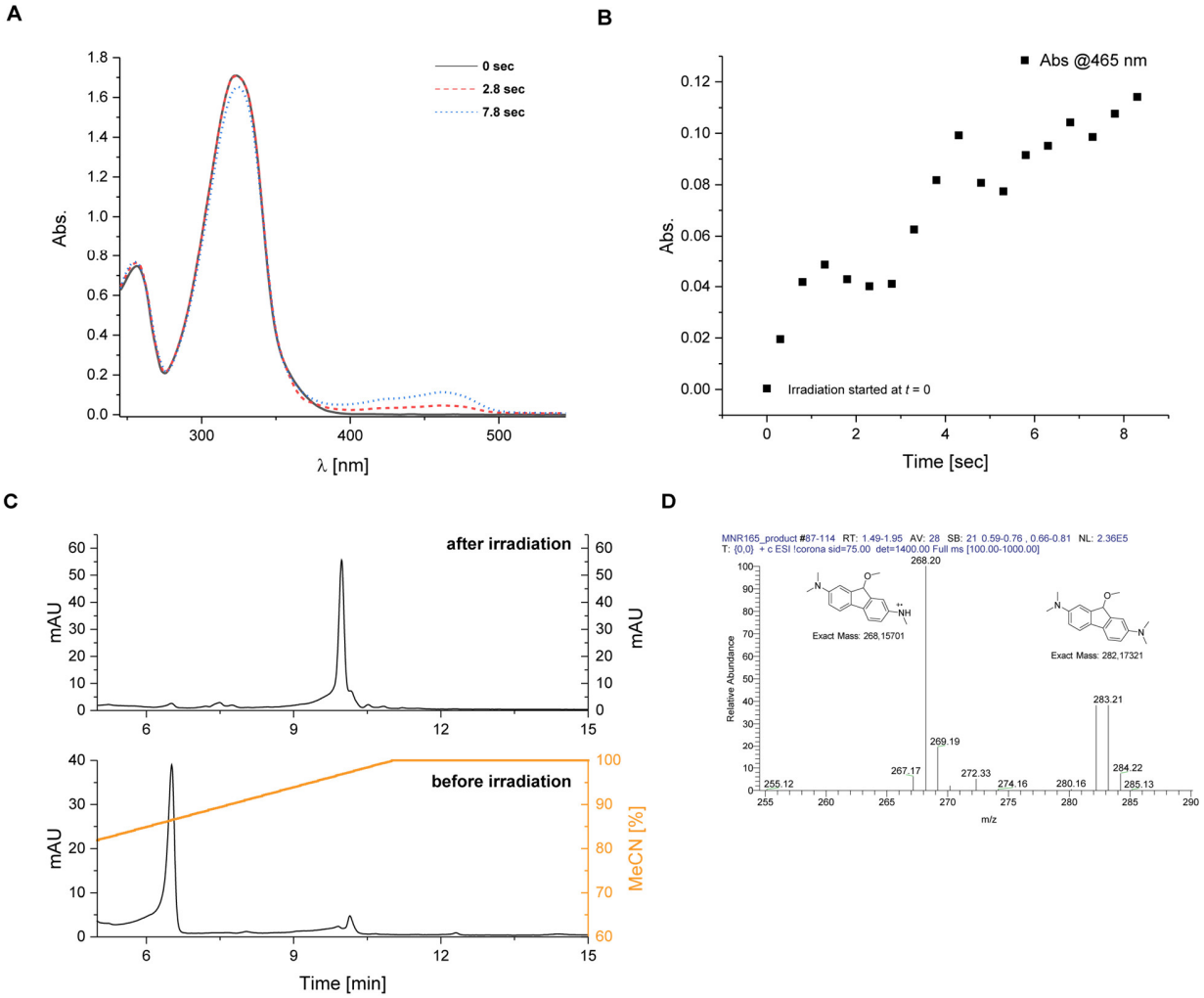

Figure 150: *A* – UV-Vis absorption spectra of the compound **177** before and during irradiation (at 365 nm). *B* – The change of absorption intensity at 465 nm upon irradiation of compound **177** at 365 nm; *C* – The HPLC analysis of the compound **177** before and after irradiation; *D* – ESI-MS analysis of the irradiation product (collected after HPLC analysis shown in the panel C).

6.2. NMR spectra

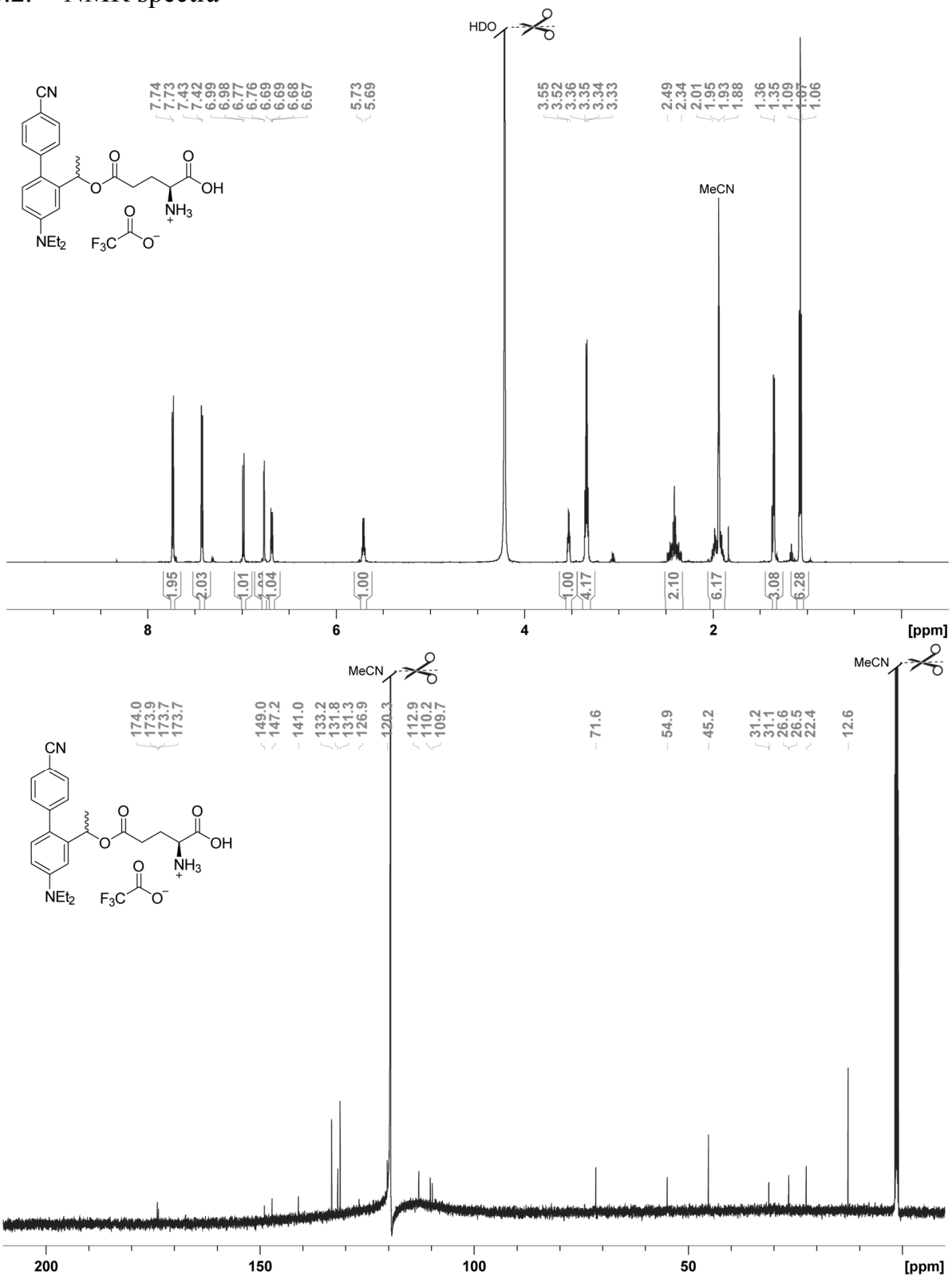

Figure 151: ^{1}H (600 MHz, MeCN-d_3 + D_2O) (upper) and ^{13}C (150 MHz, MeCN-d_3 + D_2O) (lower) NMR spectra of **137**.

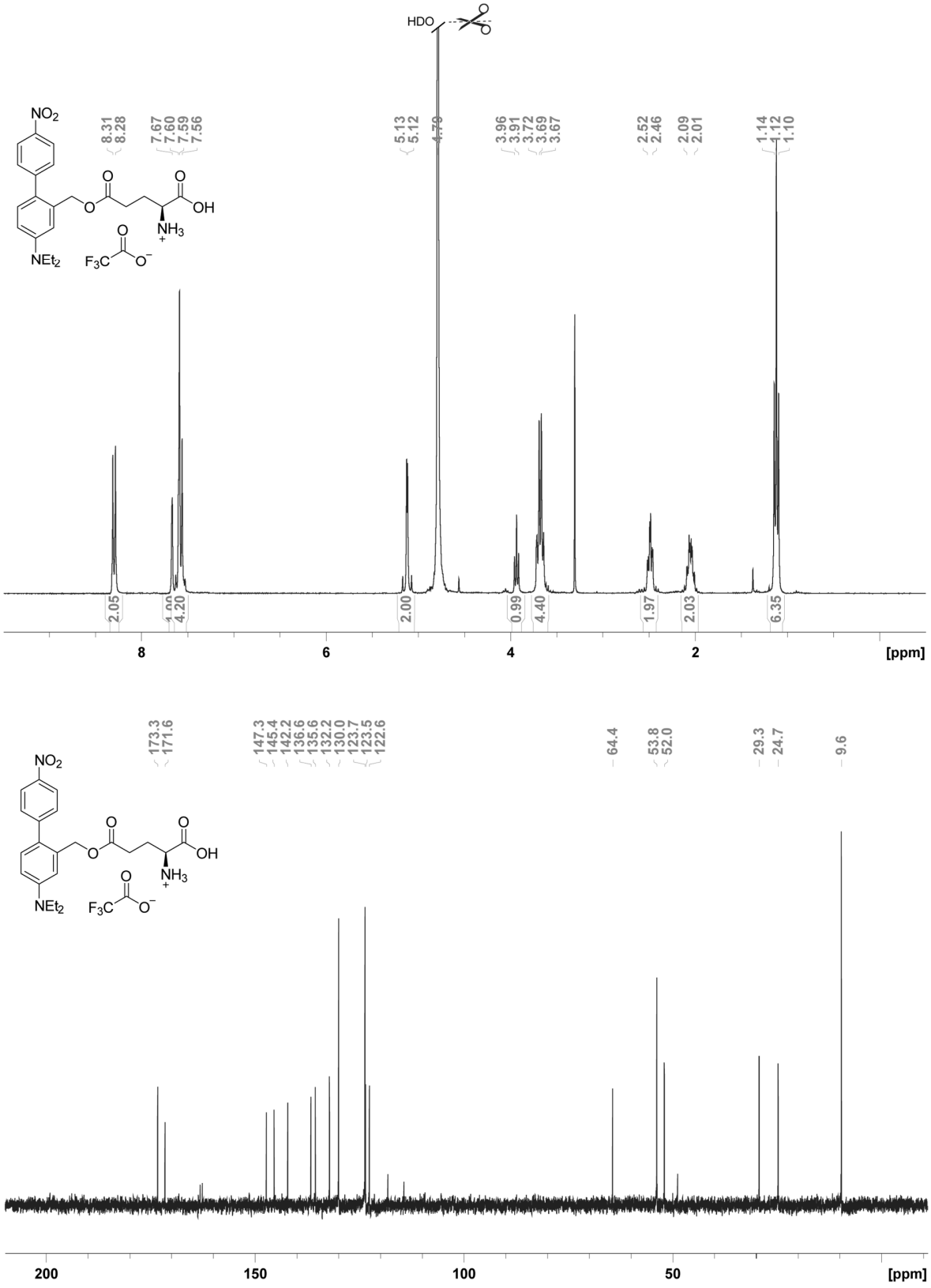

Figure 152: ^{1}H (300 MHz, D_2O) (upper) and ^{13}C (75 MHz, D_2O) (lower) NMR spectra of **133**.

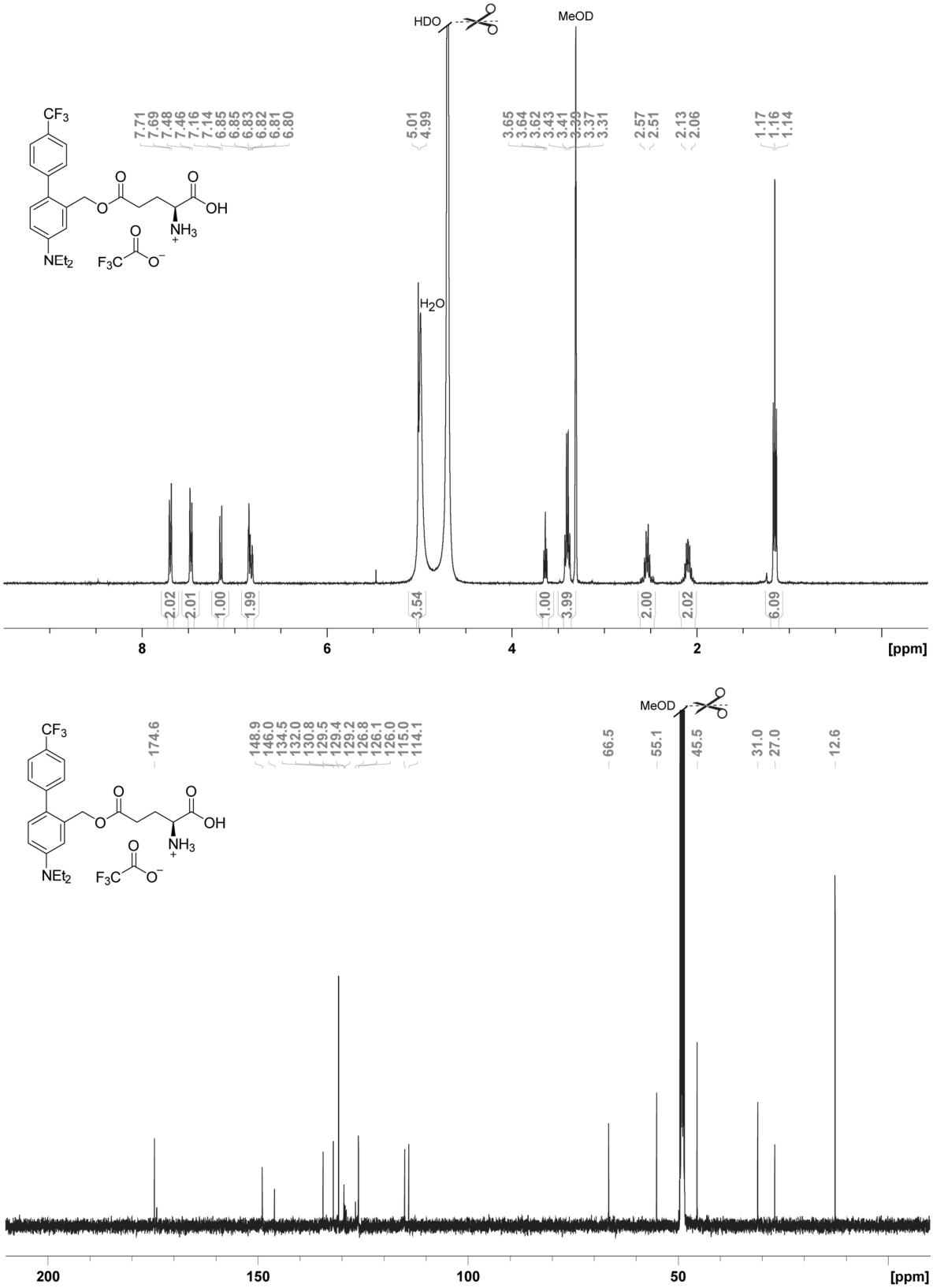

Figure 153: ^{1}H (400 MHz, MeOD-d_4 + D_2O) (upper) and ^{13}C (125 MHz, MeOD-d_4 + D_2O) (lower) NMR spectra of **128**.

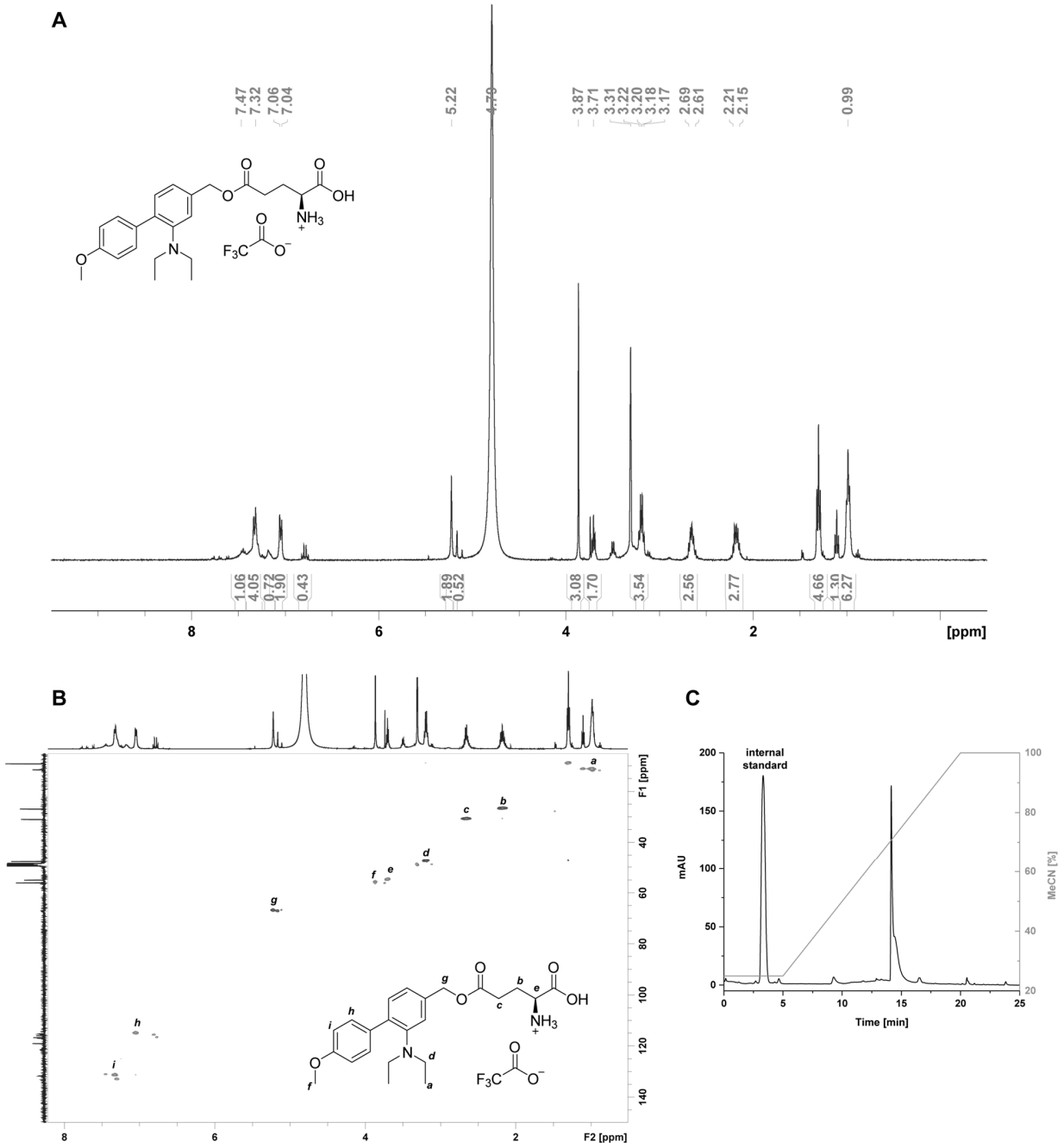

Figure 154: *A* - ^{1}H NMR (400 MHz, MeOD-d_4 + D_2O) spectra of **141**; *B* – $^{1}H^{13}C$ HSQC spectra (^{1}H 500 MHz, ^{13}C 125 MHz, MeOD-d_4 + D_2O). The relevant signals could be found and assigned; *C* – reverse phase HPLC chromatogram (detection at 254 nm) of the compound **141** at the time of photochemical characterization. Internal standard – phenylalanine.

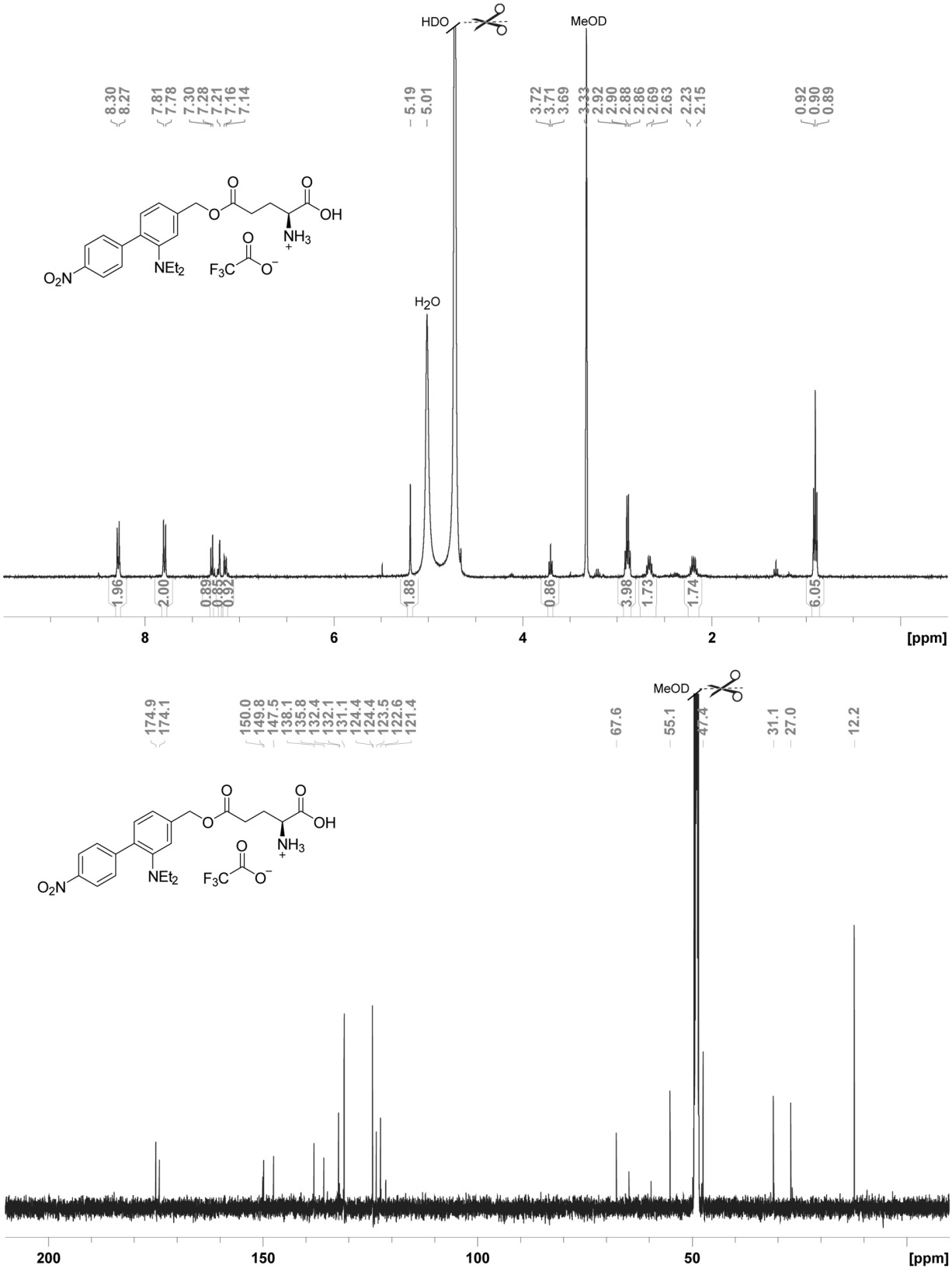

Figure 155: ^{1}H (400 MHz, MeOD-d_4 + D_2O) (upper) and ^{13}C (125 MHz, MeOD-d_4 + D_2O) (lower) NMR spectra of **143**.

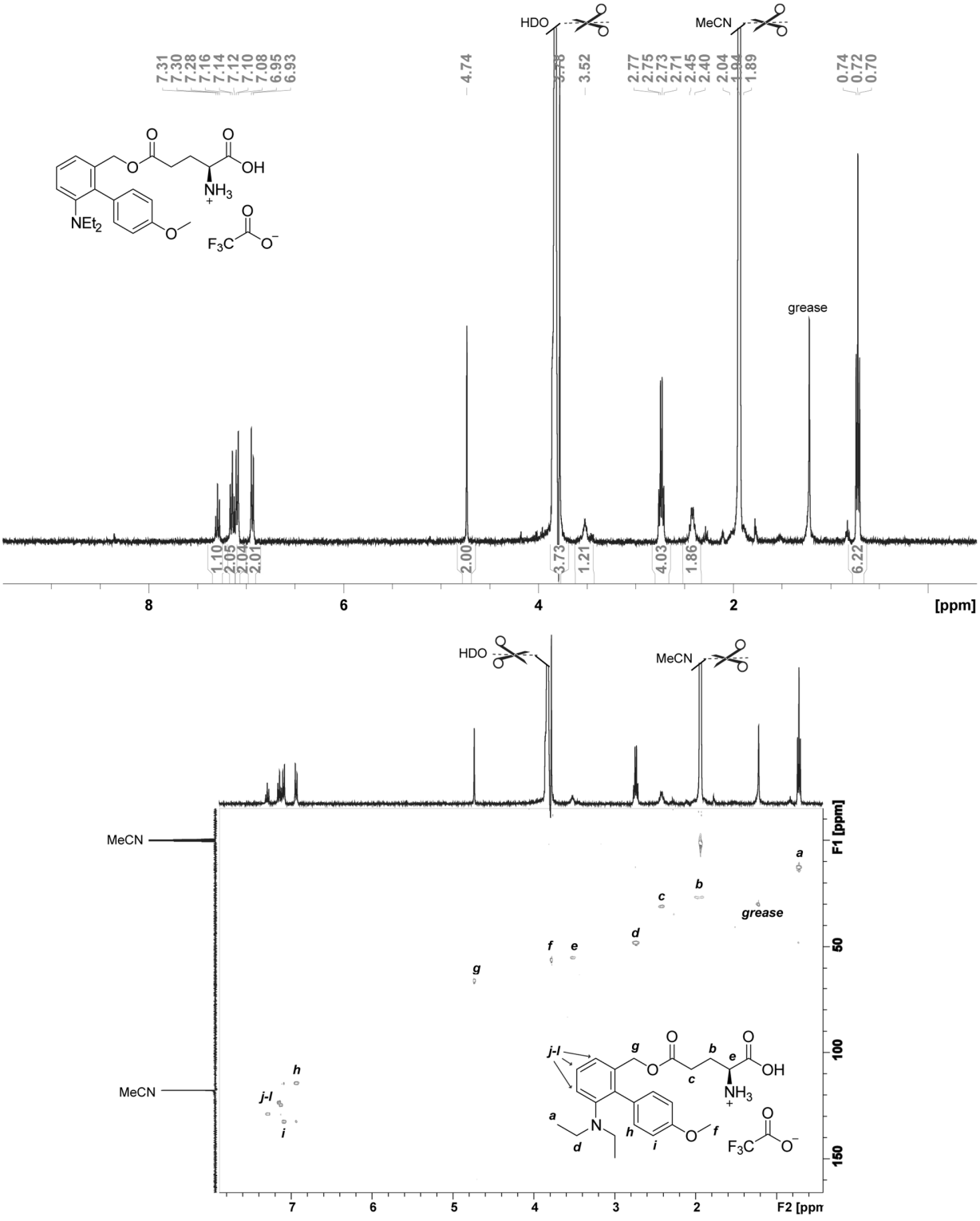

Figure 156: ^{1}H NMR (400 MHz, MeCN-d_3 + D_2O) spectra of **144** (upper); $^{1}H^{13}C$ HSQC spectra of **144** (^{1}H 400 MHz, ^{13}C 100 MHz, MeCN-d_3 + D_2O). The relevant signals could be found and assigned (lower);

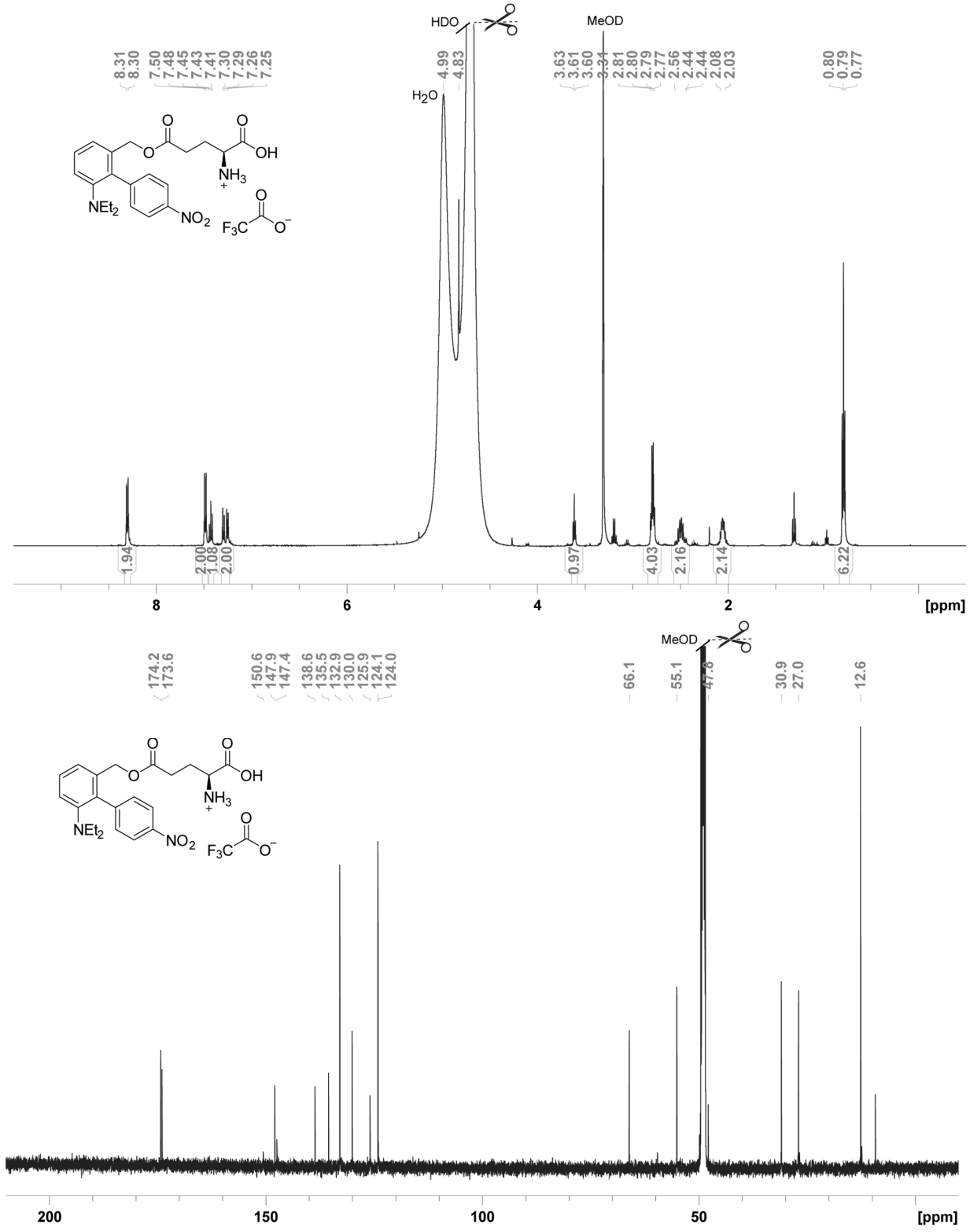

Figure 157: ^{1}H (500 MHz, MeOD-d_4 + D_2O) (upper) and ^{13}C (125 MHz, MeOD-d_4 + D_2O) (lower) NMR spectra of **146**.

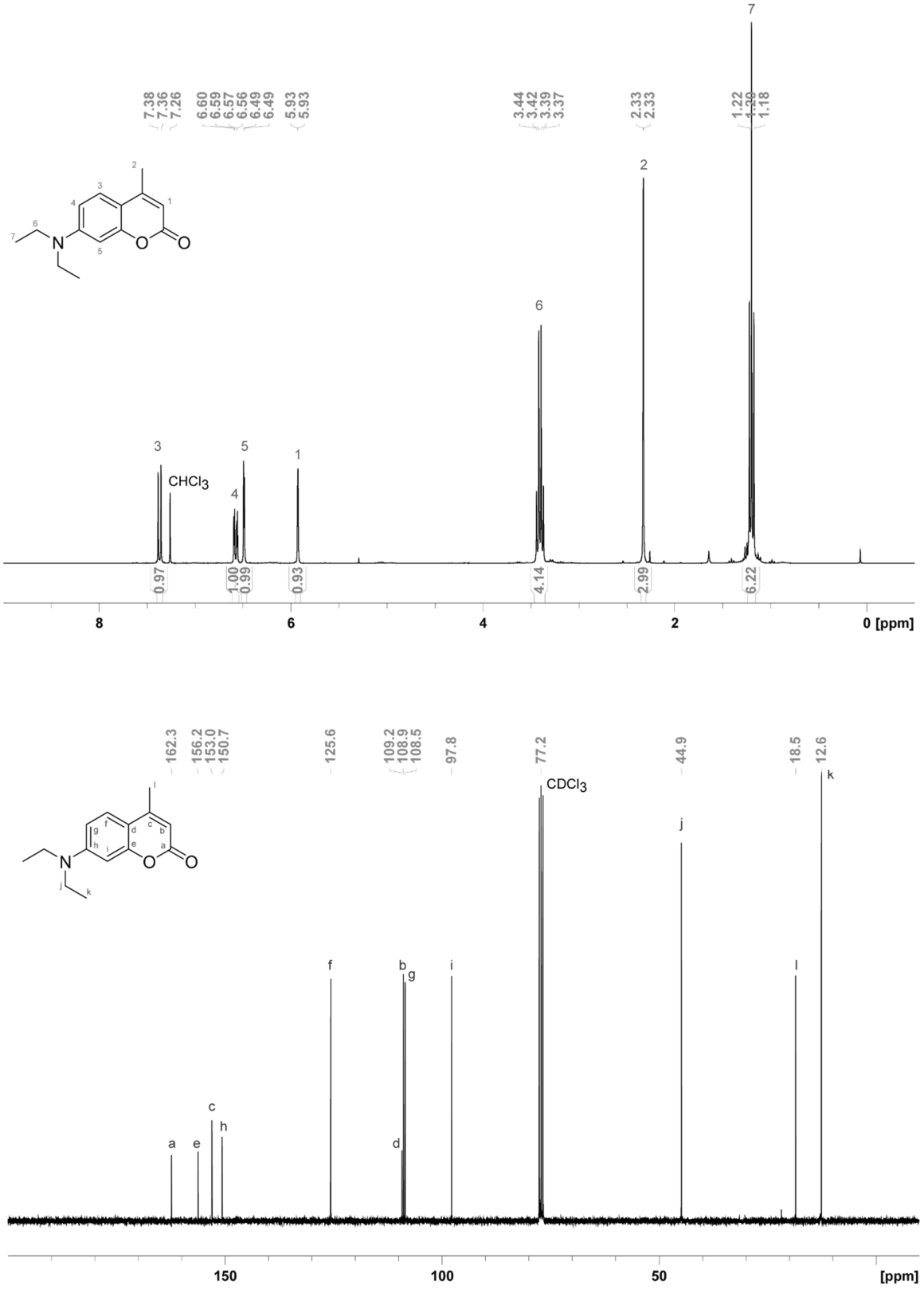

Figure 158: ^{1}H (300 MHz, $CDCl_3$) (upper) and ^{13}C (75 MHz, $CDCl_3$) (lower) NMR spectra of **207**.

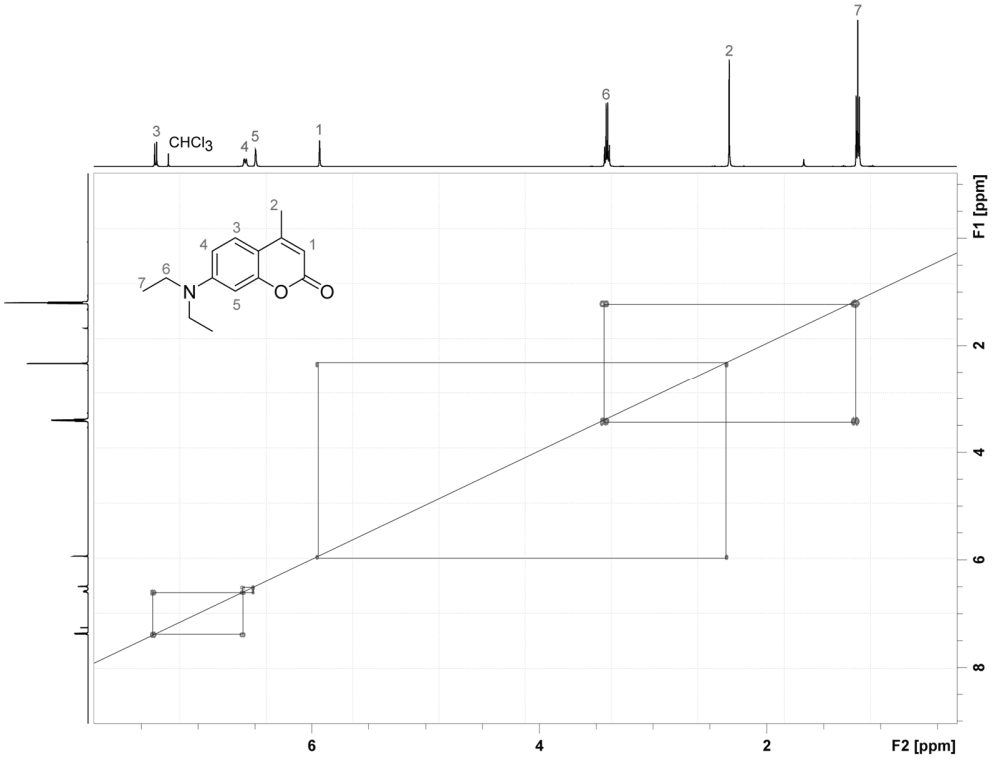

Figure 159: HH-COSY NMR (500 MHz, $CDCl_3$) spectrum of **207**.

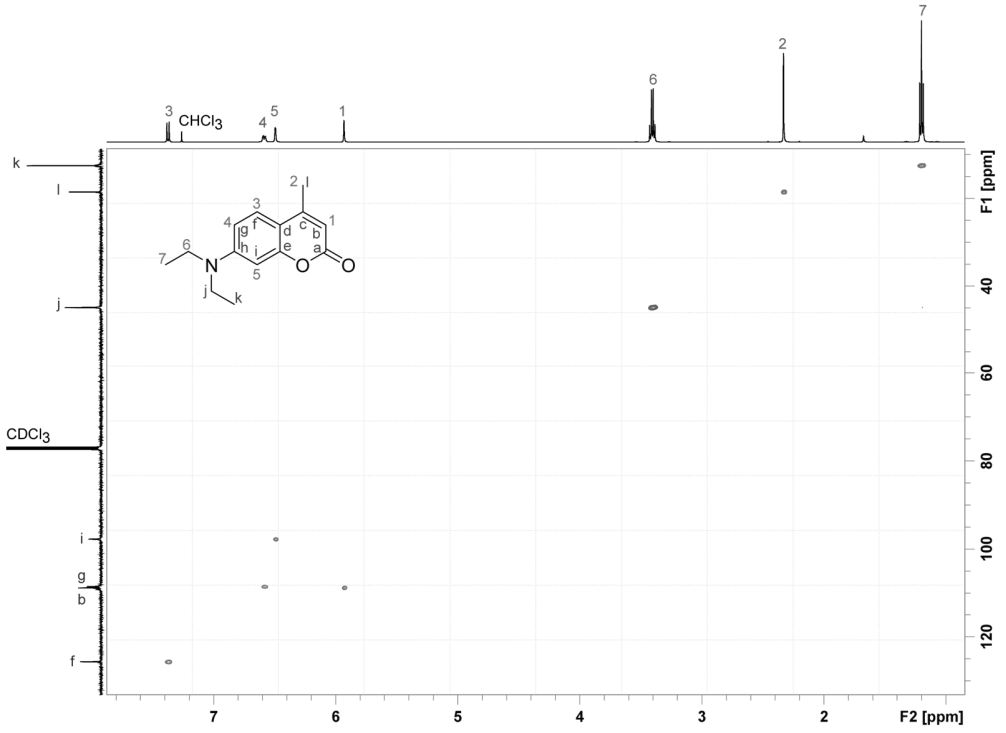

Figure 160: HSQC NMR (^{1}H 500 MHz, ^{13}C 125 MHz, $CDCl_3$) spectrum of **207**.

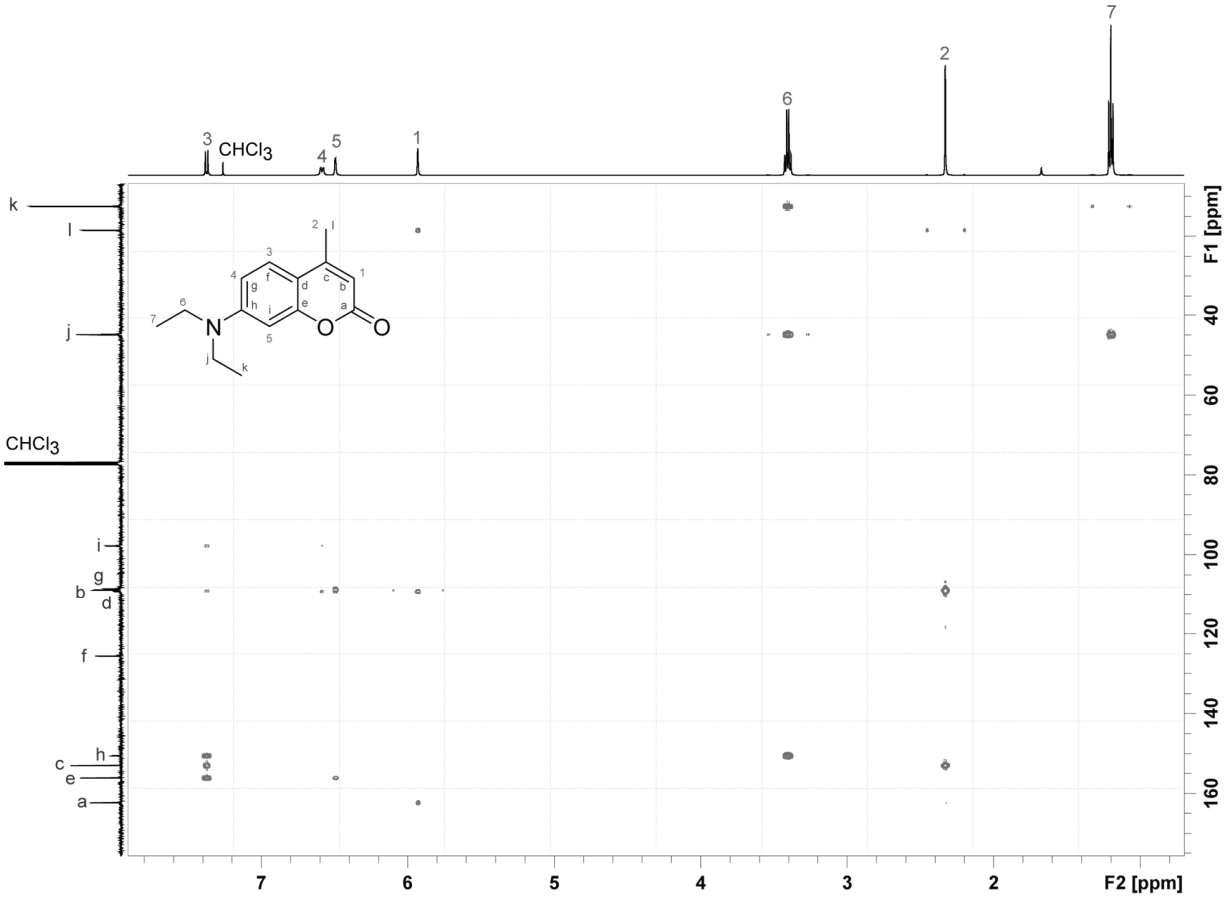

Figure 161: HMBC NMR (^{1}H 500 MHz, ^{13}C 125 MHz, $CDCl_3$) spectrum of **207**.

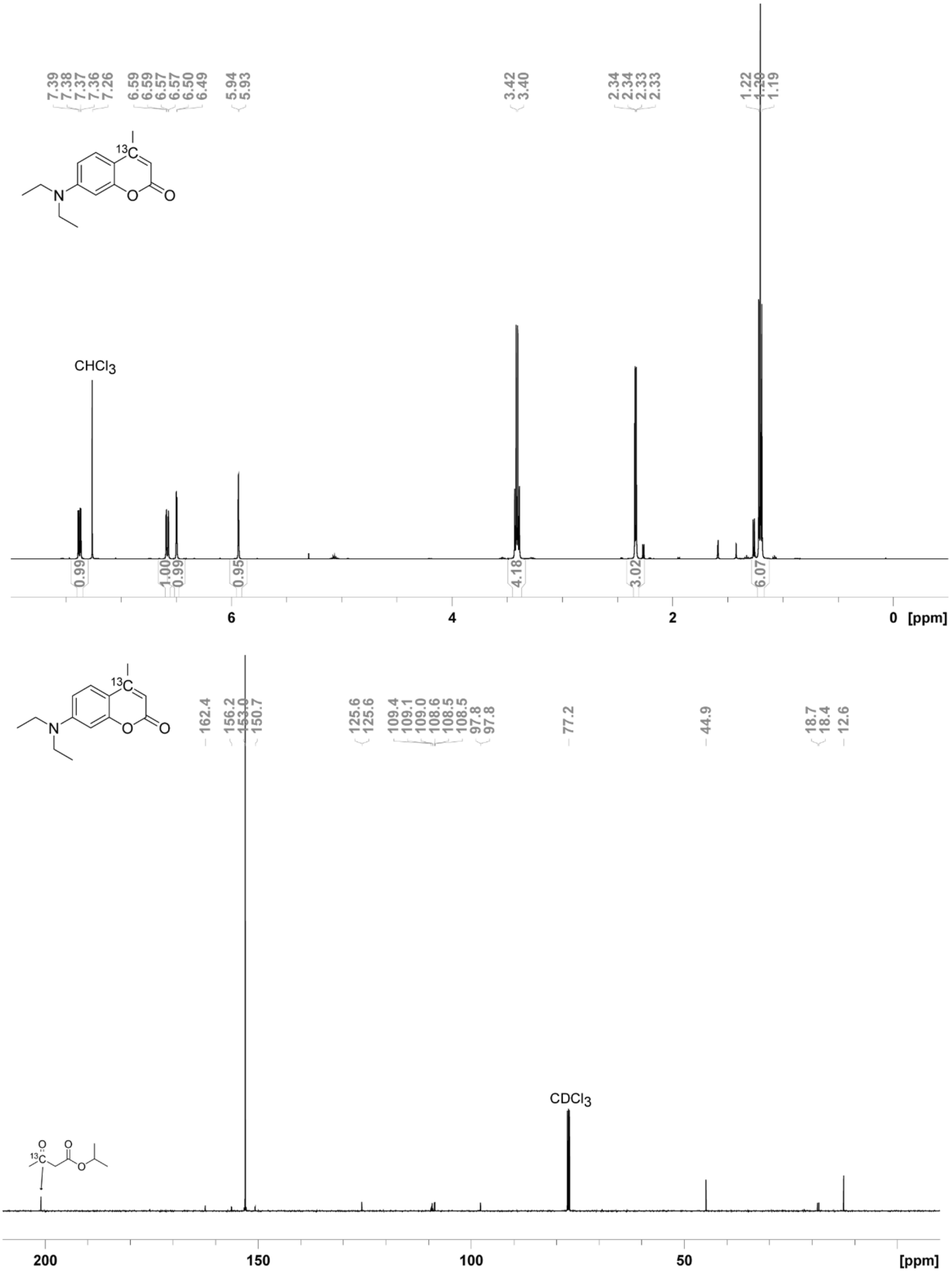

Figure 162: ^{1}H (500 MHz, CDCl3) (upper) and ^{13}C (125 MHz, CDCl3) (lower) NMR spectra of **207a**.

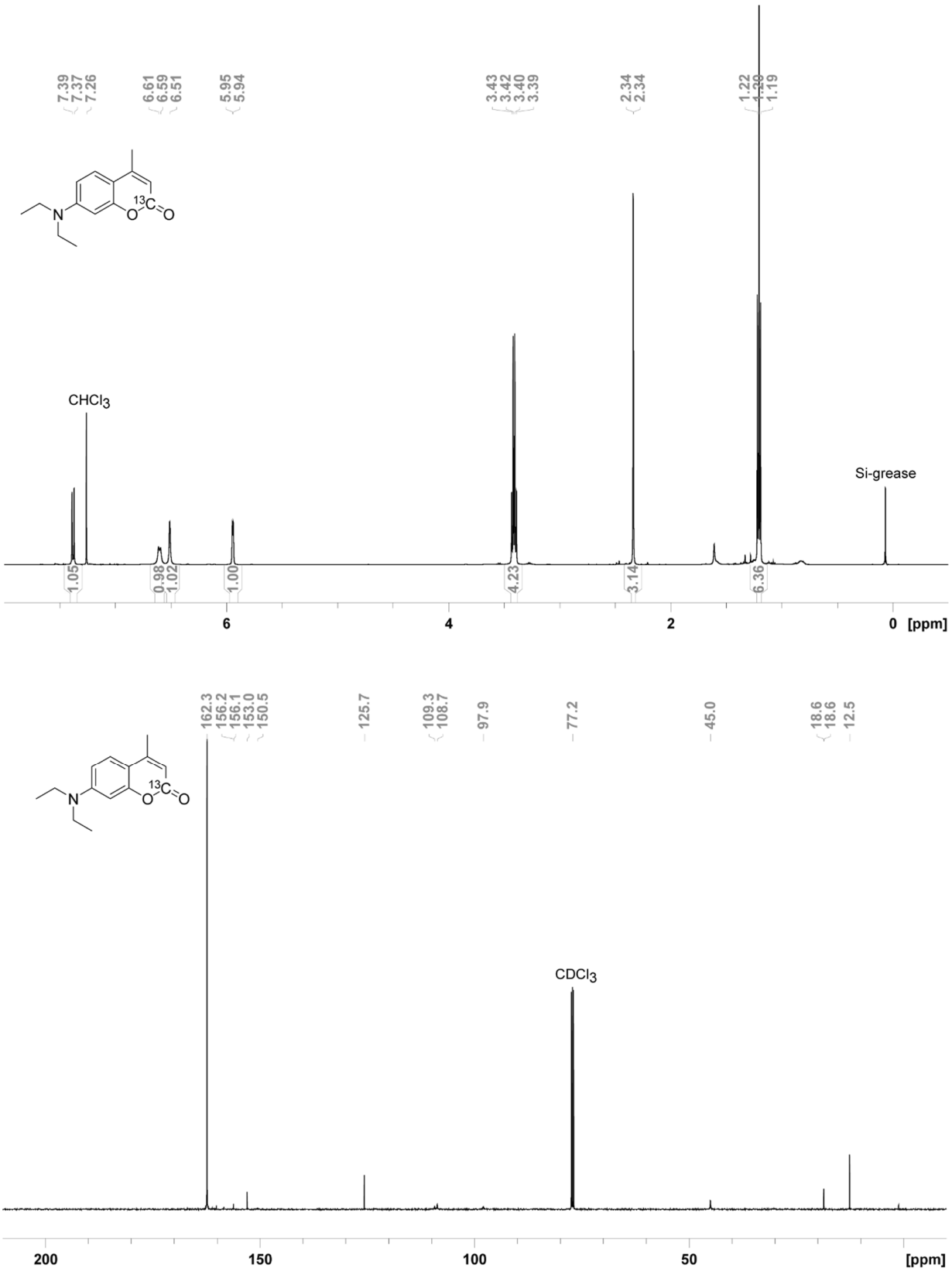

Figure 163: ^{1}H (500 MHz, $CDCl_3$) (upper) and ^{13}C (125 MHz, $CDCl_3$) (lower) NMR spectra of **207b**.

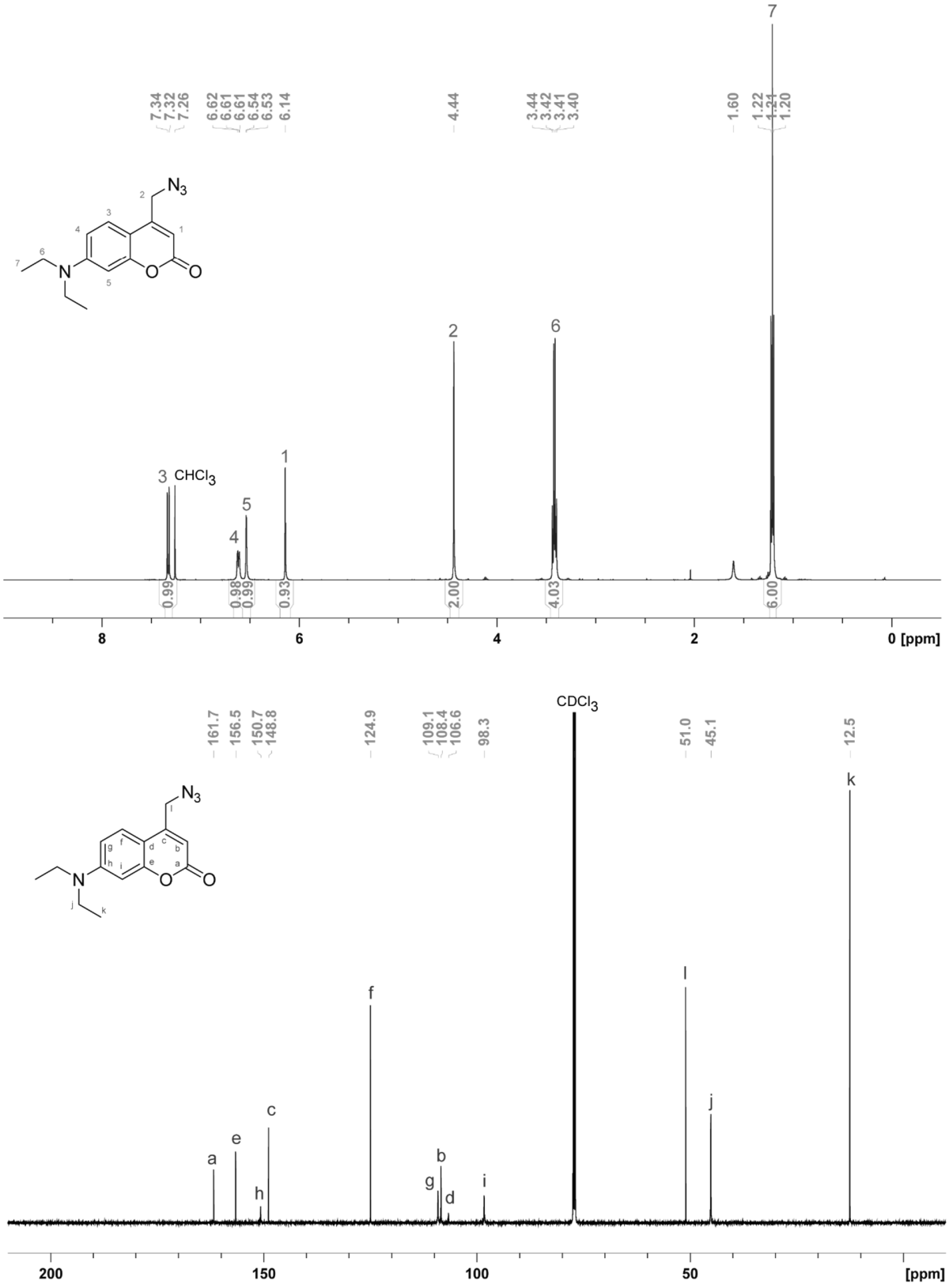

Figure 164: ^{1}H (500 MHz, $CDCl_3$) (upper) and ^{13}C (125 MHz, $CDCl_3$) (lower) NMR spectra of **203**.

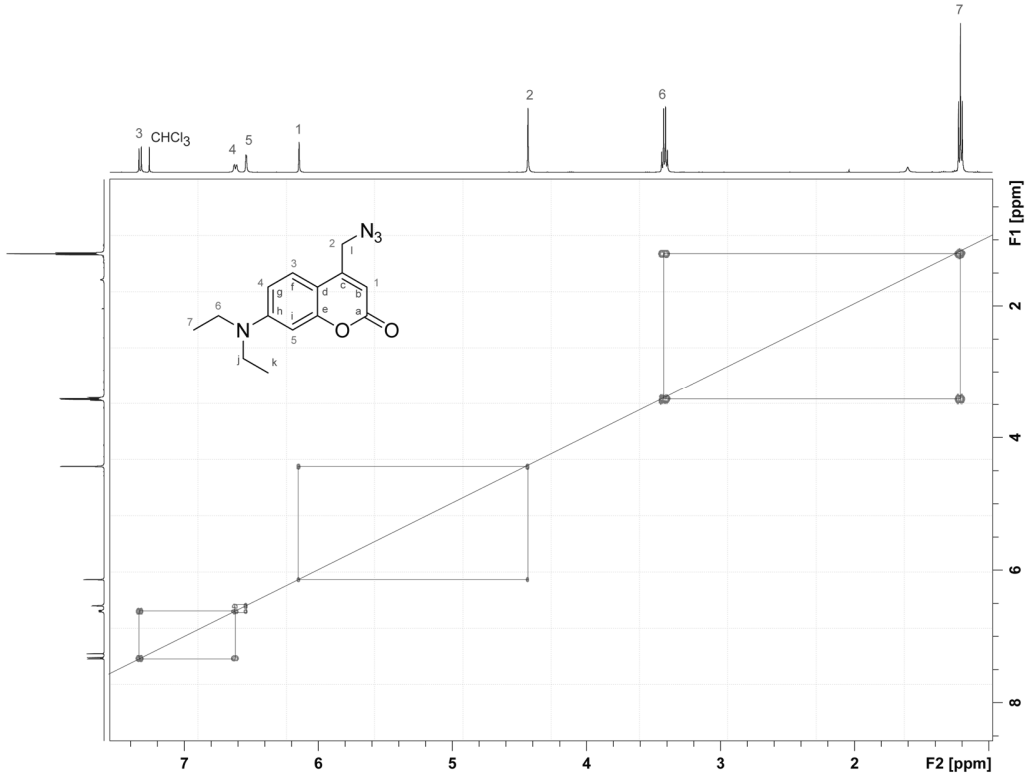

Figure 165: HH-COSY NMR (500 MHz, $CDCl_3$) spectrum of **203**.

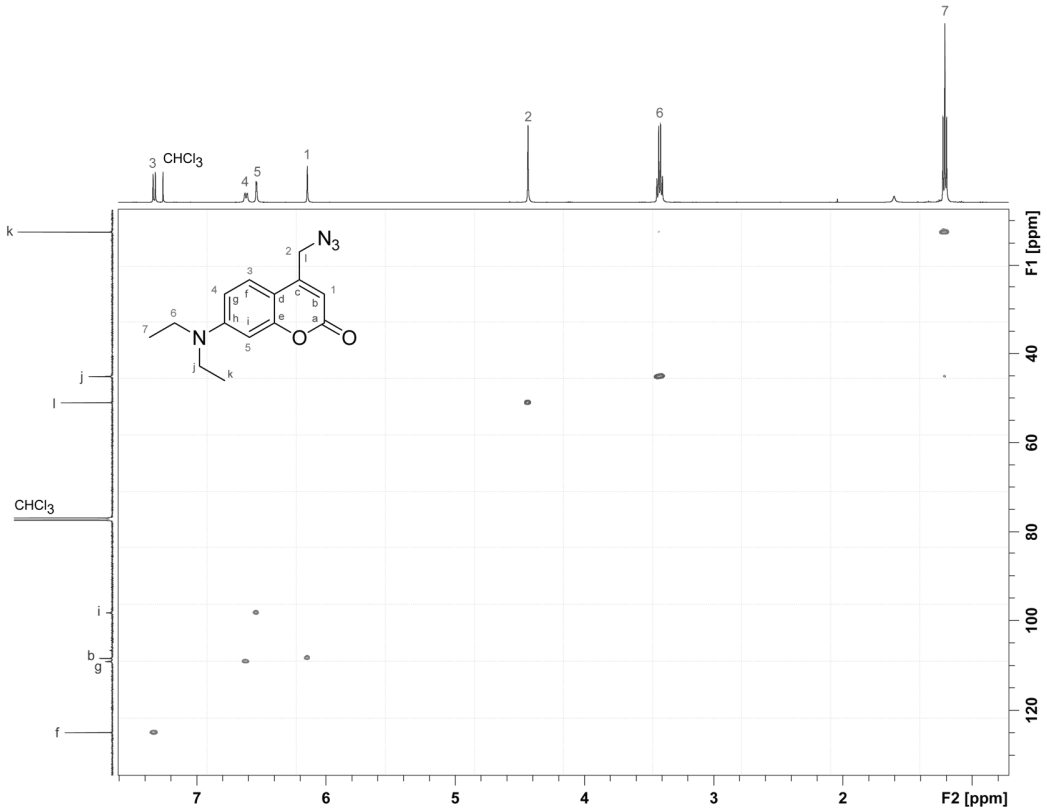

Figure 166: HSQC NMR (^{1}H 500 MHz, ^{13}C 125 MHz, $CDCl_3$) spectrum of **203**.

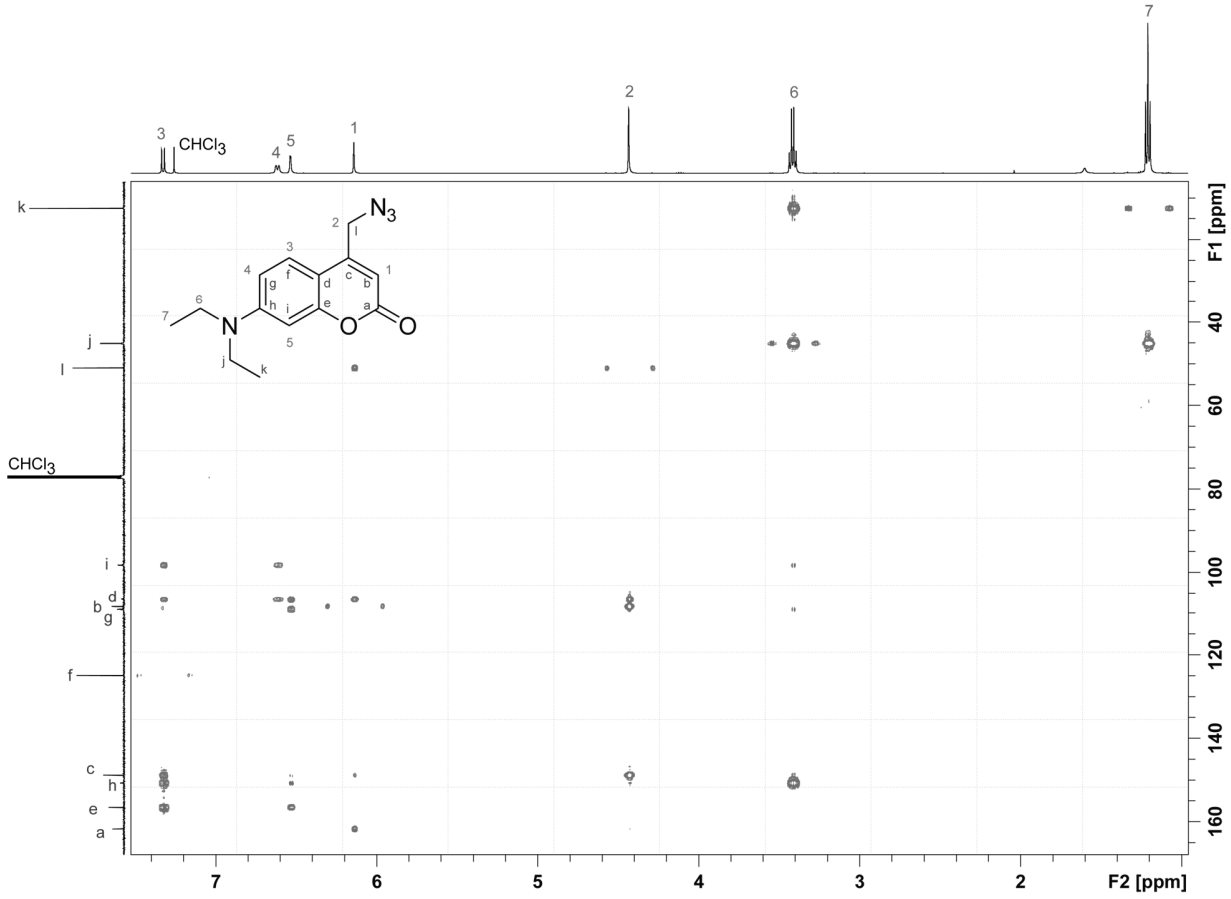

Figure 167: HMBC NMR (^{1}H 500 MHz, ^{13}C 125 MHz, $CDCl_3$) spectrum of **203**.

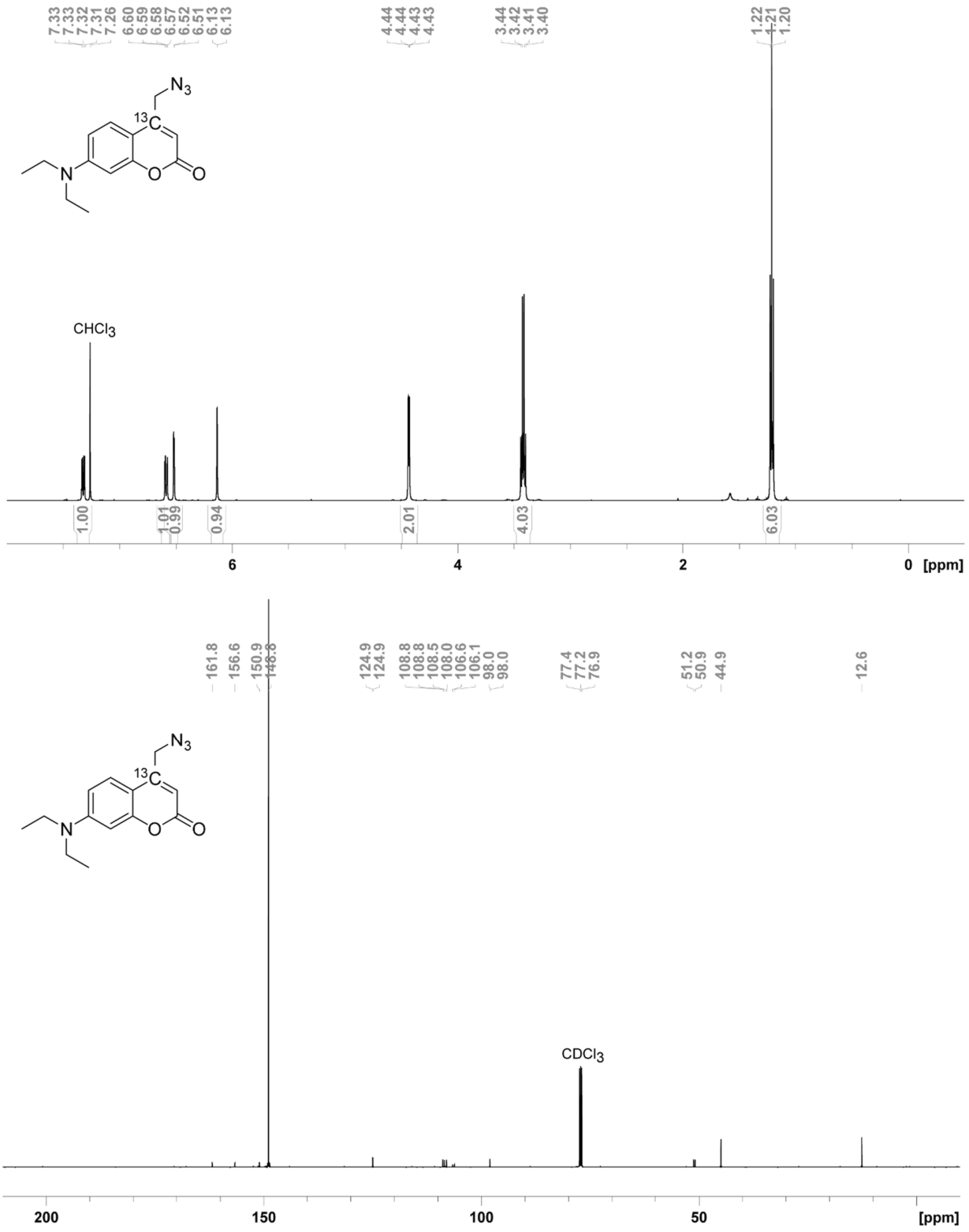

Figure 168: ^{1}H (500 MHz, $CDCl_3$) (upper) and ^{13}C (125 MHz, $CDCl_3$) (lower) NMR spectra of **201**.

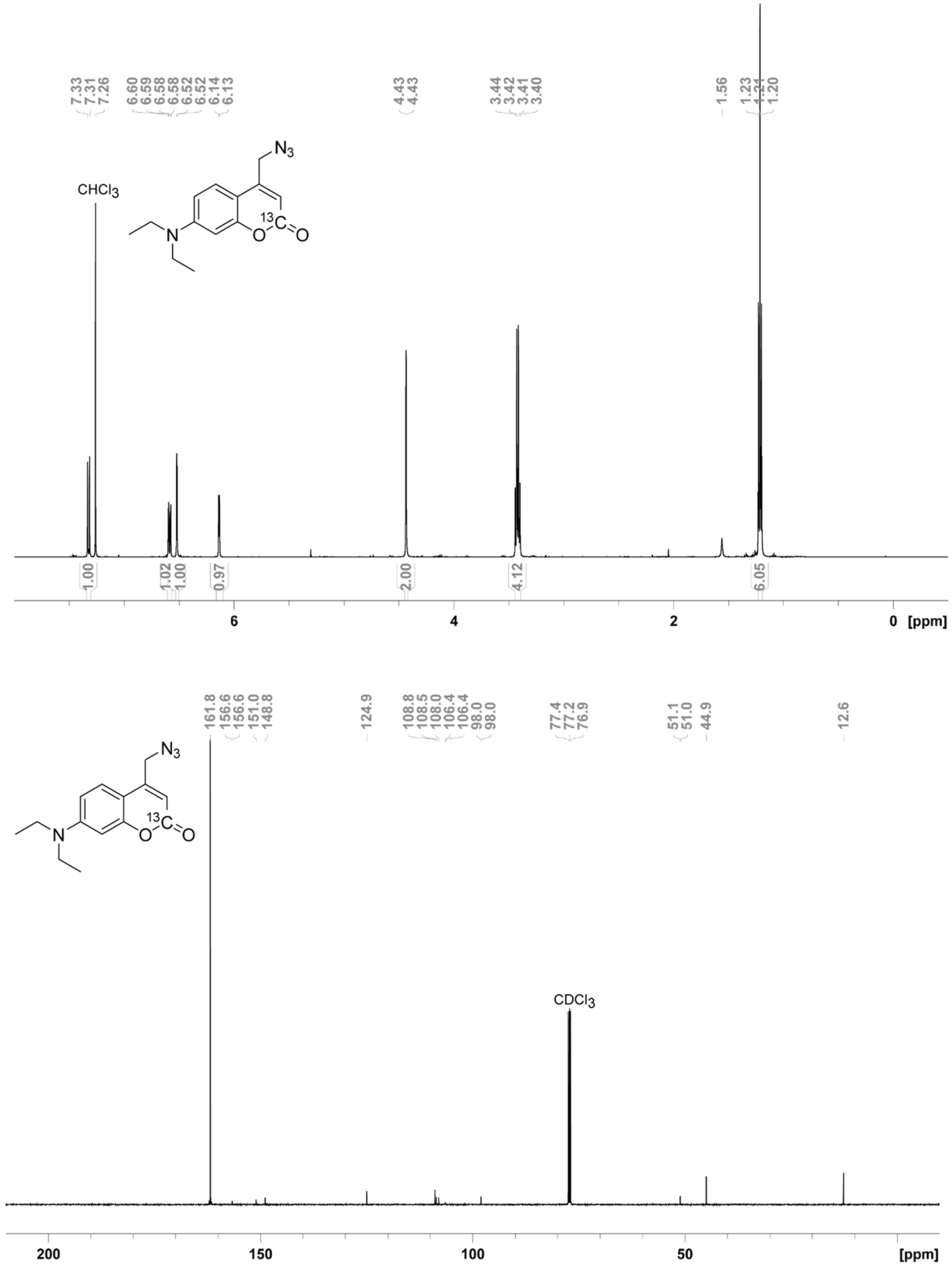

Figure 169: ^{1}H (500 MHz, $CDCl_3$) (upper) and ^{13}C (125 MHz, $CDCl_3$) (lower) NMR spectra of **202**.

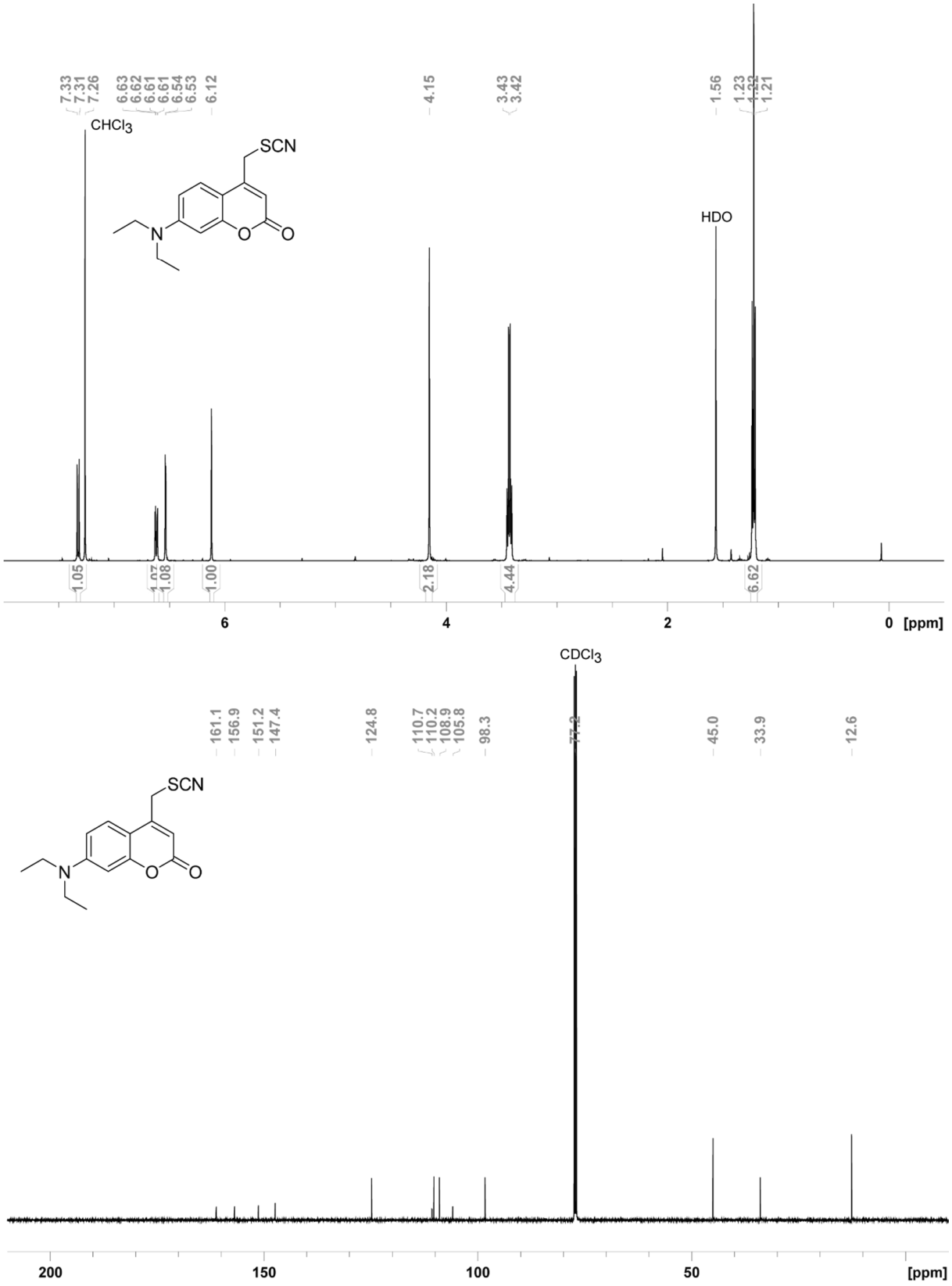

Figure 170: ^{1}H (500 MHz, $CDCl_3$) (upper) and ^{13}C (125 MHz, $CDCl_3$) (lower) NMR spectra of **204**.

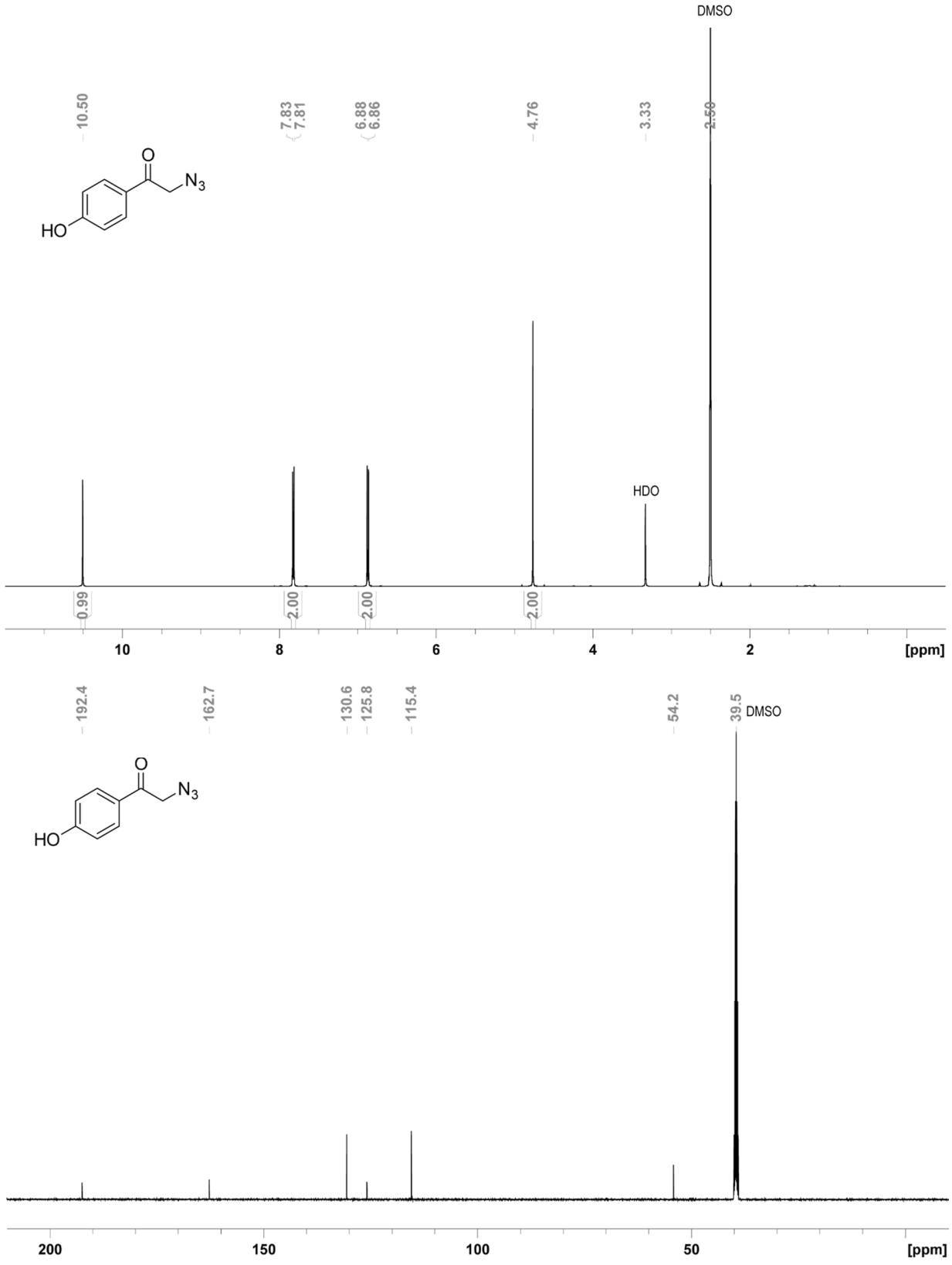

Figure 171: ^{1}H (500 MHz, DMSO-d_6) (upper) and ^{13}C (125 MHz, DMSO-d_6) (lower) NMR spectra of **217**.

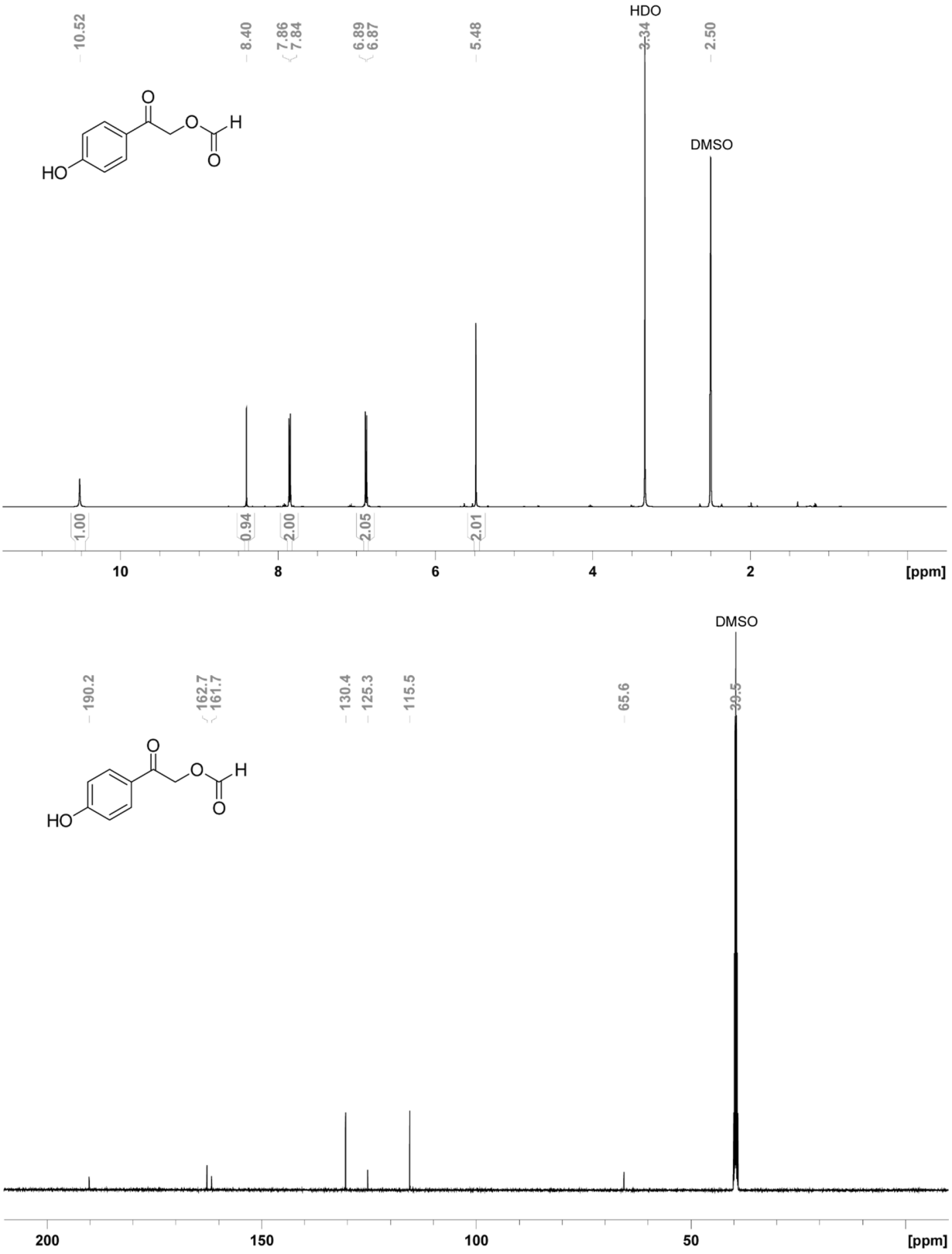

Figure 172: ^{1}H (500 MHz, DMSO-d_6) (upper) and ^{13}C (125 MHz, DMSO-d_6) (lower) NMR spectra of **219**.

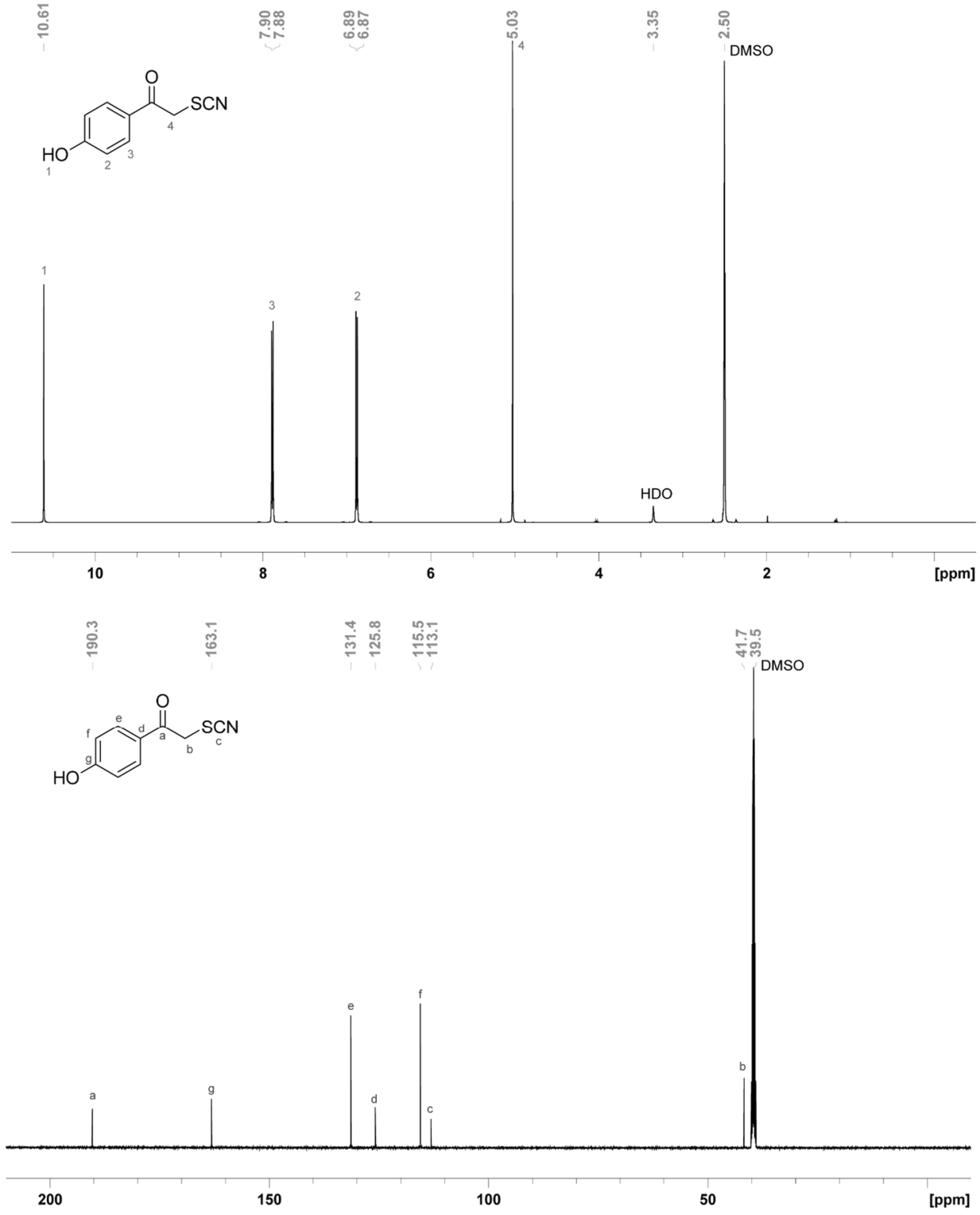

Figure 173: ^{1}H (500 MHz, DMSO-d_6) (upper) and ^{13}C (125 MHz, DMSO-d_6) (lower) NMR spectra of **218**.

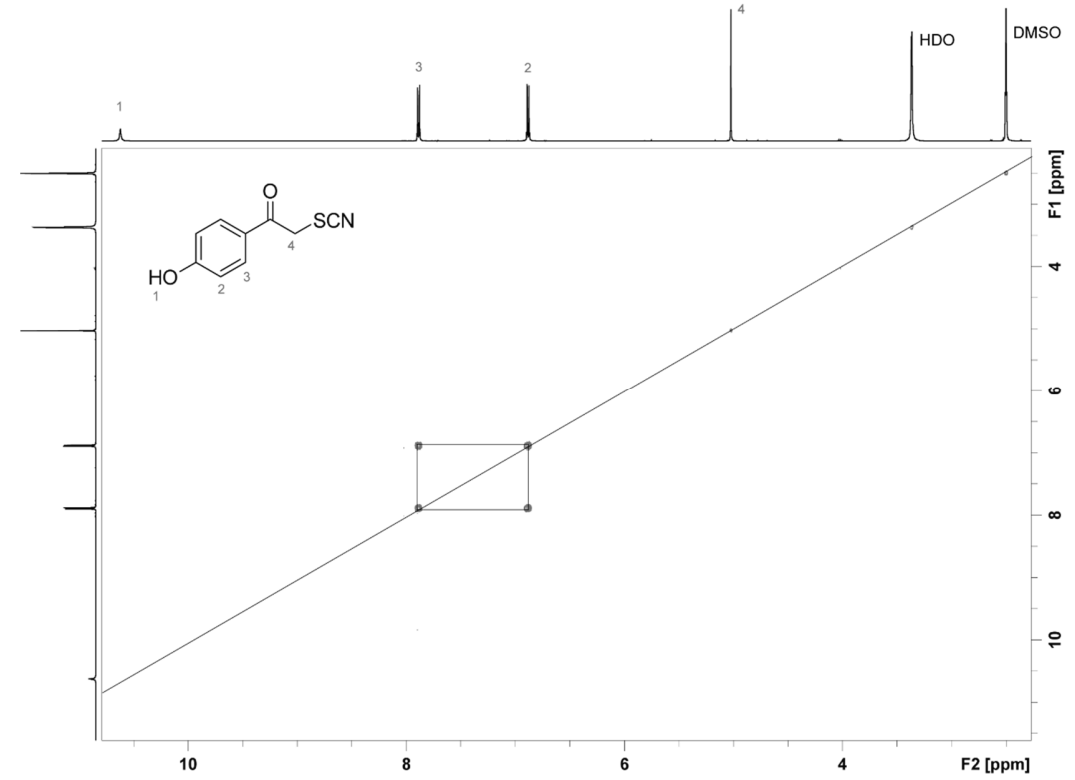

Figure 174: HH-COSY NMR (500 MHz, DMSO-d_6) spectra of **218**.

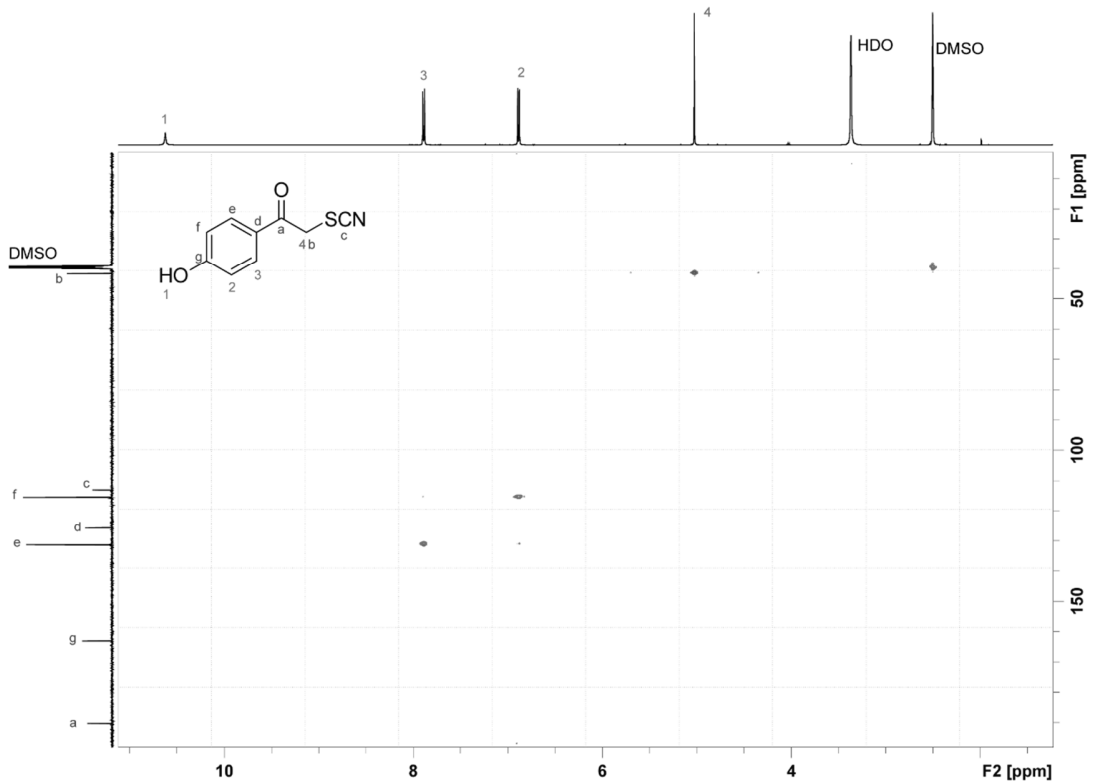

Figure 175: HSQC NMR (^{1}H 500 MHz, ^{13}C 125 MHz, DMSO-d_6) spectra of **218**.

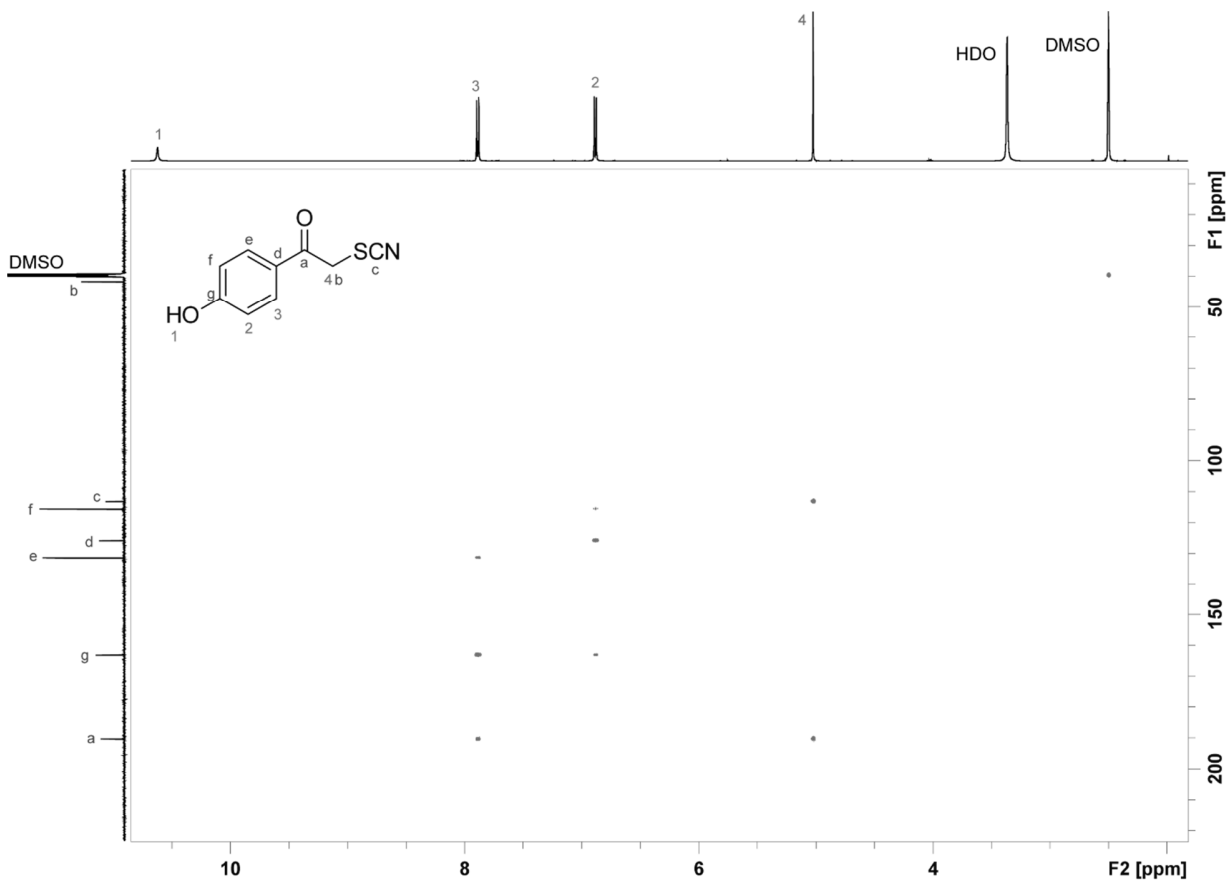

Figure 176: HMBC NMR (^{1}H 500 MHz, ^{13}C 125 MHz, DMSO-d_6) spectra of **218**.

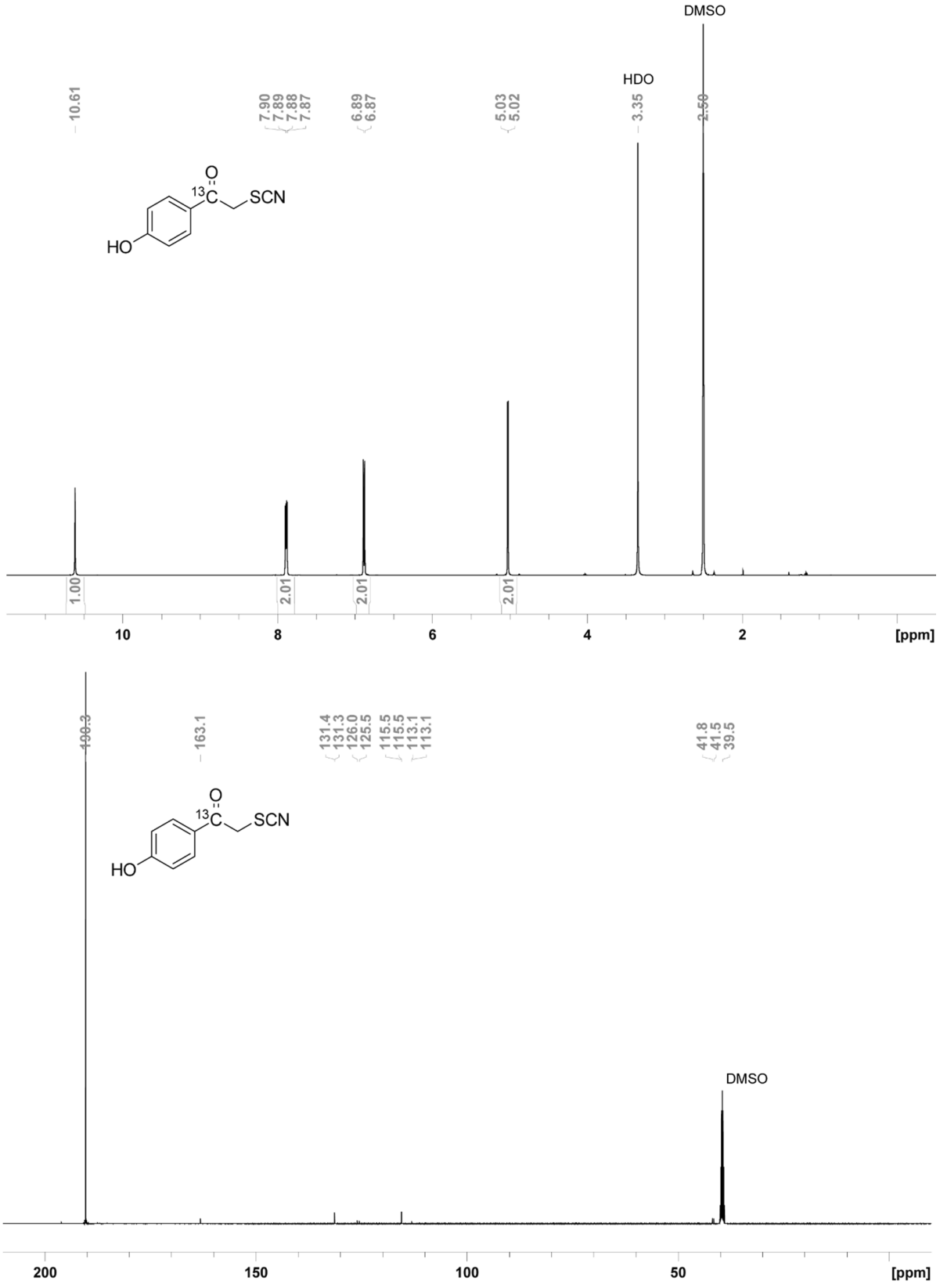

Figure 177: ^{1}H (500 MHz, DMSO-d_6) (upper) and ^{13}C (125 MHz, DMSO-d_6) (lower) NMR spectra of **228**.

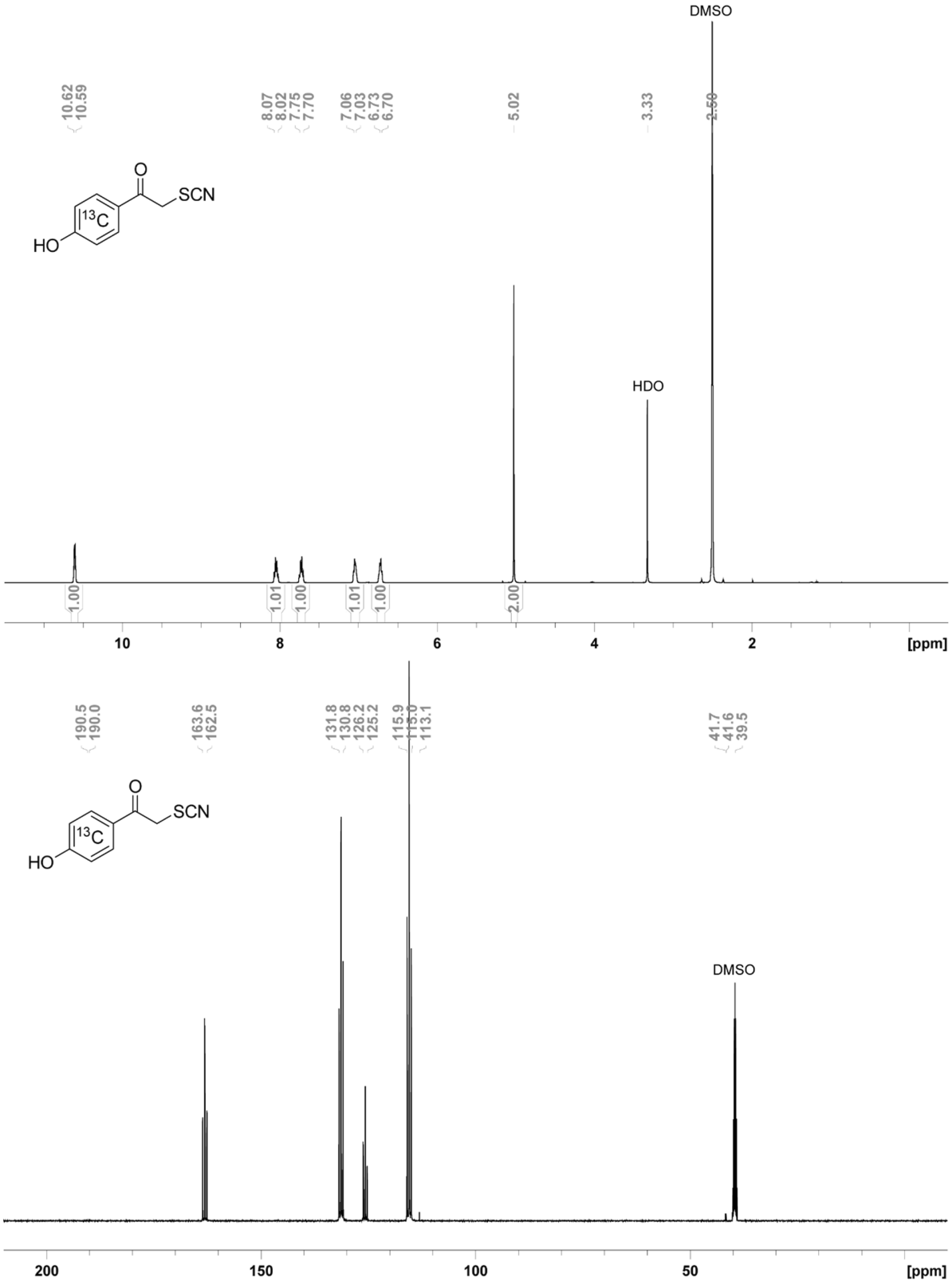

Figure 178: ^{1}H (500 MHz, DMSO-d_6) (upper) and ^{13}C (125 MHz, DMSO-d_6) (lower) NMR spectra of **230**.

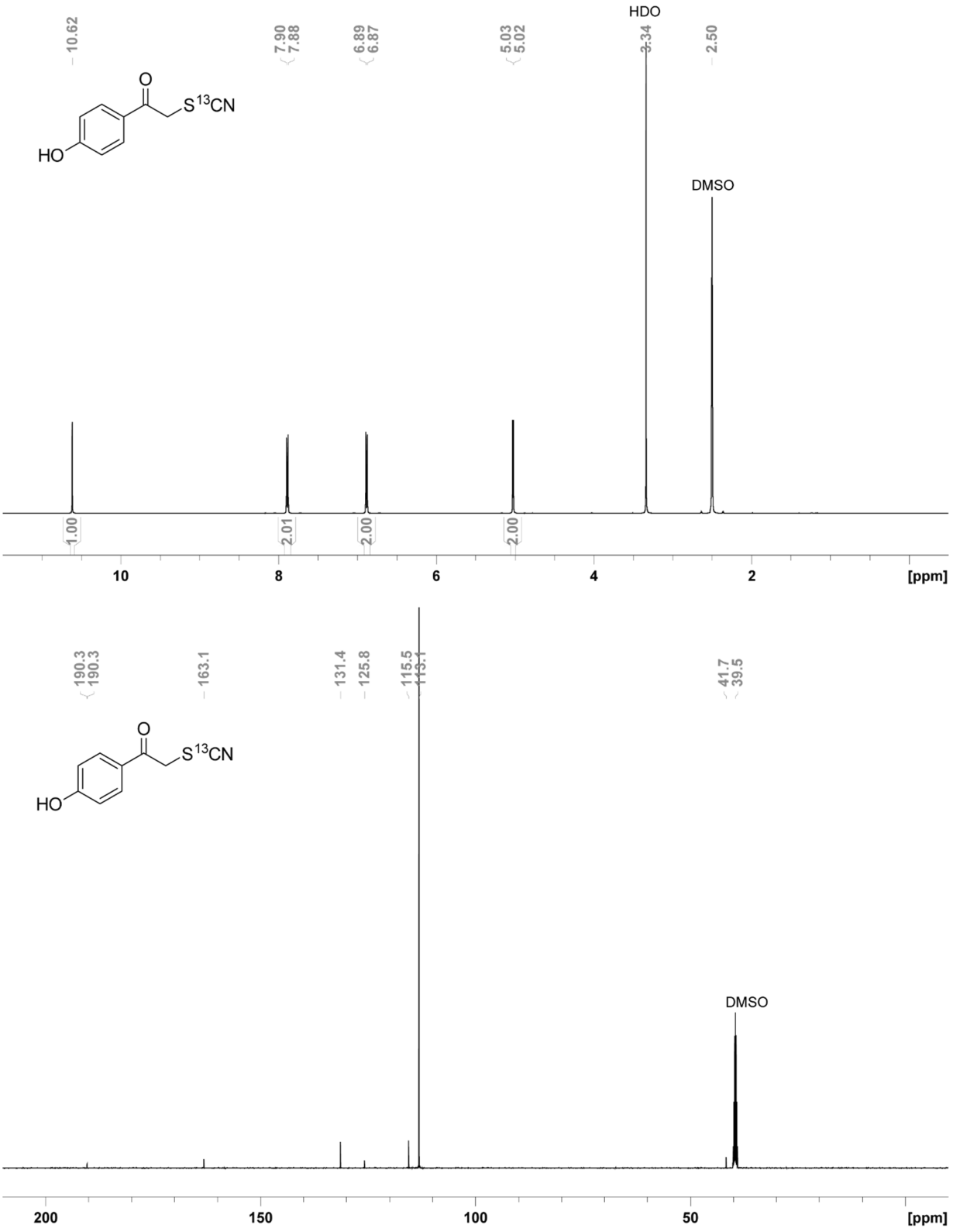

Figure 179: ^{1}H (500 MHz, DMSO-d_6) (upper) and ^{13}C (125 MHz, DMSO-d_6) (lower) NMR spectra of **231**.

6.3. Abbreviations

Ac	Acetyl
AcOH	Acetic acid
aq.	Aqueous
Ar	Aryl
Boc	*tert*-butyloxycarbonyl
BODIPY	Boron-dipyrromethene
ca.	circa (Latin) approximately
COSY	Correlation spectroscopy
Cy	Cyclohexane
DEACM	7-diethylamino coumarin
DEAMb	Diethylamino benzyl
DIPEA	*N*,*N*-Diisopropylethylamine
DMAP	4-(Dimethylamino)-pyridin
DMF-DMA	*N*,*N*-Dimethylformamide-dimethyl acetal
DMF	*N*,*N*-Dimethylformamide
DMSO	Dimethyl sulfoxide
EDC HCl	*N*-(3-Dimethylaminopropyl)-N′-ethylcarbodiimide hydrochloride
EDG	Electron donating group
e.g.	exempli gratia (Latin) for example
ESI	Electrospray ionization
et al.	et alia (Latin) and others
EtOAc	Ethyl acetate
EWG	Electron withdrawing group
HILIC	Hydrophilic interaction chromatography
HMBC	Heteronuclear Multiple Bond Correlation
HOMO	Highest occupied molecular orbital
HPLC	High-performance liquid chromatography
HSQC	Heteronuclear single quantum correlation
IR	Infrared

ISC	Intersystem crossing
LED	Light emitting diode
LG	Leaving group
LUMO	Lowest unoccupied molecular orbital
MALDI	Matrix Assisted Laser Desorption/Ionization
MO	Molecular Orbital
MsCl	Methanesulfonyl chloride
MS	Mass spectra
NMR	Nuclear magnetic resonance
Nu	Nucleophile
*o*HC	*ortho*-hydroxycinnamyl
*o*NB	*ortho*-nitrobenzene
OPA	*ortho*-phthaldialdehyde
PBS	Phosphate-buffered saline
*p*HP	*para*-hydroxy phenacyl
PPGs	Photolabile protecting groups
RP	Reverse phase
*t*Bu	*tert*-Butyl
TDDFT	Time-dependent density functional theory
TEAA	Triethylammonium acetate
TFA	Trifluoroacetic acid
TfOH	Trifluorosulfonic acid
THF	Tetrahydrofuran
TLC	Thin layer chromatography
UV-Vis	Ultraviolet-visible
VIPER	VIbrationally Promoted Electronic Resonance

6.4. References

[1] C. Brieke, F. Rohrbach, A. Gottschalk, G. Mayer, A. Heckel, *Angew. Chem. Int. Ed.* **2012**, *51*, 8446–8476.

[2] N. Ankenbruck, T. Courtney, Y. Naro, A. Deiters, *Angew. Chem. Int. Ed.* **2018**, *57*, 2768–2798.

[3] C. G. Bochet, A. Blanc, in *Handb. Synth. Photochem.* (Eds.: A. Albini, M. Fagnoni), Wiley-VCH Verlag GmbH & Co. KGaA, Weinheim, Germany, **2009**, pp. 417–447.

[4] C. Bochet, S. Mercier, in *Link. Strateg. Solid-Phase Org. Synth.* (Ed.: P.J.H. Scott), John Wiley & Sons, Ltd, Chichester, UK, **2009**, pp. 151–193.

[5] M. Sauer, M. Heilemann, *Chem. Rev.* **2017**, *117*, 7478–7509.

[6] F. M. Raymo, *Phys. Chem. Chem. Phys.* **2013**, *15*, 14840.

[7] C.-L. Ciana, C. G. Bochet, *Chim. Int. J. Chem.* **2007**, *61*, 650–654.

[8] N. J. Turro, V. Ramamurthy, J. C. Scaiano, *Modern Molecular Photochemistry of Organic Molecules*, **2017**.

[9] P. Klán, J. Wirz, *Photochemistry of Organic Compounds: From Concepts to Practice*, Wiley, Chichester, West Sussex, U.K, **2009**.

[10] S. Barman, S. K. Mukhopadhyay, S. Biswas, S. Nandi, M. Gangopadhyay, S. Dey, A. Anoop, N. D. Pradeep Singh, *Angew. Chem. Int. Ed.* **2016**, *55*, 4194–4198.

[11] L. Fournier, I. Aujard, T. Le Saux, S. Maurin, S. Beaupierre, J.-B. Baudin, L. Jullien, *Chem. - Eur. J.* **2013**, *19*, 17494–17507.

[12] N. Kamatham, J. P. Da Silva, R. S. Givens, V. Ramamurthy, *Org. Lett.* **2017**, *19*, 3588–3591.

[13] R. S. Givens, K. Stensrud, P. G. Conrad, A. L. Yousef, C. Perera, S. N. Senadheera, D. Heger, J. Wirz, *Can. J. Chem.* **2011**, *89*, 364–384.

[14] S. Draxler, T. Brust, S. Malkmus, J. A. DiGirolamo, W. J. Lees, W. Zinth, M. Braun, *Phys. Chem. Chem. Phys.* **2009**, *11*, 5019–5027.

[15] E. Riguet, C. G. Bochet, *Org. Lett.* **2007**, *9*, 5453–5456.

[16] L. Kammari, T. Šolomek, B. P. Ngoy, D. Heger, P. Klán, *J. Am. Chem. Soc.* **2010**, *132*, 11431–11433.

[17] A. Rodrigues-Correia, D. Knapp-Bühle, J. W. Engels, A. Heckel, *Org. Lett.* **2014**, *16*, 5128–5131.

[18] A. Blanc, C. G. Bochet, *J. Am. Chem. Soc.* **2004**, *126*, 7174–7175.

[19] C. G. Bochet, *Tetrahedron Lett.* **2000**, *41*, 6341–6346.

[20] C. G. Bochet, *Angew. Chem. Int. Ed.* **2001**, *40*, 2071–2073.

[21] V. San Miguel, C. G. Bochet, A. del Campo, *J. Am. Chem. Soc.* **2011**, *133*, 5380–5388.

[22] A. Rodrigues-Correia, X. M. M. Weyel, A. Heckel, *Org. Lett.* **2013**, *15*, 5500–5503.

[23] M. J. Hansen, W. A. Velema, M. M. Lerch, W. Szymanski, B. L. Feringa, *Chem. Soc. Rev.* **2015**, *44*, 3358–3377.

[24] T. Šolomek, J. Wirz, P. Klán, *Acc. Chem. Res.* **2015**, *48*, 3064–3072.

[25] C. G. Bochet, *Chim. Int. J. Chem.* **2016**, *70*, 182–185.

[26] S. Piant, F. Bolze, A. Specht, *Opt. Mater. Express* **2016**, *6*, 1679.

[27] M. Abe, Y. Chitose, S. Jakkampudi, P. Thuy, Q. Lin, B. Van, A. Yamada, R. Oyama, M. Sasaki, C. Katan, *Synthesis* **2017**, *49*, 3337–3346.
[28] L. Sansalone, S. Tang, Y. Zhang, E. R. Thapaliya, F. M. Raymo, J. Garcia-Amorós, *Top. Curr. Chem.* **2016**, *374*, 73.
[29] M. Wijtmans, S. J. Rosenthal, B. Zwanenburg, N. A. Porter, *J. Am. Chem. Soc.* **2006**, *128*, 11720–11726.
[30] D. Neuman, A. D. Ostrowski, R. O. Absalonson, G. F. Strouse, P. C. Ford, *J. Am. Chem. Soc.* **2007**, *129*, 4146–4147.
[31] C.-J. Carling, J.-C. Boyer, N. R. Branda, *J. Am. Chem. Soc.* **2009**, *131*, 10838–10839.
[32] C.-J. Carling, F. Nourmohammadian, J.-C. Boyer, N. R. Branda, *Angew. Chem. Int. Ed.* **2010**, *49*, 3782–3785.
[33] M. Delor, P. A. Scattergood, I. V. Sazanovich, A. W. Parker, G. M. Greetham, A. J. H. M. Meijer, M. Towrie, J. A. Weinstein, *Science* **2014**, *346*, 1492–1495.
[34] M. Delor, S. A. Archer, T. Keane, A. J. H. M. Meijer, I. V. Sazanovich, G. M. Greetham, M. Towrie, J. A. Weinstein, *Nat. Chem.* **2017**, *9*, 1099–1104.
[35] J. Engels, E. J. Schlaeger, *J. Med. Chem.* **1977**, *20*, 907–911.
[36] J. H. Kaplan, B. Forbush, J. F. Hoffman, *Biochemistry (Mosc.)* **1978**, *17*, 1929–1935.
[37] Y. V. Il'ichev, M. A. Schwoerer, J. Wirz, *J. Am. Chem. Soc.* **2004**, *126*, 4581–4595.
[38] T. Šolomek, C. G. Bochet, T. Bally, *Chem. - Eur. J.* **2014**, 20, 8062-8067.
[39] I. Aujard, C. Benbrahim, M. Gouget, O. Ruel, J.-B. Baudin, P. Neveu, L. Jullien, *Chem. - Eur. J.* **2006**, *12*, 6865–6879.
[40] A. Momotake, N. Lindegger, E. Niggli, R. J. Barsotti, G. C. R. Ellis-Davies, *Nat. Methods* **2006**, *3*, 35–40.
[41] A. D. Turner, S. V. Pizzo, G. W. Rozakis, N. A. Porter, *J. Am. Chem. Soc.* **1987**, *109*, 1274–1275.
[42] Y. Yu, L. Wu, X. Zou, X. Dai, K. Liu, H. Su, *J. Phys. Chem. A* **2013**, *117*, 7767–7775.
[43] N. Gagey, P. Neveu, C. Benbrahim, B. Goetz, I. Aujard, J.-B. Baudin, L. Jullien, *J. Am. Chem. Soc.* **2007**, *129*, 9986–9998.
[44] Y. Venkatesh, H. K. Srivastava, S. Bhattacharya, M. Mehra, P. K. Datta, S. Bandyopadhyay, N. D. P. Singh, *Org. Lett.* **2018**, *20*, 2241–2244.
[45] D. J. Kunsberg, A. H. Kipping, D. E. Falvey, *Org. Lett.* **2015**, *17*, 3454–3457.
[46] D. P. Walton, D. A. Dougherty, *J. Am. Chem. Soc.* **2017**, *139*, 4655–4658.
[47] C. J. Regan, D. P. Walton, O. S. Shafaat, D. A. Dougherty, *J. Am. Chem. Soc.* **2017**, *139*, 4729–4736.
[48] X. Wang, J. A. Kalow, *Org. Lett.* **2018**, *20*, 1716–1719.
[49] A. P. Gorka, R. R. Nani, J. Zhu, S. Mackem, M. J. Schnermann, *J. Am. Chem. Soc.* **2014**, *136*, 14153–14159.
[50] R. S. Givens, C.-H. Park, *Tetrahedron Lett.* **1996**, *37*, 6259–6262.
[51] C.-H. Park, R. S. Givens, *J. Am. Chem. Soc.* **1997**, *119*, 2453–2463.
[52] R. S. Givens, D. Heger, B. Hellrung, Y. Kamdzhilov, M. Mac, P. G. Conrad, E. Cope, J. I. Lee, J. F. Mata-Segreda, R. L. Schowen, et al., *J. Am. Chem. Soc.* **2008**, *130*, 3307–3309.

[53] P. Klán, T. Šolomek, C. G. Bochet, A. Blanc, R. Givens, M. Rubina, V. Popik, A. Kostikov, J. Wirz, *Chem. Rev.* **2013**, *113*, 119–191.
[54] R. S. Givens, M. Rubina, J. Wirz, *Photochem. Photobiol. Sci.* **2012**, *11*, 472–488.
[55] F. Salahi, V. Purohit, G. Ferraudi, C. Stauffacher, O. Wiest, P. Helquist, *Org. Lett.* **2018**, *20*, 2547–2550.
[56] T. Slanina, P. Šebej, A. Heckel, Richard S. Givens, P. Klán, *Org. Lett.* **2015**, *17*, 4814–4817.
[57] I. Bownik, P. Šebej, J. Literák, D. Heger, Z. Šimek, R. S. Givens, P. Klán, *J. Org. Chem.* **2015**, *80*, 9713–9721.
[58] D. Madea, T. Slanina, P. Klán, *Chem Commun* **2016**, *52*, 12901–12904.
[59] S. Barman, S. K. Mukhopadhyay, S. Biswas, S. Nandi, M. Gangopadhyay, S. Dey, A. Anoop, N. D. P. Singh, *Angew. Chem. Int. Ed.* **2016**, 55, 4194-4198.
[60] A. L. Houk, R. S. Givens, C. G. Elles, *J. Phys. Chem. B* **2016**, 120, 3178-3186.
[61] J. C. Sheehan, R. M. Wilson, *J. Am. Chem. Soc.* **1964**, *86*, 5277–5281.
[62] J. C. Sheehan, R. M. Wilson, A. W. Oxford, *J. Am. Chem. Soc.* **1971**, *93*, 7222–7228.
[63] C. Ma, W. M. Kwok, H.-Y. An, X. Guan, M. Y. Fu, P. H. Toy, D. L. Phillips, *Chem. - Eur. J.* **2010**, *16*, 5102–5118.
[64] M. C. Pirrung, T. Ye, Z. Zhou, J. D. Simon, *Photochem. Photobiol.* **2006**, *82*, 1258.
[65] H. E. Zimmerman, V. R. Sandel, *J. Am. Chem. Soc.* **1963**, *85*, 915–922.
[66] Y. Carissan, D. Hagebaum-Reignier, N. Goudard, S. Humbel, *HuLiS Code: Lewis Embedded in Hückel Theory*, **2008**.
[67] O. A. Stasyuk, H. Szatylowicz, T. M. Krygowski, C. Fonseca Guerra, *Phys. Chem. Chem. Phys.* **2016**, *18*, 11624–11633.
[68] J. A. Pincock, *Acc. Chem. Res.* **1997**, *30*, 43–49.
[69] H. E. Zimmerman, *J. Am. Chem. Soc.* **1995**, *117*, 8988–8991.
[70] H. E. Zimmerman, *J. Phys. Chem. A* **1998**, *102*, 5616–5621.
[71] S. A. Fleming, A. W. Jensen, *J. Org. Chem.* **1996**, *61*, 7040–7044.
[72] C. Raviola, M. Fagnoni, *Photochem. Photobiol. Sci.* **2018**, *17*, 107–117.
[73] R. R. Perrotta, A. H. Winter, D. E. Falvey, *Org. Lett.* **2011**, *13*, 212–215.
[74] Đ. Škalamera, V. Blažek Bregović, I. Antol, C. Bohne, N. Basarić, *J. Org. Chem.* **2017**, *82*, 12554–12568.
[75] X. Ding, P. Wang, *J. Org. Chem.* **2018**, 83, 7459-7466.
[76] A. T. Buck, C. L. Beck, A. H. Winter, *J. Am. Chem. Soc.* **2014**, *136*, 8933–8940.
[77] A. H. Winter, D. E. Falvey, C. J. Cramer, B. F. Gherman, *J. Am. Chem. Soc.* **2007**, *129*, 10113–10119.
[78] T. R. Albright, A. H. Winter, *J. Am. Chem. Soc.* **2015**, *137*, 3402–3410.
[79] J. W. Chamberlin, *J. Org. Chem.* **1966**, *31*, 1658–1660.
[80] J. F. Cameron, J. M. J. Frechet, *J. Org. Chem.* **1990**, *55*, 5919–5922.
[81] P. H. Ruane, K. M. Bushan, C. M. Pavlos, R. A. D'S, J. P. Toscano, *J. Am. Chem. Soc.* **2002**, *124*, 9806–9811.
[82] A. W. Jensen, N. K. Desai, B. S. Maru, D. K. Mohanty, *Macromolecules* **2004**, *37*, 4196–4200.
[83] Y. Wang, S. Liu, Z. Lin, Y. Fan, Y. Wang, X. Peng, *Org. Lett.* **2016**, *18*, 2544–2547.

[84] P. Wang, H. Hu, Y. Wang, *Org. Lett.* **2007**, *9*, 2831–2833.
[85] P. Wang, Y. Wang, H. Hu, C. Spencer, X. Liang, L. Pan, *J. Org. Chem.* **2008**, *73*, 6152–6157.
[86] P. Wang, W. Lu, D. A. Devalankar, Z. Ding, *Org. Lett.* **2015**, *17*, 2114–2117.
[87] P. Wang, D. A. Devalankar, W. Lu, *J. Org. Chem.* **2016**, *81*, 6195–6200.
[88] X. Ding, D. A. Devalankar, P. Wang, *Org. Lett.* **2016**, *18*, 5396–5399.
[89] P. Wang, *J. Photochem. Photobiol. Chem.* **2017**, *335*, 300–310.
[90] X. Ding, P. Wang, *J. Org. Chem.* **2017**, *82*, 7309–7316.
[91] E. Havinga, R. O. de Jongh, W. Dorst, *Recl. Trav. Chim. Pays-Bas* **n.d.**, *75*, 378–383.
[92] H. E. Zimmerman, S. Somasekhara, *J. Am. Chem. Soc.* **1963**, *85*, 922–927.
[93] J. Cornelisse, E. Havinga, *Chem. Rev.* **1975**, *75*, 353–388.
[94] P. Kuzmič, L. Pavlíčková, M. Souček, *Collect. Czechoslov. Chem. Commun.* **1986**, *51*, 1293–1300.
[95] A. Banerjee, C. Grewer, L. Ramakrishnan, J. Jäger, A. Gameiro, H.-G. A. Breitinger, K. R. Gee, B. K. Carpenter, G. P. Hess, *J. Org. Chem.* **2003**, *68*, 8361–8367.
[96] E. Riguet, C. G. Bochet, *Org. Lett.* **2007**, *9*, 5453–5456.
[97] Y. Becker, E. Unger, M. A. H. Fichte, D. A. Gacek, A. Dreuw, J. Wachtveitl, P. J. Walla, A. Heckel, *Chem. Sci.* **2018**, *9*, 2797–2802.
[98] J.-M. Mewes, E. Pepler, J. Wachtveitl, A. Dreuw, *J. Phys. Chem. A* **2012**, *116*, 11846–11862.
[99] R. S. Givens, B. Matuszewski, *J. Am. Chem. Soc.* **1984**, *106*, 6860–6861.
[100] P. Klán, T. Šolomek, C. G. Bochet, A. Blanc, R. Givens, M. Rubina, V. Popik, A. Kostikov, J. Wirz, *Chem. Rev.* **2013**, *113*, 119–191.
[101] Y. Carissan, D. Hagebaum-Reignier, N. Goudard, S. Humbel, *J. Phys. Chem. A* **2008**, *112*, 13256–13262.
[102] R. H. Abu-Eittah, B. A. H. El-Tawil, *Can. J. Chem.* **1985**, *63*, 1173–1179.
[103] X. Liu, J. M. Cole, Z. Xu, *J. Phys. Chem. C* **2017**, *121*, 13274–13279.
[104] T. A. Moore, M. L. Harter, P.-S. Song, *J. Mol. Spectrosc.* **1971**, *40*, 144–157.
[105] T. G. Pavlopoulos, *Spectrochim. Acta Part Mol. Spectrosc.* **1986**, *42*, 47–52.
[106] N. A. Kuznetsova, O. L. Kaliya, *Russ. Chem. Rev.* **1992**, *61*, 683–696.
[107] T. Eckardt, V. Hagen, B. Schade, R. Schmidt, C. Schweitzer, J. Bendig, *J. Org. Chem.* **2002**, *67*, 703–710.
[108] T. Pavlopoulos, *IEEE J. Quantum Electron.* **1973**, *9*, 510–516.
[109] X. Liu, Z. Xu, J. M. Cole, *J. Phys. Chem. C* **2013**, *117*, 16584–16595.
[110] A. N. Fletcher, D. E. Bliss, J. M. Kauffman, *Opt. Commun.* **1983**, *47*, 57–61.
[111] B. Schade, V. Hagen, R. Schmidt, R. Herbrich, E. Krause, T. Eckardt, J. Bendig, *J. Org. Chem.* **1999**, *64*, 9109–9117.
[112] R. Schmidt, D. Geissler, V. Hagen, J. Bendig, *J. Phys. Chem. A* **2007**, *111*, 5768–5774.
[113] R. Schmidt, D. Geissler, V. Hagen, J. Bendig, *J. Phys. Chem. A* **2005**, *109*, 5000–5004.
[114] L. J. G. W. van Wilderen, C. Neumann, A. Rodrigues-Correia, D. Kern-Michler, N. Mielke, M. Reinfelds, A. Heckel, J. Bredenbeck, *Phys. Chem. Chem. Phys.* **2017**, *19*, 6487–6496.

[115] M. Yamaji, K. Nozaki, X. Allonas, S. Nakajima, S. Tero-Kubota, B. Marciniak, *J. Phys. Chem. A* **2009**, *113*, 5815–5822.
[116] A. V. Pinheiro, A. J. Parola, P. V. Baptista, J. C. Lima, *J. Phys. Chem. A* **2010**, *114*, 12795–12803.
[117] M. J. G. Fernandes, M. S. T. Gonçalves, S. P. G. Costa, *Tetrahedron* **2008**, *64*, 3032–3038.
[118] A. S. C. Fonseca, M. S. T. Gonçalves, S. P. G. Costa, *Amino Acids* **2010**, *39*, 699–712.
[119] A. M. S. Soares, S. P. G. Costa, M. S. T. Gonçalves, *Tetrahedron* **2010**, *66*, 8189–8195.
[120] T. Furuta, S. S.-H. Wang, J. L. Dantzker, T. M. Dore, W. J. Bybee, E. M. Callaway, W. Denk, R. Y. Tsien, *Proc. Natl. Acad. Sci.* **1999**, *96*, 1193–1200.
[121] H. Takano, T. Narumi, W. Nomura, T. Furuta, H. Tamamura, *Org. Lett.* **2015**, *17*, 5372–5375.
[122] R. Conceição, G. Hungerford, S. P. G. Costa, M. S. T. Gonçalves, *Dyes Pigments* **2018**, *148*, 368–379.
[123] C. Bao, G. Fan, Q. Lin, B. Li, S. Cheng, Q. Huang, L. Zhu, *Org. Lett.* **2012**, *14*, 572–575.
[124] H. Suzuki, *Bull. Chem. Soc. Jpn.* **1959**, *32*, 1340–1350.
[125] H. Suzuki, *Bull. Chem. Soc. Jpn.* **1960**, *33*, 406–410.
[126] G. Bassolino, C. Nançoz, Z. Thiel, E. Bois, E. Vauthey, P. Rivera-Fuentes, *Chem. Sci.* **2018**, *9*, 387–391.
[127] G. Bassolino, E. Halabi, P. Rivera-Fuentes, *Synthesis* **2018**, *50*, 846–852.
[128] L. Fournier, C. Gauron, L. Xu, I. Aujard, T. Le Saux, N. Gagey-Eilstein, S. Maurin, S. Dubruille, J.-B. Baudin, D. Bensimon, et al., *ACS Chem. Biol.* **2013**, *8*, 1528–1536.
[129] A. Gandioso, S. Contreras, I. Melnyk, J. Oliva, S. Nonell, D. Velasco, J. García-Amorós, V. Marchán, *J. Org. Chem.* **2017**, *82*, 5398–5408.
[130] Y. Chitose, M. Abe, K. Furukawa, J.-Y. Lin, T.-C. Lin, C. Katan, *Org. Lett.* **2017**, *19*, 2622–2625.
[131] C. A. Hammer, K. Falahati, A. Jakob, R. Klimek, I. Burghardt, A. Heckel, J. Wachtveitl, *J. Phys. Chem. Lett.* **2018**, *9*, 1448–1453.
[132] J. P. Olson, M. R. Banghart, B. L. Sabatini, G. C. R. Ellis-Davies, *J. Am. Chem. Soc.* **2013**, *135*, 15948–15954.
[133] J. P. Olson, H.-B. Kwon, K. T. Takasaki, C. Q. Chiu, M. J. Higley, B. L. Sabatini, G. C. R. Ellis-Davies, *J. Am. Chem. Soc.* **2013**, *135*, 5954–5957.
[134] J. Schaal, B. Dekowski, B. Wiesner, J. Eichhorst, K. Marter, C. Vargas, S. Keller, N. Eremina, A. Barth, A. Baumann, et al., *ChemBioChem* **2012**, *13*, 1458–1464.
[135] V. Hagen, B. Dekowski, N. Kotzur, R. Lechler, B. Wiesner, B. Briand, M. Beyermann, *Chem.- Eur. J.* **2008**, *14*, 1621–1627.
[136] M. T. Richers, J. M. Amatrudo, J. P. Olson, G. C. R. Ellis-Davies, *Angew. Chem. Int. Ed.* **2017**, *56*, 193–197.
[137] P. Seyfried, L. Eiden, N. Grebenovsky, G. Mayer, A. Heckel, *Angew. Chem. Int. Ed.* **2017**, *56*, 359–363.
[138] T. Ohtsuki, S. Kanzaki, S. Nishimura, Y. Kunihiro, M. Sisido, K. Watanabe, *Nat. Commun.* **2016**, *7*, 12501.

[139] P. Šebej, J. Wintner, P. Müller, T. Slanina, J. Al Anshori, L. A. P. Antony, P. Klán, J. Wirz, *J. Org. Chem.* **2013**, *78*, 1833–1843.
[140] L. A. P. Antony, T. Slanina, P. Šebej, T. Šolomek, P. Klán, *Org. Lett.* **2013**, *15*, 4552–4555.
[141] P. P. Goswami, A. Syed, C. L. Beck, T. R. Albright, K. M. Mahoney, R. Unash, E. A. Smith, A. H. Winter, *J. Am. Chem. Soc.* **2015**, *137*, 3783–3786.
[142] N. Rubinstein, P. Liu, E. W. Miller, R. Weinstain, *Chem. Commun.* **2015**, *51*, 6369–6372.
[143] N. Umeda, H. Takahashi, M. Kamiya, T. Ueno, T. Komatsu, T. Terai, K. Hanaoka, T. Nagano, Y. Urano, *ACS Chem. Biol.* **2014**, *9*, 2242–2246.
[144] A. Takeda, T. Komatsu, H. Nomura, M. Naka, N. Matsuki, Y. Ikegaya, T. Terai, T. Ueno, K. Hanaoka, T. Nagano, et al., *ChemBioChem* **2016**, *17*, 1233–1240.
[145] M. Kawatani, M. Kamiya, H. Takahashi, Y. Urano, *Bioorg. Med. Chem. Lett.* **2018**, *28*, 1–5.
[146] T. Slanina, P. Shrestha, E. Palao, D. Kand, J. A. Peterson, A. S. Dutton, N. Rubinstein, R. Weinstain, A. H. Winter, P. Klán, *J. Am. Chem. Soc.* **2017**, *139*, 15168–15175.
[147] E. Palao, T. Slanina, L. Muchová, T. Šolomek, L. Vítek, P. Klán, *J. Am. Chem. Soc.* **2016**, *138*, 126–133.
[148] K. Sitkowska, B. L. Feringa, W. Szymański, *J. Org. Chem.* **2018**, *83*, 1819–1827.
[149] N. Vohradská, E. M. Sánchez-Carnerero, T. Pastierik, C. Mazal, P. Klán, *Chem. Commun.* **2018**, *54*, 5558–5561.
[150] J. A. Peterson, C. Wijesooriya, E. J. Gehrmann, K. M. Mahoney, P. P. Goswami, T. R. Albright, A. Syed, A. S. Dutton, E. A. Smith, A. H. Winter, *J. Am. Chem. Soc.* **2018**, 140, 7343-7346.
[151] L. J. G. W. van Wilderen, A. T. Messmer, J. Bredenbeck, *Angew. Chem. Int. Ed.* **2014**, *53*, 2667–2672.
[152] A. Lennart, Synthese neuer photolabiler Schutzgruppen basierend auf dem 3-DiethylaminobenzylGrundgerüst, Bachelor Thesis, Goethe University Frankfurt, **2015**.
[153] J. Breitenbach, Synthese und Evaluierung neuartiger photolabiler Schutzgruppen basierend auf 3-Diethylaminobenzyl Derivaten, Bachelor Thesis, Goethe University Frankfurt, **2016**.
[154] V. McKenney, Synthese und Evaluierung neuartiger photolabiler Schutzgruppen basierend auf 2-Amino-9-Fluorenol - Derivaten, Bachelor Thesis, Goethe University Frankfurt, **2017**.
[155] F. Bureš, *RSC Adv* **2014**, *4*, 58826–58851.
[156] Z. Ahmadi, J. S. McIndoe, *Chem. Commun.* **2013**, *49*, 11488–11490.
[157] N. Wu, X. Li, X. Xu, Y. Wang, Y. Xu, X. Chen, *Lett. Org. Chem.* **2010**, *7*, 11–14.
[158] A. Almenningen, O. Bastiansen, L. Fernholt, B. N. Cyvin, S. J. Cyvin, S. Samdal, *J. Mol. Struct.* **1985**, *128*, 59–76.
[159] M. P. Johansson, J. Olsen, *J. Chem. Theory Comput.* **2008**, *4*, 1460–1471.
[160] H. Suzuki, *Bull. Chem. Soc. Jpn.* **1959**, *32*, 1350–1356.
[161] Gaussian 16, Revision B.01, M. J. Frisch, G. W. Trucks, H. B. Schlegel, G. E.Scuseria, M. A. Robb, J. R. Cheeseman, G. Scalmani, V. Barone, B. Mennucci, G. A. Petersson, H. Nakatsuji, M. Caricato, X. Li, H. P. Hratchian,A. F. Izmaylov, J. Bloino, G. Zheng, J. L. Sonnenberg, M. Hada, M. Ehara, K. Toyota, R. Fukuda, J. Hasegawa, M. Ishida, T. Nakajima, Y. Honda, O. Kitao, H. Nakai, T. Vreven, J. A. Montgomery, Jr., J. E. Peralta, F.

Ogliaro, M. Bearpark, J. J. Heyd, E. Brothers, K. N. Kudin, V. N. Staroverov, R. Kobayashi, J. Normand, K. Raghavachari, A. Rendell, J. C. Burant, S. S. Iyengar, J. Tomasi, M. Cossi, N. Rega, J. M. Millam, M. Klene, J. E. Knox, J. B.Cross, V. Bakken, C. Adamo, J. Jaramillo, R. Gomperts, R. E. Stratmann, O. Yazyev, A. J. Austin, R. Cammi, C. Pomelli, J. W. Ochterski, R. L. Martin, K. Morokuma, V. G. Zakrzewski, G. A. Voth, P. Salvador, J. J. Dannenberg, S. Dapprich, A. D. Daniels, Farkas, J. B. Foresman, J. V. Ortiz, J. Cioslowski, D. J. Fox, Gaussian, Inc. Wallingford CT, 2016

[162] C. Adamo, V. Barone, *J. Chem. Phys.* **1999**, *110*, 6158–6170.

[163] F. Weigend, R. Ahlrichs, *Phys. Chem. Chem. Phys.* **2005**, *7*, 3297–3305.

[164] B. Buszewski, S. Noga, *Anal. Bioanal. Chem.* **2012**, *402*, 231–247.

[165] G. Papageorgiou, D. Ogden, G. Kelly, J. E. T. Corrie, *Photochem. Photobiol. Sci.* **2005**, *4*, 887–896.

[166] R. F. Chen, C. Scott, E. Trepman, *Biochim. Biophys. Acta BBA - Protein Struct.* **1979**, *576*, 440–455.

[167] G. G. Gurzadyan, S. Steenken, *Chem. – Eur. J.* **2001**, *7*, 1808–1815.

[168] K. H. Jensen, J. E. Hanson, *Chem. Mater.* **2002**, *14*, 918–923.

[169] A. Roxin, A. Chase, E. Jeffers, M. Lukeman, *Photochem. Photobiol. Sci.* **2011**, *10*, 920–930.

[170] D. Zivkovic, Investigations on 2,7-Diamino-9-Fluorenol Photochemistry, PhD Thesis, University of Basel, **2007**.

[171] G. Rieveschl, F. E. Ray, *Chem. Rev.* **1938**, *23*, 287–389.

[172] C. Finger, *Process for the Production of Fluorenone by Catalytic Oxidation of Fluorene*, **1980**, 4218400.

[173] P. J. Perry, M. A. Read, R. T. Davies, S. M. Gowan, A. P. Reszka, A. A. Wood, L. R. Kelland, S. Neidle, *J. Med. Chem.* **1999**, *42*, 2679–2684.

[174] O. Kwon, S. Barlow, S. A. Odom, L. Beverina, N. J. Thompson, E. Zojer, J.-L. Brédas, S. R. Marder, *J. Phys. Chem. A* **2005**, *109*, 9346–9352.

[175] T. Redzimski, J. R. Heldt, *J. Fluoresc.* **2003**, *13*, 393–401.

[176] C. A. Stout, A Molecular Orbital Correlation of Reactivities of Substituted 9-Phenylfluorenyl Systems, PhD Thesis, The Ohio State University, **1962**.

[177] S. R. D. George, T. E. Elton, J. B. Harper, *Org. Biomol. Chem.* **2015**, *13*, 10745–10750.

[178] R. A. McClelland, N. Mathivanan, S. Steenken, *J. Am. Chem. Soc.* **1990**, *112*, 4857–4861.

[179] M. Fischer, Y. Shi, B. Zhao, V. Snieckus, P. Wan, **1999**, *77*, 7.

[180] S. Ward, T. Messier, M. Lukeman, *Can. J. Chem.* **2010**, *88*, 493–499.

[181] S. Arumugam, J. Guo, N. E. Mbua, F. Friscourt, N. Lin, E. Nekongo, G.-J. Boons, V. V. Popik, *Chem Sci* **2014**, *5*, 1591–1598.

[182] P. Wan, E. Krogh, *J. Chem. Soc. Chem. Commun.* **1985**, *0*, 1207–1208.

[183] P. Wan, E. Krogh, *J. Am. Chem. Soc.* **1989**, *111*, 4887–4895.

[184] M. Rosenberg, C. Dahlstrand, K. Kilså, H. Ottosson, *Chem. Rev.* **2014**, *114*, 5379–5425.

[185] P. Klán, J. Wirz, in *Photochem. Org. Compd.*, Wiley-Blackwell, **2009**, pp. 137–182.

[186] P. Klán, J. Wirz, in *Photochem. Org. Compd.*, Wiley-Blackwell, **2009**, pp. 25–72.

[187] J. von Cosel, J. Cerezo, D. Kern-Michler, C. Neumann, L. J. G. W. van Wilderen, J. Bredenbeck, F. Santoro, I. Burghardt, *J. Chem. Phys.* **2017**, *147*, 164116.
[188] T. Weinrich, M. Gränz, C. Grünewald, T. F. Prisner, M. W. Göbel, *Eur. J. Org. Chem.* **2017**, *2017*, 491–496.
[189] J. Daru, A. Stirling, *J. Org. Chem.* **2011**, *76*, 8749–8755.
[190] S. Tyndall, K. F. Wong, M. A. VanAlstine-Parris, *J. Org. Chem.* **2015**, *80*, 8951–8953.
[191] I. K. Müller, Synthese von Testsubstraten für VIPER uncaging, Bachelor Thesis, Goethe University Frankfurt **2014**.
[192] L. Wirtz, U. Kazmaier, *Eur. J. Org. Chem.* **2011**, *2011*, 7062–7065.
[193] A. Schiavello, *Gazzetta Chim. Ital.* **1951**, *81*, 717–724.
[194] Y. Ichikawa, M. Osada, I. I. Ohtani, M. Isobe, *J. Chem. Soc. [Perkin 1]* **1997**, *0*, 1449–1456.
[195] P. Kočovský, *Tetrahedron Lett.* **1986**, *27*, 5521–5524.
[196] D. T. Mowry, *Chem. Rev.* **1948**, *42*, 189–283.
[197] K. A. Jensen, A. Holm, N. A. Sørensen, D. R. Sparrow, *Acta Chem. Scand.* **1964**, *18*, 2417–2418.
[198] D. Martin, *Angew. Chem.* **1964**, *76*, 303–303.
[199] K. A. Jensen, A. Holm, E. Larsen, A. Djurhuus, K. Gustavii, U. Junggren, B. Lamm, B. Samuelsson, *Acta Chem. Scand.* **1969**, *23*, 2183–2183.
[200] H. Bender, F. Carnovale, J. B. Peel, C. Wentrup, *J. Am. Chem. Soc.* **1988**, *110*, 3458–3461.
[201] J.-T. Yu, F. Teng, J. Cheng, *Adv. Synth. Catal.* **2017**, *359*, 26–38.
[202] D. Crich, T. K. Hutton, A. Banerjee, P. Jayalath, J. Picione, *Tetrahedron Asymmetry* **2005**, *16*, 105–119.
[203] K. A. Jensen, A. Holm, B. Thorkilsen, H. Halvarson, L. Nilsson, *Acta Chem. Scand.* **1964**, *18*, 826–828.
[204] D. Martin, *Tetrahedron Lett.* **1964**, *5*, 2829–2832.
[205] K. A. Jensen, M. Due, A. Holm, A. Kjær, R. H. Shapiro, A. Westerdahl, *Acta Chem. Scand.* **1965**, *19*, 438–442.
[206] N. Groving, A. Holm, š. Kováč, A. Kjær, R. H. Shapiro, A. Westerdahl, *Acta Chem. Scand.* **1965**, *19*, 443–450.
[207] E. Vowinkel, H.-J. Baese, *Chem. Ber.* **1974**, *107*, 1213–1220.
[208] D. Martin, *Z. Für Chem.* **1967**, *7*, 123–137.
[209] B. H. Winters, H. I. Mandelberg, W. B. Mohr, *Appl. Phys. Lett.* **1974**, *25*, 723–725.
[210] G. Jones, W. R. Bergmark, W. R. Jackson, *Opt. Commun.* **1984**, *50*, 320–323.
[211] G. Jones II, W. R. Bergmark, J*ournal of Photochemistry*, **1984**, 26, 179-184.
[212] B. C. Pemberton, A. Ugrinov, J. Sivaguru, *J. Photochem. Photobiol. Chem.* **2013**, *255*, 10–15.
[213] N. Barooah, B. C. Pemberton, J. Sivaguru, *Org. Lett.* **2008**, *10*, 3339–3342.
[214] T. Wolff, H. Görner, *Phys Chem Chem Phys* **2004**, *6*, 368–376.
[215] N. Kuş, S. Breda, I. Reva, E. Tasal, C. Ogretir, R. Fausto, *Photochem. Photobiol.* **2007**, *83*, 1237–1253.
[216] R. J. von Trebra, T. H. Koch, *Appl. Phys. Lett.* **1983**, *42*, 129–131.

[217] E. A. Kalmykova, N. A. Kuznetsova, O. L. Kaliya, *Zhurnal Obshchei Khimii* **1990**, *60*, 946–951.
[218] E. Raudonyte-Svirbutaviciene, L. Mikoliunaite, A. Drabavicius, R. Juskenas, S. Sakirzanovas, T. Jüstel, A. Katelnikovas, *RSC Adv.* **2016**, *6*, 107065–107074.
[219] F. D. Lewis, W. H. Saunders, *J. Am. Chem. Soc.* **1967**, *89*, 645–647.
[220] F. D. Lewis, W. H. Saunders, *J. Am. Chem. Soc.* **1968**, *90*, 7033–7038.
[221] F. D. Lewis, W. H. Saunders, *J. Am. Chem. Soc.* **1968**, *90*, 7031–7033.
[222] K. I. Priyadarsini, D. B. Naik, P. N. Moorthy, *J. Photochem. Photobiol. Chem.* **1990**, *54*, 251–261.
[223] D. Kern-Michler, C. Neumann, N. Mielke, L. J. G. W. van Wilderen, M. Reinfelds, J. von Cosel, F. Santoro, A. Heckel, I. Burghardt, J. Bredenbeck, *J. Am. Chem. Soc.* **2018**, *140*, 926–931.
[224] R. Shelkov, M. Nahmany, A. Melman, *Org. Biomol. Chem.* 2004, 2, 397-401.
[225] V. Lutz, J. Glatthaar, C. Würtele, M. Serafin, H. Hausmann, P. R. Schreiner, *Chem. - Eur. J.* **2009**, *15*, 8548–8557.
[226] R. Murashige, Y. Hayashi, S. Ohmori, A. Torii, Y. Aizu, Y. Muto, Y. Murai, Y. Oda, M. Hashimoto, *Tetrahedron* **2011**, *67*, 641–649.
[227] S. Ueda, M. Fujita, H. Tamamura, N. Fujii, A. Otaka, *ChemBioChem* **2005**, *6*, 1983–1986.
[228] G. Yin, M. Gao, N. She, S. Hu, A. Wu, Y. Pan, *Synthesis* **2007**, *2007*, 3113–3116.
[229] V. G. Gaikar, H. M. Anasthas, *Ind. Eng. Chem. Res.* **2002**, *41*, 1335–1343.
[230] A. Filarowski, A. Koll, A. Kochel, J. Kalenik, P. E. Hansen, *J. Mol. Struct.* **2004**, *700*, 67–72.
[231] P. N. D. Singh, S. M. Mandel, R. M. Robinson, Z. Zhu, R. Franz, B. S. Ault, A. D. Gudmundsdóttir, *J. Org. Chem.* **2003**, *68*, 7951–7960.
[232] C. Ma, P. Zuo, W. M. Kwok, W. S. Chan, J. T. W. Kan, P. H. Toy, D. L. Phillips, *J. Org. Chem.* **2004**, *69*, 6641–6657.
[233] M. C. Sauer, R. A. Crowell, I. A. Shkrob, *J. Phys. Chem. A* **2004**, *108*, 5490–5502.
[234] Photoelectric Spectrometry Group, Institut für Spektrochemie und Angewandte Spektroskopie, *UV atlas of organic compounds Vol. III. Vol. III.*, **1967**.
[235] C. G. Hatchard, C. A. Parker, *Proc R Soc Lond A* **1956**, *235*, 518–536.
[236] A. Zafar, R. Melendez, S. J. Geib, A. D. Hamilton, *Tetrahedron* **2002**, *58*, 683–690.
[237] T. Saitoh, S. Yoshida, J. Ichikawa, *J. Org. Chem.* **2006**, *71*, 6414–6419.
[238] C. J. Monceaux, C. Hirata-Fukae, P. C.-H. Lam, M. M. Totrov, Y. Matsuoka, P. R. Carlier, *Bioorg. Med. Chem. Lett.* **2011**, *21*, 3992–3996.
[239] P. J. Homnick, P. M. Lahti, *Phys. Chem. Chem. Phys.* **2012**, *14*, 11961–11968.
[240] P. J. Homnick, P. M. Lahti, *Phys. Chem. Chem. Phys.* **2012**, *14*, 11961.
[241] K. Park, L. Tsou, A. Hamilton, *Synthesis* **2006**, 3617–3620.

[242] X. Zhang, J.-B. Han, P.-F. Li, X. Ji, Z. Zhang, *Synth. Commun.* **2009**, *39*, 3804–3815.

[243] S. A. Sojka, *J. Org. Chem.* **1975**, *40*, 1175–1178.

[244] R. O. Schönleber, J. Bendig, V. Hagen, B. Giese, *Bioorg. Med. Chem.* **2002**, *10*, 97–101.

[245] B. P. Ngoy, P. Sebej, T. Solomek, B. H. Lim, T. Pastierik, B. S. Park, R. S. Givens, D. Heger, P. Klan, *Photochem. Photobiol. Sci.* **2012**, *11*, 1465–1475.

[246] D. S. Bhalerao, K. G. Akamanchi, *Synth. Commun.* **2010**, *40*, 799–807.

6.5. Acknowledgments

First of all, I want to thank my supervisor Prof. Dr. Alexander Heckel for offering me interesting projects and giving me an opportunity to conduct research in his working group. Furthermore, I want to thank Alexander Heckel for giving me scientific freedom, improving my weaknesses and helping me to address my demons all through my doctoral studies. I could not wish for a better *Doktorvater*.

To Prof. Dr. Jens Bredenbeck and Dr. Boris Fürtig for their productive contribution, encouragement and good advice as members of my mentoring committee in the CLiC program. Furthermore, I want to thank Jens Bredenbeck for accepting the role of second reviewer of this thesis. Also, the fruitful collaboration with Jens Bredenbeck and members of his group - Daniela Kern-Michler, Carsten Neumann, Nicole Mielke and Luuk van Wilderen within the VIPER project deserves acknowledgement. Your professionality, responsiveness and friendliness always made me happy to be your synthesis guy and it has been a great experience working with you.

I want to thank Prof. Dr. Irene Burghardt and the Three Musketeers of computational chemistry - Jan von Cosel, Konstantin Falahati and Carsten Hamerla for their wise and friendly guidance in the world of theoretical chemistry.

My work would have been impossible without the fast and professional service by Julia Kiedrowski, Ralf Salomon, Dana Dobbs (*Chemikalienausgabe*); Wilhelm Lohbeck and Keve Bitto (*Zentrales Zwischenlager für chemische Sonderabfälle*); Andreas Münch, Dr. Uwe Hener, Simon Zenglein and Matthias Brandl (*Serviceeinheit Massenspektrometrie*).

My thanks goes to all current and former members of AK Heckel. During the nearly 4 years of us being colleagues, you have always been most welcoming and friendly, I have had a lot of fun together with you. One may say, it has been refreshing as bread. Especially, soon-to-be Dr. Josefine Kahlstatt and notorious Ph.D Thomas Goldau, Yvonne Becker, Anja Blümler, Robin Klimek and Volker Hermanns. To Dr. Thomas Halbritter, Dr. Dean Klötzner and Andreas Jakob I want to thank for those evenings in Lahmer Esel and BBQ parties. My thanks goes also to Martin Held, Alexandra Schuck, Heike Köhler and Dr. Christian Grünewald for technical and organizational support of various kinds. Dr. Manuela Fichte for her guidance and friendly encouragement of me as a new PhD student. Patricia Müller for her patience and support with my German language practice during the countless scientific and non-scientific discussions, and her readiness to always help me out. I would like to let Dr. Patrick Seyfried know, that for all those NMR ampules he never washed he has paid back with hours and hours of helping with his advice whenever I needed it.

Furthermore, all non-science related talks we have had over the years have been pure pleasure. I thank also Dr. Tomáš Slanina for the countless, very helpful scientific discussions and being a cool guy in general. Nikolai Grebenovsky for being the most trustworthy person and an amazing laboratory mate. If only your music taste would not be so horrible!

I want to thank my great master's practicum students Beatriz Sánchez Batalla, Sina Roth (it's leviosaa!), Hong Thu Duong, Daniel Göttnauer, Victoria Aladin, Danhau Dai, Betul Ceylan, Christopher Beier, Monika Swierzy and Alexander Kaps as well as bachelor students, who entrusted me to be their thesis advisor - Lennart Alsheimer, Jennifer Breitenbach, Vivien McKenney and Daniel Scheppa.

Thanks to all the members of the CLiC graduate school for the great time together, especially, Tobias Lieblein, Dinh Du Tran and my two gypsies Christopher Hammer and Andrés Arriagada.

Special thanks to Andrés Arriagada, Christopher and Anneke Hammer, György Pintér, László Rácz, Julian de Mos and Dinh Du Tran for the nice time we have had together since I live in Frankfurt.

Further away from Frankfurt and Germany, at the shore of the Baltic Sea is Latvia and there are countless Latvians I would like to acknowledge. First of all those people, who stand behind my previous chemistry education: high school chemistry teacher Brigita Brūvere, members of Faculty of Chemistry in University of Latvia (especially Dr. Igors Kļimenkovs), Prof. Dr. Marja Lajunen and Dr. Johanna Kärkkäinen (University of Oulu), Dr. Mārtiņš Katkevičs and members of BASS group (Latvian Institute of Organic Synthesis). Also my friends, study colleagues and amazing chemists Agnese Deksne, Beatrise Bērziņa, Eduards Baķis, Kaspars Leduskrasts, Toms Reķis and Ilmārs Rikmanis. I would not be writing this chapter if it were not for you. Special thanks to Luīze Bidiņa for her friendship and inspiration throught the years.

Even more I wish to thank all member of my family for the years of their love and support. Especially, my brothers Reinis and Jānis for the guidance of their youngest brother through my childhood and also in later years up to this very day. And to my mother for everything one could possibly be his mum thankful for. Furthermore, I want to thank Brandstetter, Hasenhüttl and Schwarzl familys for their support and always making me feel welcomed as a member of family.

Finally, my biggest thank goes to Julia Brandstetter, who's love and support filled even the most difficult times during my PhD thesis with a ray of sun.

6.6. Declaration

Except where stated otherwise by reference or acknowledgment, the work presented was generated by myself under the supervision of my advisors during my doctoral studies. All contributions from colleagues are explicitly referenced in the thesis. The material listed below was obtained in the context of collaborative research:

-Figures 62, 63, 78, 145;

Whenever a figure, table or text is identical to a previous publication, it is stated explicitly in the thesis that copyright permission and/or co-author agreement has been obtained.

The following parts of the thesis have been previously published:

-Chapters 5.1 (partly), 5.2 (completely), 5.3 (completely), 5.4 (partly);

-Figures 57, 59, 60, 64, 76, 77, 89, 107, 113, 115, 116, 117, 143, 144, 146, 147, 148, 149;

-Tables 1, 2, 4, 6;

6.7. Curriculum vitae

Personal Information:

Name, last name:	Matīss Reinfelds
Address:	Ludwig-Tieck Str. 3,
	60431, Frankfurt am Main, Germany
Date and place of birth:	12.10.1990
	Rīga, Latvia

Education:

Since 11/2014	Doctoral studies in Chemistry
	Institute of Organic Chemistry and Biochemistry, Goethe University Frankfurt (Frankfurt am Main, Germany)
	Title of dissertation: "Design and Synthesis of New Photolabile Protecting Groups". Doctoral advisor Prof. Dr. Alexander Heckel
2012-2014	Master of Science in Chemistry (with distinction)
	University of Latvia (Rīga, Latvia)
	Title of master thesis: "Enantioselective synthesis of tryptophan derivatives substituted in the indole ring". Supervisor Dr. Chem., principal scientist, Mārtiņš Katkevičs, supervisor at University of Latvia, Dr. Chem., docent, Igors Kļimenkovs.
2009-2012	Bachelor of Science in Chemistry
	University of Latvia (Rīga, Latvia)
	Title of bachelor thesis: "Iron catalyzed cyclization of *N*-aryl benzamide iodo derivatives". Supervisor Dr. Chem., principal scientist, Mārtiņš Katkevičs, supervisor at University of Latvia, Dr. Chem., docent, Edgars Sūna.
1997-2009	High School Education, Secondary School No. 6 (Rīga, Latvia)

Scientific publications:

1. M. Reinfelds, J. von Cosel, K. Falahati, C. Hamerla, T. Slanina, I. Burghardt, A. Heckel, A New Photocage Derived from Fluorene, *Chem. Eur. J.* **2018**, 24, doi: 10.1002/chem.201802390.

2. D. Kern-Michler, C. Neumann, N. Mielke, L. J. G. W. van Wilderen, M. Reinfelds, J. von Cosel, F. Santoro, A. Heckel, I. Burghardt, J. Bredenbeck, Controlling photochemistry via isotopomers and IR preexcitation, *J. Am. Chem. Soc.* **2018**, 140, 926–931.

3. L. J. G. W. van Wilderen, C. Neumann, A. Rodrigues-Correia, D. Kern-Michler, N. Mielke, M. Reinfelds, A. Heckel, J. Bredenbeck, Picosecond activation of the DEACM photocage unravelled by VIS-pump-IR-probe spectroscopy, *Phys. Chem. Chem. Phys.* **2017**, 19, 6487–6496.

4. M. Reinfelds, K. Kalinins, D. Katkevica, R. Zemribo, M. Katkevics, Synthesis of tryptophans by alkylation of chiral glycine enolate equivalents with quaternary gramines, *Tetrahedron Lett.* **2015**, 56, 5882-5885